Proceedings of the International Conference “Micro- and Nanoelectronics – 2018”

IC Micro- and Nanoelectronics

with the Extended Session

Quantum Informatics

Book of

ABSTRACTS

October 1 – 5, 2018
Moscow – Zvenigorod, Russia

RUSSIAN ACADEMY OF SCIENCES
MINISTRY OF SCIENCE AND HIGHER EDUCATION
INSTITUTE OF PHYSICS AND TECHNOLOGY OF RAS

Proceedings of the International Conference «Micro- and Nanoelectronics – 2018» ICMNE – 2018

Book of Abstracts

October 1–5, 2018
Moscow – Zvenigorod, Russia

MOSCOW – 2018

УДК 621
ББК 32.85
М59

DOI 10.29003/m209.ICMNE-2018

Издание осуществлено при поддержке
Российского фонда фундаментальных исследований по проекту 18-07-20062

Под редакцией:
чл.-корр. РАН *В.Ф. Лукичева*;
д. ф.-м. н. *К.В. Руденко*

Составитель к. ф.-м. н. *В.П. Кудря*

М59 **Микро- и наноэлектроника – 2018:** Труды международной конференции (1–5 октября, 2018, г. Звенигород, РФ): Сборник тезисов / Под ред. В.Ф. Лукичева, К.В. Руденко. Составитель В.П. Кудря. – Москва : МАКС Пресс, 2018. – 218 с.
ISBN 978-5-317-05917-0

Сборник содержит тезисы докладов, представленных на Международной конференции «Микро- и наноэлектроника – 2018» (ICMNE-2018), включающей расширенную сессию «Квантовая информатика» (QI-2018). Тематика конференции охватывает большинство областей физики микро- и наноразмерных приборов, а также микро- и наноэлектронных технологий и концентрируется на освещении последних достижений в этой сфере. Она продолжает серию всероссийских (с 1994 года) и международных конференций (с 2003 года).

Ключевые слова: нанотранзисторы, затворные стеки, квантовые компьютеры, МЭМС, магнитные материалы, оптоэлектроника.

УДК 621
ББК 32.85

Publishing was supported
by Russian Foundation for Fundamental Research, project 18-07-20062

Micro- and Nanoelectronics – 2018: Proceedings of the International Conference (October 1–5, 2018, Zvenigorod, Russia): Book of Abstracts / Ed. by V.F. Lukichev and K.V. Rudenko. Compiler V.P. Kudrya. – Moscow : MAKS Press, 2018. – 218 p.

The Book of Abstracts contains the abstracts of the papers presented at the biannual International Conference "Micro- and Nanoelectronics – 2018" (ICMNE-2018) including the extended Session "Quantum Informatics" (QI-2018). The Conference topics cover the most of the areas dedicated to the physics of integrated micro- and nanoelectronic devices and related micro- and nanotechnologies. The Conference is focused on recent progress in those areas. It continues the series of the AllRussian Conferences (since 1994) and the International Conferences (since 2003).

Keywords: nanoscale transistors, gate stacks, quantum computers, MEMS, magnetic materials, optoelectronics.

ISBN 978-5-317-05917-0

© Коллектив авторов, 2018

OXFORD INSTRUMENTS

Oxford Instruments Plasma Technology

Лидер по производству систем плазмохимического осаждения/травления для научно-исследовательских целей и мелкосерийного производства

ALE
Атомно-слоевое травление

ALD
Атомно-слоевое осаждение

CNT

CVD
Плазмо-химическое осаждение

ICP CVD

Bosch

RIE
Реактивное ионное травление

IBE
Ионно-лучевое травление

PVD
Магнетронное напыление

PECVD

IBD

Crestec Corporation

CRESTEC

Передовые технологии в электронно-лучевой литографии и уникальные решения

CABL-9000 / CABL-UH
Системы нанолитографии высокого разрешения

- ускоряющее напряжение до **130 кВ**
- минимальная ширина линии **5 нм**
- диаметр пятна до **1,6 нм**
- диаметр пластин до **200 мм**
- **полевой катод (ZrO/W)**
- ручная загрузка
- размер поля 30мкм,60мкм,120мкм, 300мкм, 600мкм, 1200мкм,2400мкм)
- векторное сканирование (x,y)
- векторное сканирование (R,f)
- растровое сканирование
- компактные размеры системы
- термостатированный кожух
- минимальные затраты на подготовку помещения

TechnoInfo

Ваш надежный партнер в мире нанотехнологий

Ion Beam Services

Самое современное оборудование для ионной имплантации, разработка технологий на заказ, сервис

ibs Innovative Ion Implant

IMC-200/ IMC-400
Ионно-лучевая имплантация

- диаметр пластин до **150 мм**
- энергии **2 - 400 кэВ**
- токи до **3000 мкА**
- дозы до **10E18**
- температура **-150... 600 С**
- автоматическая, либо ручная загрузка

PULSION
Плазменная иммерсионная ионная имплантация

- диаметр пластин до **460 мм**
- энергии **1 - 30 кэВ**
- токи до **300 мА**
- дозы до **10E18**
- температура **-150... 600 С**
- автоматическая, либо ручная загрузка

- разработаны рецепты имплантации для более **60 примесей**

www.technoinfo.ru / sales@technoinfo.ru / +7(499) 243-66-26

НИКС

КОМПЬЮТЕРНАЯ
КОМПАНИЯ

БИЗНЕС, ОСНОВАННЫЙ НА НАУЧНОМ ПОДХОДЕ

Спонсор конференций ICMNE2003, Qi2004, ICMNE2005, 2007, 2009, 2012, 2014, 2016

Год основания:..........**1991**
Профиль:..........**компьютеры,**
- комплектующие,
- программное обеспечение,
- бизнес-анализ

Учредители:..........**выпускники МФТИ**
Сотрудники:..........**600 человек,**
- из них 20% выпускников МФТИ и других физико-математических вузов России

Годовой оборот:..........**$80млн**
Сайт:..........www.nix.ru
- 150 тыс. уникальных посетителей в день

Компьютерный супермаркет НИКС в рамках собственного проекта NANOSOFT® занимается всесторонней поддержкой российской науки и образования, исследований в области квантовой информатики. На гранты нашей компании многие талантливые студенты, преподаватели и российские учёные смогли успешно развивать свою научную деятельность.

NANOSOFT.RU

ваш шанс на прорыв в будущее

Nanosoft® - собственная программа Компьютерного супермаркета НИКС по поддержке российских ученых, занимающихся теоретическими и экспериментальными исследованиями квантовых приборов и нанотехнологий.

http://www.nanosoft.ru, science@nix.ru

TABLE OF CONTENTS

Monday, October, 1st	**Special Session:**	**S1-01 – S1-02**
Tuesday, October, 2nd	**Invited Papers:**	**L1-01 – L1-04**
		qL1-01 – qL1-04
	Oral Papers:	**O1-01 – O1-20**
		q1-01 – q1-09
Wednesday, October, 3rd	**Invited Papers:**	**L2-01 – L2-04**
	Oral Papers:	**O2-01 – O2-18**
		q2-01 – q2-09
	Posters:	**P1-01 – P1-46**
Thursday, October, 4th	**Oral Papers:**	**O3-01 – O3-29**
		q3-01 – q3-09
	Posters:	**P2-01 – P2-46**
		D-01 – D-02

How to search for necessary abstract?

Every Abstract has its own identification number (for instance, L1-04, O1-07, P2-28, and so on), which is printed at the top of the page. This number corresponds to the one in the *Conference Programme*. If you do not know the number of the paper, but know at least one of the authors it is possible to find the Abstract using the *Author Index* located in the end of the *Book of Abstracts*.

Как отыскать интересующие Вас тезисы доклада?

Каждый доклад имеет собственный идентификационный номер (например, L1-04, O1-07, P2-28 и т.д.), который указан вверху страницы. Этот номер совпадает с номером, присвоенным докладу в *Программе конференции*. Если Вы не знаете номера доклада, но Вам известен хотя бы один из авторов, вы можете воспользоваться *Авторским указателем*, расположенным в конце *Сборника тезисов.*

Advanced equipment for manufacturing nanostructures, 2D materials, new semiconductor devices, and other applications

A. Krynin
Technoinfo Limited, Moscow, a.krynin@technoinfo.ru

In contemporary world every laboratory need to have modern and precise equipment. It is not possible to get real good results on handmade tool anymore, especially in nanotechnology area. That's why choosing and maintaining technological tools become more and more important. The second point, it needs to understand, that hardware should strongly linked with technological processes. In this article you could find examples of irreplaceable tools for crystal manufacturing.

In condition of miniaturization of all devices every lab should possess electron beam lithography. Crestec is good choice considering its minimal width line 5nm, accelerating voltage up to 130 kV and excellent quality of lacing. In last twenty years technological processes of ion implantation for manufacturing new semiconductor devices have been redoubled. For Russian market Ion Beam Services will be good choice because of low price and overall dimensions but with quite enough performance and great flexibility and reliability.

Oxford Instruments Plasma Technology (OIPT) provides a range of high performance, flexible tools to semiconductor and electronic processing customers in both R&D and production. Today the company offers equipment and technology for Plasma Etch and Deposition, Atomic Layer Deposition, Atomic Layer Etching, Ion Beam Etch and Deposition, Nanoscale Growth. With a 30-year history of high performance tools production and process development, OIPT has great experience in this area and good worldwide reputation. More than 3000 systems were installed around the world.

Oxford Instruments has a process library of over 6000 recipes developed in own process laboratories. Processes are backed by process guarantees for key parameters and repeatability such as rate and uniformity to ensure rapid start-up during installation. Oxford Instruments' process tools offer a powerful range of stand-alone and clusterable process modules with sample sizes up to 300 mm. Nanoscale features can be formed by growth techniques ('bottom up') and etching ('top down') with temperature range up to 1200°C. Nanoscale growth processes encompass: Nanotubes/nanowires, Nanoscale thin films, 2D materials.

And of course in every device it's no way to avoid metallization and passivation processes. PVD systems from Scientific Vacuum Systems (SVS) are the best choice for this. Also SVS possesses unique technology of conformal coating of 3D structures. Flexibility in configure and possibility of combining several PVD methods in one chamber make SVS pleasing for the users.

Examples of new generation of 2D materials manufacturing on OIPT tools:

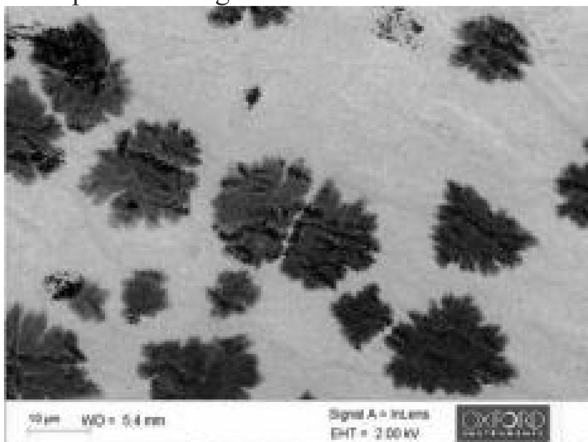

Graphene domains growing on copper substrates.

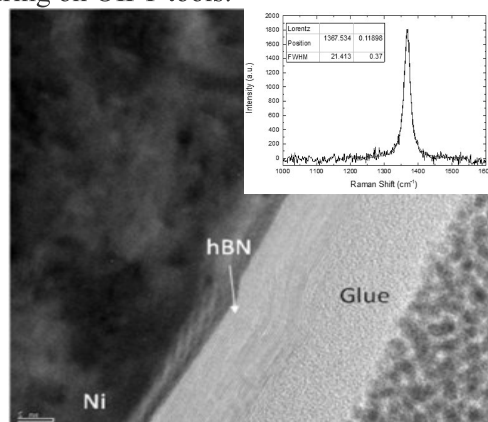

Thermal CVD hBN on Ni foils: TEM image and: Raman spectrum of hexagonal Boron Nitride.

Novelty in vacuum nanoelectronics

Yu.V. Gulyaev
Kotelnikov Institute of Radioengineering and Electronics of RAS, Moscow, Russia

Modeling and Characterization of Electron Devices for More-than-Moore Integrated Electronic Systems

C. Fiegna, S. Reggiani, A. Tallarico, E. Sangiorgi, M. Zanuccoli
DEI, ARCES University of Bologna and IUNET claudio.fiegna@unibo.

During the last decade the microelectronic industry devoted an increasing interest to “More than Moore” (MtM) technologies, “where added value to devices is provided by incorporating (new) functionalities” [1].

The present progress in both process technology and design is enhancing the compatibility between CMOS and non-digital technologies, enabling the fabrication of complex electronic systems integrated at the package (SiP) or even chip (SoC) level.

Functional diversification may be regarded as a complement of digital signal and data processing in a product. This includes the interaction with the outside world through an appropriate transduction (sensors and actuators) and the subsystem for powering the system and driving the integrated and external actuators. Heterogeneous integrated systems already represent the key driver for a wide variety of application fields, such as communication, automotive, environmental control, healthcare, security and entertainment.

Our presentation deals with characterization and modeling activities currently running at the University of Bologna in the frame of international collaborations, concerning advanced semiconductor devices for MtM applications and covering the following case studies:

- discrete and integrated power transistors based on silicon and GaN HEMTs compatible with silicon technology [2-5];
- high-efficiency, low-cost CMOS-compatible silicon solar cells based on advanced device architectures [6];
- design of micro-mirrors for micro-projectors, assisted by advanced optical simulation [7].

1. W. Arden, M. Brillouët, P. Cogez, M. Graef, B. Huizing, R. Mahnkopf. “More than Moore White Paper”, 2010 *www.itrs2.net/uploads/4/9/7/7/.../irc-itrs-mtm-v2_3.pd*
2. A.N. Tallarico, P. Magnone, G. Barletta, A. Magrì, E. Sangiorgi, C. Fiegna. *Influence of bias and temperature conditions on NBTI physical mechanisms in p-channel power U-MOSFETs*, Solid-State Elec., 2015.
3. A.N. Tallarico, S. Stoffels, P. Magnone, N. Posthuma, E. Sangiorgi, S. Decoutere, C. Fiegna. *Investigation of the p-GaN gate breakdown in forward-biased GaN-based power HEMTs*, IEEE Elec. Dev. Lett., 2017, **38**, pp. 99–102.
4. A.N. Tallarico, S. Stoffels, N. Posthuma, P. Magnone, D. Marcon, S. Decoutere, E. Sangiorgi, C. Fiegna. *PBTI in GaN-HEMTs With p-Type Gate: Role of the Aluminum Content on ΔVTH and Underlying Degradation Mechanisms*, IEEE Trans. Elec. Dev., 2018.
5. A.N.Tallarico, S. Reggiani, R. Depetro, A.M. Torti, G. Croce, E. Sangiorgi, C. Fiegna. *Hot-Carrier Degradation in Power LDMOS: Selective LOCOS-Versus STI-Based Architecture*, IEEE Journ. Elec. Dev. Soc., 2018, **6**, pp. 219–226.
6. M. Nicolai, M. Zanuccoli, F. Feldmann, M. Hermle, C. Fiegna. *Analysis of Silicon Solar Cells With Poly-Si/SiOx Carrier-Selective Base and Emitter Contacts*, IEEE Journ. Photovoltaics., 2018, **8**, pp. 103–109.
7. M. Zanuccoli, C. Fiegna, E. Cianci, C. Wiemer, A. Lamperti, G. Tallarida, L. Lamagna, S. Losa, S. Rossini, F. Vercesi, I. Semenikhin. *Simulation of micro-mirrors for optical MEMS*, in: 2017 International Conference on Simulation of Semiconductor Processes and Devices (SISPAD), 2017, pp. 81-84.

Electron Spin for Modern and Future Microelectronics

V. Sverdlov[1] and S. Selberherr[2]
1. Christian Doppler Laboratory for Nonvolatile Magnetoresistive Memory and Logic
2. Institute for Microelectronics TU Wien, Gusshausstr. 27-29, 1040 Vienna, Austria,
E-Mail: {Sverdlov|Selberherr}@iue.tuwien.ac.at

Continuous miniaturization of semiconductor devices' feature size remains the key driving force ensuring outstanding increase of performance of modern integrated circuits. While chips based on 5nm technology are already nearing production [1], the semiconductor industry is now focusing on a 3nm technology node. Although setting limits for scaling has proven to be a mere meaningless task in the past, it is obvious that the conventional transistor scaling is showing signs of saturation. To sustain the growing demand for high performance small area CPUs and high-capacity memory needed to handle an increasing information flow, an introduction of a disruptive technology employing new computing principles is anticipated. Most importantly, any emerging technology must be energy efficient, as a harmful active power penalty already prevents the clock frequency from being increased in CMOS circuits, while rapidly increasing leakages result in alarmingly growing stand-by power.

In contrast to charge, the electron spin has received less attention in microelectronics. The most significant employment of the spin degree in known devices is the magnetization direction of ferromagnetic media used to store the information in magnetic hard drives. The useful property of the magnetization to preserve its direction without energy source results in a non-volatile data storage. Introducing non-volatility is a promising way to reduce the stand-by power. Emerging spin-transfer torque (STT) magnetoresistive random access memory (MRAM) [2] is an electrically addressable non-volatile memory combining high speed, high endurance and long retention, and is suitable for replacing flash. The broad versatility of STT-MRAM with respect to the operation speed makes it a suitable candidate for embedded DRAM and low-level caches. In fact, all major foundries have announced the start of STT-MRAM production in 2018.

To further reduce the energy consumption, it is essential to replace high-level caches in modern hierarchical multi-level processor memory structures with a non-volatile memory. The development of an electrically addressable non-volatile memory combining sub-ns operation, high endurance, and long retention is thus essential for replacing SRAM. Among the newly discovered physical phenomena suitable for future MRAM generations is spin-orbit torque (SOT) assisted switching [3]. In these memory cells the free magnetic layer is grown on a material with a large spin Hall angle. By passing the current through the material, the SOT acting on the free layer is generated. As the switching current is injected in-plane along the heavy metal line, it results in a three-terminal configuration with the read and write paths separated.

SOT-MRAM is thus suitable for applications in caches. Recently, IMEC presented a technology to integrate SOT-MRAM on a 300mm CMOS wafer using CMOS compatible processes [4]. However, although the high switching current is not flowing through the tunnel barrier, the current and the current density are still high, and their reduction is the pressing issue in the field of SOT-MRAM development. In addition, inventing a switching scheme [5], which allows for deterministic switching of a perpendicularly magnetized structure without an external magnetic field, is urgently needed.

Regarding active power reduction, the availability of high-capacity non-volatile memory close to high-performance CMOS circuits allows exploring conceptually new logic-in-memory architectures. Employing the same non-volatile elements to store and to process the information paves the way for new low power and high-performance computing-in-memory paradigms [6]. Spin-based qubits also serve as building blocks for quantum logic gates to realize quantum algorithms [7] conceptually different from those based on the Boolean logic. Although it is not clear at the moment, which way microelectronics will develop, many challenges are lying ahead on the exciting journey to develop the computer architecture of the future.

1. N. Loubet et al., 2017 Symp. VLSI Technology and Circuits, p.T230.
2. D. Apalkov et al., Proc. IEEE **104**, 1796 (2016).
3. S.-W. Lee et al., Proc. IEEE **104**, 1831 (2016).
4. K. Garello et al., 2018 Symp. VLSI Technology and Circuits, C8-2.
5. A. Makarov et al., 2018 SISPAD, accepted.
6. V. Sverdlov et al., Microelectronics, Electronic Components and Materials **47**, p.195 (2017).
7. T.F. Watson et al., Nature **555**, p.633 (2018).

Ferroelectric properties of SOS and SOI pseudo-MOSFETs with HfO_2 interlayers

V.P. Popov[1], M.A. Ilnitskii[1], V.I. Vdovin[1], V.A. Antonov[1], A.V. Miakonkikh[2], K.V. Rudenko[2]

1. Institute of Semiconductor Physics of SB RAS, Novosibirsk, Russia, popov@isp.nsc.ru

2. Institute of Physics and Technology of RAS, Moscow, Russia, rudenko@ftian.ru

PEALD HfO_2 interlayers with the thickness of 10-40 nm were deposited on silicon donor wafers before direct bonding (DB) and a hydrogen transfer of <100> silicon layer on to reduce the defects and magnitude of their charge at the silicon-on-sapphire (SOS) and silicon-on-insulator (SOI) interfaces. We suggested using DB and solid state epitaxy (SSE) for the amorphous high-k oxide interlayer of hafnia between (100) Si and (0001) Al_2O_3 (c-axis of sapphire) during thermal annealing. The goal of this approach is obtaining a stable crystalline phase of HfO_2 and lower dangling bond density at the interface silicon / sapphire for SOS and thermally conductive ultrathin buried oxide (BOX) for SOI structure. Besides SSE process of hafnia can provide a ferroelectric phase with the impurities like silicon in a field effect transistor (FET) that is promising for memory applications [1]. Ferroelectric field effect transistors (FeFETs) with enhanced functionality allow new logic cell architectures for computing [2]. FeFETs and silicon-on-ferroelectric SOFFETs can change the logic cell functionality providing the two-gate threshold control via back gate for reconfigurable logic, carrying out memory and learning functions in integral circuits (IC) [3]. For the implementation of such devices we developed and studied the hafnium dioxide interlayers as the two dielectric gate in SOI and SOS pseudo-MOSFETs. The purpose of this work was to study the opportunity and properties of a hafnium oxide interlayer with possible ferroelectric phases in SOI and SOS FeFETs and using structural and electrical measurements.

The formation of a multi-crystalline HfO_2 film during SSE, containing the ferroelectric phase OII (*$Pmn2_1$*) at a high-temperature annealing (> 800°C), was experimentally observed by HREM in SOS structures on c-sapphire substrates, but not in SOI structure for transfer on Si substrate. SOS and SOI pseudo-MOS transistors demonstrate standard drain-gate characteristics with the same charge carrier mobility as in bulk silicon and a small positive charge ($\leq 1.2x10^{12}$ cm^{-2}). The clear evidences of traps and ferroelectric polarization in SOS with hafnia interlayers were obtained by the SOS pseudo-MOSFET I-V analysis with $D_{it,n,p} \leq 1 \cdot 0^{12} cm^{-2}$ and $Q_P = 0.1$ $\mu C \cdot cm^{-2}$ at $E_{Pr} = 3 \cdot 10^4$ $V \cdot cm^{-1}$. SOS pseudo-MOSFETs show the highly stable ferroelectric hysteresis after a high temperature annealing ~1000°C with memory window ΔV_G ~700 V. Large tetragonal distortions can provide a stabilization of the OII ($Pmn2_1$) HfO_2 phase.

The ferroelectric properties in the case of SOS pseudo-MOSFETs with hafnia show a new way for constructing highly stressed heterostructures and FeFET transistors promising for the embedded memory formation and negative capacitance (NC) NCFET with subthreshold swing (SS) below thermodynamic limit SS = 60 mV/dec. They extend the functionality of IC. An absence of hysteresis in SOI pseudo-MOSFETs proves that the OII phase is stabilized mainly by a high compressive stress and it is responsible for the hysteresis in the case of SOS pseudo-MOSFETs opposite to the SOI-structure. It was suggested that using $HfZrO_2$ or ALD hafnia-alumina multilayers as a buried oxide in SOI structures will be useful in decreasing back biasing voltages to sub-volt ranges instead of kilovolts in the case of SOS-heterostructures and obtaining ferroelectric hysteresis in the BOX. SOI- and SOS-structures with hafnia interlayers are the promising substrates for a new IC generation with the multifunctional transistors like FeFET, SOFFET, ISFET and similar ones being of demand in Artificial Intelligence applications.

1. T.S. Böscke, St. Teichert, D. Bräuhaus, J. Müller, U. Schröder, U. Böttger, T. Mikolajick. “Phase transitions in ferroelectric silicon doped hafnium oxide”. Appl. Phys. Lett., **99**, 112904, 2011.
2. H. Mulaosmanovic et al. "Switching kinetics in nanoscale hafnium oxide based ferroelectric field-effect transistors", ACS Appl. Mater. Interfaces, **9**, pp. 3792-3798, 2017.
3. E. Ashenafi, A. Es-Sakhi, M.H. Chowdhury. Nodal thermal analysis for multi-V_T SOFFET based subthreshold circuits". In Proc. of 2017 IEEE International Symposium on Circuits and Systems (ISCAS), Baltimore, MD, USA, DOI: 10.1109/ISCAS.2017.8050826.

Quantum Technologies: State of Art and Perspectives

S. Kulik[1,2]

1. Faculty of Physics, M.V. Lomonosov Moscow State University, 119991, Moscow, Russia
2. Quantum Technologies Centre, M.V. Lomonosov Moscow State University, 119991, Moscow, Russia
E-mail: *sergei.kulik@physics.msu.ru*

The talk reports the current state and prospects of the interdisciplinary field of knowledge - Quantum Information Processing and Computation (QIPC).

Basically, QIPC includes three large sections: quantum computation, quantum communications, and quantum information science.

The report will consider general and some special issues related to the theoretical and experimental aspects of QIPC mainly related to quantum computation, quantum communications.

The focus is on the main technologies of QIPC developed in the world, and especially in the Russian Federation, which potentially lead or have already led to the creation in the near future of quantum simulators and quantum communication systems.

In the field of quantum computation/simulators, these are technologies that exploit neutral atoms and ions in traps as working physical systems, superconducting systems, impurity structures, and linear optical systems.

In the field of quantum communication - is the creation of a global network based on fiber-optic, atmospheric and space channels.

Separately, the main problems of the implementation of certain nodes/elements of the systems of quantum simulators and quantum coupling are considered.

In the second part of the talk I will present an overview of the experimental results in the field of quantum computation and quantum coupling, which are held at the Faculty of Physics, within the framework of the Center for Quantum Technologies of the Moscow State University. Prospects for the development of these two areas will be considered in the context of the rapid growth of interest in the world in quantum technologies. On the example of two physical systems - photonic chips and neutral atoms in optical traps, the principles of quantum computation and the main stages in the construction of quantum computers will be presented.

In the final part, three particular projects will be presented. These large complex projects are carried out at the MSU Faculty of Physics together with number of partners:

- Optical Quantum Simulators;
- Development and creation of high-speed quantum encoders;
- "Quantum telephone".

Optimizing heralded single-photon sources based on spontaneous four-wave mixing in a system of coupled microresonators

I.N. Chuprina[1,2], N.S. Perminov[1,3], A.A. Kalachev[1,2]

1. Zavoisky Physical-Technical Institute, Kazan Scientific Center, Kazan, Russia
2. Institute of Physics, Kazan Federal University, Kazan, Russia
3. Kazan Quantum Center, Kazan National Research Technical University, Kazan, Russia

Optimal design for a heralded single-photon source based on spontaneous four-wave mixing in a system of coupled ring microresonators is developed. It shown that the optimal coupling parameters, in combination with the optimal spectral width of the pump pulse, give rise to the highest purity of the heralded photons for a given pump linewidth [1].

1. I.N. Chuprina, et al. "Generating pure single-photon states via spontaneous four-wave mixing in a system of coupled microresonators". Laser Physics Letters (accepted).

Decoherence in a one-dimensional system of interacting nuclear spins: experimental and theoretical investigations

G. Bochkin, E. Fel'dman, S. Vasil'ev
Institute of Problems of Chemical Physics of Russian Academy of Sciences, Chernogolovka, Moscow region, 142432, Russia, efeldman@icp.ac.ru

Decoherence of quantum states is one of the main problems in the way of creating scaled many-qubit quantum computers [1]. The research performed shows [2] that clusters created for quantum computation get more fragile and are destroyed faster with increasing number of qubits in them due to decoherence. In other words, life times of such clusters are getting so small with increasing number of qubits that those clusters cannot be used as quantum registers.

At the present time, the potential of NMR methods in solids is not fully realized for solving problems of quantum informatics. In particular, multiple quantum (MQ) NMR [3] allows us to investigate decoherence of clusters of correlated spins since MQ NMR not only creates many-qubit coherent spin clusters but also allows to study their relaxation under the action of a correlated spin reservoir. The investigations using MQ NMR methods in three-dimensional systems [2] showed that the rate of decoherence in many-qubit coherent clusters slowly increases with the number of spins. This is promising for creation of universal quantum devices. One-dimensional spin systems open new possibilities for both theoretical and experimental investigation of decoherence with MQ NMR methods. The point is that a consistent quantum-mechanical theory of MQ NMR dynamics exists only for one-dimensional systems [4]. It is also important that theory of dipolar relaxation of MQ NMR coherences is also developed for one-dimensional systems [5]. In our work the experimental study of MQ NMR dynamics and relaxation of one-dimensional systems is performed in a single crystal of calcium fluorapatite $Ca_5(PO_4)_3F$.

The growth of the coherent correlated clusters occurs on the preparation period of the MQ NMR experiment [3]. Such clusters are responsible for the emergence of MQ NMR coherences and their dipolar relaxation occurs on the evolution period [3] which starts immediately after the preparation period. We suppose that the dipolar relaxation of MQ NMR coherences can be considered as a simple model of decoherence in the correlated spin cluster [6].

Using the theory [5] we can obtain the dependence of the dipolar relaxation time on the duration of the preparation period [6]. We developed a semi-phenomenological theory allowing us to obtain the dependence of the number of correlated spins on the duration of the preparation period [6]. As a result, we found the dependence of the decoherence time (the relaxation time) on the number of the correlated spins. We showed experimentally and theoretically that the dipolar relaxation (decoherence) time decreases very slowly with the growth of the number of spins in many-qubit correlated clusters. We found also that there is a lower bound for the decoherence time in the considered model. Thus, we showed that the problem of decoherence can be overcome in the model under consideration.

The work is supported by the Russian Foundation for Basic Research (Grant № 16-03-00056) and the Program of the Presidium of RAS No 5 "ESR, time-dependent electron effects and spin technologies".

1. M.A. Nielsen, I.L. Chuang. *Quantum Computation and Quantum Information.* Cambridge University Press, Cambridge. 2000.
2. H.G. Krojanski, D. Suter. Scaling of decoherence in wide NMR quantum registers. Phys. Rev. Lett. **93**, 090501 (2004).
3. J. Baum, M. Munowitz, A.N. Garroway, A. Pines. Multiple-quantum dynamics in solid state NMR. J. Chem. Phys. **83**, 2015 (1985).
4. S.I. Doronin, I.I. Maksimov, E.B. Fel'dman. Multiple quantum dynamics of one-dimensional nuclear spin systems in solids. JETP **91**, 597-609 (2000).
5. G.A. Bochkin, E.B. Fel'dman, S.G. Vasil'ev, V.I. Volkov. Dipolar relaxation of multiple quantum NMR coherences in one-dimensional systems. Chem. Phys. Lett. **680**, 56-60 (2017).
6. G.A. Bochkin, E.B. Fel'dman, S.G. Vasil'ev, V.I. Volkov. Dipolar relaxation of multiple quantum NMR coherences as a model of decoherence of many-qubit coherent clusters. Appl. Magn. Reson. **49**, 25-34 (2018).

Three-body Förster resonances in cold Rydberg atoms and their applications in quantum information

D.B. Tretyakov[1,2], I.I. Beterov[1,2], E.A. Yakshina[1,2], V.M. Entin[1,2], I.I. Ryabtsev[1,2], P. Cheinet[3], P. Pillet[3]

1. Institute of Semiconductor Physics, SB RAS, Novosibirsk, Russia, E-mail address: dtret@isp.nsc.ru

2. Novosibirsk State University, Novosibirsk, Russia

3. Laboratoire Aime Cotton, CNRS, Univ. Paris-Sud, ENS Paris-Saclay, Orsay, France

Strong long-range interactions between highly excited Rydberg atoms form the basis for quantum information processing with neutral trapped atoms [1]. For example, two-qubit gates, which provide quantum entanglement of two qubits, can be implemented using a temporary excitation of two ground-state atoms to highly-excited Rydberg states exhibiting strong long-range interactions. Up to date, an experimental Bell state fidelity of 73% has been achieved for two-qubit neutral Cs atom experiment [2].

Besides two-qubit quantum gates, the implementation of universal three-qubit Toffoli gate is of great interest. This gate is important for faster realizations of some quantum algorithms, such as the Shor's algorithm [3]. The Toffoli gate has been demonstrated with different quantum objects. For example the experimental fidelity of 71% and 1.5 ms duration of the gate has been achieved with $^{40}Ca^{+}$ ions [4].

In this report we present a scheme of a fast Toffoli gate for ultracold neutral Rb atoms [5]. This gate is shown to be much faster than in Ref. [4] and can provide approximately 3 μs duration and 96.8% fidelity. In our gate we use the three-body Förster resonance in ultracold Rydberg atoms. Such resonances were first predicted and observed in a large ensemble of cold Cs Rydberg atoms [6] and then investigated by us recently for a few cold Rb Rydberg atoms in a magneto-optical trap [7].

Earlier we have observed for the first time a Stark-tuned Förster resonance between two cold Rb Rydberg atoms confined to a small laser excitation volume [8]. Due to resonant dipole-dipole interaction, an energy transfer between two Rydberg atoms occurs. In the case of three interacting Rydberg atoms, one of the atoms carries away an energy excess preventing the two-body resonance, leading thus to a Borromean type of Förster energy transfer [6]. As the observed three-body resonances appear at the different dc electric field with respect to the two-body resonance, they represents an effective three-body operator, which can be used to directly control the three-body interactions in quantum simulations and three-qubit quantum gates with Rydberg atoms. The results of our experimental and theoretical studies of three-body Förster resonances at long-range interactions of three cold Rydberg atoms are also presented [7, 9].

This work was supported by the Russian Science Foundation Grant No 16-12-0083 in the part of the numerical model and Grant No 18-12-00313 in the part of the analytical calculations, the RFBR Grant No 17-02-00987 in the part of simulation of the off-resonant Rydberg interactions and Grant No 16-02-00383 in part of simulation of coherent three-body Forster resonances, the Novosibirsk State University, the public Grant CYRAQS from Labex PALM (ANR-10-LABX-0039) and the EU H2020 FET Proactive project RySQ (Grant No. 640378).

1. I.I. Ryabtsev et al. "Spectroscopy of cold rubidium Rydberg atoms for applications in quantum information". Physics – Uspekhi, **59**, 196, 2016.
2. K.M. Maller et al. Phys. Rev. A, **92**, 022336, 2015.
3. P. Shor. SIAM Review, **41**, 303, 1999.
4. R. Blatt et al. Phys. Rev. Lett., **102**, 040501, 2009.
5. I.I. Beterov et al. "Fast three-qubit Toffoli quantum gate based on the Borromean three-body Förster resonances in Rydberg atoms", submitted in PRA.
6. R. Faoro et al. Nature Commun., **6**, 8173, 2015.
7. D.B. Tretyakov et al. "Observation of the Borromean Three-Body Förster Resonances for Three Interacting Rb Rydberg Atoms". Phys. Rev. Lett., **119**, 173402, 2017.
8. I.I. Ryabtsev et al. "Observation of the Stark-Tuned Förster Resonance between Two Rydberg Atoms". Phys. Rev. Lett., **104**, 073003, 2010.
9. I.I. Ryabtsev et al. "Coherence of the Borromean three-body Förster resonances in Rydberg atoms". arXiv: 1807.09125 (2018); submitted in PRA.

2D Ferromagnetism and Charge Transport in Silicene and Graphene

D.V. Averyanov, A.M. Tokmachev, O.E. Parfenov, I.A. Karateev,
I.S. Sokolov, A.N. Taldenkov, and V.G. Storchak
National Research Center "Kurchatov Institute", Kurchatov Sq. 1, Moscow 123182, Russia
E-mail: mussr@triumf.ca

The appeal of ultra-compact spintronics drives intense research on magnetism in low-dimensional materials. Recent years have witnessed remarkable progress in engineering two-dimensional (2D) magnetism via defects, edges, adatoms and magnetic proximity. However, intrinsic 2D ferromagnetism remained elusive until recent discovery of magneto-optical response in Cr-based layers, stimulating the search for novel 2D magnets with tunable properties. We employ a bottom-up approach to produce layered structures of silicene (a Si counterpart of graphene) functionalized by rare-earth atoms, ranging from the bulk down to one monolayer (Fig. 1). We track the evolution from the antiferromagnetism of the bulk to intrinsic 2D ferromagnetism of ultrathin layers of $GdSi_2$ and $EuSi_2$ [1]. Remarkably, the charge transport is found to be layer-dependent once silicene structures are scaled to a few-monolayers limit: it evolves from a Kondo-like trend to an insulating behavior once a gap opens up in its charge excitation spectrum. The discovery of a class of robust 2D magnets, compatible with the mature Si technology, is instrumental for engineering new spintronic devices.

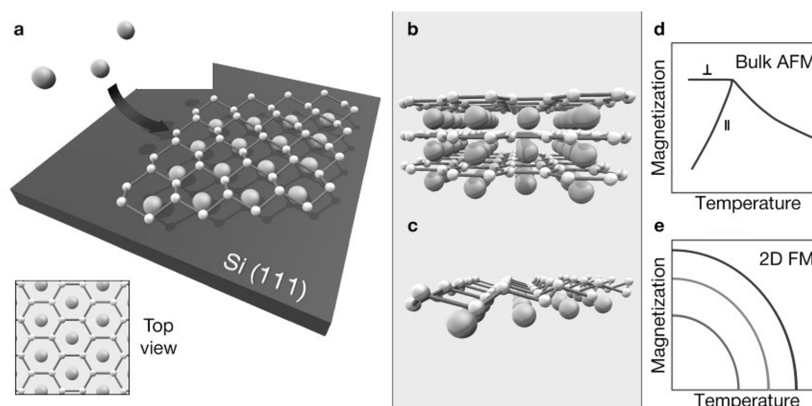

Fig.1. **a** MBE synthesis of MSi_2 silicene materials by directing metal atoms (Gd or Eu) at the Si(111) substrate leading to formation of **b** a bulk (multilayer) material or **c** a monolayer. The AFM state of the bulk **d** transforms into 2D ferromagnetism with its characteristic dependence of the transition temperature on magnetic fields **e**.

Addition of magnetism to spectacular properties of graphene may also lead to novel spintronics. A significant progress is made in defect-induced magnetism in graphene - selective elimination of p_z orbitals (by vacancies or adatoms) tailors graphene magnetism. Proximity to a magnetic insulator is a less invasive way, which is being actively explored now. Integration of graphene with the ferromagnetic semiconductor EuO has much to offer, particularly in terms of proximity-induced spin−orbit interactions. We synthesize films of EuO on graphene using reactive molecular beam epitaxy. Their quality is attested by electron and X-ray diffraction, cross-sectional electron microscopy, and Raman and magnetization measurements. Studies of electron transport reveal a magnetic transition at $T_C \approx 220$ K, well above the Curie temperature 69 K of EuO. Up to T_C, the dependence $R_{xy}(B)$ is strongly nonlinear, suggesting the presence of the anomalous Hall effect. The results justify the use of the EuO/graphene system in spintronics [2].

We acknowledge support from RSF (14-19-00662) and RFBR (16-29-03027 and 17-07-00170).

1. A.M. Tokmachev, D.V. Averyanov, O.E. Parfenov, A.N. Taldenkov, I.A. Karateev, I.S. Sokolov, O.A. Kondratev, and V.G. Storchak, "Emerging two-dimensional ferromagnetism in silicene materials", Nature Communications **9**, 1672-9 (2018).
2. D.V. Averyanov, I.S. Sokolov, A.M. Tokmachev, O.E. Parfenov, I.A. Karateev, A.N. Taldenkov, and V.G. Storchak, "High-temperature magnetism in graphene induced by proximity to EuO", ACS Applied Materials & Interfaces **10**, 20767-20774 (2018).

Simulation of Graphene Field-Effect Transistors and Resonant Tunneling Diodes Based on Carbon Nanomaterials

I. Abramov, V. Labunov, N. Kolomejtseva, I. Romanova, I. Shcherbakova
Belarusian State University of Informatics and Radioelectronics, Minsk, Belarus, E-mail: nanodev@bsuir.edu.by

The development of field-effect transistors (GFETs), resonant-tunneling diodes (RTDs) and other device structures on the basis of graphene is one of the important tasks for producing a new element base for micro- and nanoelectronics.
The report presents the simulation results of the GFET based on monolayer graphene in various operating modes, as well as the RTD based on bilayer graphene and carbon nanotubes.
The main model of GFET [1, 2] was developed on the basis of the quantum drift-diffusion model. It is a combination of electrical and physical models. According to the model the electrostatic potential of the channel is calculated self-consistently. The report describes the modification of the model for the case of GFET transfer characteristics calculation. The optimization method of dichotomy is used for this purpose. A satisfactory agreement with the experimental data not only of the output, but also of the transfer characteristics of a single- and dual-gate GFET was obtained with the use of the modified model. In the report, the influence of various factors on the characteristics of the investigated GFET was analyzed with the use of the model.
The wave function formalism was applied in the development of numerical models of resonant-tunneling device structures based on graphene and carbon nanotubes. It was also taken into account that RTD includes not only nanostructures (active regions) but also extended (passive) regions. Combined self-consistent models of RTD based on graphene and carbon nanotubes [3, 4] were developed in accordance with quantum-mechanical and semiclassical approaches. The influence of various factors (height and shape of potential barriers, contact areas extension) on the characteristics of the RTD based on bilayer graphene was investigated with the use of the developed models. The IV-characteristics were calculated for RTD based on carbon nanotubes with different chiral indices and geometric dimensions.
The programs realizing the models of GFET and graphene-based RTD were included in the nanoelectronic devices simulation system developed at the BSUIR since 1995 [5,6].

1. I.I. Abramov, N.V. Kolomejtseva, V.A. Labunov, I.A. Romanova. "Combined models of graphene field-effect transistors with the single and dual gates". 27th International Crimean Conference "Microwave & Telecommunication Technology" (CriMiCo'2017), Sevastopol: Weber Publishing, **4**, pp. 1076-1083, 2017. (in Russian).
2. I.I. Abramov, N.V. Kolomejtseva, V.A. Labunov, I.A. Romanova. "Simulation of graphene field-effect transistors with the single and dual gates". J. of Nano- and Microsystem Technique, no. 12, pp. 714-721, 2017.
3. I.I. Abramov, N.V. Kolomejtseva, V.A. Labunov, I.A. Romanova. "Simulation of graphene resonant tunneling diodes on the substrates of various types". J. of Nano- and Microsystem Technique, no 11, pp. 3-10, 2015.
4. I.I. Abramov, N.V. Kolomejtseva, V.A. Labunov, I.A. Romanova. "Simulation of resonant tunneling devices based on carbon nanomaterials". Nanotehnologii: razrabotka, primenenie — XXI vek, **3**, pp. 3–11, 2017. (in Russian).
5. I.I. Abramov, I.A. Goncharenko, S.A. Ignatenko, A.V. Korolev, E.G. Novik, A.I. Rogachev. "NANODEV: A nanoelectronic-device simulation software system". Russian Microelectronics, **32**, N 2, pp. 97-104, 2003.
6. I.I. Abramov, A.L. Baranoff, I.A. Goncharenko, N.V. Kolomejtseva, Y.L. Bely, I.Y. Shcherbakova. "A nanoelectronic device simulation software system NANODEV: New opportunities". Proc. of SPIE, **7521**, edited by Kamil A. Valiev, Alexander A. Orlikovsky, pp. 75211E1-1-11, 2010.

Theoretical and experimental graphene's electron transparency

E. Il'ichev[1], V. Khaustov[1], A. Kuleshov[1], D. Migunov[1], R. Nabiev[1], G. Petrukhin[1,2], E. Teverovskaya[1], G. Rychkov[1]

1. National Research University of Electronic Technology, Zelenograd-Moscow, Russia, start_94@mail.ru
2. LLC "CNEL Devices", Zelenograd-Moscow, Russia, cneldevices@gmail.com

Due to its electronic and mechanical properties graphene attracts many developers of electronic devices. Especially the unique properties of graphene membranes as micro- and nanoresonators should be noted [1]. The property of electronic transparency of the graphene membrane becomes essential. That has been discussed in a number of papers [2, 3, 4] the results of which are rather contradictory. At energies of 1-100 eV to describe the dynamics of reflection and passage of an electron through graphene it is necessary to use the time-dependent Schrödinger equation. In work [5] calculations based on quantum mechanics for energies of 20-200 eV were carried out. The results obtained for 20-40 eV showed sharp transparency fluctuations which are strange and might be caused by insufficient accuracy in the approximation of graphene by a potential field. Therefore even with normal incidence of the electron the calculations are difficult to perform. Taking into account the secondary fall of the reflected electron at an arbitrary angle leads to a complication of quantum mechanical calculations because of the resonant phenomena [6].

In this paper the electron incident on a graphene was considered as elastically scattered particle. The scattering angle of electron depended on electron energy (E) and impact parameter (b) and was calculated in the centrally symmetric field of attractive forces using Thomas-Fermi screening potential. The angle of electron's trajectory deflection determined cases of transparency (T) or reflection (R). The T and R coefficients were determined as the ratio of the area which is limited by the b corresponding to the case of passage or reflection to the area of one sixth of the graphene hexagon (area per one carbon atom).

In the real case the electron reflected from graphene would return back by the decelerating field and it would have the probability to pass through graphene again.

In this work the photoemission experiment on electron transparency was also presented. The electron source was a photocathode irradiated by a vacuum ultraviolet (VUV) with a wavelength of 185-225 nm. Passing through the anode grid and graphene membranes the VUV stream falls on the surface of the photocathode and generates photoelectrons at the point of incidence. Photoelectrons in a vacuum of ~ 10^{-7} Torr move toward graphene membranes under the electric field created by voltage sources. Those electrons might be reflected or they might pass throw graphene.

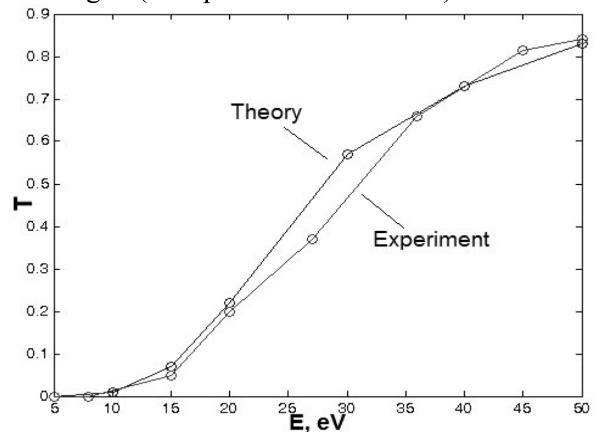

Fig. 1. Theoretical and experimental transparency

We compared theoretical and experimental data for the sample from Graphenea Inc (Fig. 1). The theoretical results showed practically identical dependence of the transparency coefficient to experimental results in the range 10-50 eV.

1. C. Chen, S. Lee, W. Deshpande, et al. "Graphene mechanical oscillators with tunable frequency". Nature nanotechnology, **8**, pp. 923-927, 2013

2. C. Li, M.T. Cole, W. Lei et al. " Highly Electron Transparent Graphene for Field Emission Triode Gates". Adv. Funct. Mater., **24**, pp. 1218-1227, 2014.

3. E.A. Il'ichev et al. "The use of graphene in vacuum micro-and nanoelectronics". Technical Physics Letters, **39**, pp. 808-810, 2013.

4. G. Hassink, R. Wanke, I. Rastega, et al. "Transparency of graphene for low-energy electrons measured in a vacuum-triode setup". APL Materials, **3**, p. 076106, 2015.

5. J.-A. Yan, J.A. Driscoll, B.K. Wyatt, et al. "Time-domain simulation of electron diffraction in crystals". Phys. Rev., **84**, p. 224117, 2011.

6. F. Wicki, J.-N. Longchamp, et al. " Mapping unoccupied electronic states of freestanding graphene by angle-resolved low-energy electron transmission ". Phys. Rev., **94**, p. 075424, 2016.

Planar ring-shaped matrix field emission nanostructure based on multigraphene/SiC

I. Jityaev, A. Svetlichnyi, O. Ageev
Southern Federal University, Institute of Nanotechnologies, Electronics and Equipment Engineering, Taganrog, Russia, izhityaev@sfedu.ru

Improving the performance of the element base by miniaturization approaches the physical and technological limits. A qualitatively different approach is required to solve this problem. One of the possible solutions is the use of a nanosized field emission element base. It is estimated that it will allow switching to the terahertz frequency range. At the same time, field emission elements are characterized by increased resistance to X-ray and electromagnetic radiation, low noise level, high current-voltage characteristics steepness.

The emitter and substrate material and the design of the emission cell have a great influence on the characteristics of the field emission elements. Materials based on graphene are promising for field emission application due to their unique electrophysical properties [1, 2]. Multigraphene field emission structures were studied in this work. Multigraphene was obtained by high-temperature destruction of the silicon carbide in vacuum and consisted of about ten graphene layers. This method makes it possible to obtain uniform films on the entire surface of the substrate and to vary the thickness of the multigraphene film by the parameters of the technological process. Multigraphene film was characterized by Raman spectroscopy.

Multigraphene films on the silicon carbide surface are excellent material for planar edge field emission structures [3]. The nanometer film thickness contributes to the high form-factor. The interelectrode distance is an important parameter of the field emission cell, which affects the form-factor. Thus, planar field emission cells with a nanoscale interelectrode distance and an emitter of the tip shape were fabricated using focused ion beams. This made it possible to form a multigraphene cathode and an anode in one operation and contributed to threshold voltages of less than 1 V.

The geometric parameters of the experimental sample of a nanoscale field emission cell formed the basis for the model parameters with 3 and 5 planar-type tips. Simulation was performed to evaluate the efficiency of the field-emission cell design by finding the electric field strength at the emitter tops. The electric field strength is an important parameter of field emission structure, as field emission appears when an external electric field applied. Simulation of the multi-emitter structure showed that the difference in the values of the electric field strength is observed at the emitter tops. The electric field strength increases in the direction from the central to the outermost emitter. As a result, the design of the field emission cell with an anode in the form of a disk and a surrounding cathode in the form of a ring containing uniformly spaced tips directed inward has been proposed. This positioning of the tips in matrix emitter made it possible to eliminate the screening effect, obtaining uniform electric field strength at their tops, and to increase the density of the emission current, in proportion to the number of tips. Thus, the set of proposed constructive and technological solutions will allow forming nanoscale field emission structures characterized by high compactness, low threshold voltages, high current density, stability of emission characteristics and durability.

The equipment of the Collective Usage Center “Nanotechnologies” and the Research and Educational Center "Nanotechnologies" of Southern Federal University was used for this study. This work was funded by Internal grant of the Southern Federal University No. VnGr-07/2017-26.

1. G. Eda, H.E. Unalan, N. Rupesinghe, G.A.J. Amaratunga, and M. Chhowalla. "Field emission from graphene based composite thin films". Appl. Phys. Lett. **93**, pp. 233502, 2008.
2. W. Wang, X. Qin, N. Xu, and Z. Li. "Field electron emission characteristic of graphene". J. Appl. Phys. **109**, pp. 044304, 2011.
3. I.L. Jityaev, O.A. Ageev, A.M. Svetlichnyi, A.S. Kolomiytsev, and O.B. Spiridonov. "Planar nanosized field emission cathodes on the basis of graphene/semi-insulating silicon carbide fabricated by focused ion beam". J. Phys.: Conf. Ser. **741**, 012011 (2016).

O1-05

Laser reduction of graphene oxide thin films for nanoelectronic application

I.A. Komarov[1], N.S. Struchkov[2], D.D. Levin[2], E.E. Danelyan[1], M.A. Orlov[1], S.N. Sherbin[1], V.V. Bogachev[1], N.K. Lagodenko[1]

1. Bauman Moscow State Technical University, Moscow, Russia, ikomarov@emtc.ru.

2. National Research University of Electronic Technology, Moscow, Russia, skaldd@yandex.ru

Management of material properties is one of the most important goals in todays' science. One of the most interesting and promising class of material for wide range of applications from flexible electronic to new energy storage and harvesting units and sensing devices is graphene derivatives [1]. This class of materials include graphene oxide, reduced graphene oxide, graphene nanoribbons etc. In our work we paid attention to graphene oxide and its reduction due to possibility of easy formation of relatively large area but thin films and opportunity to vary reduction level of this film that makes its attractive at first for sensor applications [2].

We designed a new device and methodic for aerosol deposition and showed thin and uniform film formation with subsequent laser reduction of the film. Graphene oxide film was made by aerosol deposition of graphene oxide solution with 50 μg/ml under low spray flow. Substrate was heated up to 80 °C during deposition process. We also made graphene oxide films by spin-coating on Si and PET substrates with 100 mm^2 area. With these techniques we made graphene oxide films with thickness from 10 to 100 nm. Both approaches allowed us to make uniform low roughness graphene oxide films on different substrates (fig.1).

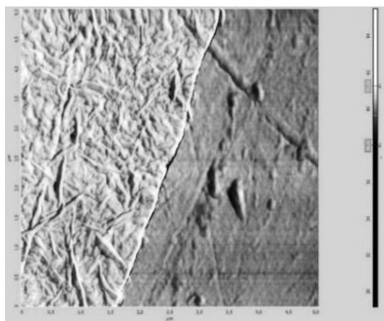

Fig. 1. AFM image of 40 nm graphene oxide film on PEN substrate.

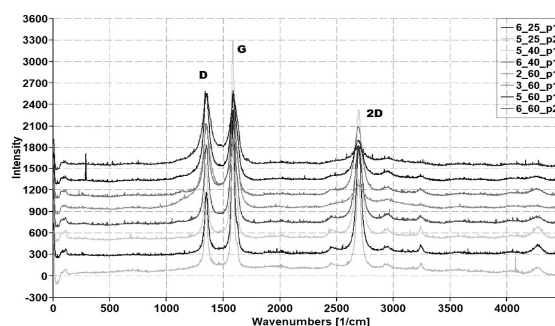

Fig. 2. Raman spectra of graphene oxide films with different reduction level.

By varying of reduction parameters (laser power and movement speed) we achieved different reduction level (fig.2). We observe reduction level from poor (low I_{2D}/I_G) to high (large I_{2D}/I_G) similar to represent in [3] and thus we can, for example, form basis for sensing platforms with different sensing substances or highly conductive flexible coatings.

In this work we developed new methodic and device for aerosol deposition, made low thickness uniform graphene oxide films. We also showed possibility of reduction with manageable reduction rate that is important for different electronic and other application.

This work is done with the financial support of the Ministry of Education and Sciences of Russian Federation, grant number 14.574.21.0184 (grant unique I.D. RFMEFI57417X0184).

1. R.K. Singh, R. Kumar, D.P. Singh. "Graphene oxide: strategies for synthesis, reduction and frontier applications". RSC Adv., **6**, pp. 64993–65011, 2016.
2. M.-S. Chae et al. "Enhancing surface functionality of reduced graphene oxide biosensors by oxygen plasma treatment for Alzheimer's disease diagnosis". Biosensors and Bioelectronics, **92**, pp. 610-617, 2017.
3. M. Kasischke et al. "Simultaneous nanopatterning and reduction of graphene oxide by femtosecond laser pulses", Applied Surface Science, **445**, pp. 197-203, 2018.

Silicon oxides and silicon nitrides: structure, properties and applications in memristors

V.A. Volodin[1,2], G.N. Kamaev[1], V.N. Kruchinin[1], V.A. Gritsenko[1,2,3]
1. A.V. Rzhanov Institute of Semiconductor Physics, Siberian Division of the Russian Academy of Sciences, Lavrenteva 13, Novosibirsk 630090, Russia, E-mail: volodin@isp.nsc.ru.
2. Novosibirsk State University, Pirogova street, 2, 630090, Novosibirsk, Russia.
3. Novosibirsk State Technical University, K. Marks ave., 20, 630073, Novosibirsk, Russia.

The capacity of memory matrices grows exponentially, but in many approaches the degree of integration of memory elements already reaches physical limits, which stimulates research into the development of new physical principles and new materials for memory elements. Memristors are very promising elements of memory. The memristors are the basis for high-speed, non-volatile, radiation-resistant flash memory matrices of the new generation.

In nonstoichiometric amorphous silicon oxides SiO_x ($x<2$) and silicon nitrides SiN_x ($x<4/3$), excess silicon can be distributed randomly in the atomic network or segregated to clusters. In the first case, there is some probability of formation of the tetrahedral Si–SiO_3(or N_3), Si–Si_2O_2(or N_2), Si–Si_3O(or N), and Si–Si_4 groups. This situation is described by so called random bonding (RB) model [1]. In the latter case, the nonstoichiometric silicon oxide (or silicon nitride) film presents a mixture of amorphous SiO_2 (or Si_3N_4) and amorphous Si. This situation is described by the random mixture (RM) model [1]. The actual structure of the SiO_x or SiN_x films cannot be rigorously described by one of these two models; as follows from some experimental data, the structure can be treated in the context of a combination of these two approaches [1]. The films contain various tetrahedral groups as well as separated phases, and the structure of the films heavily depends on the preparation procedure [1]. Moreover, it was recently investigated, that even nearly stoichiometric SiN_x ($x\approx4/3$) and silica there are local Si-Si bonds, appearing as substitution defects [2]. These defects are traps for electrons and holes and play significant role in conductivity of SiO_x and SiN_x films.

The SiO_x films of various stoichiometry were prepared using evaporation of Si, SiO and SiO_2 targets and deposition in high vacuum. The SiN_x ($0.5<x\leq4/3$) films were deposited using chemical vapor deposition and plasma enhanced chemical vapor deposition (PECVD).

Raman scattering spectroscopy, photoluminescence spectroscopy, visible and infrared (IR) absorbance spectroscopy and spectral ellipsometry and electro-physical methods were used for studies of the films.

According to Raman spectroscopy data, the as-deposited SiN_x ($x\leq1.1$) contain amorphous Si clusters, high temperature annealings lead to crystallization of the clusters and forming of Si nanocrystals in such films. As for SiO_x films, amorphous Si clusters were observed in as-deposited films with $x\leq1.7$. These data were confirmed from analysis of ellipsometry data with the use of Bruggemann model. Furnace and pulse laser annealings lead to growth of amorphous Si clusters and to its crystallization.

The red-shift of optical gap was observed for SiO_x and SiN_x films with reducing of stoichiometry parameter x. The hydrogen bonds were observed in PECVD as-deposited from analysis of IR-absorbance spectra. Annealing lead to evaporation of hydrogen from N-H bonds, but absorption peaks related to Si-H bonds were still registered in nearly stoichiometric SiN_x films even after 1 hour annealing at 1100 ^oC, as it was observed earlier [3].

The current-voltage (I-V) characteristics of the films were studied. Effects of switching from high resistance state (HRS) to low resistance state (LRS) were observed for SiO_x based films. Stability and reproducibility of switching and HRS\LRS ratio are determined by the ratio of Si, SiO and SiO_2 targets during deposition. These switching can be used in memristors.

Acknowledgements: The work was supported by Russian Science Foundation, project No. 18-49-08001.

1. V.A. Gritsenko. "Atomic structure of the amorphous nonstoichiometric silicon oxides and nitrides". Phys. Usp., **51**, pp. 699-708, 2008.
2. V.A. Volodin, V.A. Gritsenko, A. Chin. "Local Oscillations of Silicon–Silicon Bonds in Silicon Nitride". Technical Physics Letters, **44**, pp. 424–427, 2018.
3. V.A. Volodin, K.O. Bugaev, A.K. Gutakovsky, L.I. Fedina, M.A. Neklyudova, A.V. Latyshev, A. Misiuk. "Evolution of silicon nanoclusters and hydrogen in SiN_x:H films: Influence of high hydrostatic pressure under annealing". Thin Solid Films, **520**, pp. 6207-6214, 2012.

Influence of the vacuum-plasma etching on the electrophysical characteristics of thin ferroelectric PZT films

D.A. Abdullaev[1,2], D.S. Seregin[2], D.N. Zubov[1], K.A. Vorotilov[2]

1. Institute of Nanotechnology of Microelectronics, Russian Academy of Science, Russia, 119991 Moscow, Leninsky Prospekt, 32A

2. MIREA - Russian Technological University (RTU-MIREA), 119454 Moscow, Vernadsky Prospekt, 78, abdullaev@mirea.ru.

Ferroelectric lead zirconate titanate (PZT) films due to its high electrophysical characteristics such as the dielectric permittivity, the remanent polarization, the piezoelectric coefficient very interesting for integration into micro- and nanoelectronics devices, fabrication of non-volatile ferroelectric memory, MEMS elements, sensors and other devices [1, 2]. To create elements in the micro- and nanoelectronics prefer used vacuum plasma etching (VPE) processes provided a high degree control of the structures formation [3, 4].

In our work we research influence of two VPE modes – reactive-ion etching (RIE) and ion beam etching (IBE) on the dielectric permittivity and polarization. The PZT films, formed sol-gel method, were deposited on silicon substrates with structure Pt (150 nm)–TiO_2 (10 nm)–SiO_2 (300 nm)–Si (fig. 1). Our experiments show that IBE and RIE processes lead to negative effect on the electrophysical parameters of the PZT film. The etching process decreases the maximum value of dielectric permittivity, remanent polarizations and increases of the coercive field and asymmetry (emergence large at IBE) of the values *ε(E)* and *P(E)* under forward and reverse bias (fig. 2). The obtained results can be explained by the forming of the surface "dead layer" (amorphization, ion implantation) during etching and overall reduce of the PZT film thickness. Subsequent, after RIE, thermal annealing leads to recovery PZT properties, but after IBE the annealing leads to their further degradation.

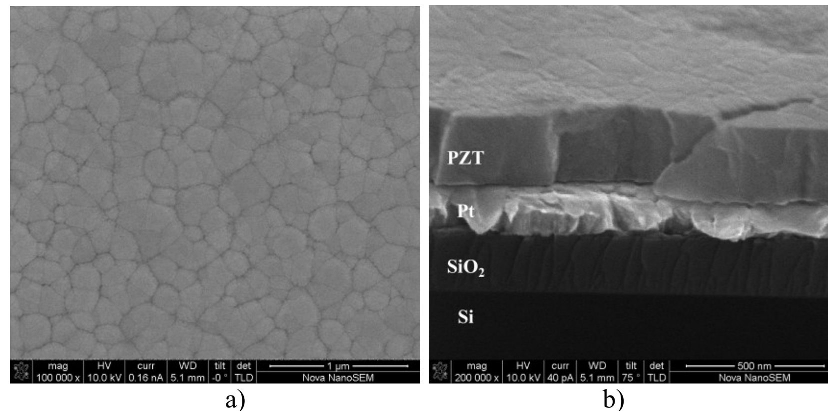

a) b)

Fig. 1. SEM image of surface (a) and cross-section (b) PZT films.

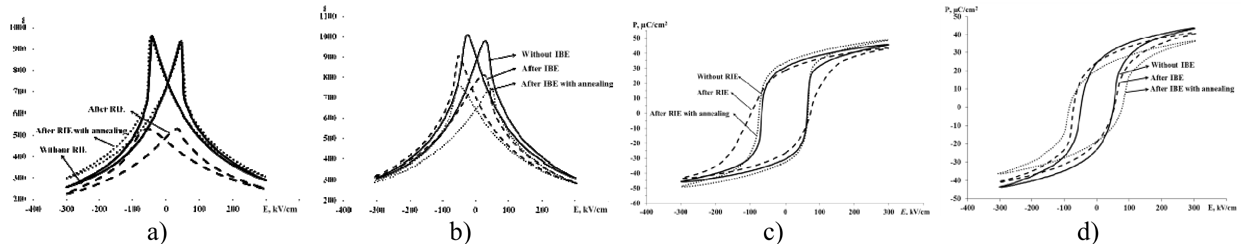

a) b) c) d)

Fig. 2. *ε(E)* (a, b) and *P(E)* (c, d) characteristics of PZT films during RIE (a, c) and IBE (b, d) without etching, after etching and after etching with annealing.

1. Ishiwara H. "Ferroelectric random access memories," J. Nanosc. Nanotech., **12**(10), 7619-7627, (2012).
2. Vorotilov K.A., Sigov A.S. "Ferroelectric memory," Physics of the Solid State, **54**(5), 894-899, (2012).
3. Nojiri K. [Dry etching technology for semiconductors], Springer, Switzerland, (2016).
4. Abdullaev D.A., Vorotilov K.A., Zubkova E.N., Seregin D.S., and Sigov A.S. "Reactiv-ion etching of lead-zirconate titanate," Nano- and Microsystems Technology, **18**(12), 721-729, (2016).

Electronic and optical properties of MoS_2 thin films deposited by magnetron sputtering studying

A.I. Belikov, Z.P. Kyaw, A.I. Semochkin
Bauman Moscow State Technical University (BMSTU), Moscow, Russia, belikov@bmstu.ru,

In the recent years, many kinds of 2D materials have attracted tremendous research interest; their unique electronic properties allow using them in a wide range of nano-electronic applications became possible [1]. Molybdenum disulphide (MoS_2), which is a semiconductor from the family of layered transition metal dichalcogenides (TMDs), is an attractive material for optoelectronic and photo-detection applications because of its large effective mobility (up to 500-1000 cm^2/Vs) [2], excellent current ON/OFF ratio (exceeding 10^8) [3]. MoS_2 has intrinsic and tunable bandgap that varies with the thickness from a bulk to monolayer film (1.2-1.8 eV) [3]. In the present work, we have used magnetron sputtering method to deposit MoS_2 thin films on the different substrates such as Si and sapphire, with the different processing conditions. MoS_2 films were prepared by magnetron sputtering MoS_2 (99.9% purity) target on the substrates at the different pressure and power discharge. MoS_2 thin films thickness and morphology were analyzed by atomic force microscope; spectrophotometer ("Epsilon") was used for the reflectance detecting and then to calculate thin films bandgap.
In Figure 1 shows MoS_2 thin films reflection spectra's for the samples on the Si substrates (1a) and on the sapphire substrates (1b) showing deposition parameters effect on the optical properties of MoS_2 films.

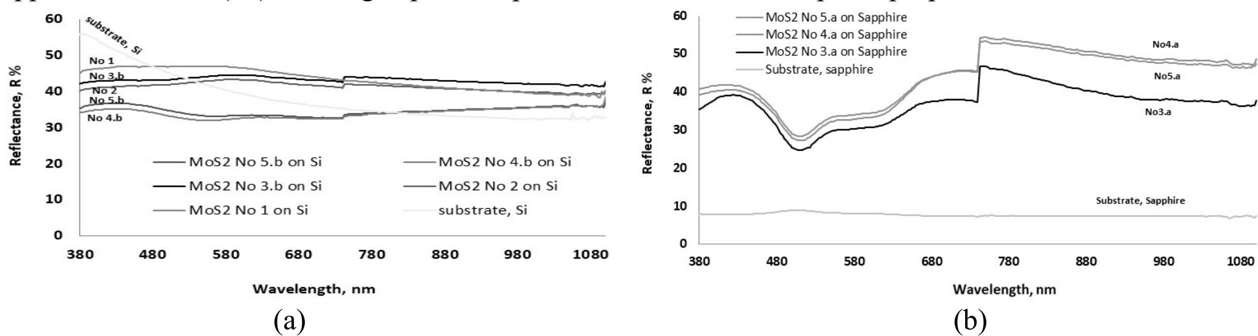

Fig. 1. Sputtered MoS_2 thin films samples on Si (a) and sapphire (b), and substrates, reflection spectra's.

Using spectrophotometer reflectance coefficients data's the values for the absorption function *F(R)* were determined based on the Kubelka-Munch method. Then the calculated absorption coefficient values were used to plot the dependence $(F(R)h\nu)^{1/2}$ on *hν*. Using a Tauc plot we obtained MoS_2 thin films indirect bandgap for all samples. Consolidated experimental data's presented at the table 1.

Table1. MoS_2 thin films experimental values of thickness, roughness and the bandgap E_g

No	Target power,W	Argon pressure, Pa	Substrate	Thickness, nm	Roughness,nm	Bandgap E_g, eV
1	10	5×10^{-1}	Si	33	0.787	1.4
2	10	9×10^{-1}	Si	45	2.063	1.39
3	30	5×10^{-1}	a.Sapphire	66	1.319	1.41
			b.Si	66	1.618	1.35
4	30	9×10^{-1}	a.Sapphire	60	1.847	1.46
			b.Si	60	2.622	1.36
5	50	9×10^{-1}	a.Sapphire	37	1.660	1.49
			b.Si	37	2.152	1.45

In this report reveal that lower roughness MoS_2 thin films can be observed on sapphire substrates and the influence of deposition parameters and MoS_2 thin films thickness on its structural and optical properties.

1. Wang Q.H. et al. "Electronics and optoelectronics of two-dimensional transition metal dichalcogenides". Nat. Nanotechnol., **7**, pp. 699–712, 2012.
2. Baugher B.W. et al. "Intrinsic electronic transport properties of high-quality monolayer and bilayer MoS_2". Nano Letters, **13**, pp. 4212-4216, 2013.
3. Duan X. et al. "Two-dimensional transition metal dichalcogenides as atomically thin semiconductors: opportunities and challenges". Chem. Soc. Rev., **44**, pp. 8859, 2015.

Study of the Co_2FeAl Heusler alloy films growth on R- and A-plane sapphire substrates and investigation of their magnetic properties

I.V. Malikov, L.A. Fomin, V.A. Berezin, and G.M. Mikhailov
Institute of Microelectronics Technology and High Purity Materials RAS, 142432 Chernogolovka, Russia,
E-mail: mikhailo@iptm.ru

Attempts to implement half metals (HMs) by application of binary compounds were not successful enough. Among the materials that exhibit the properties of HMs, the most promising are Heusler ternary alloys, which are currently being intensively studied. Application of HMs would lead to a significant increase of magnetoresistive effects in devices used in spintronics.

Thin films of the ferromagnetic Co_2FeAl Heusler alloys were grown by pulse laser deposition technique on *R*- and A-plane monocrystalline sapphire substrates with and without epitaxial refractory metal seed layer. In all cases the magnetoresistance of the films strongly depends on the films growth temperature demonstrating in their longitudinal and transverse magnetoresistances a behavior specific for an anisotropic magnetoresistance. Nonmonotonic dependences of the morphological and magnetic properties of the films on their growth temperature were also found.

In particular, the coercive fields H_c and full widths at half maximum of the magnetoresistance peaks sharply increase at first and then sharply decrease again with the growth temperature. This indicates to the structural transformation in Heusler alloys films in different growth temperature ranges. The Co_2FeAl films grown on A-sapphire plane possess growth-induced uniaxial magnetic anisotropy (Fig. 1) in contrast to the previously published results for Co_2FeSi Heusler films [1].

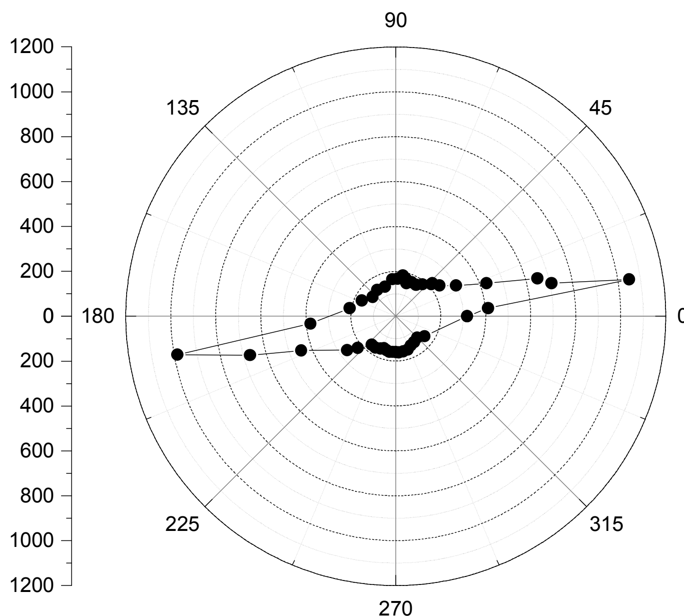

Fig. 1. Polar figure of the coercive field H_c (vertical scale in Oe) against the direction of the in-plane magnetic field for the Co_2FeAl film that grown on the A-plane monocrystalline sapphire substrate with Mo(011) seed layer.

The Co_2FeAl films grown on the *R*-plane sapphire substrate show four-fold magnetic anisotropy. The microstructures fabricated by subtractive nanotechnology from the grown films exhibit magnetic domain patterns, which were studied by magnetic force microscopy in the presence of external magnetic field. For Co_2FeAl stripes the regular domain patterns, the formation of which is in agreement with the magnetic anisotropy found from magnetoresistive experiments, were observed. This could be useful for applications in magnetic storage and spin transfer torque devices.

The work is supported by RFBR grant No. 17-57-45024.

1. H. Schneider, Ch. Herbort, G. Jakob, H. Adrian, S. Wurmehl, C. Felser. "Structural, magnetic and transport properties of Co_2FeSi Heusler films". J. Phys. D: Appl. Phys. **40**, pp. 1548–1551, 2007.

Nanocrystalline diamond films heavily doped by boron: structure, optical and electrical properties

V.A. Volodin[1,2], S.G. Cherkova[1], V. Kumar[3], V.A. Sachkov[4], V. Mortet[5], A. Taylor[5], Z. Remes[5], T.H. Stuchliková[5], J. Stuchlik[5]

1. A.V. Rzhanov Institute of Semiconductor Physics, Siberian Division of the Russian Academy of Sciences, Lavrenteva 13, Novosibirsk 630090, Russia, E-mail: volodin@isp.nsc.ru.

2. Novosibirsk State University, Pirogova street, 2, 630090, Novosibirsk, Russia.

3. Indian Institute of Information Technology Design & Manufacturing, Kancheepuram Melakottaiyur, Off Vandalur-Kelambakkam Road, Chennai - 600127, Tamil Nadu, India.

4. Omsk Scientific Center, Siberian Branch, Russian Academy of Sciences, 644024, Omsk, Russia.

5. Institute of Physics ASCR, v. v. i., Cukrovarnická 10/112, 162 00 Praha 6, Czech Republic.

Doped diamond films attract the interest of researchers due to many reasons. From some threshold concentration of boron, the diamond is low-temperature superconductor [1]. Since the diamond is a wide-gap semiconductor, it is promising for use in optoelectronic devices as transparent electrodes [2].

The set of nanocrystalline diamond films was grown using PECVD on glass substrates from methane (CH_4) diluted by hydrogen: without doping gases and with addition of trimethylborane (C_3H_9B). The ratio B/C was varied from 0 to 8,000 particles per million (ppm). The heavily boron doped nanocrystalline diamond films were investigated using electron microscopy, atomic-force microscopy, Raman spectroscopy, transmittance spectroscopy and electro-physical methods. The spectrometer T64000 (Horiba Jobin Yvon) with micro-Raman setup was used. The Ar^+ (514.5 nm), HeCd (325 nm) and solid-state (660 nm) lasers were used for excitation of Raman scattering. The spectral resolution was better than 2 cm^{-1}. The radiation power reaching the sample was ~1 mW, laser spot was about 10 microns, which is insufficient to cause significant local heating. The back-scattering geometry was used; the polarization of scattered light was not analyzed.

For analysis of Raman spectra of heavily doped p-type nanocrystalline diamond using Fano contour one should take into account the shift and broadening of phonon line due to phonon confinement in grains, or phonon scattering by defects. The Raman spectra were calculated using phonon confinement model and Fano contour. A good agreement was found between the calculated and experimental spectra. Analysis of the spectra showed both the phonon confinement effect in nanocrystalline grains and Fano interference effect due to the contribution of electron Raman scattering in heavily doped p-type diamond films. Increase of boron concentration led to decrease of the size of crystalline diamond grains and also to formation of defects (supposedly inclusion of sp^2-hybridizated carbon) in the diamond nanocrystals. These Raman spectroscopy data were approved by data of electron microscopy and atomic-force microscopy.

The conductivity of not-doped film (0 ppm of C_3H_9B) was 0.066 $Ohm^{-1}cm^{-1}$, the conductivity of doped film grow with increasing of C_3H_9B concentration and reach 418 $Ohm^{-1}cm^{-1}$ (8000 ppm of C_3H_9B). The films were semitransparent and have good conductivity, so its can be used as transparent electrodes in giant-scale electronics and optoelectronics.

So, it was shown, that increase of boron concentration led to decreasing of phonon correlation length in nanocrystalline diamond films. The films are semitransparent and have good conductivity and can be used as transparent electrodes.

Acknowledgements: The work was carried out according to the state research program of ISP SB RAS project number 0306-2016-0015. This work was also supported by the MEYS project LTC17029 INTER-COST Action MP1406, Grant CFS 17-05259S and the J.E. Purkyně fellowship awarded to V. Mortet by CAS, Czech Republic.

1. M. Nesládek, D. Tromson, C. Mer, P. Bergonzo, P. Hubik, and J.J. Mares. “Superconductive B-doped nanocrystalline diamond thin films: Electrical transport and Raman spectra”. Appl. Phys. Lett. **88**, 232111, 2006.

2. V.A. Volodin, V. Mortet, A. Taylor, Z. Remes, T.H. Stuchliková, and J. Stuchlik. “Raman scattering in boron doped nanocrystalline diamond films: manifestation of Fano interference and phonon confinement effect”. Solid State Communications **276**, 33-36, 2018.

O1-11

Scaled-up deposition of 2D materials and heterostructures: Technology and processes

F. Reale, R.S. Sundaram, T. Miller, O. Thomas
Oxford Instruments Plasma Technology, Yatton, UK, Francesco.Reale@oxinst.com

Traditional vapour-phase synthesis methods of bulk semiconductors have recently undergone a resurgence of research interest for the growth of two-dimensional (2D) materials and heterostructures [1-3]. In particular, the chemical vapour deposition (CVD) has been extensively rediscovered to achieve atomic planes of Van der Waals solids such as transition metal dichalcogenides [4, 5]. Heterostructures created by stacking layers with complementary characteristics to achieve novel functionality have also been demonstrated [6]. These nanomaterials have revealed unforeseen electrical, optical and mechanical properties which make them unique candidates for next-generation nanotechnologies, ranging from large scale consumer electronics to quantum electronics.

For the successful scaling up of prototypical applications demonstrated to date, technologies and processes for the wafer-sized deposition of these materials need to be developed. In this talk I will give an overview of the progress we have made at Oxford Instruments Plasma Technology towards the high-performance growth of various low-dimensional materials (e.g. MoS_2, graphene, h-BN, CNTs, Ge NWs) by CVD/PECVD (Fig. 1). Further, we compare the relative merits of CVD and atomic layer deposition (ALD) to grow 2D materials, and introduce results on the atomic layer etching. Finally, I will discuss our developments in technology for device fabrication processes such as dielectric deposition and device pattern etching.

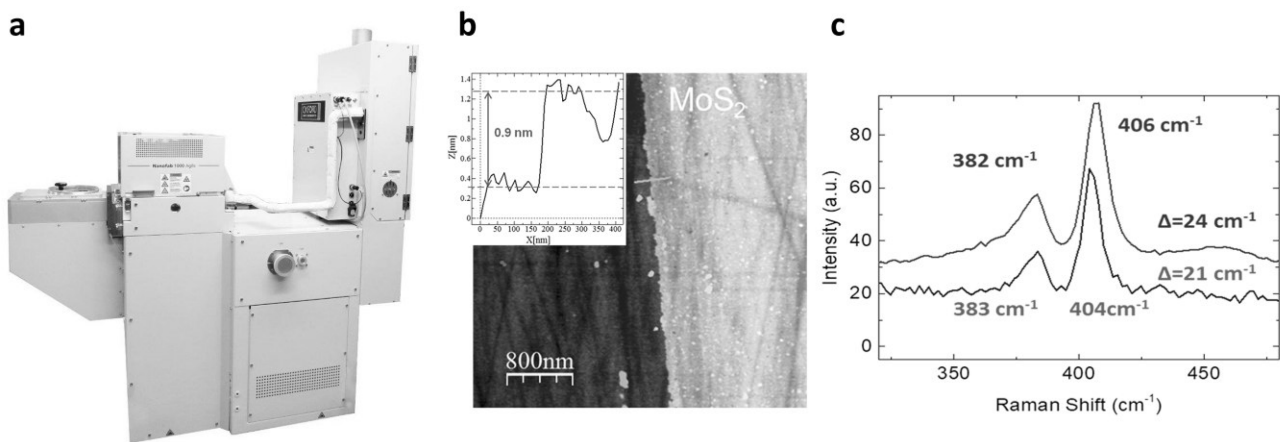

Figure 1: (a) Oxford Instruments Nanofab system for the growth of 1D/2D nanomaterials and heterostructures. (b) AFM characterization of CVD-deposited monolayer MoS_2 on c plane Sapphire substrates. (c) Characteristic Raman spectra of single (blue line) and few layer (red line) MoS_2 (λ=532 nm).

1. X. Li et al. “Large-area synthesis of high-quality and uniform graphene films on copper foils”. Science, **324**, pp. 1312-1314, 2009.
2. S. Bae et al. “Roll-to-roll production of 30-inch graphene films for transparent electrodes”. Nat. Nanotech., **5**, pp. 574-578, 2010.
3. K. Kang et al. “High-mobility three-atom-thick semiconducting films with wafer-scale homogeneity”. Nature, **520**, pp. 656-660, 2015.
4. F. Reale et al. "From bulk crystals to atomically thin layers of group VI-transition metal dichalcogenides vapour phase synthesis". Applied Materials Today, **3**, pp. 11-22, 2016.
5. E. Mercado et al. “A Raman metrology approach to quality control of 2D MoS_2 film fabrication”. J. Phys. D Appl. Phys., **50**, 184005, 2017.
6. L. Yuan, “Van der Waals heterostructures and devices”. Nature Reviews Materials, **1**, 16042, 2016.

Flicker Noise Reduction for 110nm Technology

N. Belova, T. Myers, B. Huang, E.A. Process, J. Kimball, N. Menninger
ON Semiconductor, Phoenix, AZ, USA, E-mail Nadya.Strelkova@onsemi.com. Tracy.Myers@onsemi.com

The 110nm technologies emerged on the market around beginning of 2000 employed very thin oxynitrided gate for the 1.2V minimum design rule transistors. Nitrided gate oxide enhances digital I_{on}/I_{off} characteristics but influences unfavorably analog parameters by degrading the flicker 1/f noise and NBTI (Negative Bias temperature Instability) performance. MOS transistors have the highest 1/f noise of all active semiconductors. Improving flicker noise performance is important to be competitive in the semiconductor industry.

There are two strong theories for explaining flicker noise: the mobility fluctuation model and the number fluctuation model. Mobility model explains flicker noise by random mobility fluctuation at Si/SiO_2 interface. In the number fluctuation model the 1/f noise is explained by the random trapping and detrapping of the mobile carriers in the trap located at $Si\text{-}SiO_2$ interface and within the gate oxide. Nitrided gate oxide is considered having high trap density which increases flicker noise. One of the known noise improvement solutions is to remove Nitride from the gate oxide. It results in increasing Boron penetration through thin oxide into channel and degrading PMOS transistors. To prevent Boron penetration we selected to build the Nitrogen barrier in the Poly film after gate oxide formation similar to [1].

Test Vehicle (TV) and Process: The Noise test vehicle was built to support automated data collection. Following factors were investigated: (a) Gate-Ox Pre-Clean; (b) Gate-Ox-Annl; (c) Nitrogen-Imp into blanket Poly followed by the Rapid Temperature Anneal (RTA); (d) Fluorine-Implant. Boron penetration was evaluated by measuring MOS capacitor electrical thickness and long channel transistor saturation current and threshold voltage. Noise measurements done on long channel L_xW=1x10um and 10x10um transistors.

Results:

(1) Screening experiments confirmed noise reduction by replacing NO-Anneal with N_2-Anneal in the thin gate module but resulted in increasing Boron Penetration into PMOS transistor channel.
(2) Optimization of the N-Implant into Polysilicon was done to suppress Boron penetration.
(3) The high performance thin gate PMOS transistors (PHP) with adjusted channel implants showed approximately 10x Noise reduction (fig.1).

Conclusions: The 110nm experiments demonstrated the way of modulating noise signal to (1) roughness of Si/SiO_2 interface; (2) Thin-Gate-Oxidation conditions; and (3) Nitrogen Implant Conditions.

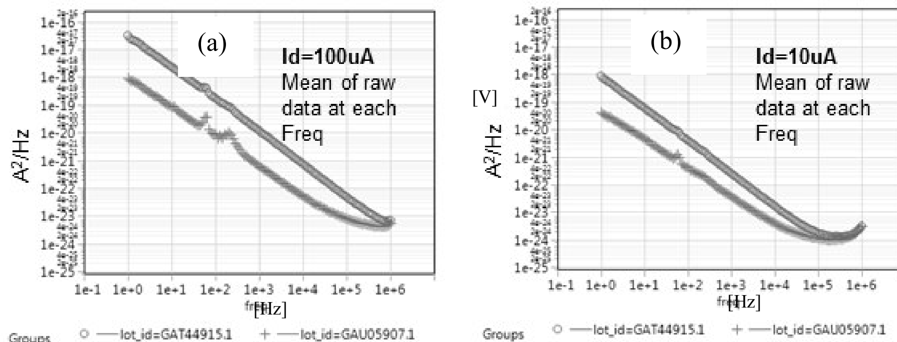

Fig. 1. Comparison of the 10x10um PHP Transistor Noise between process of record (red) and the optimized conditions (blue). Measurements done at two different I_d: 100uA (a) and 10uA (b). Y-axis scales from 1e-25 to 1e-16 A^2/Hz. Blue curves show ~ 10x lower noise than POR at 10Hz and 1000Hz.

1. A.J. Bauer, etc. “Implantation of Nitrogen into Polysilicon to Suppress Boron Penetration through the Gate Oxide”, 1999 IEEE.

Alternative BEOL approach: gap filling with CSD low-*k* dielectric

V. Gvozdev[1], D. Seregin[2], P. Kuznetsov[1], A. Valeev[1], K. Vorotilov[2], O. Gushin[1], G. Krasnikov[1], A. Sigov[2]

1. Molecular Electronics Research Institute (JSC MERI), Zelenograd, Russia, v_gvozdev@mail.ru
2. MIREA – Russian Technological University, Moscow, Russia, vorotilov@mirea.ru

Subtractive BEOL technique was widely used in semiconductor manufacturing technology during era of aluminum metallization. According to this technique Al is deposited over the entire wafer, after that it is patterned by reactive ion etching (RIE) and interlevel silicon dioxide dielectric is deposited by PECVD. Replacement of Al by Cu required dramatic changing BEOL process from subtractive to Damascene process, as Cu cannot be patterned by RIE due to a low vapor pressure of reaction products. According to Damascene technique low-*k* interlevel dielectric is deposited firstly and subjected to plasma etching with the following Cu deposition. This technique is used in semiconductor manufacturing technology from 180 nm to the current 7 nm. However, the plasma etching of porous dielectric is the main challenge as vacuum ultraviolet irradiation leads to degradation of low-*k* dielectric properties due to its composition change. Now semiconductor industry calls for new low-*k* dielectric materials with lower *k* value and higher porosity, however integration of these materials in Damascene process is highly conjectural. For this reason, some research groups started research works on alternative BEOL process: subtractive technique in which metal (Cu, Co or some other metal) would be deposited first [1, 2]. This process does not require plasma etching of low-*k* dielectric; however, it lays down condition of good filling of gaps between metal lines. PECVD provides bad gap filling properties, whereas chemical solution deposition (CSD) could give good results, along with good composition control [3, 4].

This work devotes to experimental research of this alternative subtractive techniques with the use of CSD low-*k* dielectric obtained by molecular self-assembly process. Organosilicate low-*k* dielectric with methyl terminal groups was used as a low-*k* material. Porous structure was obtained by evaporation-induced self-assembly of nonionic surfactant Brij 30, the total porosity was about 30% and the mean pore radius was 0.9 – 1.2 nm. The film-forming solution was spin-on deposited onto substrates with the test structure: 90 nm Cu lines with TaN/Ta barrier at the side walls and CuSiN or SiCN barrier on the top of Cu lines. It was demonstrated that CSD technique provides good planarization properties, planarization coefficient is increased with the decrease of the gap width up to 90-95% (see Figure 1). It was shown, that new BEOL approach is very promising for the current and the next technology nodes, however additional efforts are needed to obtain good properties of metal barriers with minimal thickness.

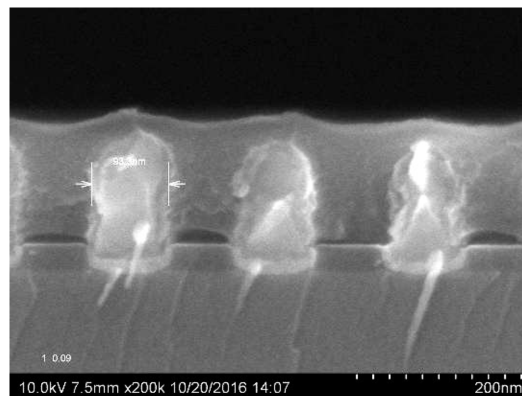

Fig.1. SEM microphotography of 90 nm test structure after CSD low-*k* deposition.

The study was supported by the Ministry of Education and Science (project No. 11.2259.2017/4.6).

1. L. Zhang et al. Appl. Phys. Letters, **109**, p. 232901, 2016.
2. Patent 2548523 Russian Federation, IPC H01L 21/768, Valeev A.S. et al.
3. R. Nenashev et al. ECS J. Sol.-St. Sci. Techn., **6** (10), pp. 182-188, 2017.
4. C. Liu et al. Jap. J. Appl. Phys., **57**, p. 07MC01, 2018.

Investigation of technological operations for manufacturing 3D micro-assemblies with embedded elements

S. Kruchinin, S. Timoshenkov
National Research University of Electronic Technology – MIET, Zelenograd, Moscow, Russia
E-mail: sergeycx075@mail.ru

The internal mounting technology is the mounting of unpackaged dies in a functional radio-electronic module substrate structure. This method does not require the microcircuits packaging, since the package task carry out the microelectronic product substrate.
To produce flexible boards, polymer materials such as polyimides are actively used. That material is characterized by wide regulation possibilities of composition, structure and properties. The internal mounting technology implies the open-dies embedding into the polymer material, followed by etching to the die contact pad (CP), and the added ability to integrate 3D design will significantly improve the technology in many parameters.
The following aspects of the technology have been emphasized: (1) substrate performed the printed circuit board function after the conductive (metal) pattern deposition process of the electronic circuit onto the substrate through a technological mask; (2) when the circuit pattern was deposited, the open-die contact pads were connected to the module conductive track. This allowed us not to use welding or soldering.
Internal mounting ensured high speed, stability of frequency characteristics, absence of parasitic phenomena of inductive and capacitor nature, as well as high reliability, insensitivity to external unauthorized electromagnetic influences, high vibration resistance.
This option allowed improving the performance, noise immunity and, as a result, the total capacity of the device due to shorter electrical connections, since the contact from the external pad was realized directly on the open die contact pad. Plane and qualitative hole was formed with a minimum clearance to produce such contact by plasma-chemical etching operation. Combination of isotropic and anisotropic etching made it possible to create through holes with a small pitch between them and with a good steps coating in the polyimide layer.
The report presents technological operation results such as the plasma-chemical etching process of domestic polymer materials PI-LC “Raduga” and AD 9103. Optimal conditions for their implementation have been offered. The adhesion properties to open dies and sealants were investigated. The tests have been carried out on the LDS V455 shaker confirmed the special adhesion parameters of polyimide varnish PI-LC “Raduga” 6 (N), as well as the ability of 3D micro-assemblies to withstand high vibrational effects at a frequency of 20 to 2000 Hz with an amplitude of 5g.
Practical recommendations on the use of polyimide varnish PI-LC “Raduga” 6 (N), which allows you to set up in 80 minutes to 20 crystals per working surface without loss of the original adhesive properties have been done. The deep plasma-chemical etching process of polyimide for the interlayer compounds formation was studied. Basic technological parameters such as etching rate, uniformity of etching on samples, anisotropy and others were established.

Graphoepitaxial growth of $Y:ZrO_2$ thin films on tilted-axes substrates

P.B. Mozhaev[1], J.E. Mozhaeva[1], A.V. Khoryushin[2], I.M. Kotelyanskii[3], V.A. Luzanov[3], J.B. Hansen[2], C.S. Jacobsen[2]

1. Institute of Physics and Technology of Russian Academy of Sciences, Moscow, 117218, Russia, pbmozh@gmail.com
2. Department of Physics, Technical University of Denmark, Kongens Lyngby, DK-2800, Denmark, jbh@fysik.dtu.dk
3. Institute of Radio Engineering and Electronics RAS, Moscow, 125009, Russia, valery@luzanov.ru

$Y:ZrO_2$ (YSZ) thin films were deposited on tilted-axes $NdGaO_3$ substrates (TAS NGO) by pulsed laser deposition. A specific growth mode resulting in a tilt of crystallographic planes of the top layer from that of the substrate was observed. A simple geometrical growth model can be proposed, taking into account faceting of the surface of the substrate. The height of the growth steps of the film c_f is not equal to the height of the steps on the substrate surface c_s. As a consequence, the inclination of the crystallographic planes of the film from the substrate surface plane γ' increases compared to the substrate tilt γ when $c_f > c_s$, and decreases when $c_f < c_s$. Assuming simultaneous seeding of the grain of the film on neighboring edge-terrace joints on the substrate surface, we obtain a simple formula explaining the observed dependences (see Figure **a**) well:

$$\gamma' = \arcsin((c_f / c_s) \cdot \sin \gamma) \quad (1)$$

The adjustment of the film and the substrate is essentially three-dimensional, with graphoepitaxial matching in the substrate plane normal to the substrate tilt axis, so the observed growth mechanism may be called three-dimensional graphoepitaxial (3DGE).

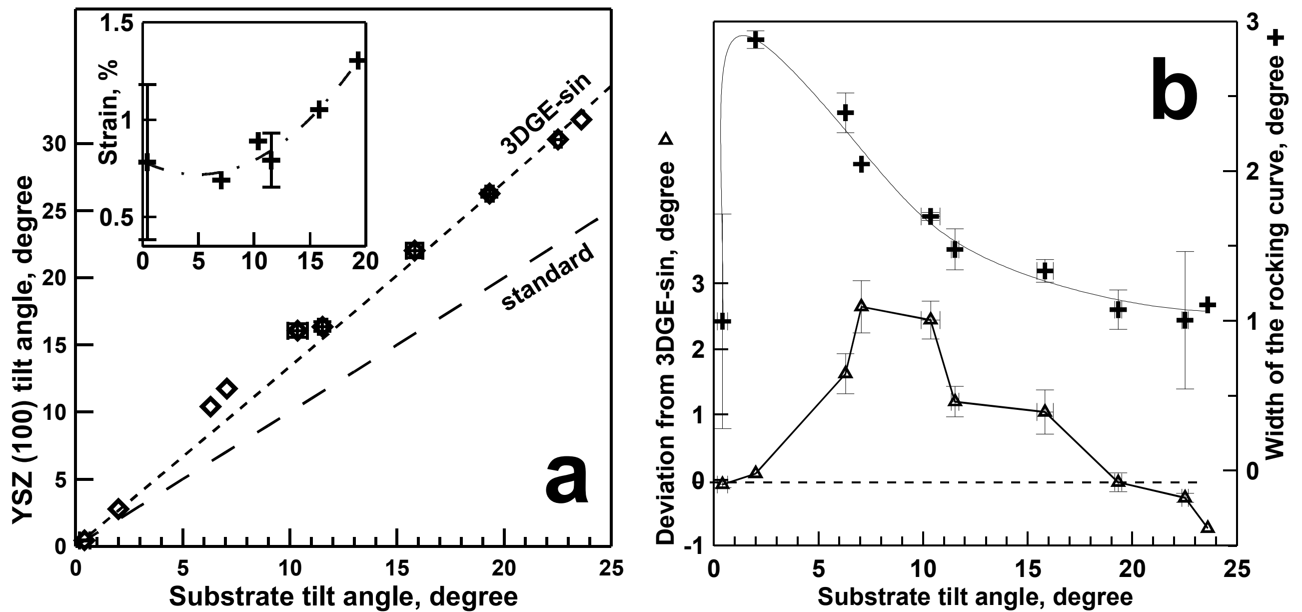

Orientational relations of YSZ films on TAS NGO: a) the film orientation follows the 3DGE growth mode at high substrate tilt angles and slightly exceeds the calculated value for 5-15º. Inset: dependence of the strain in the film on the substrate tilt angle; b) deviation from calculated tilt angle (triangles) shows maximum in the 7-10º range, correlating with the width of the rocking curve dependence on tilt angle (crosses).

The orientational features (Figure **b**) confirm assumption of simultaneous seeding mechanism. Such seeding is more probable for smaller distances between the neighboring joints, so for small angles the films shows an increased tilt compared to the calculated (bottom curve). The variety of distances between the seeding joints increases with decreasing substrate tilt angle, resulting in a broad spread of film grains orientation for very low tilt angles (top curve).

Effects of deposition parameters, deposition rate, and film thickness on properties of the YSZ 3DGE films were studied. The YSZ orientation did not change after deposition of films on top of the YSZ 3DGE layer, providing a possibility of film orientation control using the 3DGE growth mode.

A New Universal Physics Based Strategy for the Field-Effect Transistor Modeling

G.I. Zebrev

National Research Nuclear University MEPHI, Moscow, Russia, e-mail: gizebrev@mephi.ru

The silicon CMOS technology and the field-effect transistors occupy a dedicated place in the modern electronics and industry. The promising material-based (graphene, MoS_2, etc) electronics has been most often implemented via the field effect device technologies. At the present time, a large number of different configurations of the field-effect transistors (FinFET, FD and PD SOI, Double Gate and Multi Gate transistors) from different materials (silicon or different 2D monolayers) are manufactured, developed or discussed. This requires developing the new compact models for design of advanced chip architectures [1]. As a rule, each configuration or type of transistors uses its own compact model.
We propose a different approach, which consists of decomposition the FET model into the two independent parts: (i) the charge neutrality based electrostatics, and (ii) the current continuity based kinetics. The former part is specific for different transistor configurations, strongly dependent on material characteristics, sizes and geometry, and can be considered as a separate task. At the output of the device electrostatics modeling is dependence of the channel charge on gate bias. The latter part of modeling is based on the current continuity equation leading to obtaining of the electrical and chemical potentials and the carrier density distributions as functions of the total channel charge. This diffusion-drift kinetics is a universal for all FETs, and its physics is relied upon the fundamental physical characteristics. Particularly, we intend to discuss a fundamental role of the quantum capacitance and compressibility of the 2D electron gas in the silicon or graphene FET operation. We found that the quantum capacitance should enter the expression for the drain current for any FETs in explicit way. A concise universal FET model, presented in a transparent physical form, will be discussed.

1. B. Das and S. Mahapatra, npj 2D Materials and Applications (2018) 2:28; doi:10.1038/s41699-018-0073-3

Modeling of the submicron MOSFETs characteristics for UTSi technology

A.S. Adonin[1], K.O. Petrosyants[2], D.A. Popov[2]
1. OJSC "Research-and-production enterprise "Pulsar", Moscow, Russia adonin@pulsarnpp.ru
2. National Research University Higher School of Economics (Moscow Institute of Electronics and Mathematics, Department of Electronics Engineering), Moscow, Russia kpetrosyants@hse.ru

Traditional technology on bulk silicon has such disadvantages as non-linear parasitic capacitances between the structure of the transistor and the substrate, and also the low substrate resistivity. The authors [1] proposed the design of a MOSFET manufactured on an Al_2O_3 substrate – silicon on sapphire (SOS). This design has a lower capacity and, therefore, higher performance at lower power [2]. However, a large number of defects in the silicon film resulted in a small number of suitable yields and a correspondingly high cost.

Further SOS technology development was made possible by Peregrine Semiconductor. They proposed a method for manufacturing SOS MOSFETs with a silicon film thickness of about 100 nm and the minimum number of defects – UTSi technology [3].

Adonin A.S. proposed the design of the SOS MOSFET [4] allowing us to increase the transistor dynamic characteristics to 30-40% while reducing the power consumption. The design feature is the presence of high-resistance undoped silicon of intrinsic conductivity in the channel region near the source (see Fig. 1).

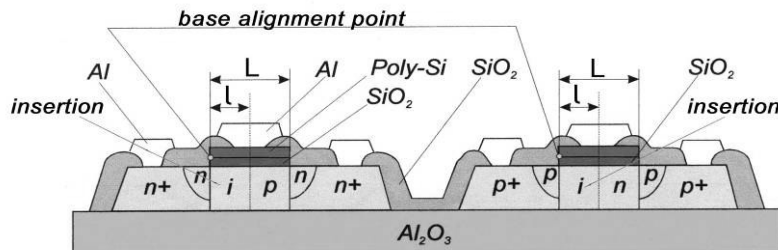

Fig. 1. CMOS structure with the insertion of intrinsic conductivity area in a channel [4].

Table 1 shows the simulated n-channel SOS MOSFET parameters with topological channel lengths of 0.75 and 0.5 μm. The simulation results for SOS MOSFETs with using the "insertion" show that such parameters as threshold voltage, saturation current and delay time are improved, but the leakage current increases by 5 orders of magnitude when the insertion region occupies 75% of the channel length.

Table 1. The value of the simulated structures parameters

Gate Length	0.75 um								0.5 um
t_{Si}	0.3 um				0.1 um				0.1 um
«insertion», %	0%	25%	50%	75%	0%	25%	50%	75%	0%
V_{th}, V	0.94	0.86	0.81	0.6	0.67	0.62	*0.55*	0.43	0.6
I_{off}, A	8E-14	2E-13	4E-13	9E-10	3E-13	5E-13	*6E-12*	8E-09	9E-12
I_{on}, mA	4.90	5.78	7.00	9.71	6.25	6.95	*7.47*	8.60	7.67
$t_{delay01}$, ps	20,5	–	–	–	17,6	15,0	*13,6*	11,8	10,9
$t_{delay10}$, ps	20,7	–	–	–	18,3	15,8	*14,4*	13,1	11,0

Thus, a new design of 0.75 μm SOS MOSFET with the use of an "insertion" makes it possible to obtain the transistor with characteristics corresponding to a transistor with a topological channel length of 0.5 μm. This allows the factories to produce new competitive products without significant capital expenditures for the modernization of production capacities.

1. C.W. Mueller, P.H. Robinson. "Grown-film silicon transistors on sapphire". Proc. of the IEEE (Vol. 52, Issue 12, Dec. 1964), pp. 1487-1490, 1964.
2. E.R. Ronald. Application of UTSi® CMOS On Sapphire to RF and Mixed Signal Requirements in Advanced Space Systems. Microwave Engineering Europe, pp. 1-4, 2002.
3. M.L. Burgener, R.E. Reedy. Patent US №5600169, 1993.
4. A.S. Adonin. Patent RU №2298856, 2004.

A linear "extrinsic" compact model for short-channel MOSFET drain current asymptotic dependence on drain bias in saturation regime

V. Turin[1], R. Shkarlat[1,2], V. Poyarkov[2], O. Kshensky[2], G. Zebrev[3], B. Iñiguez[4], M. Shur[5]
1. Orel State University after Ivan Turgenev, Orel, Russia, voturin@ostu.ru
2. JSC "Bolkhov Plant of Semiconductor Devices", Bolkhov, Orel region, Russia, oaobzpp@list.ru.
3. National Research Nuclear University "MEPHI", Moscow, Russia, gizebrev@mephi.ru.
4. Rovira i Virgili University, Tarragona, Spain, benjamin.iniguez@urv.cat.
5. Rensselaer Polytechnic Institute, Troy, NY, USA, shurm@rpi.edu

In [1, 2], we developed an approach for an "intrinsic" compact modeling of the MOSFET drain current (without accounting for the contact resistances) with the correct account of the differential conductance in saturation regime. To generalize this approach for the "extrinsic" compact modeling (accounting for the contact resistances), we need to modify the equation describing the linear regime:

$$I_{LIN}= g_{CH}\, V_{DS} \quad \text{with} \quad g_{CH}\,(V_{GT})= \beta\, V_{GT} = \beta\,(V_{GS} - V_{th}). \tag{1}$$

(g_{CH} is MOSFET conductance in the linear regime and V_{th} is threshold voltage). In addition, we need to modify the drain current asymptotic in the saturation regime given by

$$\text{Level 1:} \quad I_{ASY}= I_{SAT} + g_{ASY}\, V_{DS}\,; \qquad \text{BSIM3/4:} \quad I_{ASY}= I_{SAT}+ g_{ASY}\,(V_{DS}\text{-}V_{SAT}). \tag{2}$$

(in both equations $g_{ASY} = \lambda\, I_{SAT}$). The relations between the "extrinsic" and "intrinsic" voltages are [3]

$$V_{ds} = V_{DS} + I\,(R_S+R_D), \quad V_{gs} = V_{GS} + I\,R_S. \tag{3}$$

The "intrinsic" saturation current and voltage are

$$I_{SAT} = \beta V_L^2/\,\alpha \times [\{1 + \alpha\,(V_{GT}/V_L)^2\}^{1/2}\text{-}1], \quad V_{SAT} = V_L \times [1 + \alpha\, V_{GT}/V_L\, - \{1 + (\alpha\, V_{GT}/V_L)^2\}^{1/2}]. \tag{4}$$

(with the carrier's velocity saturation characteristic voltage $V_L = v_s\, L/\mu$). The "extrinsic" output MOSFET resistance in linear regime is equal to the sum of the contact resistances and the "intrinsic" MOSFET output channel resistance. Hence, we have [3]:

$$I_{lin}= g_{ch}\, V_{ds} \quad \text{with} \quad 1/g_{ch} = 1/g_{CH}(V_{gt}) + R_S + R_D\,. \tag{5}$$

Here $V_{gt} = V_{gs} - V_{th}$. From (2) and (3) we have implicit equation for "extrinsic" drain current I_{asy}:

$$\text{Level 1: } I_{asy}=I_{SAT}(V_{gt} - I_{asy}R_S)\times[1+\lambda\{V_{ds} - I_{asy}(R_S+R_D)\}]; \tag{6.1}$$

$$\text{BSIM3/4: } I_{asy}=I_{SAT}(V_{gt} - I_{asy}R_S)\times[1+\lambda\{V_{ds} - I_{asy}(R_S+R_D)\text{-}V_{SAT}(V_{gt} - I_{asy}R_S)\}]. \tag{6.2}$$

We suggest using in "extrinsic" case a linear approximation for the drain current asymptotic dependence on the "extrinsic" drain-to-source bias in saturation regime:

$$\text{Level 1:} \quad I_{asy}= I_{sat}+ g_{asy}\, V_{ds}\,; \qquad \text{BSIM3/4:} \quad I_{asy}= I_{sat}+ g_{asy}\,(V_{ds}\text{-}V_{sat}). \tag{7}$$

With use of (3) and (4) we can obtain the equation for I_{sat} [3, 4]:

$$I_{sat}=\beta V_L^2/\alpha \times [\{1+2\alpha\beta R_S V_{gt}+\alpha\,(V_{gt}/V_L)^2\}^{1/2}\text{-}\,(1+\alpha\beta\, R_S\, V_{gt})]/(1\text{–}\beta^2\, R_S^2\, V_L^2). \tag{8}$$

The equation for the "extrinsic" saturation voltage is

$$V_{sat}= V_{SAT}\,(V_{gt} - I_{sat}\, R_S) + I_{sat} \times (R_S+R_D). \tag{9}$$

The "extrinsic" differential conductance in saturation regime is:

$$g_{asy} = \partial I_{asy}/\partial V_{ds}\,|_{I_{asy} = I_{sat}\,,\; V_{ds}=V_{sat}} \tag{10}$$

yielding

$$\text{Level 1:} \quad 1/\,g_{asy} = 1/g_{ASY} + R_D + R_S; \qquad \text{BSIM3/4: } 1/\,g_{asy} = 1/g_{ASY} + R_D + (1+g_m/g_{ASY} - b_m)\, R_S. \tag{11}$$

The equation for MOSFET "intrinsic" transconductance: $g_m = \partial I_{SAT}/\,\partial V_{GS} = \alpha\,\beta\, V_{GT}/\{1 + (\alpha\, V_{GT}/V_L)^2\}^{1/2}$. The function b_m is determined as $b_m = \partial V_{SAT}/\,\partial V_{GS} = \alpha\,\{1 - g_m\,/\,\beta\, V_L\}$. In all functions g_{ASY}, g_m, b_m, I_{SAT}, and V_{SAT} the argument $V_{GT} = V_{gt} - I_{sat}\, R_S$ is used with I_{sat} given by equation (8). Note, that the same approach to drain current "extrinsic" compact modeling can be applied to OFET and TFT.

1. V.O. Turin, A.V. Sedov. G.I. Zebrev, B. Iñiguez and M.S. Shur. "Intrinsic compact MOSFET model with correct account of positive differential conductance after saturation". Proc. SPIE, 7521, 75211H, 2009.
2. V. Turin et al. "The correct account of nonzero differential conductance in the saturation regime in the MOSFET compact model". Int. J. Numer. Model. El., 1969, 2014.
3. M.S. Shur. *Physics of Semiconductor Devices*. Prentice Hall, New. Jersey, 1990.
4. T. Ytterdal, Y. Cheng, T.A. Fjeldly. *Device Modeling for Analog and RF CMOS Circuit.* John Willey and Sons, New York, 2003.

A linear "extrinsic" compact model for OFET drain current in saturation regime with nonzero differential conductance

V. Turin[1], B. Rakhmatov[1], C.-H. Kim[2]
1. Orel State University after Ivan Turgenev, Orel, Russia, voturin@ostu.
2. Gachon University, Seongnam, Republic of Korea. chang-hyun.kim@gachon.ac.kr

In [1], we have suggested an approach for an "intrinsic" (without accounting of contacts resistances) compact modeling of the organic field-effect transistor (OFET) drain current with correct account of the differential conductance in saturation regime based on model developed for MOSFET [2]. To generalize this approach for the "extrinsic" compact modeling (accounting for the contact resistances), first, we need to modify the equation describing the linear regime:

$$I_{LIN} = g_{CH} V_{DS} \quad \text{with} \quad g_{CH} = K \mu_{FET} V_{GT} = K \mu_{FET} (V_{GS} - V_{th}), \tag{1}$$

where g_{CH} is the OFET channel differential conductance in linear regime, V_{th} is threshold voltage, $K = W / L \times C_i$, W is the channel width, L is the channel length, $C_i = \varepsilon_0 \varepsilon_{OX} / d$ is the insulator capacitance per unit area, $\mu_{FET} = \mu_0 (V_{GT}/V_{aa})^{\gamma}$ field-effect mobility, μ_0 is the conversion mobility set to 1 cm^2/V·s. Second, we need to modify equations for the saturation voltage and current:

$$V_{SAT} = \alpha_S V_{GT}, \qquad I_{SAT} = g_{CH} V_{SAT}, \tag{2}$$

(α_S is a dimensionless parameter related to the influence of the substrate). Correspondingly, the transconductance and function b_m is determined by the following equations:

$$g_m = \partial I_{SAT}/ \partial V_{GS} = \alpha_S K \mu_0 (\gamma + 2) V_{GT}^{\gamma+1}/V_{aa}^{\gamma}; \qquad b_m = \partial V_{SAT}/ \partial V_{GS} = \alpha_S. \tag{3}$$

Third, we need to convert the drain current asymptotic in saturation regime. There are two approaches: #1 like in MOSFET Level 1 compact model and #2 like in BSIM3/4:

$$\#1: \quad I_{ASY} = I_{SAT} + g_{ASY} V_{DS}; \qquad \#2: \quad I_{ASY} = I_{SAT} + g_{ASY} (V_{DS} - V_{SAT}) \tag{4}$$

(in both equations $g_{ASY} = \lambda I_{SAT}$). The relations between the "extrinsic" and "intrinsic" voltages are

$$V_{ds} = V_{DS} + I (R_S + R_D), \quad V_{gs} = V_{GS} + I R_S . \tag{5}$$

The "extrinsic" output OFET resistance in linear regime for small drain-to-source voltages is equal to the sum of the contact resistances and the "intrinsic" OFET output channel resistance. Hence, we have:

$$I_{lin} = g_{ch} V_{ds} \quad \text{with} \quad 1/g_{ch} = 1/g_{CH}(V_{gt}) + R_S + R_D . \tag{6}$$

Here $V_{gt} = V_{gs} - V_{th}$. From (2) and (5) we have implicit equation for "extrinsic" saturation current:

$$I_{sat} = I_{SAT}(V_{gt} - I_{sat} R_S) = \alpha_S K \mu_0 / V_{aa}^{\gamma} \times (V_{gt} - I_{sat} R_S)^{\gamma+2}. \tag{7}$$

We found, that the following equation gives an acceptable accuracy for a sufficiently large range of V_{gt}:

$$I_{sat} \approx I_{SAT}(V_{gt})/(1+g_m(V_{gt})R_S). \tag{8}$$

The equation for the "extrinsic" saturation voltage is

$$V_{sat} = V_{SAT} (V_{gt} - I_{sat} R_S) + I_{sat} \times (R_S + R_D). \tag{9}$$

From (4) and (5) we have implicit equation for "extrinsic" drain current asymptotic in saturation regime:

$$\#1: I_{asy} = I_{SAT}(V_{gt} - I_{asy}R_S)\times[1+\lambda\times\{V_{ds} - I_{asy}\times (R_S+R_D)\}]; \tag{10.1}$$

$$\#2: I_{asy} = I_{SAT}(V_{gt} - I_{asy}R_S)\times[1+\lambda\times\{V_{ds} - I_{asy}\times(R_S+R_D) - V_{SAT}(V_{gt} - I_{asy}R_S)\}]. \tag{10.2}$$

We suggest using in "extrinsic" case a linear approximation for the drain current asymptotic dependence on the "extrinsic" drain-to-source bias in saturation regime:

$$\#1: \quad I_{asy} = I_{sat} + g_{asy} V_{ds}; \qquad \#2: \quad I_{asy} = I_{sat} + g_{asy} (V_{ds} - V_{sat}). \tag{11}$$

The "extrinsic" differential conductance in saturation regime is:

$$g_{asy} = \partial I_{asy}/\partial V_{ds} |_{I_{asy} = I_{sat},\ V_{ds}=V_{sat}} \tag{12}$$

yielding

$$\#1: \quad 1/ g_{asy} = 1/g_{ASY} + R_D + R_S ; \qquad \#2: 1/ g_{asy} = 1/g_{ASY} + R_D + (1+g_m/g_{ASY} - b_m) R_S. \tag{13}$$

In all functions g_{ASY}, g_m, b_m, I_{SAT}, and V_{SAT} the argument $V_{GT} = V_{gt} - I_{sat} R_S$ is used with I_{sat} given by equation (8). Note, that the same approach can be applied to MOSFET and TFT compact modeling.

1. V.O. Turin, B.A. Rakhmatov, C.H. Kim, B. Iñiguez. "An approach to organic field-effect transistor above-threshold drains current compact modeling that provides monotonic decrease of the output conductance with drain bias increasing". IOP Conference Series: Materials Science and Engineering. **151**(1), pp. 1-5, 2016.
2. V.O. Turin, A.V. Sedov. G.I. Zebrev, B. Iñiguez, and M.S. Shur. "Intrinsic compact MOSFET model with correct account of positive differential conductance after saturation". Proc. SPIE, **7521**, 75211H, 2009.

TCAD-based performance analysis of nanoscale vacuum field-emission transistors at advanced technology nodes

I.D. Evsikov, N.A. Djuzhev, G.D. Demin
National Research University of Electronic Technology (MIET), Moscow, Russia, evsikov.ilija@yandex.ru.

At the present time, the significant progress has been made in the area of scaling of solid-state nanoelectronic devices, where minimal design standards approach a level of 10 nm and below [1]. With the decrease in the lithographic dimensions of MOS transistors, the influence of interface effects near the border with the conductive channel region becomes critical. In particular, the complexity of technological control of the gate oxide thickness and the occurrence of additional leakage current can lead to rapid degradation of operating characteristics in harsh environment. Simultaneously, electron-phonon scattering in a semiconductor material initially limits performance of MOS transistor. Field emission of electrons into the vacuum provides maximum charge-carrier lifetime and high frequency (in the THz range)/power ratio, which makes field-emission transistors with nanoscale vacuum channel the most attractive for the high-speed electronic devices which operate under the high radiation and temperature conditions. However, low stability of current emission and strong power consumption in the modern vacuum microelectronic devices demands improvements in the fabrication process of the vacuum transistors.

Recent development of vacuum transistor with nanoscale air channel [2] opens the way to the creation of a new class of vacuum nanoelectronic devices in which electrons move in a "quasi-vacuum" with a minimum probability of collision with gas molecules at a channel length of less than 100 nm. This approach significantly reduces the power consumption of vacuum nano-transistors and prevents the degradation of emission characteristics. In addition, increasing emission current from a single cathode requires a reduction of the emitter radius up to the nanometers. Technological computer-aided device (TCAD) simulation becomes an important tool for the reducing the cost of producing the test structures of vacuum transistors.

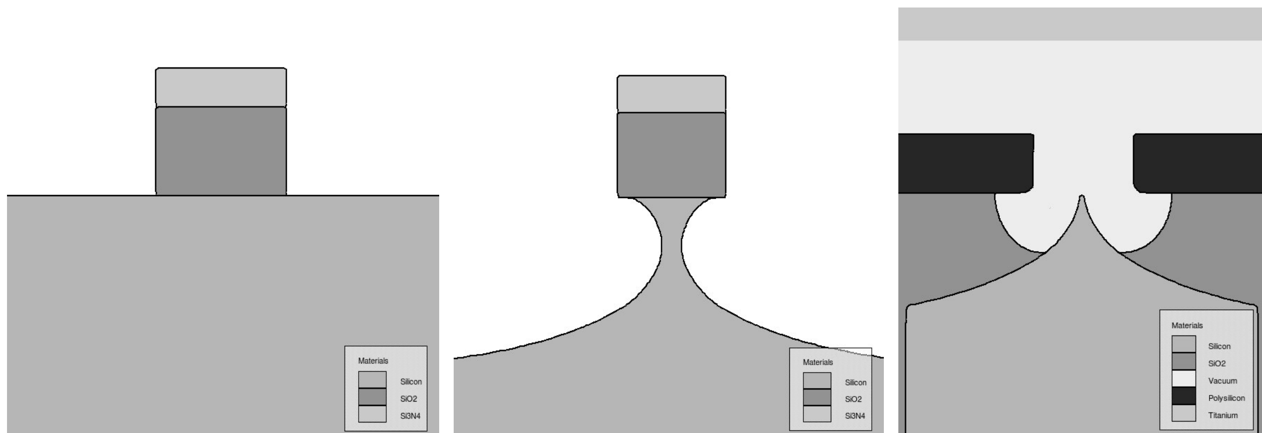

Figure 1. Technological steps of the fabrication process of nanoscale vacuum transistor.

In this work the full fabrication process of both gate-all-around nanowire and nanoscale vacuum channel transistors (Fig. 1) has been simulated using Silvaco TCAD (Victory Process and Victory Device simulation modules [3]). The analysis of electric characteristics of the obtained structure of vacuum transistor shows the comparability of the operating currents with an improved performance compared to its solid-state analog for different technology nodes varied from 50 to 5 nm. The obtained parameters of fabrication process can serve as recommendations for the development of a new generation of high-speed nanoscale vacuum transistors.

1. R. Courtland. “Moore’s Law’s Next Step: 10 Nanometers”. IEEE Spectrum, **54**, pp. 52-53, 2017.
2. J.W. Han, D.I. Moon, and M. Meyyappan. “Nanoscale Vacuum Channel Transistor”. Nano Lett., 17 (4), pp. 2146–2151, 2017.
3. Silvaco TCAD tools: Victory Process User's manual, Process Simulation Software, 2018.

Quantum wavelet transforms as alternative to the quantum Fourier transforms for a quantum computing

A.A. Kokin
Institute of Physics and Technology, Russian Academy of Sciences, Russia

The results of studying the using of wavelet transforms in the linear antiferromagnetic multiqubit spin chain with uniaxial anisotropy in a transverse magnetic field are presented. Wavelet and Fourier transforms can be viewed as a rotation in function space to a different domain. For the Fourier transform this domain contains basis trigonometric functions. For the wavelet transform, this new domain contains more complicated basis functions called mother wavelets, Wavelet transforms are characterized by the absence of such operations as a controlled phase shift, which is responsible for increasing the time-cost of the Fourier transform.

The other interesting difference between these two transforms is that individual wavelet functions are localized in space. The trigonometric Fourier functions are not localized. This property, along with the localization of the packet of frequency, leads to the fact, that many functions and operators use sparse when converted to the area of the wavelet memory. This feature makes many functions and operators, using wavelets sparse when transformed into the wavelet domain. This sparseness, in turn, results in a number of useful applications, such as data compression, detecting features in images, and moving noise from time series.

The simplest transformation is the Haar transformation.

For a one-dimensional chain of $N >> 1$ spins, located at equal distances from each other, the states of chain are almost not affected by the boundary conditions at its ends. By using for them periodic Born-Karman conditions and Haar wavelet representation for the spin operators, we will have $\mathbf{S}^{-}(l) = \mathbf{S}_{\mathrm{x}}(l) - i\mathbf{S}_{\mathrm{y}}(l) = \sum_{l=1}^{l=N} \mathbf{w}(n,m)\psi_{n,m}(l)$**,** where $\mathbf{w}(n,m)$ is quantum operator (amplitude) of Haar wavelet transform, $\psi_{n,m}(l) = 2^{n/2}\psi(2^n l - m)$ are pairwise orthogonal Haar functions, where, $\psi(x) = \begin{cases} 1 & 0 \le x < 1/2, \\ -1 & 1/2 \le x < 1, \\ 0 & otherwise \end{cases}$ is the Haar wavelet's mother function, It follows from this formulas , that for positions on the scale m, this amplitude is different from zero for values of N lying in the intervals $2^{-n} m \le l \le 2^{-n}(m+1$. Each pair of the value n,m correspond to a comparable small group of such wavelet transforms, if $2^{-n} m = 1$ is equal to a non-large group of integers. Since the wavelet amplitudes $w(n,m)$ decrease from the values of the negative values of $n,$ it is necessary to restrict the intensity to their small negative values, say $n = 0, -1, -2,...$ Then the position of the most intense wavelet amplitudes corresponds to the values, using the set of products of the $2^{-n} m = 1$, the corresponding probabilities of wavelet amplitudes,

Quantum wavelet transform of Haar's type as an alternative to the quantum Fourier transform in the Shor's-factorization algorithm in a quantum computer we considered earlier in [1]

1. K.A. Valiev, A.A Kokin. Quantum computers: hopes and reality, Moscow-Ishevsk, R&C Dynamics, 2001 (in Russian).

Homogeneous atomic ensembles and single-mode field: review of simulation results

A.V. Kulagin[1], V.Y. Ladunov[1], Y.I. Ozhigov[1,2] ,N.A. Skovoroda[1], N.B. Victorova[3]
1. Faculty of CMC, M.V.Lomonosov Moscow State University, Russia, E-mail address alexfmsu@mail.ru
2. Institute of Physics and Technology of RAS, Moscow, Russia, E-mail address ozhigov@cs.msu.su
3. Russian State University for the Humanities, Institute of informational sciences and secure technologies, Chair of fundamental and applied mathematics, E-mail address nbvictorova@list.ru

The results of analytical, computer and supercomputer modeling of homogeneous ensembles of two-level atoms and single-mode field in the optical cavity system are reviewed. The analytical solution of the problem of relaxation of one atom [1, 2] was found, where the exact expression for the population dynamics of the three basic states of the system and the boundary separating the oscillatory form of the dynamics from the smooth form is found. An analytical solution for the cavity immersed in a single-mode photonic thermostat with one atom revealed the presence of stationary states of a Gibbs type for the field and the corresponding states of the atom; for two-atomic ensembles in a similar cavity the computer simulation revealed the presence of attractors of the density matrix of the system, the nature of which comes from the dark states of atoms [3, 4]; it is shown the results of visualization, constructed by the method of triangulation.
For a bipartite atomic ensemble of more than 40 atoms, simulations on the supercomputer Lomonosov revealed the presence of ensemble oscillations of non-Rabi type [5], related to quantum echo; their character is revealed for systems with one cavity and two cavities connected by optical fiber. A criterion of a similar optical conductivity for a pair of systems of resonators in the absence of atoms is represented. It was also shown the example of computational task, for which one way quantum control on the distributed quantum computations with EPR pairs (atomic or photonic) can improve the quality of the result [6].

1. Y.I. Ozhigov, N.A. Skovoroda, Simulation of a Relaxation of Electron Shells of a Pair of Two Level Atoms in Qubit Representation, Moscow University Computational Mathematics and Cybernetics, 2014, Vol. 38, No. 4, pp. 167–173. © Allerton Press, Inc., 2014
2. Y.I. Ozhigov and N.A. Skovoroda, Computer Simulation of Atomic Excitation Conductivity Using the Quantum Master Equation, Mathematical Models and Computer Simulations, 2018, Vol. 10, No. 4, pp. 450–458. © Pleiades Publishing, Ltd., 2018.
3. Y.I. Ozhigov, N.A. Skovoroda, V.Y. Ladunov, Computer simulation of quantum effects in Tavis-Cummings model and its applications, Proc. SPIE, 10224, International Conference on Micro- and Nano-Electronics 2016, 102242X (30 December 2016); doi: 10.1117/12.2267190.
4. Y.I. Ozhigov, Dark states of atomic ensembles: properties and preparation, Proc. SPIE **10224**, International Conference on Micro- and Nano-Electronics 2016, 102242Y (30 December 2016); doi: 10.1117/12.2264516.
5. Yu.I. Ozhigov, N.A. Skovoroda, and N.B. Victorova, Quantum revivals of a non-Rabi type in a Jaynes-Cummings model, Theoretical and Mathematical Physics, **189**(2), pp. 1673–1679, 2016.
6. Y.I. Ozhigov, Distributed synthesis of chains with one-way biphotonic control, Quantum Information and Computation, Vol. 18, No. 7&8 pp. 0592-0598, 2018.

Secure quantum devices on dark atomic states

Y.I. Ozhigov[1,2]
1. Faculty of CMC, M.V. Lomonosov Moscow State University, Moscow, Russia
2. Institute of Physics and Technology of RAS, Moscow, Russia, E-mail address ozhigov@cs.msu.su

A "quantum lock" on dark atomic states is proposed: a scheme of a safe access device based on the products of singlet states of two-level atomic ensembles. The advantage over the classical secure access system is the impossibility of extracting the code, which is ensured by the impossibility of cloning quantum states. The principle of operation of the lock is based on the movement of pairs of atoms from the main cavity to the control one with the help of optical tweezers. Verification of the secret code-the splitting of the atomic ensemble into pairs-is carried out with the help of two detectors located opposite the cavities. The error in the operation of the quantum lock is associated with the false operation of the protection system for the correct code. The technical improvement of the method of preparation of such states proposed by the author earlier on the basis of Stark-Zeeman effect [1] gives a performance of more than 30%, which allows using this method of preparation of singlets as a base for the quantum lock.

1. Y.I. Ozhigov, "Dark states of atomic ensembles: properties and preparation," Proc. SPIE **10224**, International Conference on Micro- and Nano-Electronics 2016, 102242Y (30 December 2016); doi: 10.1117/12.2264516.

Representation of Boolean functions in terms of quantum computation

Yu.I. Bogdanov[1,2,3], N.A. Bogdanova[1,2], D.V. Fastovets[1,2], V.F. Lukichev[1]
1. Institute of Physics and Technology, Russian Academy of Sciences, Russia
2. National Research University of Electronic Technology (MIET), Russia
3. National Research Nuclear University (MEPhI), Russia

Present report considers the fundamental relationship between quantum physics and discrete mathematics. We present our findings in Boolean algebra, which is one of the most important discrete mathematics fields. It is shown that discrete mathematics objects can be interpreted in terms of quantum computation. The connection between Zhegalkin polynomials, which define the algebraic normal form of Boolean function, and quantum logic circuits is described. The algorithm for converting an arbitrary multibit Boolean function to quantum circuit analogue in terms of quantum transformations is presented.

The domain of definition x of a one-bit function will be considered as the basis vector e_1 of a two-dimensional vector space: $e_1 = x = \begin{pmatrix} 0 \\ 1 \end{pmatrix}$. As the second basic vector, consider the following column vector: $e_0 = x + 1 = \begin{pmatrix} 1 \\ 0 \end{pmatrix}$. The basis vectors e_0 and e_1, introduced by us to describe one-bit functions, also form the basis for the representation of arbitrary multi-bit functions. It is possible to show the validity of the following statement (an algorithm for constructing a Boolean function in the form of a Zhegalkin polynomial). An arbitrary Boolean function is a superposition of the following basic functions: $e_{j_1 j_2 \cdots j_n} = e_{j_1} \otimes e_{j_2} \otimes \ldots \otimes e_{j_n}$. The index j_k corresponds to the multiplier $\left(x_{j_k} + 1\right)$ for $j_k = 0$ and the multiplier x_{j_k} for $j_k = 1$. As an example, the figure shows quantum schemes for two-qubit basis functions and the corresponding Zhegalkin polynomials

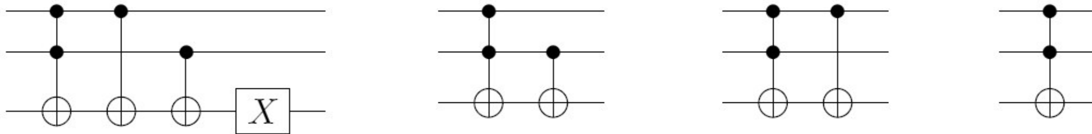

$e_{00} = x_1 x_2 \oplus x_1 \oplus x_2 \oplus 1$ $\quad e_{01} = x_1 x_2 \oplus x_2$ $\quad e_{10} = x_1 x_2 \oplus x_1$ $\quad e_{11} = x_1 x_2$

All developed methods can be applied to realization of quantum computer algorithms which are based on classical Boolean functions. Such approaches are the first steps for transition from classical machine logic to quantum hardware.

Jumps of optimal measurement angle and fractures on the curves of quantum correlation functions in two-qubit systems

M.A. Yurischev
Institute of Problems of Chemical Physics of the Russian Academy of Sciences, Chernogolovka, Moscow Region, 142432 Russia, E-mail address: yur@itp.ac.ru

A measure of quantum correlation, namely, the one-way quantum work deficit [1] exhibits the domains with the bimodal behavior of post-measurement entropy versus the measurement angle $\theta \in (0, \pi/2)$ [2, 3]. This can under certain conditions lead to the finite jumps $\Delta\vartheta > 0$ of optimal measurement angle ϑ from the endpoint 0 or $\pi/2$ to the interior minimum and vice versa. In turn, such jumps lead to the fractures on the dependences of quantum correlation against the state parameters. In the talk, a possibility to observe these jumps and fractures in an experiment will be discussed.

1. G. Adesso, T.R. Bromley, and M. Cianciaruso. "Measures and applications of quantum correlations". J. Phys. A: Math. Theor., **49**, 473001, pp. 1-82, 2016.
2. M.A. Yurischev. "Bimodal behavior of post-measured entropy and one-way quantum deficit for two-qubit X states". Quantum Inf. Process., **17**:6, pp. 1-14, 2018.
3. M.A. Yurischev. "Phase diagram for the one-way quantum deficit of two-qubit X states". ArXiv:1804.03755v1 [quant-ph], pp. 1-20, 2018.

MQ-coherence matrix transfer and remote block-scaled states creation

G.A. Bochkin, E.B. Feldman, A.I. Zenchuk
Institute of Problems of Chemical Physics of RAS, Chernogolovka, Russia, E-mail address: zenchuk@itp.ac.ru

The remote creation [1] of the density matrices is a consequent development of the state transfer problem first formulated by Bose in [2]. Although the one-qubit state creation can be completely described [3], the description of creatable multi-qubit states is much more complicated. Therefore, methods for characterizing the creatable states are meaningful.

We consider the remote creation of multiple-quantum coherence matrices as a particular problem associated with the remote state creation [4]. The n-order coherence matrix $\rho^{(n)}$ is a submatrix of the density matrix ρ collecting elements responsible for the transition in the state space changing the z-projection of the total spin momentum by n. We show that these multiple-quantum (MQ) coherence matrices evolve without mutual interaction if the Hamiltonian governing the spin dynamics commutes with the operator I_z of the z-projection of the total spin momentum. Such dynamics generates the set of conserved quantities which are the intensities of MQ-coherences

$$I_n = \mathrm{Tr}\,\rho^{(n)}\rho^{(-n)}. \qquad (1)$$

We show that the MQ-coherence matrices of the initial sender's state can be transferred to the receiver without mutual mixing if only the initial state of the rest of the communication line includes only the zero-order coherence matrix. Among such initial states is the thermal equilibrium state. But elements of each such matrix become mixed in the receiver's state. It is important that this mixing can be partially removed using the unitary transformation of the receiver. A particular example of such state-restoring is represented.

In addition we show that the initial sender's states having a special structure can be transferred to the receiver with the minimal deformation which reduces to multiplying each of sender's MQ-coherence matrix (except the zero-order one which provides the trace condition) by a scalar factor [5]. In this protocol, each of such special coherence matrices carries one arbitrary parameter from the sender to the receiver.

This work is partially supported by the program of the Presidium of RAS No. 5 "Electron resonance, spin-dependent electron effects and spin technology" and by the Russian Foundation for Basic Research (Grant No. 16-03-00056).

1. N.A. Peters, J.T. Barreiro, M.E. Goggin, N.-C. Wei, P.G. Kwiat, "Remote state preparation: arbitrary remote control of photon polarization". Phys. Rev. Lett. **94**, 150502, 2005.
2. S. Bose, "Quantum communication through an unmodulated spin chain". Phys. Rev. Lett. **91**, 207901, 2003.
3. G.A. Bochkin, A.I. Zenchuk, "Remote one-qubit-state control using the pure initial state of a two-qubit sender: selective-region and eigenvalue creation". Phys. Rev. A **91**, 062326, 2015.
4. E.B. Fel'dman and A.I. Zenchuk, "Coherence Evolution and Transfer Supplemented by Sender's Initial-State Restoring". JETP, **125**, pp.1042-1050, 2017.
5. G.A. Bochkin, E.B. Fel'dman, and A.I. Zenchuk, "Transfer of scaled multiple-quantum coherence matrices". Quantum Inf. Process. **17**, 218, 2018.

An investigation of entanglement in trimer clusters

E. Fel'dman, E. Kuznetsova
Institute of Problems of Chemical Physics, of Russian Academy of Sciences, Chernogolovka, Moscow region, 142432, Russia, kuznets@icp.ac.ru

Quantum entanglement is a measure of quantum correlations which are responsible for effective work of quantum devices (in particular, quantum computers) which significantly outperform their classical counterparts [1]. We investigate here quantum entanglement in the trimer clusters [2] consisting of three electron spins sited in vertexes of an isosceles triangle. We consider entanglement of two subsystems of the system. The first subsystem consists of spins sited on the triangle baseline and the second subsystem consists of spin equidistant from others. It is suggested that the temperature dependence of the magnetic susceptibility can be used for an experimental investigation of entanglement. Earlier it has been successfully demonstrated at the investigation of entanglement of dimers in the nitrosyl iron complexes [3]. We generalized the Bleany-Bowers equation [4, 5], describing the dependence of magnetic susceptibility on temperature, for trimer clusters. It is shown that entanglement can emerge only in the case of the antiferromagnetic interaction of the subsystems. An equation for the temperature of the entanglement emergence is derived. The criterion of the double negativity [6] is used in order to find the dependence of the entanglement on the temperature.

The work is supported by the Russian Foundation for Basic Research (Grant № 16-03-00056), the Program of the Presidium of RAS No 1.38P "Investigations of fundamental problems of synthesis and the "structure-property" dependence for creation of new compounds and materials", RFBR and NSFC (Grant No. 18-57-53007).

1. M.A. Nielsen, I.L. Chuang. *Quantum Computation and Quantum Information.* Cambridge University Press, Cambridge. 2000.
2. B.S. Tsukerblat, M.I. Belinskii. *Magnetochemistry and Radiospectroscopy of Exchange Clusters.* Shtiintsa. Kishinev. 1983.
3. S.M. Aldoshin, E.B. Fel'dman, M.A. Yurishchev. "Quantum Entanglement in Nitrosyl Iron Complexes". JETP **107**, pp. 804-811, 2008.
4. B. Bleany, K.D. Bowers. "Anomalous paramagnetism of copper acetate". Proc. R. Soc. London **A 214**, pp. 451-465, 1952.
5. R.L. Carlin. *Magnetochemistry.* New York, 1986.
6. K. Zyczkowski, P. Horodecki, A. Sapera, and M. Lewenstein. "Volume of the set of separable states" Phys. Rev. A **58**, pp. 883-892, 1998.

The multiple quantum coherence transfer and quantum correlations in NMR experiments in solids

G. Bochkin, A. Fedorova, E. Fel'dman, A. Zenchuk
Institute of Problems of Chemical Physics of Russian Academy of Sciences, Chernogolovka, Moscow region, 142432, Russia, bochkin.g@yandex.ru

NMR methods in solids are very suitable for solving problems of quantum informatics due to relatively long relaxation times, well-developed methods of creation and control of superposition quantum states, and the simple methods for processing experimental data.
We investigated [1] a transfer of multiple quantum (MQ) NMR coherences, which can be obtained experimentally in MQ NMR, from sender to the remote receiver. This transfer occurs without mixing of MQ coherences and distortions. The only effect of spin transfer is scaling of the certain blocks of sender's density matrix of MQ coherences [1]. Such a block-scaled transfer is an alternative to the perfect state transfer. We showed [1] that equal scaling of MQ coherences of higher orders can be obtained. Examples of block-scaled transfer in spin-1/2 communication lines for several different line lengths with two-qubit sender and receiver are demonstrated [1].
We investigated [2] quantum correlations in a two-spin system with the dipole-dipole interaction (DDI) in the NMR multi-pulse spin locking experiment [3]. We consider two schemes of the multi-pulse spin locking. The first scheme consists of $\pi/2$-pulses only, and delays between pulses can differ. The second scheme uses φ-pulses ($0<\varphi<\pi$) and has equal delays between them. We calculated [2] entanglement for both schemes for an initial separable state. We showed that entanglement is absent for the first scheme in the case of equal delays between pulses at any temperature. Entanglement emerges after several periods of the pulse sequence in the second scheme for $\varphi=\pi/4$ at milliKelvin temperatures for suitably chosen pulse delays. We investigated [2] the dependence of entanglement on temperature, the pulse delay and the number of the sequence periods irradiating the spin system.

The work is supported by the Russian Foundation for Basic Research (grant No. 16-03-00056) and the Program of the Presidium of RAS No. 5 "Electron spin resonance, spin-dependent electron effects and spin technologies".

1. G.A. Bochkin, E.B. Fel'dman, and A.I. Zenchuk. "Transfer of scaled multiple-quantum coherence matrices". Quant. Inform. Processing **17**, article 218, 2018.
2. S.A. Gerasev, E.I. Kuznetsova, A.V. Fedorova, and E.B. Fel'dman. "Theoretical investigations of quantum correlations in NMR multiple-pulse spin-locking NMR experiments". Quant. Inform. Processing **17**, article 72, 2018.
3. M. Goldman. *Spin Temperature and Nuclear Magnetic Resonance in Solids.* Clarendon Press, Oxford, 1970.

Quantum information processing with macroscopic BEC qubits

A.N. Pyrkov[1], T. Byrnes[2,3]
1. Institute of Problems of Chemical Physics RAS, 142432, Russia, Chernogolovka, Acad. Semenov av. 1,
E-mail address: pyrkov@icp.ac.ru
2. New York University Shanghai, 1555 Century Ave, Pudong, Shanghai 200122, China
3. Department of Physics, New York University, New York, NY 10003, USA

The achievements of quantum information theory such as Shor's factoring algorithm, Grover's search algorithm, algorithms of quantum machine learning and so on, motivate a lot of efforts to realize quantum computers with a variety of different physical systems from photons to superconducting circuits. Among systems proposed for quantum information processing macroscopic BEC qubits appear promising for overcoming some decoherence effects due to duplication of information in a huge number of bosons in the same state. In particular, the protocol of generation of entanglement between two macroscopic BEC qubits and protocol for teleportation of macroscopic BEC qubit were proposed [1-3].

Here we consider an artificial chain of macroscopic BEC qubits mutually connected by optical fiber and investigated entanglement between the ends of the chain depends on length of the chain and measurement results of the qubits in between. We show that entanglement decays slow with number of sites for the most probable measurement results. We investigate fidelity of the entanglement propagation protocol [4].
Furthermore, we shortly consider a new approach to quantum adiabatic computations on the basis of macroscopic BEC qubits and show that it gives an equivalent formulation of the original qubit-based problem with a constant no-zero value of minimum energy gap in the limit of huge number of particles in the ensemble [5]. This work is supported by the RFBR-NSFC collaborative program (Grants No. 18-57-53007, 81811530112).

1. A.N. Pyrkov, T. Byrnes, *Entanglement generation in quantum networks of Bose-Einstein condensates*, New J. Phys. **15**, 093019 (2013).
2. A.N. Pyrkov, T. Byrnes, *Quantum teleportation of spin coherent states: beyond continuous variables teleportation*, New J. Phys. **16**, 073038 (2014).
3. T. Byrnes, D. Rosseau, M. Khosla, A. Pyrkov, A. Thomasen, T. Mukai, S. Koyama, A. Abdelrahman, E. Ilo-Okeke, *Macroscopic quantum information processing using spin coherent states*, Optics Communications **337**, 102 (2015).
4. A.N. Pyrkov, T. Byrnes, *Entanglement distribution in a chain of macroscopic BEC qubits*, in preparation.
5. N. Mohseni, M. Narozniak, A.N. Pyrkov, V. Ivannikov, J.P. Dowling, T. Byrnes, *Adiabatic quantum computing with qubit ensembles*, submitted.

Graphene-based 2D heterostructures for terahertz photonic and plasmonic light-sources applications

D. Yadav[1], T. Watanabe[1], S. Boubanga-Tombet[1], A. Satou[1], V. Ryzhii[1,2], M. Ryzhii[3], A.A. Dubinov[4], W. Knap[5], V.V. Popov[6], and T. Otsuji[1]

1. Research Institute of Electrical Communication, Tohoku University, Sendai, Japan, otsuji@riec.tohoku.ac.jp
2. Institute of Ultra-High-Frequency Semiconductor Electronics, Moscow, Russia
3. Department of Computer Science and Engineering, University of Aizu, Aizu-Wakamatsu, Japan
4. Institute for Physics of Microstructures, RAS, Lobachevsky State University of Nizhny Novgorod, Nizhny Novgorod, Russia
5. Laboratory Charles Coulomb, University of Montpellier and CNRS, Montpellier, France
6. Kotelnikov Institute of Radio Engineering and Electronics (Saratov Branch), RAS, Saratov, Russia

Graphene has attracted considerable attention due to massless and gapless energy spectrum of Dirac Fermions as well as strong light-matter interactions via plasmon-polaritons. Carrier-injection pumping of graphene can enable negative-dynamic conductivity in the terahertz (THz) range, which may lead to new types of THz lasers [1-3]. Current-driven plasmon instabilities in graphene can promote the generation and amplification of THz waves [4, 5], leading to intense, room-temperature THz lasing. This paper highlights recent advances in related experimental studies and demonstrations.

The dual-gate graphene channel transistor (DG-GFET) structure serves carrier population inversion in the lateral p-i-n junctions under current-injection pumping, promoting spontaneous incoherent THz light emission [1, 2]. A laser cavity structure implemented in the active gain area can transcend the incoherent light emission to the single-mode lasing. We designed and fabricated the distributed feedback (DFB) DG-GFET [3]. The DG forms the DFB cavity having the fundamental mode, modal gain and the Q factor of 4.96 THz, ~5 cm^{-1}, and ~240, respectively. THz emission from the sample was measured using a Fourier-transform spectrometer with a 4.2K-cooled Si bolometer. Broadband rather intense (~10 ~ 100 μW) amplified spontaneous emission from 1 to 7.6 THz and weak (~0.1~1μW) single-mode lasing at 5.2 THz [3] were observed at 100K in different samples. When the substrate-thickness dependent THz photon field distribution could not meet the maximal available gain-overlapping condition, the DFB cavity cannot work properly, resulting in broadband LED-like incoherent emission. To increase the operating temperature and lasing radiation intensity, further enhancement of the THz gain and the cavity Q factor are mandatory.

Plasmonic metasurface structures promoting the instabilities [4,5]and/or superradiance [6] as well as double-graphene-layered van der Waals heterostructures promoting photon/plasmon-assisted resonant tunnelling [7,8] are promising for giant THz gain enhancement.

This work was financially supported by JSPS-KAKENHI No. 16H06361 and No. 16K24374, Japan.

1. M. Ryzhii and V. Ryzhii. “Injection and population inversion in electrically induced p–n junction in graphene with split gate”. Jpn. J. Appl. Phys., **46**, pp. L151-L153, 2007.
2. V. Ryzhii, M. Ryzhii, V. Mitin, and T. Otsuji. “Toward the creation of terahertz graphene injection laser”. J. Appl. Phys., **110**, 094503, 2011.
3. D. Yadav, G. Tamamushi, T. Watanabe, J. Mitsushio, Y. Tobah, K. Sugawara, A.A. Dubinov, A. Satou, M. Ryzhii, V. Ryzhii, and T. Otsuji. “Terahertz light-emitting graphene-channel transistor toward single-mode lasing”. Nanophoton., **7**, pp. 741-752, 2018.
4. Y. Koseki, V. Ryzhii, T. Otsuji, V.V. Popov, and A. Satou, “Giant plasmon instability in a dual-grating-gate graphene field-effect transistor”. Phys. Rev. B, **93**, 245408, 2016.
5. S. Boubanga-Tombet, D. Yadav, W. Knap, V.V. Popov, and T. Otsuji. “Plasmonic instabilities and terahertz waves amplification in graphene metamaterials”. arXiv 1801.04518, 2018.
6. V.V. Popov, O.V. Polischuk, A.R. Davoyan, V. Ryzhii, T. Otsuji, and M.S. Shur. “Plasmonic terahertz lasing in an array of graphene nanocavities”. Phys. Rev. B, **86**, 195437, 2012.
7. V. Ryzhii, A.A. Dubinov, T. Otsuji, V.Ya. Aleshkin, M. Ryzhii, and M. Shur. “Double-graphene-layer terahertz laser: concept, characteristics, and comparison”, Opt. Exp., **21**, pp. 31567-31577, 2013.
8. D. Yadav, S. Boubanga-Tombet, T. Watanabe, S. Arnold, V. Ryzhii, T. Otsuji. “Terahertz wave generation and detection in double-graphene layered van der Waals heterostructures”. 2D Mater., **3**, 045009, 2016.

Graphene-phosphorene hybrid structures and their applications

V. Ryzhii[1,2,3,4], T. Otsuji[1], M. Ryzhii[5], V. Leiman[4], D. Ponomarev[2,4], P.P. Maltsev[2], D. Svintsov[4], V. Mitin[6], and M.S. Shur[7]

1. Research Institute of Electrical Communication, Tohoku University, Sendai, Japan
2. Institute of Ultra-High-Frequency Semiconductor Electronics, RAS, Moscow, Russia
3. Center of Photonics and Infrared Engineering, Bauman Moscow State Technical University, Moscow
4. Center of Photonics and Two-Dimensional Materials, Moscow Institute of Physics and Technology, Russia
5. Department of Computer Science and Engineering, University of Aizu, Aizu-Wakamatsu, Japan
6. Department of Electrical Engineering, University at Buffalo, Buffalo, USA
7. Department of Electrical, Computer, and Systems Engineering, Rensselaer Polytechnic Institute, Troy, USA
E-mail: v-ryzhii@riec.tohoku.ac.jp

The hybrid structures comprising graphene (G) and phosphorene (P), i.e., a two-dimensional form of black phosphorus, are very promising for different device applications. We analyze the nonlinear carrier transport in the gated G-P hybrid structures - the G-P -field-effect transistors (G-P-FETs) using a phenomenological model. Figure 1 shows the G-P-FET under consideration and the band diagram and the energy dependence of the density of state of its G-P-channel. The developed model assumes that due to high carrier densities in the G-P-channel, the carrier system, including the electrons and holes in both the G- and P-layers, is characterized by a single effective temperature. We demonstrate that a strong electric-field dependence of the G-P-channel dc and ac conductivity and substantially non-linear current-voltage characteristics, exhibiting a negative differential conductivity [1], are associated with the carrier heating and the real-space carrier transfer between the G- and P-layers. The predicted features of the G-P-systems can be used in the detectors [2], modulators [3], and sources of electromagnetic radiation and in the logical circuits. Applying our model for the detectors and electrically-controlled modulators of the terahertz radiation [2], we evaluated their characteristics and show that these devices can compete or surpass the existing devices.

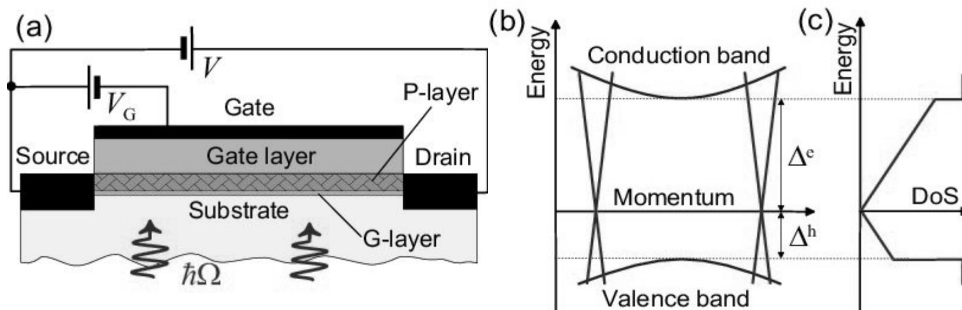

Fig. 1. Schematic view of (a) the G-P-FET structure with generally asymmetric with respect to the Dirac point energy spectrum, (b) the G-P energy spectrum with the G-Dirac cones and the parabolic extrema corresponding to the P-layer, and (c) density of state (DoS).

1. V. Ryzhii, M. Ryzhii, D. Svitsov, V.G. Leiman, P.P. Maltsev, D.S. Ponomarev, V. Mitin, M.S. Shur, and T. Otsuji,"Real-space-transfer mechanism of negative differential conductivity in gated graphene-phosphorene hybrid structures: Phenomenological heating model". arXiv:1806.06227 (2018).
2. V. Ryzhii, M. Ryzhii, D.S. Ponomarev, V.G. Leiman, V. Mitin, M.S. Shur, and T. Otsuji, "Negative photoconductivity and detection of terahertz radiation in gated graphene-phosphorene hybrid structures" (unpublished).
3. V. Ryzhii, T. Otsuji, M. Ryzhii, D.S. Ponomarev, V.G. Leiman, V. Mitin, and M.S. Shur, "Electrical modulation of terahertz radiation using graphene-phosphorene heterostructures" (unpublished).

Photonic Double-Mixing by InGaAs-HEMTs for Optical to MMW/THz Carrier Frequency Down-Conversion

A. Satou[1,3], Y. Omori[1,3], S. Manabe[1,3], T. Hosotani[1,3], T. Suemitsu[2,3], and T. Otsuji[1,3]

1. Research Institute of Electrical Communication, Tohoku University, Sendai, Japan, a-satou@riec.tohoku.ac.jp
2. Center for Innovative Integrated Electronic Systems, Tohoku University, Sendai, Japan
3. Research Organization of Electrical Communication, Tohoku University, Sendai, Japan

For future high-capacity, seamless convergence of fiber and wireless networks, a carrier-frequency down-converter from optical data signals to millimeter-wave (MMW)/terahertz (THz) data signals is needed. We have studied the so-called photonic double-mixing functionality of InGaAs-channel high-electron-mobility transistors (InGaAs-HEMTs) to perform the conversion of the 1.5-μm bands to the MMW bands[1,2]. The photonic double-mixing comprises two mixing functionalities: the usual photomixing of a optical carrier signal and an optical subcarrier signal, which generates the difference-frequency beat-note signal, and the RF mixing of the beat-note signal and an RF signal, which generates an IF data signal (i.e., a double-mixed signal) with a desired frequency. The photomixing can be realized using a transistor structure with high-speed photodetection functionality, if the photomixed current is generated either by the direct photoabsorption in the channel or by the injection from a certain absorption layer into the channel, while the RF mixing can be realized by impinging the RF signal to the gate and utilizing the nonlinear I-V characteristics. We have demonstrated the frequency down-conversion of a 10-Gbps-class ASK or BPSK modulated optical data signal into an IF signal at 22.5 GHz by using an InGaAs-HEMT[2]. However, the double-mixing conversion gain of the InGaAs-HEMT is very low due to its very thin absorption layer (i.e., the channel layer) and also due to generation of photoholes in the channel, which limit the high-speed operation due to their very low mobility. Besides, in order to extend the RF/IF bands further to the THz region, the limitition of the operation frequency bandwidth by the electron transit time must be overcome.

In this work, we investigated two strategies to overcome those issues: (i) integration of the uni-traveling-carrier photodiode (UTC-PD) structure in an InGaAs-HEMT for improvement of photoabsorption efficiency and fast extraction of photogenerated holes and (ii) utilization of plasmon resonances in the channel for the THz double-mixing. We fabricated an InGaAs-HEMT integrated with the UTC-PD structure on its source side (Fig. 1), measured its photomixing performance in the MMW region (Fig. 2), and observed more than 10-dB enhancement of photomixing conversion gain by the introduction of the UTC-PD structure, compared with a standard InGaAs-HEMT without the UTC-PD structure. We also conducted a theoretical study of the THz double-mixing utilizing the hydrodynamic nonlinearities of the 2D plasmons and the plasmon-resonance effect by extending the hydrodynamic model. We demonstrated that they can be utilized to extend the operation frequency bandwidth of the double-mixing to the THz region.

1. K. Sugawara *et al.*, "Photonix frequency double-mixing conversion over the 120-GHz band using InP- and graphene-based transistors," J. Lightwave Technol., **34**, 2011-2019, 2016.
2. A. Satou and T. Otsuji, "Millimeter-wave/terahertz detection and photonic double-mixing by transistors," Proc. SPIE, **10403**, 104030S 1-12, 2017.

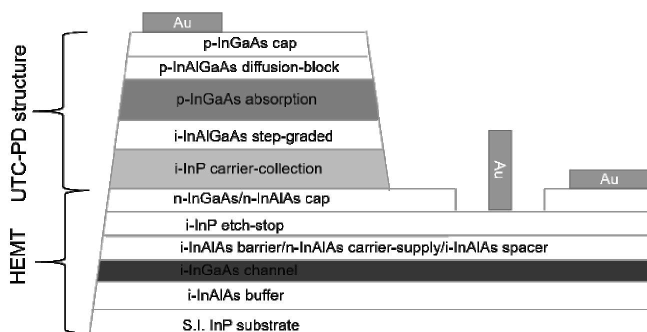

Fig. 1. Cross-sectional schematic view of a UTC-PD-integrated InGaAs-HEMT.

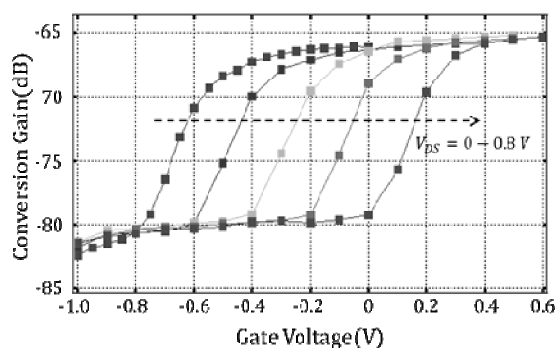

Fig. 2. The measured bias dependence of photomixing conversion gain of a UTC-PD-integrated InGaAs-HEMT.

Graphene plasmonics for resonant voltage-tunable terahertz detectors

D. Svintsov[1], D. Bandurin[2], I. Gayduchenko[3], G. Fedorov[1], A. Geim[2], G. Goltsman[3]
1. Moscow Institute of Physics and Technology, Dolgoprudny 141700, Russia
2. School of Physics and Astronomy, University of Manchester, Manchester M13 9PL, UK
3. Moscow State University of Education (MSPU), Moscow 119435, Russia

High electron mobility transistors can act as resonant detectors of terahertz (THz) radiation due to the possibility of plasmon excitation by incident field [1]. Graphene, a prototypical high-electron mobility material, was proposed as efficient resonant photodetector. However, measurements of THz photocurrent in antenna-coupled graphene field-effect transistors (FETs) so far demonstrated only broadband response [2, 3].

In this paper, we report the observation of resonant plasmonic THz detection in graphene FETs [4]. Source and gate terminals of the FET were connected to the THz antenna, the dc photovoltage was read out between source and drain (Fig. 1) and peaked at the values of gate voltage corresponding to standing wave plasmon resonances in the FET channel (Fig. 2). The key factor enabling the observation of plasma resonances is the use of bilayer graphene (BLG) encapsulated in hexagonal boron nitride as FET channel. Compared to single-layer, BLG has larger effective mass and comparable mobility (~10 m^2/Vs at 10 K), which results in long momentum relaxation time ~2 ps and high plasmon quality factor. By varying the plasmon velocity with gate, we observe eight resonant harmonics on both electron- and hole doping sides.

The observed resonances not only enable high-responsivity THz detection with graphene FETs. We show that photocurrent spectroscopy can be also used as a tool to study the plasmon dispersion and damping. Particularly, we elaborated the density dependence of plasmon wavelength, which reached up to 150 times smaller values compared to free-space wavelength. The width of plasmon resonances provided us with valuable information on plasmon lifetime. The proposed technique is readily extended to other 2d electronic systems and to plasmon spectroscopy under non-ambient conditions (low temperatures, high magnetic fields, non-equilibrium carrier populations). It can be also used for the search of novel collective modes, particularly those arising from strong carrier-carrier interactions.

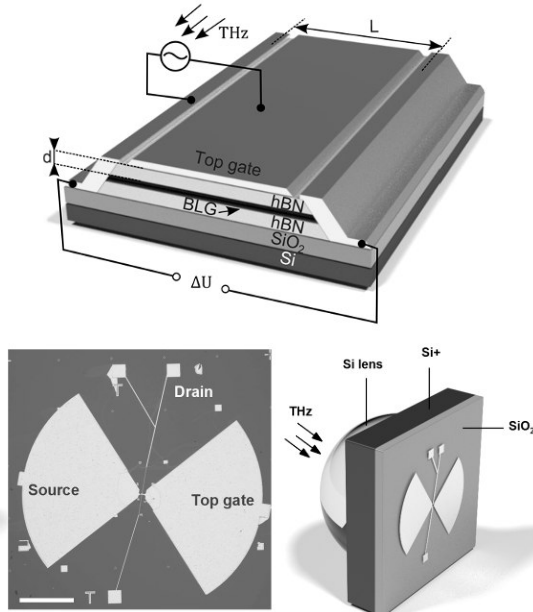

Fig. 1. (top) Schematic of graphene-based THz detector (bottom left) Optical image of the device with antenna (bottom right) Arrangement of device on substrate for THz measurements.

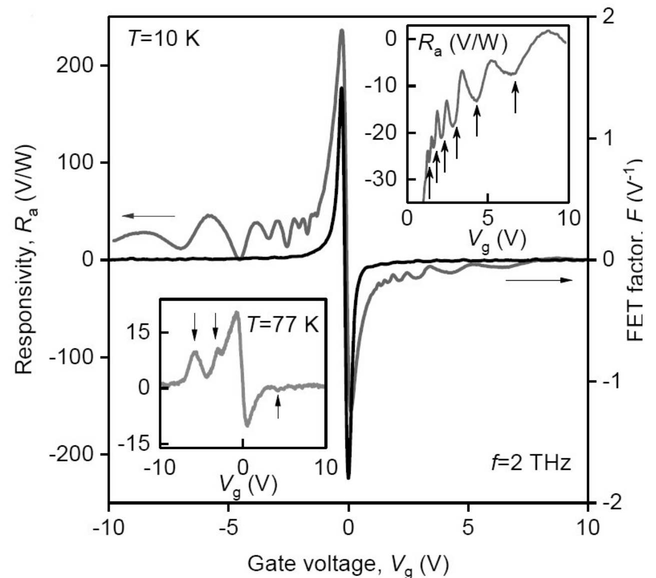

Fig. 2. Measured dependence of photovoltage on gate voltage at f=2 THz and T=10 K (red) and T=77 K (blue, inset). Black line shows the measured sub threshold slope.

1. M. Dyakonov, M. Shur, *IEEE Trans. El. Dev.* **43**, 380-387 (1996).
2. L. Vicarelli *et.al. Nature Materials* **11**, 865 (2012).
3. D. Bandurin, I. Gayduchenko, Y. Cao, M. Moskotin, A. Principi, I. Grigorieva, G. Goltsman, G. Fedorov, D. Svintsov, *Appl. Phys. Lett.* **112**, 141101 (2018).
4. D. Bandurin, D. Svintsov, I. Gayduchenko, S. Xu, A. Principi, M. Moskotin, I. Tretyakov, D. Yagodkin, S. Zhukov, T. Taniguchi, K. Watanabe, I. Grigorieva, M. Polini, G. Goltsman, A. Geim, G. Fedorov, *arXiv preprint arXiv:1807.04703* (2018).

Maskless nanolithography on the basis of microfocus X-ray tubes: conversion of electron energy into the BeKα line

N.I. Chkhalo[1], A.Ya. Lopatin[1], A.E. Pestov[1], N.N. Salashchenko[1], G.D. Demin[2], N.A. Dyuzhev[2], M.A. Makhiboroda[2]

1. Institute for physics of microstructures RAS, Nizhny Novgorod, Russia, lopatin@ipmras.ru

2. National University Research Institute of Electronic Technology, Zelenograd, Russia, djuzhev@ntc-nmst.ru

Projection photolithography (PPL) is the key technology of micro (nano) electronics, which determines the critical topological size of microcircuits. The most advanced topologies are achieved with the use of immersion at a wavelength of 193 nm and the extreme ultraviolet (EUV), at a wavelength of 13.5 nm, photolithography [1, 2]. The most complex and expensive elements of the infrastructure of the PPL are masks. A set of masks only in the production of a single chip can cost up to several million dollars. Therefore, because of the high cost of equipment, the high cost of masks, complex and expensive infrastructure, the PPL becomes competitive only for mass (global) production, while the market for small- and medium-scale production (up to hundreds of thousands of chips per year) is not inferior in value expression global. Therefore, it is extremely urgent to find new tools for nanolithography.

The hypothetical nanolithograph should provide the same topological norms, which gives the PPL in the region of 100-10 nm and less. The performance of such a nanolithograph can be one to three orders of magnitude lower, there should be no masks, and the cost of the lithographic process should not depend heavily on the scale of production. It is also important that the cost of a lithograph is comparable to the cost of an industrial single-beam electron lithograph. In this case, we can say that the production of nanoelectronics will become available not only to single global companies, but also to smaller companies, which is critically important for our country.

At present, multi-beam electron lithography (MBEL) is considered the most promising for such kind of the lithography. However, despite the successes, in particular in productivity [3], the prospects of MBEL are not obvious due to the strong heating of the wafer with resist in the litho process and the inter-beam interaction. As an alternative, also maskless EUV lithography is considered [4]. However, the unresolved problem of creating an effective spatial light modulator for the EUV radiation suppresses its development.

In [5], we proposed a new approach to nanolithography - a maskless X-ray lithography based on a microfocus X-ray tube chip with a thin-film target. This report discusses the basic principles of this method of nanolithography, gives the results of measurements of the conversion efficiency of electron energy to the energy of the BeKα characteristic line ($\lambda = 11.4$ nm), considers alternative wavelengths, gives data on the expected productivity of the lithograph at the most promising wavelengths.

1. S. Jones. “TSMC's 10 nm process offers the highest transistor density”. 2018. https://seekingalpha.com/article/4151376-tsmc-intel-lead-semiconductor-processes
2. S.-S. Kim, R. Chalykh, H. Kim et al. “Progress in EUV lithography toward manufacturing”. Proc. SPIE, **10143**, p. 1014306, 2017.
3. I. Servin, N.A. Thiam, P. Pimenta-Barros, et al. “Ready for multi-beam exposure at 5kV on MAPPER tool: Lithographic & process integration performances of advanced resists/stack”. Proc. SPIE, **9423**, p. 94231C, 2015.
4. N. Choksi, D.S. Pickard, M. McCord, et al. “Maskless extreme ultraviolet lithography”. JVST B, **17**, p. 3047, 1999.
5. N.A. Dyuzhev, G.D. Demin, T.A. Gryazneva et al. “Microfocus X-ray tubes with a silicon field emission nanocathode as a source of X-ray radiation”. Brief Communications on Physics AS, **12**, pp. 56-63, 2017.

Cellular automata method for directed self-assembly modeling

E. Gornev[1,2], M. Litavrin[1,2], I. Matyushkin[1], O. Gushin[1]
1. Molecular Electronics Research Institute, Zelenograd, Russia, niime@niime.ru.
2. Moscow Institute of Physics and Technology, Dolgoprudny, Russia, intoff@mipt.ru

Advanced immersion scanners can provide a resolution of single lithography down to 38 nm, which is clearly not enough for technology node 22 nm and lower. Further scaling 22-14- ... nm is carried out by multipatterning, which is expensive, especially at advanced technology nodes. Thus, alternative advanced lithographic methods are intensively being developed, one of which is Directed Self-Assembly (DSA) [1]. The work is aimed on the self-assembly process modeling with the method of cellular automata (CA) and using the theory of copolymers relations. The use of CA is relevant, because they are convenient [2] for describing the self-organization processes.

The DSA-method is based on using the thermodynamic properties of block copolymers for the controlled formation of a nanoscale structure, which is subsequently used as a mask for etching. This structure is formed in the process of thermodynamic microphase separation during annealing. Self-assembly control is carried out by means of a previously formed guiding structure. The method allows us to form both lamellar domains (for metallization lines) and cylindrical domains (for contact holes and via). One type of the formed domains can be removed selectively for domains of a different type (usually in a plasma). The sizes of domains lie within the limits of 5-50 nm.

The proposed CA is three-dimensional and consists of several horizontal layers of hexagonal "washers" displaced relative to each other in order to obtain a better uniformity. The size of the CA cell correlates with the Kuhn segment length l = 1.67 nm for the block-copolymer polystyrene-poly(methylmethacrylate) (PS-b-PMMA). The length of the polymer chain is about 400 segments and about 30 segments fit into one cell of the CA (the total number of chains is 500). The CA operates in a pair-asynchronous mode with a unified neighborhood. The cell state is a set of records <polymer number, number of PS links, number of PMMA links>; each polymer is distributed between the cells. The local transition function is specified with an alternation controlled by: a) a configuration filter for continuity of the circuit (which is new for the CA-technique); b) transition probabilities. In a first approximation, polymer chains move independently, and the only correlation is given by the amount of free volume (in Kuhn segments).

The transition probabilities are parameterized based on the data [4] on the change in the Gibbs energy. The key question of the computational experiment is to reveal the influence of boundary conditions on the dynamics of CA from an initial, globally "indefinite" state. The results of preliminary calculations are given.

1. G. Krasnikov, O. Gushin, M. Litavrin, E. Gornev. Complementary resolution enhancing technique for immersion lithography DSA // Electronnaya Technika. Series 3: Mikroelectronica, 2017. P. 4-17 (in Russian).
2. G. Krasnikov, E. Gornev, I. Matyushkin, R. Vildanov, S. Korobov. Cellular automata and nanoindustry // Nauchnoe obozrenie, 2015, №1, P. 161-172 (in Russian).
3. G. Willson et al. High χ Block Copolymers: A Progress Report / Conference Paper / 1st DSA symposium, At Leuven, Belgium, 2015.
4. F. Delachat et al. Advanced surface affinity control for DSA contact hole shrink applications, Proc. SPIE **10144**, Emerging Patterning Technologies, 101440O (21 March 2017).

E-beam lithography of dense 10 nm line/space pattern using the HSQ mask

A.A. Tatarintsev[1], A.V. Miakonkikh[1], K.V. Rudenko[1], A. Shishlyannikov[2]
1. Institute of Physics and Technology of Russian Academy of Science, Moscow, Russia.
2. JSC Molecular Electronics Research Institute, Zelenograd, Russia
E-mail: tatarintsev@ftian.ru

Sub-10-nm nanostructures or gaps in metal structures is very important in modern nanoscale devices such as plasmonic devices, plasmonic antennas [1], the silicon nanoscale integrated transistors [2], the molecular-electronics devices, and THz sources [3] and receivers. Various approaches were developed to form the sub-10-nm elements in such devices; however, despite this, the reproducible direct formation of nanoscale structures by electron-beam lithography always preferable.

The electron beam resist based on hydrogen silsesquioxane (HSQ) is a widely used nonorganic-silicon negative electron beam resist which possesses ultrahigh resolution, comparatively good etch resistivity in reactive ion etching (RIE) process, and mechanical durability. With the emergent of the method of the high-contrast development of the negative electron beam HSQ resist in an alkali-salt solution, lines of 10 nm in width [4] were achieved. A novel method for the formation of ultrasmall gaps in metal structures by electron-beam lithography on a negative electron beam HSQ resist was shown in [1].

This report presents the main features and methods for patterning of the structures with an increased density of elements using the e-beam resist HSQ XR-1541 manufactured by Dow Corning. Obtained structures with lines ~ 10 nm in size with an interval between adjacent lines ~ 20 nm and ~ 30 nm are shown on figure 1.

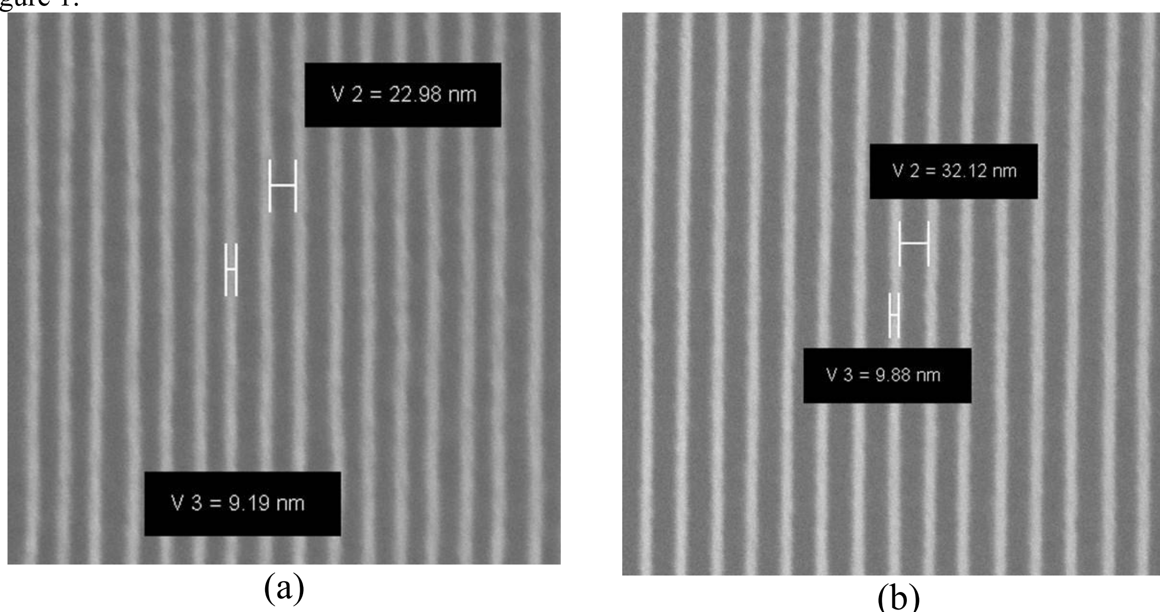

(a) (b)

Fig. 1. Lines with a width of ~ 10 nm with an interval between neighboring lines ~ 20 nm (a) and ~ 30 nm (b).

1. Duan H., Hu H., Hui H.K., Shen Z., Yang J. K. W. Free-standing sub-10 nm nanostencils for the definition of gaps in plasmonic antennas // Nanotech. 2013. **24**. 185301.
2. Franklin A.D., Luisier M., Han S.J., Tulevski G., Breslin C.M., Gignac L., Lundstrom M.S., Haensch W. Sub-10 nm carbon nanotube transistor // Nano Lett. 2012. **12**(2). 758-762.
3. R. Khabutdinov et al. Low-dimensional transit-time diodes for terahertz generation // Proc. SPIE V. 10224. P. 102240M.
4. Yang J. K. W., Berggren K.K. Using high-contrast salty development of hydrogen silsesquioxane for sub-10nm-half-pitch lithography // J. Vac. Sci. Technol. B. 2007. **25**(6). 2025.

Simulation of hybrid e-beam lithography: experimental evidence

A. Rogozhin[1,2], F. Sidorov[1,2], M. Bruk[1,3], E. Zhikharev[1]
1. Institute of Physics and Technology of RAS, Moscow 117218, Russia, rogozhin@ftian.ru
2. Moscow Institute of Physics and Technology (MIPT), Moscow, Russia
3. L.Ya. Karpov Institute of Physical Chemistry, Moscow 105064, Russia

Formation of modern integrated circuits, micro- and nanostructures requires lithography resolution of less than 10 nm. The resolution of e-beam lithography is high enough but its throughput is extremely low. It is possible to increase throughput using highly-sensitive resists, for example chemically amplified resists [2]. Unfortunately high resist sensitivity results in lower resolution. Recently great progress has been achieved in the field of chemical amplification but required doses are still high [3].

At the elevated temperatures (higher than glass transition temperature of the resist) sensitivity of the resist grows manifold [4, 5]. This amplification has similar nature as in chemically amplified resists. E-beam exposure launches chain depolymerization reaction. Thermal amplification of resist has lots in common with chemical amplification of resist. It could be one of possible approaches to improve throughput of e-beam lithography. Thermal amplification of resist can provide sensitivity increase by a factor of hundreds. For example in our experiments the same trench depths were obtained by ordinary e-beam lithography with exposure dose of 50 μC/cm2 and by thermally amplified e-beam lithography with exposure dose of 0.48 μC/cm2. Some structures obtained by the hybrid e-beam lithography (and exposure doses) are presented on fig. 1 (a). As a result throughput of the e-beam lithography could be increased dramatically.

For the simulation of electron tracks in PMMA/Si system “direct” Monte Carlo method is applied. In this method, all the dominant processes (elastic scattering, excitation, ionization and secondary electron generation for E < 20 keV) are simulated separately. The results of the simulation are presented. Simulated profiles and some other parameters (fig. 1(b)) are compared to the experimental result.

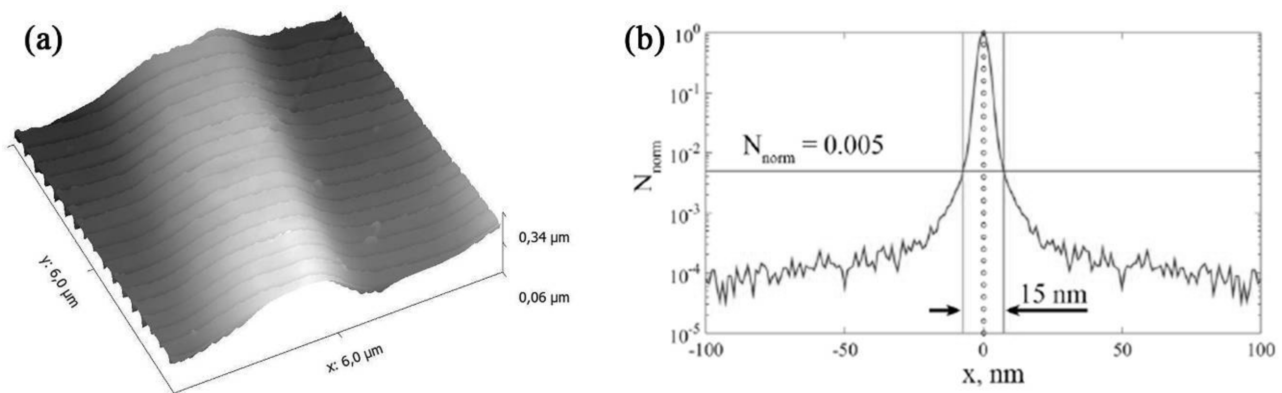

Fig. 1. (a) 3D AFM image of the sample obtained by hybrid e-beam lithography; (b) simulated distribution of electron scattering events in PMMA.

1. M. Hori, T. Naruoka, H. Nakagawa, T. Fujisawa, T. Kimoto, M. Shiratani, T. Nagai, R. Ayothi, Y. Hishiro, K. Hoshiko, T. Kimura, Proc. SPIE, **9422** (2015), Article 94220P.
2. D.X. Yang, A. Frommhold, A. McClelland, J. Roth, M. Rosamond, E.H. Linfield, J. Osmond, R.E. Palmer, A.P.G. Robinson, Microelec. Eng., **155**, 97-101 (2016).
3. M.A. Bruk, E.N. Zhikharev, D.R. Streltsov, V.A. Kalnov, A.V. Spirin. Microelec. Eng., **112**, 1 (2013).
4. M.A. Bruk, E.N. Zhikharev, A.E. Rogozhin, D.R. Streltsov, V.A. Kalnov, S.N. Averkin, and A.V. Spirin. Microelec. Eng., **155**, 92 (2016).

Simulation algorithm of PMMA depolymerization in dry e-beam etching of resist

A. Rogozhin[1], F. Sidorov[1,2], M. Bruk[1], E. Zhikharev[1]

1. Institute of Physics and Technology of RAS, Moscow 117218, Russia
2. Moscow Institute of Physics and Technology, Dolgoprudny, 141701, Russia

Method of dry e-beam etching of resist (DEBER) proposed by Bruk et al. [1] is based on chain reaction of resist depolymerization during e-beam exposure at temperatures higher than glass transition. DEBER provides high throughput of the etching process, but lateral its resolution is low (about 300 nm). In order to optimize process parameters for various purposes, reconstruction of e-beam interactions with resist has been carried out with subsequent simulation of resist thermal depolymerization.

The reconstruction of e-beam interactions with resist includes simulation of electron interactions with resist atoms and simulation of polymer chains. The simulation of electron interactions with resist atoms is based on Direct Monte-Carlo (DMC) algorithm [2], which covers dominant processes at energies of interest ($E < 20$ keV) – elastic scattering, ionization with secondary electron generation and excitation [3]. DMC algorithm allows independent simulation of processes mentioned above, which provides the information on local chemical changes. The simulation of polymer chains has been performed in 'intermediate scale', with resist monomers generated as beads arranged on string, satisfying rigid-bond model [4]. The pitch and cone between successive monomers are 0.28 nm pitch and 109° respectively, while the rotation angle is determined by random, avoiding chain overlap with itself. The separated chains are then combined in required area taking into consideration resist density (1.19 g/cm^3 for PMMA).

Electron interaction events and resist monomer coordinates are then mapped in cubic lattice with 0.5 nm size, which provides the positions of scission events. The distribution of chain lengths after exposure and structure of reaction products are determined then. Simulation of chain resist depolymerization is based on the approach described in the study of Bruk et al [5], which suggests sequential detachment of ~1000 monomers by every scission event in PMMA.

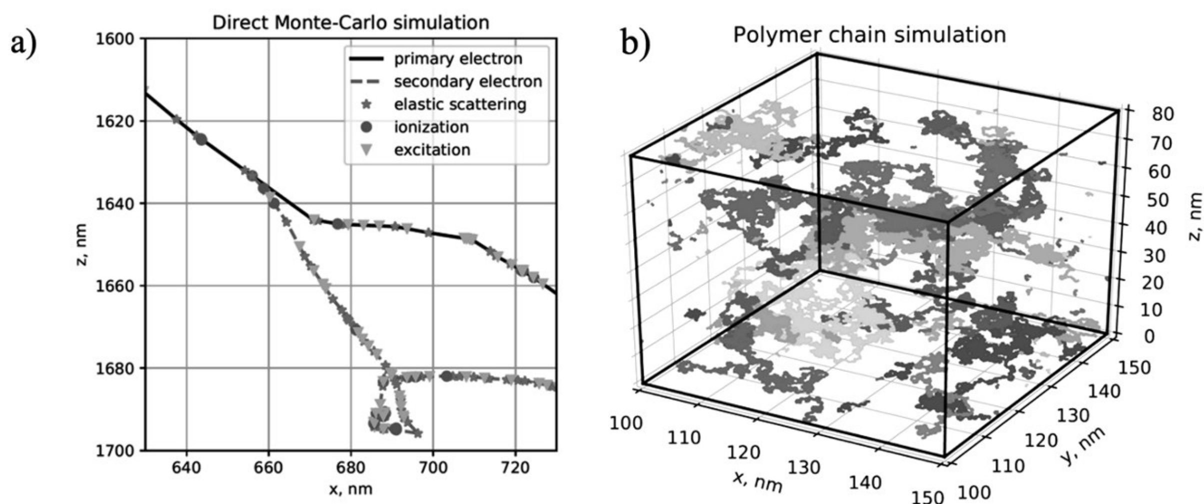

Fig. 1. a) Primary and secondary electron tracks simulated using Direct Monte-Carlo algorithm, b) simulation of PMMA 950K chains (some chains are ignored for visibility).

1. M.A. Bruk, E.N. Zhikharev, D.R. Streltsov, V.A. Kalnov, A.V. Spirin. Microelectron. Eng., **112**, 1, 2013.
2. G. Han, M. Khan, Y. Fang, F. Cerrina. J. Vac. Sci. Technol. B, **20**, 6, 2002.
3. D.E. Cullen et al., Lawrence Livermore National Lab., UCRL-50400, 6, 5, 1997.
4. G. Han, M. Khan, F. Cerrina. J. Vac. Sci. Technol. B, **21**, 3166 (2003).
5. M.A. Bruk et al., Rus. Microelectron., **42** (5), pp. 261–269, 2013.

Diffraction model of the electronic transport in rough normal metal and ferromagnetic nanowires

G.M. Mikhailov[1], L.A. Fomin[1], and A.E. Rassadin[2]
1. Institute of Microelectronic Technology and High Purity Materials RAS, Chernogolovka, Russia, mikhailo@iptm.ru. 2. Member of the Board of Nizhny Novgorod Mathematical Society, Nizhny Novgorod, Russia, brat_ras@list.ru

In recent years, the scientific interest in the studies of electronic transport in nanosized metallic conductors with a rough surface has renewed because of its potential application in sub-10-nm-electronics. It is well known that the electrical conductor with translational symmetry will not resist the current. However, such symmetry can be disturbed by thermal phonons, as well as by static defects, that violate the perfect crystalline structure. The conductors of such a small size have to be considered as rough waveguides for electron waves, in which the morphology of the boundaries determines the electrical conductivity of them.

In this work an application of the diffraction model to the electronic transport in rough nanowires is reported. In this model a quasiclassic approximation is used to some extent [1]. The model introduces the diffraction angle for each $\alpha_d = \pi/(dk_F)$, where d is characteristic transverse size of the conductive wire, and also the blocking angle $\alpha_b = a/b$, where a is the square root of the roughness dispersion, and b is the correlation length. The condition when the sum of the diffraction angle and the blocking angle is equal to the effective angle $\alpha^* = (d/(Ql_0))^{1/2}$, is considered. Here the parameter $Q = -\partial p/\partial\alpha$ characterizes the intensity of the electron momentum dissipation by the surface scattering, and the l_0 is the mean free path of conductive electrons in the bulk of the nanoconductor. It includes electron scattering on phonon and bulk static defects. It is important that there is a minimal restriction angle $\alpha_r = \alpha_d + \alpha_b$ of the incidence to the surface for small-angle electrons. Otherwise, if $l_0 \to \infty$, the conductivity of a nanowire is diverged. This circumstance changes the classic small-angle model of the electronic transport. As a result, the diffraction model gives the following expression for the conductivity of the wire:

$$\frac{\sigma}{\sigma_0} = \frac{l}{l_0} = 3\alpha^{*2}\left(\sqrt{1+\alpha^{*2}}\,\ln\left(\left(\frac{1}{\alpha^*} + \sqrt{1+\frac{1}{\alpha^{*2}}}\right)\frac{\gamma}{\sqrt{1+\gamma^2}}\right) - 1\right) \quad (1),$$

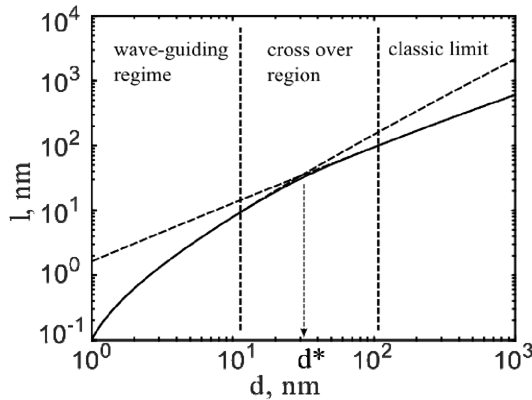

Figure 1. The effective mean free path of electrons as a function of the nanowire's diameter. The asymptotes are indicated by dashed lines. A characteristic diameter value for the transition from a classic to a wave-guiding limit is shown by an arrow.

where l is the effective mean free path of electrons, and $\gamma = \alpha^*/\alpha_r$. The result of the calculation with use of this expression is shown in figure 1. In the region of large wire diameters there is a classic limit where the dependence of l upon the diameter is close to linear. When the diameter is small we have a wave-guiding regime [2]. In the transition region where $d \approx d^*$ the dimensional dependence of l is nonlinear. There is some analogy between wave-guiding regime of electron transport in the films [3] and wires. However, no microscopic model that relates surface scattering parameters of rough nanowire has been developed yet.

The conductivity of the wires made from ferromagnetic metals is a sum of conductivities belonged to electrons of each spin subbands. In a simple two spin channel model there are two conductivities for spin-up and spin-down electrons. Both of them depend on the surface roughness that defines electron scattering parameters.

1. K. Fuchs. "The conductivity of thin metallic films according to the electron theory of metals". Proc. Cambridge Phil. Soc., **34**, pp. 100-108, 1938.
2. N.M. Makarov, Yu.V. Tarasov. "Electron localization in narrow surface-corrugated conducting channels: Manifestation of competing scattering mechanism". Phys. Rev. B, **64**, pp. 235306-1-14, 2001.
3. G.M. Mikhailov, I.V. Malikov, A.V. Chernykh. "Influence of quantum size effect for grazing electrons on electron conductivity of metallic films". JETP Letters **66**, pp. 725-732, 1997.

Static and dynamic spin-torque-diode sensitivity induced by the thermoelectric charge and spin currents in magnetic tunnel junctions

G.D. Demin[1,2], A.F. Popkov[1,2]

1. Moscow Institute of Physics and Technology (State University), Dolgoprudny, Russia, demin.gd@phystech.edu

2. National Research University of Electronic Technology (MIET), Moscow, Russia, gddemin@edu.miet.ru

The search for new applications of spin caloritronics, which determines the relationship between charge, spin and heat currents in the presence of temperature gradient across the tunnel barrier in magnetic tunnel junctions (MTJ), is still of particular interest to researchers [1, 2]. An intersection of this field and the rectification effect of an alternating current, which generates the rectified direct-current (DC) voltage in MTJ-based spin-torque diode [3], can open an original method for the thermal control of the spin-torque-diode sensitivity, caused by the inhomogeneous heating of MTJ during its microwave irradiation (Fig. 1). In the static regime, this contribution to the spin-torque sensitivity can be related to the tunnel magneto-Seebeck effect in MTJ, while in the dynamic regime the sensitivity additive shift is determined by the magnetodynamic response of the free layer of MTJ to the thermal spin-transfer torques due to the non-zero temperature gradient across the tunnel barrier [4].

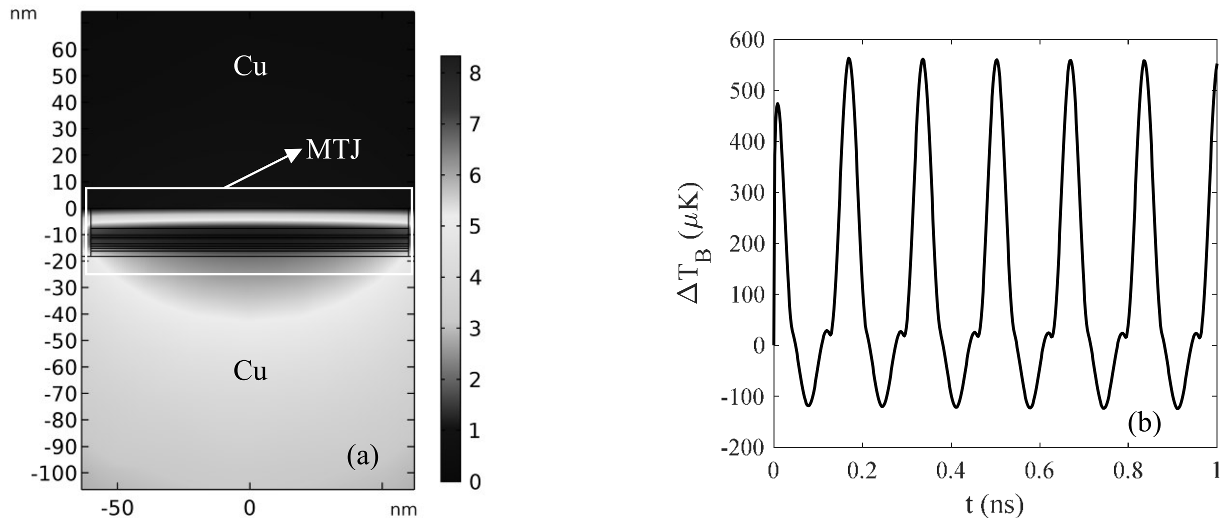

Fig. 1. (a) The temperature increment $T\text{-}T_0$ (in mK) of MTJ generated by the input microwave power of 1 μW, where T_0 = 20 K is the room temperature. (b) Time dependence of the temperature drop on both sides of the tunnel barrier of MTJ, induced by the input microwave power of 1 μW at the current frequency of 6 GHz.

Based on the quantum-mechanical transport calculations of the charge and spin fluxes associated with the inhomogeneous thermal heating of three-dimensional structure of MTJ by the input RF microwave power, finite-element analysis of the thermal contribution to the spin-torque sensitivity of MTJ was carried out in the case of nonzero bias current. Within the magnon-induced spin-transfer torque model suggested by J. Slonczewski in [5], the amplification of DC rectifying voltage in the spin-torque diode initiated by the spin pumping to the tunnel barrier from magnons was also estimated. The results obtained can be used for the development of new types of microwave detectors based on spin thermoelectric effects in MTJ. The work was supported by the Russian Science Foundation (project № 16-19-00181).

1. G.E.W. Bauer, E. Saitoh, and B.J. van Wees. "Spin caloritronics". Nat. Mater., **11**, pp. 391-399, 2012.
2. H. Yu, S.D. Brechet, and J.-P. Ansermet. "Spin caloritronics, origin and outlook". Phys. Lett. A, **381**(9), pp. 825-837, 2017.
3. A.A. Khudorozhkov, P.N. Skirdkov, K.A. Zvezdin, P.M. Vetoshko, and A.F. Popkov. "Spin-torque diode frequency tuning via soft exchange pinning of both magnetic layers". Phys. Rev. B, **96**, p. 214410, 2017.
4. M. Wilczyński. "Thermopower, figure of merit and spin-transfer torque induced by the temperature gradient in planar tunnel junctions". J. Phys.: Condens. Matter, **23**, p. 456001, 2011.
5. J.C. Slonczewski. "Initiation of spin-transfer torque by thermal transport from magnons". Phys. Rev. B, **82**, p. 054403, 2010.

Quantization and thermal effects during the scalability of magnetic-nanobridge-based STT-MRAM towards sub-20-nm technology nodes

A.V. Popov[1], G.D. Demin[1,2], A.F. Popkov[1,2]

1. Moscow Institute of Physics and Technology (State University), Dolgoprudny, Russia, demin.gd@phystech.edu.

2. National Research University of Electronic Technology (MIET), Moscow, Russia, alexcoretex@gmail.com

An important criterion ensuring the extended scalability of nonvolatile magnetoresistive memory (STT-MRAM), based on spin-transfer-torque phenomena in magnetic tunnel junctions (MTJ), towards sub-20-nm technology node is the possibility to maintain high thermal stability (>80k_BT) when demonstrating low switching voltage (not more than 0.5 V) at reduced MTJ dimensions (Fig. 1a). It was found in [1, 2], that at such technology nodes a good thermal stability can be achieved by increasing the magnetic anisotropy field with the thickness of free layer. At the same time, Joule heating in the MTJ structure caused by the electrical current can additionally reduce the voltage thresholds needed for the magnetization reversal in STT-MRAM, which should be taken into account when considering current-induced magnetization dynamics of free layer at the nanoscale. As it was shown in [3] in the case of magnetic nanobridge Au/Co/Au/Co/Au, when the magnetic structure is scaled below 10 nm, the quantization of spin-transfer torquances (first derivatives of spin-transfer torques with respect to voltage) begin, which can lead to resonant magnetodynamic switching effects in the MTJ and requires to be studied.

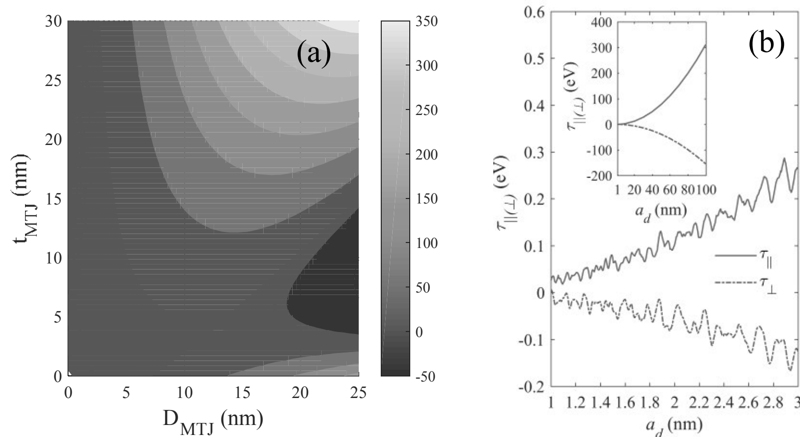

Fig. 1. (a) Dependence of the thermal stability factor on the dimensions of MTJ. (б) Quantization of the spin-transfer torques with scaling of the transverse dimensions of the magnetic nano-bridge.

In connection with the above, the complex development of a fundamentally new SPICE model of MTJ is needed, which takes into account both these nanoscale quantum and thermal effects, as well as the variation of magnetic and thermodynamic properties of MTJ with a change in its dimensions at sub-20-nm design rules. In this work we describe SPICE-compatible compact model of nano-sized MTJ for a given thermal stability factor depending on the given technology node, which, in turn, causes a change of the MTJ dimension. The spatial quantization of the spin-transfer torques in MTJ is also considered within this model when the transverse size of the MTJ cross-section scales below 10 nm (Fig. 1b). Implementation of the magnetization dynamics into the SPICE model of sub-20 nm MTJ is based on the equivalent circuit for the Landau-Lifshitz-Slonczewski-Bloch equation solver with an effective field term responsible for thermal calculations. This model can be useful for predictive simulation of STT-MRAM performance at advanced technology nodes. The work was supported by the Russian Science Foundation (project № 16-19-00181).

1. K. Watanabe, B. Jinnai, S. Fukami, and H. Sato. "Shape anisotropy revisited in single-digit nanometer magnetic tunnel junctions". Nature Communications, **9**(633), pp. 1-6, 2018.
2. N. Perrissin, S. Lequeux, N. Strelkov, A. Chavent, L. Vila, L.D. Buda-Prejbeanu, S. Auffret, R.C. Sousa, I.L. Prejbeanu, and B. Dieny. "Highly thermally stable sub-20nm magnetic random-access memory based on perpendicular shape anisotropy". Nanoscale, **10**(25), pp. 12187-12195, 2018.
3. G.D. Demin, A.F. Popkov. "Quantum oscillations of the microwave sensitivity of a spin-torque diode in a magnetic nanobridge". JETP Lett., **106**(12), pp. 821-827, 2017.

Quality control of multilayer spin-tunnel structure using combination of methods

O.S. Trushin[1], S.V. Vasiliev[1], S.G. Simakin[1], A.N. Pestova[2]
1. Yaroslavl Branch of the Institute of Physics and Technology of RAS, Yaroslavl, Russia, otrushin@gmail.com
2. P.G. Demidov Yaroslavl State University, Yaroslavl, Russia

Magnetic Tunneling Junction (MTJ) is an important element of modern MRAM cell. It is believed that MRAM might be the next generation of computer memory because it combines both fast access rate and nonvolatility [1]. Therefore optimization of the technology for MTJ fabrication is of very important task. Achievement of high functional characteristics of MTJ requires intensive quality control at different stages of the technological route. In this work we discuss different aspects of quality control during this process with emphasis on the depth profiling of multilayer structure using combination of methods including Transmission microscopy of the cross-section and Time of Flights Secondary-Ion Mass Spectrometry (TOF SIMS). A multilayer structure of the following composition (from bottom up to the top layer):
5 Ta/30 CuN /5 Ta/3 NiFe/16 IrMn/2.0 CoFe/0.9 Ru/2.5 CoFeB/MgO /2.5 CoFeB/10 Ta/ 7 Ru has been deposited on Si wafer using magnetron sputtering at Singulus Timaris PVD cluster tool [2]. Here the numbers in front of chemical elements show thicknesses of corresponding layers given in nm. Before starting the lithography process for MTJ fabrication it is very important to get complete information about quality of as-deposited multilayer film. For this purpose visual inspection of the cross section of the structure has been performed using Transmission Electron Microscopy. Typical result of such analysis is shown in Fig. 1.

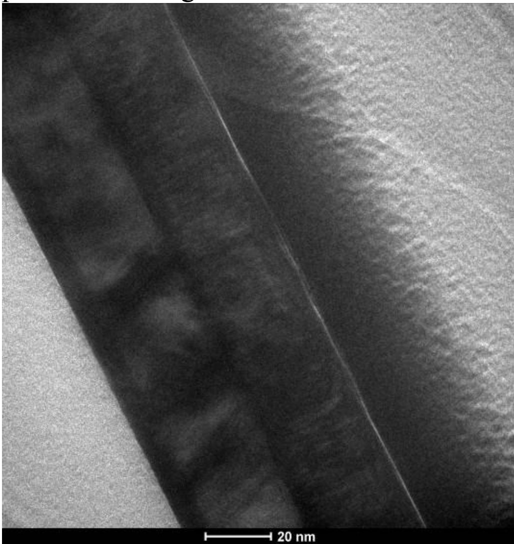

Fig. 1. TEM bright field image of the cross section of the MTJ multilayer structure (Tecnai G2 F20 U-TWIN).

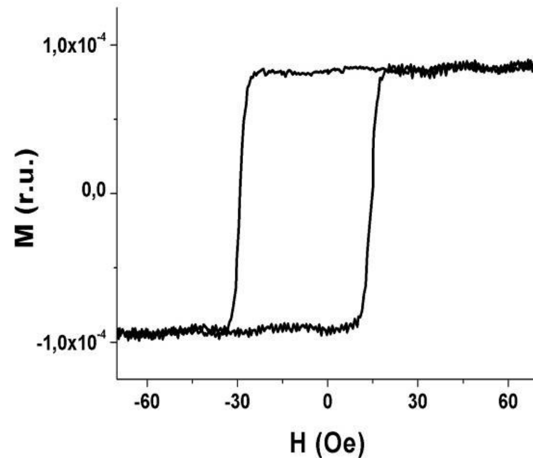

Fig. 2. Magnetization reversal of spin-tunnel structure.

Magnetic reversal curve of as deposited structure has been measured using Kerr effect magnitometry. The result is shown in Fig.2. Only single hysteresis loop corresponding to free layer switching can be seen due to limitation of external magnetic field. SIMS depth profiling has been done using ION TOF. Overall satisfactory agreement with initial requested multilayer structure in layer thicknesses and chemical composition has been obtained based on comparing the results of TEM and SIMS analysis.. However available deviations might be attributed to the artefacts of analytical methods and sample preparation procedure. The work has been done on the equipment of the Center for Collective Use of Scientific instruments “Micro and Nanodiagnostics” [4].

1. H. Yoda, *MRAM Fundamentals and Devices*, Handbook of Spintronics: Springer Reference, Berlin, 2016.
2. O.S Trushin, S.V. Vasiliev, S.G. Simakin, E.A Smirnov. "Quality control of multilayer spin-tunnel structure using combination of methods of analysis". Russian Microelectronics, accepted for publication in 2018.

Field-effect transistors for ULSI

A. Krivospitsky[1], A. Miakonkikh[1,2], V. Vyurkov[1,2], D. Svintsov[1,2],
Yu. Semin[1], K. Rudenko[1,2], V. Lukichev[1,2]

1. Institute of Physics and Technology of RAS, Moscow, Russia, miakonkikh@ftian.ru
2. Moscow Institute of Physics and Technology (State University) Moscow, Russia

Scaling of field-effect transistors (FETs) to smaller sizes required introduction of high-k gate dielectric and silicon-on insulator (SOI) wafers. Further development leads to FETs with Schottky source and drain contacts (SB FET) instead of Ohmic ones usually created by heavy doping.
The advantages of such transistors are the absence of technological operations associated with contact doping, which include the processes of ion implantation and fast annealing at high temperature (above 1000 °C), causing an undesirable diffusion of impurity and metal atoms through the structure.
Fig. 1a shows the calculated I-V curves (current vs. gate voltage) of a classical silicon transistor with physical doping and single gate and a transistor with electrical doping and several gates. There an idealized model of a sharp doping boundary at the p-i junction was used. This approximation overestimates the subthreshold slope as it does not take into account fluctuations of the density of dopants. Feasibly, due to those fluctuations the experimental values of the subthreshold slope in doped tunnel transistors are much lower, namely, $(53\ mV/dec)^{-1}$ for silicon transistors and $(47\ mV/dec)^{-1}$ for transistors at based on materials A_3B_5.

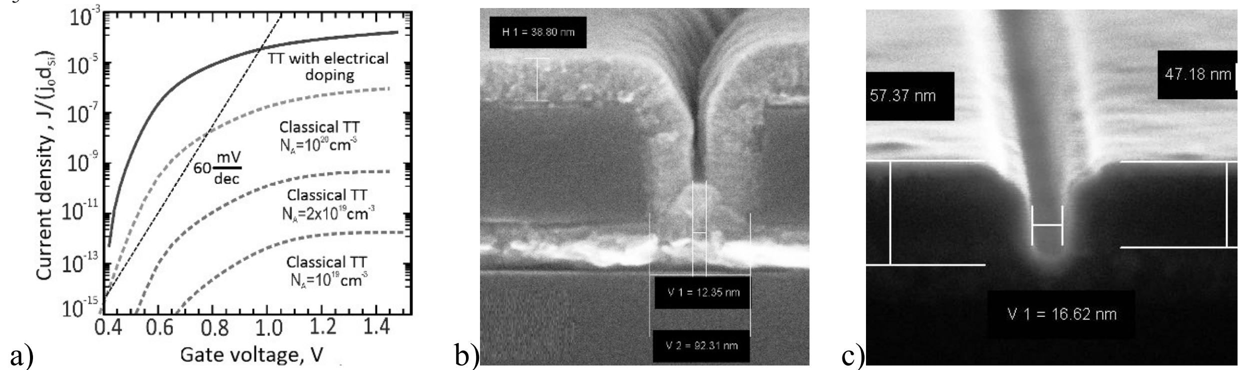

Fig. 1. (a) I-V curves for classical and electrically doped FET-transistors, (b) SEM picture after deposition of gate and spacer materials in the trench, (c) the same after their removal from the bottom.

The fabrication of a tunnel undopped multi-gate nano-FET with Schottky contacts can be carried out using high-resolution lithography, for example, e-beam, but to increase throughput the approach of patterning nanotransistor with conventional photolithography and methods of self-alignment and self-formation were developed. The method includes the stage of creating on a silicon wafer an auxiliary layer of a dielectric with a thickness of 50-100 nm and forming of 30-120 nm wide trench depending on the required number of closures. The multigate structure is then formed on the side walls of the slot by atomic layer deposition (ALD) of the conductive material of the gates (HfN or TaN) and dielectric of the spacers (HfO_2), followed by anisotropic plasma etching of the bottom of trench. These operations are repeated to achieve the required number of gates. Plasma enhanced ALD of HfO_2 performed using TEMAH precursor and O_2 plasma produces a conformal coating of trench structure with desired breakdown and leakage characteristics. Materials of conductive electrodes (gates) are deposited by PEALD with TEMAH or TBTDET as first precursor and hydrogen plasma as a second. Anisotropic etching is performed in ICP plasma etch tool in BCl_3-based plasma at relatively low pressure (1 mTorr) and DC bias of 120-200 V. Selectivity of the process with respect to silicon is optimized to insure the silicon recess lower than 1 nm.
Fig. 1b shows a photograph of the gap in the auxiliary layer obtained by means of a scanning electron microscope after the deposition of gate and spacer materials, and Fig. 1c shows the same cross-section after plasmochemical removal of gate and spacer materials from the trench bottom. Developed method allows forming the odd number of 10 nm gates and high-k spacers (4-6 nm) between them.

Quantum interference molecular inverter

A.A. Gorbatsevich[1,2,3], G.Ya. Krasnikov[3], and N.M. Shubin[1,2,3]

1. P.N. Lebedev Physical Institute of the Russian Academy of Sciences, Moscow, 119991, Russia.
2. National Research University of Electronic Technology, Zelenograd, Moscow, 124498, Russia.
3. JSC MERI, Zelenograd, Moscow, 124460, Russia.

Coherent quantum transport through molecular conductors is strongly affected by different interference effects. Formation of transmission resonance peaks and/or antiresonance dips can occur in a molecular system due to the presence of interference between different tunneling paths. Therefore, in order to control the electron transport through single molecule devices one should control its transmission spectrum resonances. Recently the effect of resonance coalescence was studied in detail in the context of PT-symmetry breaking of some non-Hermitian auxiliary Hamiltonian [1] and, moreover, the unified theory of resonances and antiresonances in quantum conductors has been developed [2]. Thus, based on this formalism one can think of a way to utilize interference effects to provide an external control to the transmission spectrum of a certain molecular conductor.

The idea of exploiting the interference effects in the electronic transport switches is not new, however, in this work we propose a novel type of quantum interference switch and an all-electrical molecular device composed of two such switches, acting as a conventional CMOS inverter. Without any external control (gate) voltage the switch is highly conductive. Application of an electric potential to the gate terminal deeply modifies the transmission spectrum of the system and significantly reduces its conductance. The underlying physical mechanism of such transition is twofold. Firstly, there is a collapse of resonances, resulting in coalescence of two perfect transmission peaks into one with smaller amplitude and also there is a transmission antiresonance dip formation (shift), which additionally lowers the transmission. From the microscopic point of view the model system, possessing the described phenomenon, involves (at least) two degenerate states. The applied external control (gate) voltage lifts this degeneracy. Therefore, we propose diradical molecules [3] to be candidates for an experimental realization of such quantum switches and inverters. Moreover, diradicals are already known for the antiresonance formation in the transmission spectrum [4]. Here we show that the resonance coalescence can accompany the antiresonance formation in diradicals. In particular, in this work we calculate transmission spectrum, currents and estimate transfer characteristics of quantum interference inverters composed of disjoint and non-disjoint diradicals within tight-binding (Huckel) approximation. From the analysis of derived transfer characteristics of the inverter, we show that by varying systems parameters the gain of the inverter (its absolute value) can be made greater than 1 for arbitrary small supply voltage.

The transition of the proposed quantum switch from the high conductive to the low conductive states and vice versa happens due to the interference effects, which destruct (build up) the transmission peaks rather than shift them out of (into) the energy range between Fermi levels of the leads. Therefore, the gate voltage, i.e. operating voltage needed, is independent of the temperature and in the ideal case can be made arbitrary small even at room temperature. This fact may provide a dramatic improvement in the power consumption and, thus, it is the main advantage of the proposed quantum interference device. In the case of such small signals, the influence of noise is of great importance. Shot noise spectral power is proportional to the current through the system and, hence, it becomes negligible as the voltages and, correspondingly, the currents are scaled down. On the other hand, at finite (room) temperature thermal noise can influence the transport dramatically. In our work, we estimate thermal noise and determine approximate restrictions on the operating frequency of the proposed quantum devices.

1. A.A. Gorbatsevich and N.M. Shubin. “Coalescence of resonances in dissipationless resonant tunneling structures and PT-symmetry breaking”, Ann. Phys., **376**, pp. 353-371, 2017.
2. A.A. Gorbatsevich and N.M. Shubin. “Unified theory of resonances and bound states in the continuum in Hermitian tight-binding models”, Phys. Rev. B, **96**, 205441, 2017.
3. M. Abe, “Diradicals”, Chem. Rev., **113**, pp. 7011–7088, 2013.
4. Y. Tsuji et al. “Close relation between quantum interference in molecular conductance and diradical existence”, Proc. Natl. Acad. Sci., **113**, pp. E413–E419, 2016.

Development of a molecular single-electron transistor with a single-atom charge center

V. Gaydamachenko[1], E. Morozova[1], S. Dagesyan[1,2], E. Soldatov[1,2], E. Beloglazkina[1]
1. M.V. Lomonosov Moscow State University, Moscow, Russia, soldatov.es@physics.msu.ru
2. The Center for Quantum Technologies of M.V. Lomonosov Moscow State University, Moscow, Russia, soldatov.es@physics.msu.ru

Single-electron transistor, parameters and characteristics of which are fundamentally improved with decreasing element sizes [1], is a promising element of extremely small, atomic-molecular scale. An atomic transistor consisting of a monatomic charge center inside a molecule connected to source and drain electrodes by aurofilic terminal groups of this molecule is the most promising, limiting version of such a transistor. However, the creation of a reliable technology for the manufacture of such nanoelements is not yet completed and is a very urgent task. In this paper, a version of such a molecular-atom nanotransistor has been developed and implemented.

To create a planar nanostructure of such a transistor on a silicon substrate coated with silicon dioxide, the bottom gate electrode was first formed in the lower layer of the element using a scanning electron microscope Supra40 with a Raith lithography attachment. The bottom gate was separated from top layer of transistor by a thin (20 nm) dielectric film that provided insulation leakage resistance of more than 1 TOhm at a voltage of 50 V. The structure of nanowires from thin (18 nm) gold films serving as a blank for the formation of transport and side control electrodes of a transistor was formed on this insulating layer by the methods of electron nanolithography. Further, the electrodes of the manufactured side gates were covered by a layer of alumina (Al_2O_3) 30 nm thick through the "windows" in the positive PMMA A2 resist mask. After removing the mask, a nanostructure was obtained in which the alumina film completely insulates the side gates, without affecting the nanowire. The leakage current measurements between the nanowire and the gate showed that the insulation resistance exceeds 1 TOhm. Then, the molecules of the aurophilic terpyridine derivative based on single rhodium atoms [2], having a length of 4.7 nm, were fixed on the surface of the nanowires during the "self-assembly". After that, by means of electromigration, a nanosized gap of 2-4 nm was formed [3] in a nanowire, during which one of the molecules fixed on the nanowire was built in the gap, thereby forming a tunnel system with charge center for electron tunneling through it. Measurements of electron transport through manufactured systems have shown the presence of a molecule in the gap and typical single-electron characteristics with a Coulomb blockade of about 250 mV.

Thus, molecular single-electron transistors with single molecules of aurophilic terpyridine derivative based on single rhodium atoms as an island with charge energy up to 250 meV are manufactured, which ensures their high operating temperature up to room temperature.

1. K.K. Likharev. “Single-electron devices and their applications”. Proc. IEEE, **87**, pp. 606-632, 1999.
2. E.K. Beloglazkina, A.G. Majouga, E.A. Manzheliy et al. “Mononuclear ruthenium(II) and rhodium(III) complexes with S-[4-(2,2:6′,2″-terpyridin-4′-yl)phenoxy]butyl ethanethioate and 4′-[4-(1,2-dithiolane-3-yl)butylcarboxy)phenyl]-2,2′:6′,2″-terpyridine: Synthesis, electrochemistry, antibacterial activity and catalytical application”. Polyhedron, **85**, pp. 800-8008, 2015.
3. S.A. Dagesyan, A.S. Stepanov, E.S. Soldatov et al. “Properties of Extremely Narrow Gaps Between Electrodes of a Molecular Transistor”. Journal of Superconductivity and Novel Magnetism, **28**, pp. 787-790, 2015.

Simulation of single-electron transistor based on the molecule with single-atom charge center

A.A. Parshintsev, V.V. Shorokhov, E.S. Soldatov
Quantum Technology Centre, Faculty of Physics, M.V. Lomonosov Moscow State University, Leninskie Gory, 1(2), Moscow, 119991, Russia, parshincev@physics.msu.ru

Solid state single-electronics based on the transistors with a single-atom charge center is a new promising direction of nanoelectronics [1]. Realization of single-atom single-electron devices is possible using molecules with accentuated single-atom detached charge center. One of the basic elements for such investigation is a single-electron monomolecular transistor (SET). The scheme of SET is provided on figure 1. In this work transport characteristics of SET with a charge center based on Sc, Cr, Ru, Rh, and Pt atoms were investigated by computer simulation.

Unrestricted Hartree-Fock method in NWChem [2] with DZP basis set [3] was used to calculate electron energy spectra of the molecules in various charge states. Analytical parametric model for obtaining the molecule energy spectra was proposed. Transport characteristics of the SET were calculated using Monte-Carlo simulation and the approach described in [4].

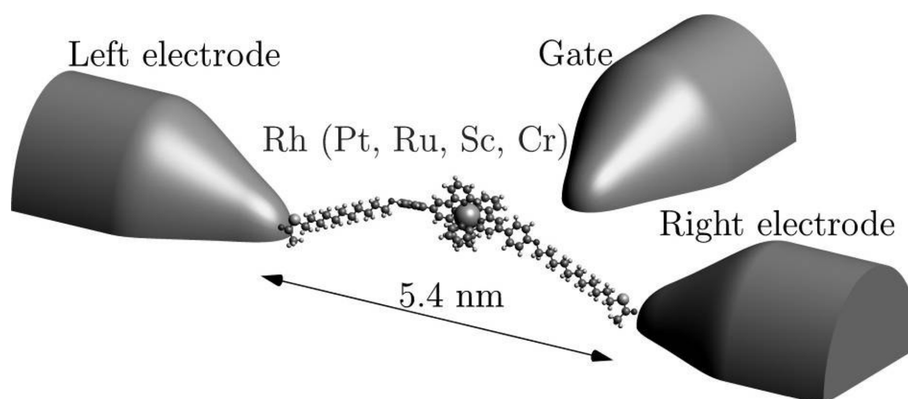

Figure 1. The scheme of SET with a charge center based on Sc, Cr, Ru, Rh, and Pt atoms.

In the course of the work the following results were obtained: transport characteristics of SET with five various charge centers (Sc, Cr, Ru, Rh, and Pt), the influence of energy electron spectra's features is studied, charge features of molecules with various charge centers are discovered. Discovered features can be used to make the certain polarization conditions in systems with many charge centers.

This work was funded by RFBR according to the research project № 18-32-00907.

1. *Fuechsle M. et al.* // Nat. Nanotechnol. **7**, 242–246, 2012.
2. *Valiev M., et. al.* // Computer Phys. Comm. 2010. V. **181**. P. 1477.
3. EMSL Basis Set Exchange Library, https://bse.pnl.gov/bse/portal
4. *Shorokhov V.V.* // MSU Phys. Bulletin 2017. V. **72**. P. 279.

Transit-time transistors for terahertz generation

V. Vyurkov[1,2], D. Svintsov[1,2], M. Rudenko[1], A. Borzdov[3],
V. Borzdov[3], K. Rudenko[1,2], V. Lukichev[1.2]
1. Institute of Physics and Technology RAS, Moscow, Russia, vyurkov@ftian.ru
2. Moscow Institute of Physics and Technology (State University) Moscow, Russia
3. Belarusian State University, Minsk, Belarus, borzdov@bsu.by

The breakthrough to the deep gap in generation power existing in the range 0f 0.1-10 THz is nowadays undertaken from both sides, that is, from optic devices and from electronic devices. One of the proposals of terahertz generation with the help of low-dimensional electronic structures (namely, ballistic quantum wires) was put forward in 1994 [1]. It turned out that ballistic regime is sufficient for the negative dynamic conductivity at THz frequencies necessary for generation. Up to date the facilities in silicon technology allow fabrication of thin layers (2D) and arrays of nanowires (1D) [2].
However, the negative conductivity of transit-time structures has a threshold with respect to scattering rate like a similar threshold of generation in optical and plasmonic devices. Fortunately, there is an effect which guarantees negative conductivity even in case of rather strong scattering. We mean the operation on barrier injection in BARITT diodes [3].
In present communication we discuss a BARITT transistor which could be realized in silicon nanostructutes and demonstrate a possibility of negative conductivity at THz frequencies with high efficiency (Fig. 1). The advantage of a transistor-like structure over that of a diode is as follows. In a diode (when the floating gate is erased from Fig. 1) the influence of the drain voltage on the height of the potential barrier near source contact is weak. The same weak is the variation in injection current. When a floating gate is inserted in the structure, the gate voltage with respect to the drain contact strongly operates over the barrier height and, therefore, injection current. This results in higher efficiency of generation. The oscillating current could be transmitted from the floating gate and the drain contact to a wave-guide (or antenna).

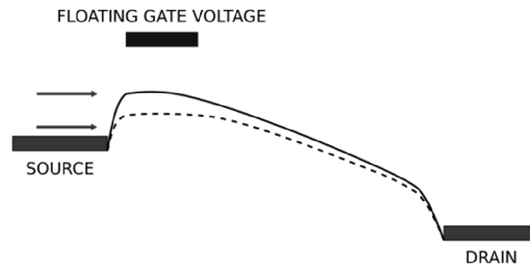

Fig. 1. Schematic view of a THz-generator based on a transit-time transistor. The gate voltage strongly affects the barrier height, i.e. the injection current, compared to variation of injection current in diodes.

1. L. Fedichkin and V.V'yurkov, "Quantum ballistic channel as an ultrahigh frequency generator," Appl. Phys. Lett., vol. **64**, pp. 2535-2536, 1994.
2. R. Khabutdinov, I. Semenikhin, F. Davydov, V. Vyurkov, L. Fedichkin, K. Rudenko, A.V. Borzdov, V.M. Borzdov. Low-dimensional transit-time diodes for terahertz generation. Proc. SPIE, **10224**, 102240M, 2016.
3. D.J. Coleman, Jr. "Transit-Time Oscillations in BARITT Diodes". J. Appl. Phys., **43**, pp.1812-1818, 1972.

Polarons in Resonant-Tunneling Diodes and Their Possible Application in Terahertz Emission

V.G. Popov[1], V.G. Krishtop[1], T.I. Ahmedov[1], S.G. Chigarev[2], M. Henini[3]

1. Institute of Microelectronics Technology of RAS, Chernogolovka, Russia, popov@iptm.ru.
2. Institute of Radio-engineering and Electronics of RAS, Fryazino, Russia.
3. School of Physics and Astronomy of Nottingham University, Nottingham NG7 2RD, UK.

Polarons are frequently considered in resonant-tunneling diodes (RTD) to explain some exotic behavior of spectral features in strong magnetic and electric fields [1]. In particular a model of the polaron resonant-tunneling was proposed to describe phonon replicas in a current-voltage characteristic of the RTD made of a heterostructure of polar semiconductors [2]. Recently this model was applied to consider transformation of the phonon replica as a transition of polarons into magnetopolarons in quantizing magnetic fields [3].

We discuss the polarons formed in a quantum well between tunnel barriers of the RTD. In this case there are two branches of bulk LO-phonons in the heterostructure. For the investigated heterostructure those are GaAs and AlAs LO-phonons with energy ε_{p1} = 36 meV and ε_{p2} = 51 meV accordingly. Considering electron-LO-phonon interaction it is more appropriate to speak about a low mass or light polaron formed by electrons and virtual LO-phonons and heavy that formed by virtual electrons and LO-phonons. Following this approach the LO-phonons should be considered as intersubband polaron excitation. Moreover the polaron model admits the intersubband transitions between polaron states formed on different LO-phonons. The energy of the transition is close to the phonon-energy difference $\varepsilon_{12} = \varepsilon_{p2} - \varepsilon_{p1}$ = 15 meV. Similar excitations have been observed in tunnel spectra of the RTD at low density of electrons and liquid helium temperatures when the electron-LO-phonon interaction is weakly screened [4]. Another way to decrease the electron screening is a temperature increase [5]. This gives a chance for polarons to survive even at room temperature. Thus one can expect the polaron intersubband transitions at room temperatures and even higher those.

In this report we will review our old and new experimental results confirmed the polaron picture in different RTDs made of GaAs/$Al_XGa_{1-X}As$ heterostructures. We shell discuss also theoretical aspects of the temperature dependence of the electron-phonon interaction, polaron density of states and probability of intersubband transitions and their coupling with electromagnetic waves.

1. G.S. Boebinger, A.F.J. Levi, S. Schmitt-Rink, A. Passner, L.N. Pfeiffer, and K.W. West, Phys. Rev. Lett. **65**, 235 (1990).
2. V.G. Popov, V.G. Krishtop, O. Makarovskii, M. Henini, *Magnetotunneling Spectroscopy of Polarons in a Quantum Well of a Resonant Tunneling Diode.* JETP **111**, 220 (2010).
3. V.G. Popov, V.G. Krishtop, L. Eaves, M. Henini, J-C. Portal. Polarons and magnetopolarons in GaAs quantum wells of resonant-tunneling diodes. Proceedings of XXIIth International Simposium "Nanophysics and nanoelectronics". Nizhniy Novgorod, March 12-15, 2018, p. 735-736 (2018) (http://nanosymp.ru/ru/proceedings, in Russian).
4. V.G. Popov, O.N. Makarovskiy, L. Eaves, M. Henini, J.-C. Portal. *Polaron states in GaAs quantum wells in GaAs/AlGaAs heterostructures with strong and weak electron-phonon interaction*. Proceedings of XXth International Simposium "Nanophysics and nanoelectronics". Nizhniy Novgorod, March 14-18, 2016, p. 695-697 (2016) (http://nanosymp.ru/ru/archive; in Russian).
5. T. Ando, A. Fowler, F. Stern. *Electronic Properties of Two Dimensional Electron Systems*. Rev. Mod. Phys. **54**, p. 155 (1982).

Plasmonic terahertz emitters with high-aspect ratio metal gratings

A. Yachmenev[1,2], D. Lavrukhin[1,2], I. Glinskiy[1], R. Khabibullin[1,3], R. Galiev[1], A. Pavlov[1], Yu. Goncharov[4], I. Spektor[4], M. Ryzhii[5], T. Otsuji[6], K. Zaytsev[2,4], D. Ponomarev[1,2,3]

1. Institute of Ultra High Frequency Semiconductor Electronics of RAS, Moscow, Russia; ponomarev_dmitr@mail.ru
2. Bauman Moscow State Technical University, Moscow, Russia
3. Center for Photonics and 2D Materials, Moscow Institute of Physics and Technology, Dolgoprudny, Russia
4. Prokhorov General Physics Institute of RAS, Moscow, Russia
5. University of Aizu, Aizu-Wakamatsu, Japan
6. Research Institute of Electrical Communication, Tohoku University, Japan

The state-of-the-art plasmonic terahertz (THz) sources and detectors are of considerable interest due to its wide applications in security systems, biology, medicine and material science [1, 2]. Despite the variability of existing THz devices photoconductive antennas (PCAs) are still promising THz emitters/detectors for broadband THz spectroscopy and imaging [3].

In present article we propose a novel technology for fabricating plasmonic SI-GaAs PCAs with increased height of plasmonic grating up to 100 nm. By means of numerical calculations we show sharp dependency of absorption coefficient as well as electric field enhancement in the absorption layer with an increase of aspect ratio of plasmonic gratings (a ratio between a width and a height of metal gratings). In our experiments, we passivated the surface of a photoconductor by 230 nm Si_3N_4, etched there windows and deposited 50/450 nm Ti/Au antenna metallization. Plasmonic gratings were formed by electron-beam lithography with 18/75 nm Ti/Au metallization followed by lift-off. Then 80 nm Al_2O_3 anti-reflection coating layer for reduction of the Fresnel reflection losses was used on the top of plasmonic gratings also serving for maintaining its mechanical stability and providing the excitation of guided modes at the resonant wavelengths of the subwavelength slab waveguide formed by the metal gratings. A SEM image of the fabricated plasmonic PCA with log-spiral topology and a magnified image of plasmonic gratings are shown in Fig. 1. Current-voltage measurements reveal a strong increase of a photocurrent generated by the proposed plasmonic PCA – 50 times higher than for a traditional one and the experimental THz spectra demonstrate 60–100 times increase of amplitude of THz radiation in plasmonic PCA (see Fig. 2).

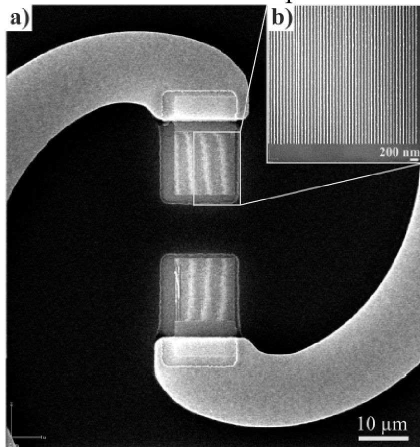

Fig. 1 SEM image of the fabricated plasmonic PCA (*a*) with a magnified image of plasmonic gratings (*b*).

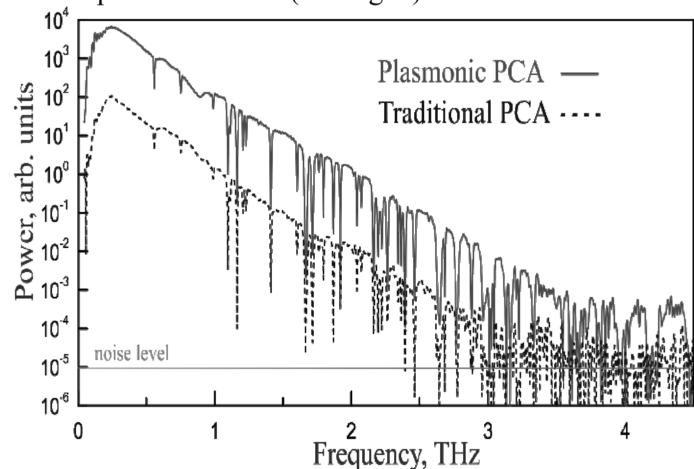

Fig. 2. Radiated power in the frequency-domain for the plasmonic and traditional PCAs based on SI-GaAs photoconductor.

1. N. Yardimci et al. "A high-power broadband terahertz source enabled by three-dimensional light confinement in a plasmonic nanocavity". Sci. Rep., **7**, pp. 4166, 2017.
2. D. Ponomarev et al. "Lateral terahertz hot-electron bolometer based on an array of Sn nanothreads in GaAs". J. Phys. D: Appl. Phys., **51** (13), pp. 135101, 2018.
3. D. Lavrukhin et al. "Numerical simulations and experimental study of terahertz photoconductive antennas based on GaAs and its ternary compounds". Proc. SPIE, 10680M, 2018.

Silver-based double metal waveguide for terahertz quantum cascade laser

R.A. Khabibullin[1,2,3], N.V. Shchavruk[1,2], D.S. Ponomarev[1,2,3], D.V. Ushakov[4], A.A. Afonenko[4], O.Yu. Volkov[5], V.V. Pavlovskiy[5], and A.A. Dubinov[2]
1. Institute of Ultra High Frequency Semiconductor Electronics of RAS, Moscow, Russia, khabibullin@isvch.ru
2. Institute for Physics of Microstructures of RAS, Nizhny Novgorod, Russia
3. Center for Photonics and 2D Materials, Moscow Institute of Physics and Technology, Dolgoprudny, Russia
4. Belarusian State University, Minsk, Belarus
5. Institute of Radio-Engineering and Electronics of RAS, Moscow, Russia

In present article we propose two designs of THz QCLs based on three- and four-well active module with gain maximum at 3.2 and 2.3 THz. The laser structures were grown by molecular beam epitaxy with 10 μm active region thickness. We fabricate ridge structures with Au-Au double metal waveguide [1]. The device were die bonded to a copper submount with wire bonding to ridge structures. Measurements were made with an abutted to laser facet sapphire hyperhemispherical lens.

By fitting the dependence of threshold current J_{th} on temperature to the empirical expression J_{th}~exp(T/T_0), we obtain the characteristic temperature T_0 = 20 and 30 K for 3.2 THz QCL and 2.3 THz QCL, respectively. From the experimental dependence of the output power on the operating temperature, we obtain the maximum operation temperature 84 and 106 K for 3.2 THz QCL and 2.3 THz QCL, respectively. In measured at 58 K spectrums of 3.2 THz QCL and 2.3 THz QCL, there are three equidistant spectral lines corresponding to the longitudinal Fabry-Perot modes with $\Delta f = c/2nL$ = 50 GHz for L=1 mm.

Metal film of Ti/Au (30/500 nm) and Ti/Ag (30/500 nm) were deposited on SI-GaAs, and their resistivities were measured for calculation of metal loss (Fig. 1). As was shown in Ref. [2], the use of Ag-Ag DMW leads to a reduction in losses of ~3 cm^{-1} compared with Au-Au DMW.

We investigate the postgrowth processing for THz QCL with Ag-Ag DMW. This processing includes the Ag–Ag thermocompression bonding of QCL heterostructures with a doped n^+-GaAs substrate, mechanical lapping and selective wet etching of the substrate, and dry etching of QCL ridge structures through a Ti/Ag metallization mask 100 μm wide. Reactive-ion-etching recipe with an inductively coupled plasma source in a BCl_3/Ar gas mixture are selected to obtain vertical walls of the QCL ridge structure with minimum Ti/Ag mask sputtering (Fig. 2).

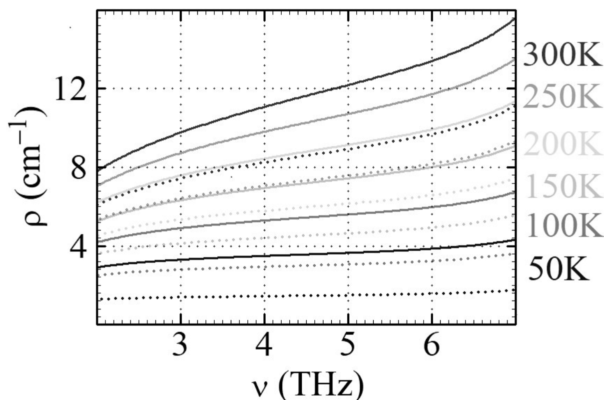

Fig. 1. Temperature dependence of metal loss for double metal waveguide based on Au-Au (solid line) and Ag-Ag (dashed line).

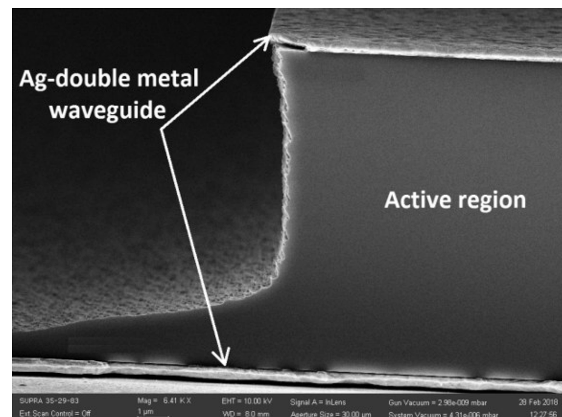

Fig. 2. SEM image of THz QCL with Ag-Ag double metal waveguide.

1. R.A. Khabibullin et al., Semiconductors, **50** (10), pp. 1377-1382, 2016.
2. Y.J. Han et al., Optics Exp., **26** (4), pp. 3814-3827, 2018.

Silicon hot-electron bolometer for terahertz radiation

V. Smirnov[1], D. Kibalov[1], V. Vyurkov[2,3], M. Rudenko[2], A. Miakonkikh[2,3], A.Rogozhin[2,3], K. Rudenko[2,3], V. Lukichev[2,3]
1. Quantum Silicon Ltd, Moscow, Russia, vsmirnov@wostec.com
2. Institute of Physics and Technology RAS, Moscow, Russia, *vyurkov@ftian.ru*
3. Moscow Institute of Physics and Technology (State University) Moscow, Russia

Recently the lateral terahertz hot-electron bolometer (HEB) based on an array of Sn nanothreads in GaAs was proposed in Ref. 1. The nanothread formation has been achieved by implantation of Sn atoms on the vicinal GaAs surface. The period of the structure was 50nm. Surely, the realization of a similar device on a silicon wafer is challenging for practical application.
Here we put forward a construction (Fig. 1) and technology of manufacturing a silicon HEB for terahertz radiation. The doping with the period of tens nanometer could be produced with via implantation through the mask. The mask could be fabricated by the especial WoS technology [2] which is much cheaper compared to an electron-beam lithography. The operation of the device much reminds that of a quantum-well bolometer. The current flows perpendicularly to threads and involves only delocalized electrons. The incident radiation heats electrons that results in the increase in their temperature. The associated increase in both mobility and density of delocalized electrons occurs, the latter does not exist for uniform doping. The developed semi-analytical model allows optimization of the structure in a wide range of parameters (Fig. 2).

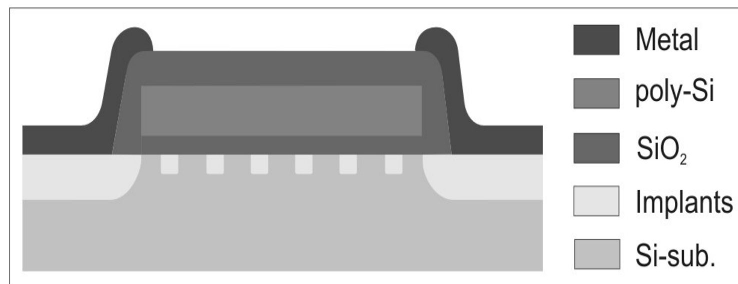

Fig. 1. Schematic view of a Si-HEB.

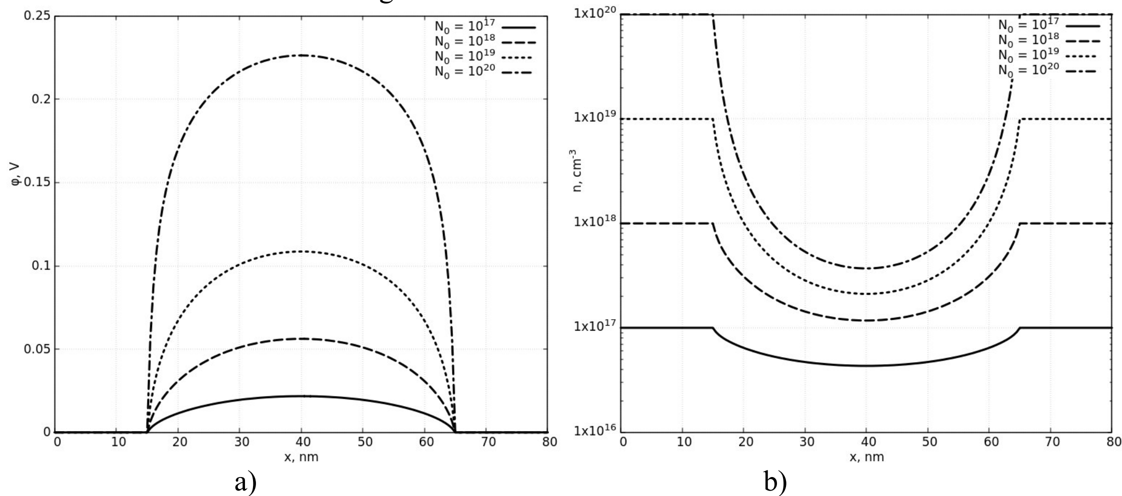

Fig. 2. Calculated potential profile (a) and electron density (b) between nanothreads for their various doping levels at room temperature.

1. D.S. Ponomarev, V. Lavrukhin, A.E. Yachmenev, R.A. Khabibullin, I.E. Semenikhin, V.V. Vyurkov, M. Ryzhii, T. Otsuji, and V. Ryzhii. Lateral terahertz hot-electron bolometer based on an array of Sn nanothreads in GaAs. J. Phys. D: Appl. Phys. **51** 135101 (2018).
2. V.K. Smirnov, D.S. Kibalov, O.M. Orlov, and V.V. Graboshnikov, Technology for nanoperiodic doping of a metal–oxide–semiconductor field-effect transistor channel using a self-forming wave-ordered structure, Nanotechnology **14**, 709–715 (2003).

Photon echo schemes for quantum memory in optical and microwave resonators reasons

S.A. Moiseev
Kazan Quantum Center, Kazan National Research Technical University, Kazan, Russia.
E-mail: samoi@yandex.ru

We analyze a number of possible schemes for photon echo quantum memory in optical and microwave resonators. It is shown that using a multi-resonator scheme provides an efficient interface for the quantum storage of broadband fields. Possible experimental implementations are also discussed.

Revival of silenced echo quantum memory in the optical resonator

M.M. Minnegaliev, K.I. Gerasimov, R.V. Urmancheev, and S.A. Moiseev
Kazan Quantum Center, Kazan National Research Technical University named after A.N. Tupolev-KAI, Kazan, 420111 Russia

The revival of silenced echo quantum memory protocol on a Tm^{3+}: $Y_3Al_5O_{12}$ crystal ($c = 0.1\%$) placed in the impedance matched optical Fabry-Perot resonator is experimentally implemented. The recovery efficiency of 21% at storage time of 36 μs was achieved. The main loss mechanisms and their effect on the quantum efficiency as well as the advantages of the realized quantum memory scheme and the possibility of further improvement of its basic parameters are discussed.

Quantum computer based on triangular atom-photon molecule

S.N. Andrianov[1], F.M. Ablayev[2], S.A. Moiseev[3], A.V. Vasiliev[2]

1. Institute of Applied Research of Tatarstan Republic Academy of Sciences
2. Kazan Federal University
3. Quantum Center of Kazan National Research Technical University

Configuration of three ring cavities in triangular scheme is considered. Each of the cavities can be coupled with its three-level atom and with neighbor cavity at any specific moment of time. Regimes for realization of single- and two-qubit gates in such atom-photon molecule are theoretically investigated. With that, the realization of two-qubit gate is considered in two different variants: at sequential switching of interactions with step transfer of excitation and when central cavity is coupled simultaneously with two by side cavities and excitation is transmitted in the course of single process. The comparison of two approaches is carried out and the recommendations on the construction of quantum computer on atom-photon molecule are given.

We analyze the architecture of the proposed quantum computer and set of the basic operations in order to construct its mathematical model. We investigate the universality of this model, i.e. the possibility of performing arbitrary quantum computations.

The photon concentrator and source on the quantum well/dot cascade nanostructure in optical microcavity for charge qubit control

A.V. Tsukanov and I.Yu. Kateev
Institute of Physics and Technology of the Russian Academy of Sciences, Moscow, Russia, ikateyev@mail.ru

A combined tunneling-emission single-electron process in a semiconductor nanostructure is proposed to generate terahertz radiation. Electrons are injected one-by-one into the active region due to the source and drain Fermi energy difference induced by dc electric field. The structure is placed inside a microcavity (1D-PhC) stimulating the electronic transition in the quantum dot accompanied by the emission of a photon to the cavity mode. Due to Coulomb blockade in the dot this transition is strictly single-photon per single tunneling event. As shown, there exist several regimes to obtain Fock or nearly coherent or fully thermalized photons. This field can be used for a local effect on the charge qubits. The node-to-waveguide dynamics for the field output is analyzed as well.

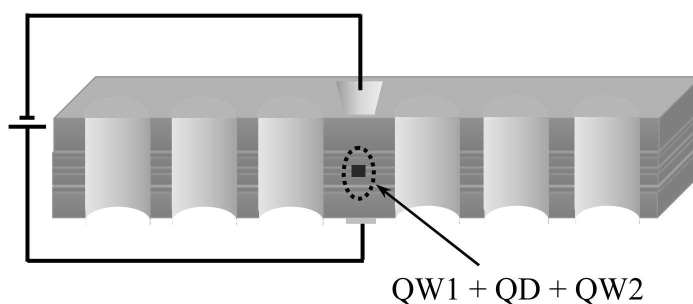

Fig. 1. Scheme of the photon concentrator. A semiconductor quantum dot (QD) is formed inside a central layer of heterostructure. This layer has adjacent layers, which form quantum wells (QWs). The active region is placed in the vicinity of a defect area of 1D photonic crystal (1D-PhC). Metal contacts providing dc electric field are deposited on the upper and lower surfaces of 1D-PhC.

Multiphoton subtracted thermal states: description, preparation, measurement and utilization

K.G. Katamadze[1,2,3,4], G.V. Avosopiants[1,2,4], B.I. Bantysh[1,5], Yu.I. Bogdanov[1,4,5], S.P. Kulik[2,3]
1. Institute of Physics and Technology, Russian Academy of Sciences, Russia
2. Faculty of Physics, M.V. Lomonosov Moscow State University, Russia
3. Quantum Technology Centre, M.V. Lomonosov Moscow State University, Russia
4. National Research Nuclear University (MEPhI), Russia
5. National Research University of Electronic Technology (MIET), Russia

Photon creation and annihilation are two basic operators in quantum optics. Their experimental implementation provides a perfect toolbox for quantum state engineering. The simplest quantum states, which can be modified both by photon creation and annihilation are thermal states of light. Therefore, the multiphoton subtracted thermal states (MPSTS) draw attention of quantum optics experimentalists last decade. Despite its simplicity they serve as a good testing area for study of a number of quantum phenomena.

In the current work we give a theoretical description of MPSTSs [1] and experimental technique of their generation and measurement [2]. Next we experimentally explore their non-Gaussianity [3]. Further we show some preliminary results of multimode MPSTSs generation and measurement. Finally, we demonstrate, how to utilize MPSTSs for studding the “quantum vampire” effect [4].

1. Yu.I. Bogdanov, N.A. Bogdanova, K.G. Katamadze, G.V. Avosopyants, and V.F. Lukichev, "Study of photon statistics using a compound Poisson distribution and quadrature measurements," Optoelectron. Instrum. Data Process. **52**(5), 475–485 (2016).
2. Yu.I. Bogdanov, K.G. Katamadze, G.V. Avosopiants, L.V. Belinsky, N.A. Bogdanova, A.A. Kalinkin, and S.P. Kulik, "Multiphoton subtracted thermal states: Description, preparation, and reconstruction," Phys. Rev. A **96**(6), 063803 (2017).
3. G.V. Avosopiants, K.G. Katamadze, Yu.I. Bogdanov, B.I. Bantysh, and S.P. Kulik, "Non-Gaussianity of multiple photon-subtracted thermal states in terms of compound-Poisson photon number distribution parameters: theory and experiment," Laser Phys. Lett. **15**(7), 075205 (2018).
4. K.G. Katamadze, G.V Avosopiants, Yu.I. Bogdanov, and S.P. Kulik, "How quantum is the “quantum vampire” effect?: testing with thermal light," Optica **5**(6), 723–726 (2018).

Quantum algorithms implementation on noisy quantum computers: from digital modeling of spin dynamics to quantum machine learning

A.A. Zhukov[1,2], E.O. Kiktenko[3,4], D.V. Babukhin[1,5], A.A. Elistratov[1], S.V. Remizov[1,6], W.V. Pogosov[1,7], Yu.E. Lozovik[1,8]

1. Dukhov Research Institute of Automatics (VNIIA), Moscow, Russia
2. National Research Nuclear University (MEPhI), Moscow, Russia
3. Steklov Mathematical Institute, Russian Academy of Sciences, Moscow, Russia
4. Russian Quantum Center, Skolkovo, Moscow, Russia
5. Department of Physics, Lomonosov Moscow State University, Moscow, Russia
6. Kotel'nikov Institute of Radio Engineering and Electronics, Russian Academy of Sciences, Moscow
7. Institute for Theoretical and Applied Electrodynamics, Russian Academy of Sciences, Moscow, Russia
8. Institute of Spectroscopy, Russian Academy of Sciences, 142190 Moscow, Russia
zugazoid@gmail.com

Quantum computers are prospective for the resolution of problems which are hard to solve using conventional computing systems. However, state-of-the-art quantum machines still suffer from decoherence and quantum gate errors. The implementation of efficient error correction codes is associated with the enormous overhead of quantum resources. Therefore, the important question is what tasks can be performed without full error correction? In the present contribution, we suggest some ideas on what could be done, on new benchmarks of capabilities of quantum computers; we also develop various ideas how error mitigation can be accomplished. Our ideas are illustrated with 5- and 16-qubit superconducting quantum machines of IBM Quantum Experience.

In the first part [1], we point out that programmable quantum computers are prospective for the simulation of far-from-equilibrium dynamics of many-body systems and perform proof-of-principle digital simulations of unitary evolution for two spin models. We argue that this task does not require phase estimation algorithms, which are very fragile with respect to gate errors. Besides, there is no need for the chemical accuracy. We also show that, in such simulations, errors can be mitigated even if noise is significant - moreover, in some cases, noise can help extracting valuable information from raw data.

In the second part, we argue that quantum communication protocols can be implemented in quantum computers by measuring entropy-based characteristics of their performance and exploring whether ”quantum advantage” is achieved. This modeling provides deep benchmarks for capabilities of noisy quantum machines. We implement superdense coding and quantum key distribution BB84 and focus on efficiency of information transfer between distant parts of the processors by placing Alice and Bob at different qubits. We also examine the ability of quantum chips to serve as quantum memory used to store entangled states for quantum communication. In the third part, we develop algorithms, which can classify ”patterns”, these ”patterns” being purely quantum and characterizing an entanglement. We concentrate on circuits, which solve a classification problem for maximally entangled states in low-dimensional Hilbert spaces and also perform proof-of-principle simulations supplemented by error mitigation.

1. A.A. Zhukov, S.V. Remizov, W.V. Pogosov, Yu.E. Lozovik, "Algorithmic simulation of far-from-equilibrium dynamics using quantum computer", Quantum Inf. Process. **17**, p. 223, 2018.

Two-Way Quantum and Classical Machines with Small Memory for Online Minimization Problems

K. Khadiev[1], A. Khadieva[2]
1. Smart Quantum Technologies Ltd.; Kazan Federal University, Kazan, Russia; Center for Quantum Computer Science, Faculty of Computing, University of Latvia, Riga, Latvia;e-mail: kamilhadi@gmail.com
2. Kazan Federal University, Kazan, Russia; University of Latvia, Riga, Latvia; e-mail: aliya.khadi@gmail.com

Online algorithms are a well-known computational model for solving optimization problems. An online algorithm reads an input piece by piece and should return output variables after some of the input variables immediately, even if the answer depends on the whole input.

An online algorithm should return the answer for minimizing an objective function. The most standard is the competitive ratio [3]. It is the ratio of the cost of the online algorithm's solution and the cost of a solution of an optimal offline algorithm. Typically, online algorithms have unlimited computational power. The main restriction is a lack of knowledge on future input variables. At the same time, it is quite interesting to solve online minimization problems in a case of a big input stream such that it cannot be stored in a memory. In that case, we can discuss online algorithms with restricted memory. As the algorithms, we can consider Turing Machines with restricted memory or two-way automata with nonconstant size (a number of states). In the paper, we focus on two-way automata.

Moreover, we are interested in an advice complexity measure [1, 6]. In this case, an online algorithm gets some bits of advice. Trusted Adviser sending advice bits knows the whole input and has an unlimited computational power. Researchers pay attention to deterministic and probabilistic or randomized online algorithms with advice [2, 6]. If we consider online streaming algorithms with advice, then the quantum model can be better than classical ones [4, 5]. It is interesting to compare the power of quantum online algorithms and classical ones in a case of two-way automata.

We provide a problem for a separation between the power of quantum and classical two-way automata using this method. Suppose that algorithms use only $o(\log n)$ bits of memory in a case of exponential expected working time and $o((\log n)^{0.5-\alpha})$ bits of memory in a case of polynomial expected working time, where n is the length of an input, $0 < \alpha < 0.5$.

1. There is a special online minimization problem that has a two-way automaton with classical and quantum states with better competitive ratio than any two-way classical (probabilistic or deterministic) automata, even if the classical ones have $o(\log n)$ advice bits.
2. For the same problem, a two-way automaton with classical and quantum states has a better competitive ratio than any deterministic online algorithm with unlimited computational power has.

1. J. Boyar, L.M. Favrholdt, C. Kudahl, K.S. Larsen, and J.W. Mikkelsen. *Online algorithms with advice: A survey*. ACM Computing Surveys, **5**0(2), p.19, 2017.
2. J. Hromkovic. *Design and analysis of randomized algorithms: Introduction to design paradigms*, 2005.
3. A.R. Karlin, M.S. Manasse, L. Rudolph, and D.D. Sleator. Competitive snoopy caching. In FOCS, 1986, pp 244-254. IEEE, 1986.
4. K. Khadiev, A. Khadieva, D. Kravchenko, A. Rivosh, I. Yamilov, R. and I. Mannapov *Quantum versus classical online algorithms with advice and logarithmic space.* ArXiv:1710.09595, 2017.
5. K. Khadiev, M. Ziatdinov, I. Mannapov, A. Khadieva, and R. Yamilov. *Quantum online streaming algorithms with constant number of advice bits.* ArXiv:1802.05134, 2018.
6. D. Komm. An Introduction to Online Computation: Determinism, Randomization, Advice. Springer. 2016.

Applications of Machine Learning for Noisy Intermediate-Scale Quantum Devices

Y. Kharkov[1,2], A. Karazeev[1,3], E. Kiktenko[1,4], and A. Fedorov[1]
1. Russian Quantum Center, Skolkovo, Moscow 143025, Russia
2. University of New South Wales, Sydney, Australia
3. Moscow Institute of Physics and Technology, Dolgoprudny, Moscow Region 141700, Russia
4. Steklov Mathematical Institute of Russian Academy of Sciences, Moscow 119991, Russia

Machine learning techniques are remarkably useful for finding atypical patterns in data. It is known quantum computers perform exponentially faster than their classical counterparts for various computational tasks, in particular, for machine learning. In this contribution, we review potential applications of near-term noisy intermediate-scale quantum (NISQ) devices for applications in machine learning tasks [1].

The combination of quantum physics, quantum information theory, and machine learning represent a relatively new research filed – quantum machine learning. There are several important directions in this scope: (i) research on quantum algorithms for universal quantum computers that could act as the building blocks of machine learning programs; (ii) development of programmable special-purpose machines that are not universal quantum computers yet possess some quantum properties that enhance training classical neural networks; (iii) using classical neural networks in order to obtain variational solutions for many-body quantum-mechanical problems.

Recently explored research avenue for implementation of machine learning methods in the quantum area is quantum state tomography [2]. As it is well-known, exact brute-force approaches to quantum state tomography place a high demand on computational resources, making them unfeasible for anything except small systems. Here we realize and experimentally test a neural-network-based approach for quantum state tomography. We discuss its performance and possible extensions for tomography of quantum processes.

Another important area is learning quantum phases of matter [3]. This includes revealing exotic quantum states (phase transitions, many-body localization, and etc.) and understanding quantum dynamics. Here we demonstrate that conventional machine learning methods, such as convolution neural networks, can be used for precise identification of the transition between regular and non-integrable regimes as well as for learning complex features of quantum chaotic states with remarkably high accuracy >99%.

This work is supported by the RFBR.

1. J. Biamonte, P. Wittek, N. Pancotti, P. Rebentrost, N. Wiebe, and S. Lloyd, Nature **549**, 195 (2017).
2. G. Torlai, G. Mazzola, J. Carrasquilla, M. Troyer, R. Melko, and G. Carleo, Nature Physics, **14**, 447 (2018).
3. J. Carrasquilla and R.G. Melko, Nature Physics **13**, 431 (2017).

Machine learning methods in quantum computing theory

D.V. Fastovets[1,2], Yu.I. Bogdanov[1,2,3], V.F. Lukichev[1]
1. Institute of Physics and Technology, Russian Academy of Sciences, Russia
2. National Research University of Electronic Technology (MIET), Russia
3. National Research Nuclear University (MEPhI), Russia

Classical machine learning theory and theory of quantum computations are among of the most rapidly developing scientific areas in our days. Set of problems, solved by these theories, is growing constantly. Machine learning algorithms learn input-output correlation from training data to interpret new inputs. It is very useful for image and speech recognition tasks or business strategy optimization. Many articles have been written recently on ideas about improvement (or speed-up) classical machine learning methods by quantum algorithms [1-3]. For example, it was shown that basic algorithms (K-means, SVM, PCA and ANN) can be extended to quantum versions [4].
Our results are presented the approaches to quantum machine learning methods. We introduce tree tensor network (TTN) quantum circuit that can be used as binary classifier. We demonstrate efficiency of these methods on several classical datasets (Fisher's Iris and MNIST for example). Also we demonstrate TTN approach on the IBM quantum processor.
Quantum analogue of artificial neural networks is presented. Here, we introduce the quantum autoencoder. It is analogue of classical variational autoencoder neural network which used to code data in latent smaller space. Quantum analogue can be used for compressing quantum data. Expressing quantum state using small number of qubits is crucial, especially when trying to maximize quantum device efficiency while considering it limitations. Another way to use neural network in quantum computer science is using classical neural nets for quantum data. Here, we demonstrate quantum tomography with using neural networks approach. Such classical-quantum approach can be applied in various experiments to reveal latent dependence between input data and output measurement results.

1. *D. Kopczyk* Quantum machine learning for data scientists, Quantee Limited, Manchester, United Kingdom, 46, arXiv:1804.10068 [quant-ph].
2. *J. Biamonte, P. Wittek, N. Pancotti, P. Rebentrost, N. Wiebe, and S. Lloyd* Quantum machine learning, Nature **549**, 195-202 (2017).
3. *P. Wittek* Quantum Machine Learning: What Quantum Computing Means to Data Mining (Academic Press, New York, NY, USA, 2014).
4. *M. Schuld, I. Sinayskiy, and F. Petruccione* An introduction to quantum machine learning. Contemp. Phys. **56**, 172–185 (2015).

AlGaN/AlN/GaN HEMT with regrown ohmic contacts

V.Yu. Pavlov, D.N. Slapovskiy, A.Yu. Pavlov, M.V. Maytama, Yu.V. Fedorov
Institute of Ultrahigh Frequency Semiconductor Electronics RAS, Moscow, Russia, e-mail: alexup@bk.ru

In the conditions of increasing operating frequencies of the devices, which are determined by the electron drift velocity and the HEMT gate length, strict requirements are imposed on the growth technology of GaN-based heterostructures and on the post-growth technology of the transistor forming. The increasing of the frequencies of present-day HEMT is provided by decreasing of the gate length and decreasing of the drain-source distance [1]. Nonalloyed ohmic contacts make it possible to preserve the smooth relief and sharp edges of the HEMT ohmic contacts due to the lack of high-temperature treatment after deposition of the contact metallization. This, in turn, make it possible to form registration marks for electron beam lithography in one layer with the contact metallization, which provides better gate positioning between the ohmic contacts of the transistor with source-drain distances which can range from hundreds of nanometers to several microns. Moreover, the value of specific contact resistance of nonalloyed ohmic contacts is several times smaller than the value of the specific contact resistance of alloy ohmic ones, which is an additional advantage of their applying [2]. The results of manufacturing of AlGaN/AlN/GaN HEMT with nonalloyed ohmic contacts are presented in this paper. Nonalloyed ohmic contacts were fabricated using the technology of epitaxial regrowth of heavily doped GaN under ohmic contact. The AlGaN/AlN/GaN HEMT structure with nonalloyed ohmic contacts is shown in Fig. 1. The AlGaN/AlN/GaN HEMT was manufactured using a structure without cap-layer and with the composite barrier layer consisted of AlGaN 13 nm and AlN 0.7 nm. Before the mesa isolation was formed, the heterostructure was covered with a 5 nm dielectric Si_3N_4 which was as a protective layer of the active region of the heterostructure and a part of the future dielectric mask for the epitaxial regrowth of GaN. Then, mesa isolation and a two-layer dielectric mask Si_3N_4/SiO_2 were formed, followed by plasmochemical recess through this mask to a depth of 2DEG. With the resulting two-layer dielectric mask, a selective growth of heavily doped GaN was carried out on the heterostructure by the method of ammonia MBE at a temperature of 800 – 850 °C. After growth, the Cr/Pd/Au ohmic contacts were formed by vacuum deposition on heavily doped GaN using the resistive method. This metallization system does not require thermal treatment and provide thermal stability up to 400 °C [3]. The value of resistance of the ohmic contacts was 0.16 Ω · mm. After the ohmic contacts formation, a Schottky T-gate of Ni/Au with a gate length of 0.18 μm was formed. The static and dynamic characteristics of AlGaN/AlN/GaN HEMTs fabricated with nonalloyed ohmic contacts were measured. The maximum specific drain current (I_s) of 1.4 A/mm with the 0 V gate voltage was obtained, the maximum specific transconductance (G_m) was 360 mS/mm, the cutoff voltage was 5 V. The output I-V characteristics of AlGaN/AlN/GaN HEMT are shown in Fig. 2. The f_T of 66 GHz and f_{MAX} of 118 GHz were obtained.

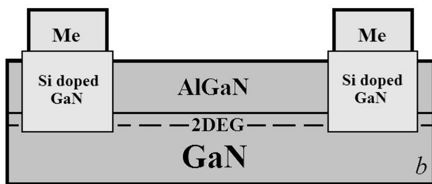

Fig. 1. The AlGaN/AlN/GaN HEMT structure with nonalloyed ohmic contacts.

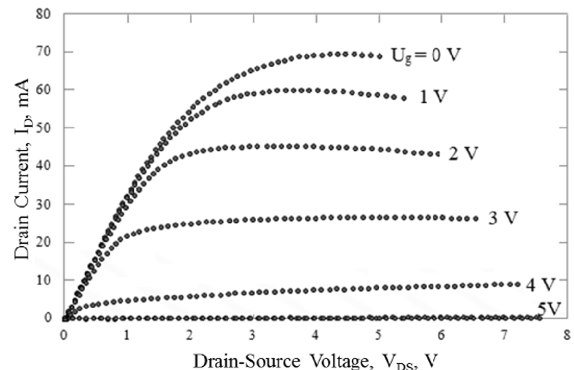

Fig. 2. Output I-V characteristics of the resulting AlGaN/AlN/GaN HEMT.

1. K. Shinohara et al. "Scaling of GaN HEMTs and Schottky Diodes for Submillimeter-Wave MMIC Applications". IEEE Transactions on Electron Devices, Vol. **60**, No 10, pp. 2982-2996, 2013.
2. V.Yu. Pavlov, A.Yu. Pavlov. "Technologies for Formation of the Alloyed and Unalloyed Ohmic Contacts to the Heterostructures on the Basis of GaN. Review". Nano- and Microsystems Technology, **18**, pp. 635-644, 2016.
3. A.Yu. Pavlov et al. "The thermal stability of nonalloyed ohmic contacts to AlGaN/GaN heterostructures". Technical Physics Letters, **43,** pp. 1043-1046, 2017.

Fabrication of electrodes for a logic element based on a disordered dopant atoms network

S. Dagesyan[1], S. Ryzhenkova[1], D. Presnov[2], I. Sapkov, V. Gaydamachenko[1], G. Zharik[1], A. Stepanov[2]

1. Lomonosov Moscow state University, Faculty of Physics, Russia, dagesyan@physics.msu.ru.
2. Skobeltsyn Institute of Nuclear Physics, Moscow, Russia

Recently it was proposed to create tunable logic electronic devices based on a disordered array of coupled nanoscale charge centers [1]. In work [2] an array of gold nanoparticles with 8 electrodes leading to them, were used to demonstrate possibility of their creation. The aim of this work is to make possible creation of similar devices but based on group of dopant atoms in semiconductor crystalline lattice, which will be much more interesting for practical applications. However, this challenge is more demanding to nanolithographic techniques used for the electrodes creation. It is required to reduce the distance between electrodes to the scale of several tens of nanometers due to the smaller size of dopant atoms.

Two methods of creating of the electrodes system leading to nanoscale region (30 – 100 nm in diameter) were developed and investigated in this work. The first one uses a high resolution negative tone electron-beam resist (low molecular weight polystyrene) and ion etching of metal similar with [3]. The second one is based on positive tone e-beam resist (PMMA) in combination with cold development and lift-off technique similar with [4]. We demonstrated that both methods provide required resolution. At least 4 electrodes leading to 30 nm region and at least 6 electrodes leading to 60 nm region can be created using the developed methods. Also they allow creating additional system of gate electrodes at 100 nm distance from the nanoscale region.

Described methods were used to form systems of electrodes on the top of silicon on insulator (SOI) substrates. The top layer of SOI substrate was 110 nm thickness undoped silicon. The electrical conductivity between pairs of electrodes was measured for different temperatures (4.2, 77 and 300 K). The electrical properties of samples created by different methods radically differed. Conductivity between the electrodes created using lift-off technique was several orders of magnitude smaller than between the same electrodes created by ion etching process. This difference can be since of penetration of dopant atoms in crystalline lattice during ion etching process. Most likely conductivity provided by these atoms will interfere with a proper work of the desired logic element. That’s why we conclude that the method using a positive tone resist with the lift-off technique is preferable for our purpose.

This work is supported by Russian Foundation for Basic Research (grant № 18-37-00414)

1. Tour J.M. et al. “Nanocell logic gates for molecular computing”. IEEE Transactions on Nanotechnology, **99**(2), pp. 100-109, 2002.
2. Bose S.K. et al. “Evolution of a designless nanoparticle network into reconfigurable Boolean logic”. Nature Nanotechnology, **10**(12), pp. 1048, 2015.
3. Zharik G.A. et al. “Nanometer Scale Lithography with Evaporated Polystyrene”. Moscow University Physics Bulletin, **72**(6), pp. 627-632, 2017.
4. Hu W. et al. “Sub-10 nm electron beam lithography using cold development of poly (methylmethacrylate)”. Journal of Vacuum Science & Technology B, **22**(4), pp. 1711-1716, 2004.

Compact Modeling of Electrical Characteristics of p-MNOS Based RADFETs

E. Mrozovskaya[1,2], P. Zimin[1,2], P. Chubunov[1,2], G. Zebrev[1]
1. National Research Nuclear University MEPhI, Moscow, Russia
2. "United Rocket and Space Corporation" - "Institute of Space Device Engineering", Moscow, Russia,
e-mail: liza.mrozovskaya @mail.ru (*poster presentation*)

Radiation has a detrimental effect on living organisms and electronics. Radioactive sources of dose are some natural and anthropogenic objects, and widely distributed on Earth: in the air, water and soil contain radioactive elements, which are sources of natural radiation; radionuclides used in agriculture, light industry; medical equipment; mining, enrichment, nuclear fuel, nuclear waste treatment, and recovery; building materials. Also, the space radiation is a serious challenge for spaceborne electronics. To control the effects of ionizing radiation in terms of dose effects, the most promising is the CMOS compatible dose detectors based on the stacked p-MOSFETs (RADFETs) (see Fig.1a) [1]. The operation of such detectors relies upon degradation of electrical characteristics with dose accumulation. Particularly, the radiation-induced threshold voltage shift is a quantitative indicator of the absorbed dose in such devices. The considered RADFETs are characterized by simplicity of performance, low cost, low consumption, compatibility with the mainstream CMOS technology, and high sensitivity. For design, prediction and proper application of the RADFETs in the radiation monitoring equipment, it is necessary to proceed combined electrical, radiation and environmental modeling of I-V characteristics of p-MNOS transistors. Particularly, we investigated experimentally behavior of its parameters and I-V characteristics as a function of total dose, dose rate, and temperature. Further, we have extracted the electrical parameters of the transistor model at different temperatures (see Fig.1b).

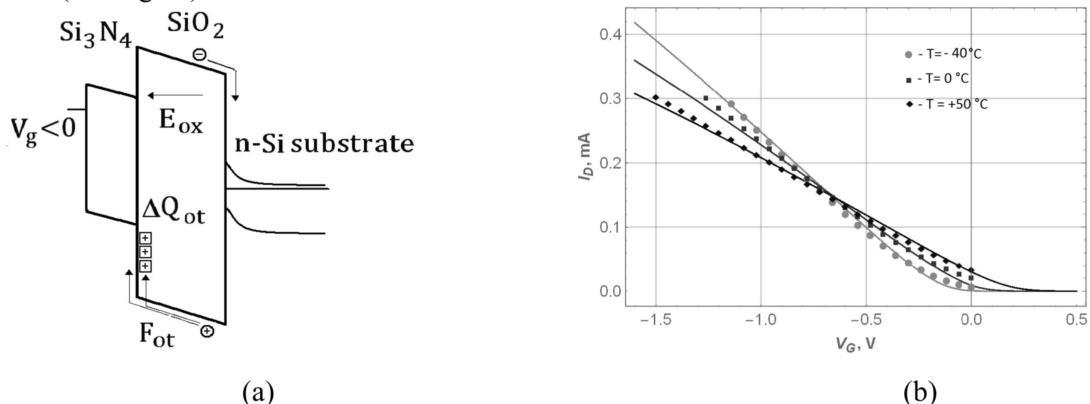

(a) (b)

Fig. 1. (a) The band diagram of the p-MNOS based RADFET. (b) The electrical simulation characterization of the RADFETs at different temperatures.

The obtained parameters were then used for validation of radiation model and simulation of I-V characteristics at different doses and temperatures. The recently published MOSFET compact model was used for this aim [2]. Such combined modeling of the electrical and radiation characteristics is a necessary condition of proper design of the promising device. The full version of the work will present the simulation results for several p-MOSFET samples with different layouts and oxide thickness under different operating conditions.

1. P. Zimin et al., "ELDRS in p-MOS and p-MNOS Based RADFETs with Thick Gate Insulators," a report accepted to RADECS 2018, Sweden, September 16th-21st, 2018.
2. G.I. Zebrev et al., "Compact Modeling of MOSFET I-V Characteristics and Simulation of Dose-Dependent Drain Currents," IEEE Trans. Nucl. Sci., V. **64**, No.8, pp. 2212-2218, 2017.

A Study of Junctionless MOSFET Using TCAD Simulations

A. Korolev, A. Krasukov, T. Krupkina, Yu. Chaplygin
National Research University of Electronic Technology, Moscow, Russia, a_kras@org.miet.ru

It is well known that CMOS technology dimensions are being aggressively scaled and limited by short-channel effects mainly by space-charge distribution from drain-substrate junction to the channel. From this point there is a very interesting device – the junctionless MOSFET (JLT) developed by Jean-Pierre Colinge form Tyndall National Institute [1].

Such device has not any p-n-junctions with space-charge regions limited transistor scaling. This device can be described as gate (field-effect) thin-film resistor. The major device advantage is simple construction which led to simplification of the fabrication process and decreasing its cost. In its initial form, JLT was constructed as a silicon nanowire with diameter d = 20 nm uniformly doped to high concentration Nsi = 10^{19} cm^{-3} to increase the threshold voltage and decrease the subthreshold current. Such concentration increases the electric field near the drain side and the band-to-band tunneling significantly increases the subthreshold current for JLT. Some methods for suppressing the band-to-band tunneling [2] while retaining high doping concentration significantly complicate the JLT structure and fabrication process.

This article presents Sentaurus TCAD [3] simulation results of JLT electrical characteristics. Simulated device is the double-gate junctionless MOSFET with n^+-source, drain and n-channel with Nsi ~ 10^{17} cm^{-3} (fig.1). Such device structure may have the following advantages with the conventional planar device:
- decreasing the transistor area;
- decreasing the effective silicon body thickness. This allows to increase Nsi with constant value of the threshold voltage;
- double gate JLT has bulk (not surface) channel. This increases the effective channel mobility and correspondingly increases the device drain current.

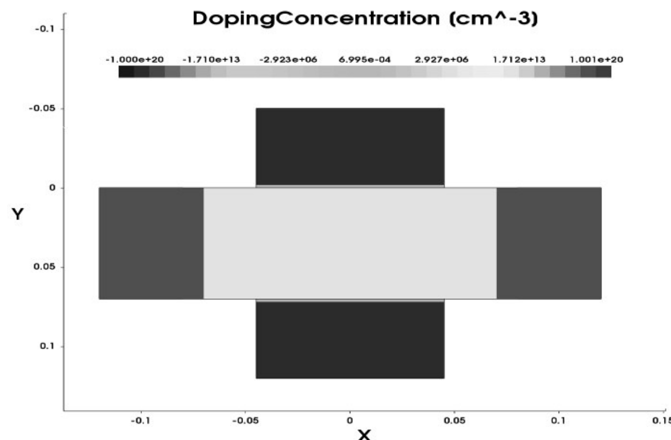

Fig. 1. TCAD model for double gate junctionless MOSFET.

The JLT model for TCAD simulation was created using 90nm SOI-CMOS design rules. $I_d(V_{gs})$ characteristics were calculated at low (0.1 V) and high (1.2 V) drain-source voltages. Dependences of threshold voltage, subthreshold slope, saturation and subthreshold currents versus the silicon body doping concentration (Nsi) were also calculated. It was shown that double gate device can have high saturation current 320 uA/um; very low off-state subtheshold current 0.3·pA/um and low subtherhold slope 82 mV/dec in comparison to conventional (inversion-mode) double-gate MOSFET parameters.

1. Lee C.-W., Afzalian A., Akhavan N.D., Yan R., Ferain I., Colinge J. Junctionless multigate field-effect transistor // Appl. Phys. Lett. 2009. Vol. 94. No. 5. P. 053511.
2. Lee C., Yan R., Ferain I., Kranti A., Akhvan N., Razavi P., Yu R., Colinge J. Nanowire zero-capacitor DRAM with transistors and without junctions // Proc. 10th IEEE-NANO. Aug. 2010. P. 242–245.
3. Yung-Chun W. Yi-Ruei J. 3D TCAD Simulation for CMOS Nanoeletronic Devices // 2018. Springer Nature Singapore Pte Ltd.

Charge effects in dielectric films of MIS structures being under high-field injection of electrons at ionizing radiation

V.V. Andreev[1], V.M. Maslovsky[2], D.V. Andreev[1], A.A. Stolyarov[1]
1. Bauman Moscow State Technical University, the Kaluga branch, Kaluga, Russia, vladimir_andreev@bmstu.ru
2. Moscow Institute of Physics and Technology (State University), Dolgoprudnyi, Moscow region, Russia, acdmaslovsky@mail.ru

Charge effects in MIS devices and integrated circuits (IC) based on these at influence of different ionizing radiation are widely studied few last decades [1]. Basically these studies are addressed to research degradation processes in MIS devices under influence of different kinds of radiations. A lowering of linear dimensions of elements of modern ICs results in fact that high-fields and tunnel injection become working modes for a wide range of MIS devices [2]. The main purpose of these studies is a discovering of method to raise radiation stability and reliability of MIS devices functioning in conditions of open space, military, atomic power, etc. Another purpose of these studies is to research a possibility of utilizing of MIS structures and devices based on these as sensors of radiation. Thus, a research of processes of radiation ionization in MIS structures being under high-field injection of electrons into the dielectric film is a great interest since high-fields stimulate processes of ionization and accelerate charge moving on the bulk of the dielectric film. At the same time this is a great interest since injected electrons can interact with charges occurring as a result of radiation ionization. Besides, an important concern is a control of change of charge characteristics of MIS structures directly at the time of influence of ionizing radiation and high-field injection of electrons into the dielectric.

In this work we study influence of α-particles, electrons, neutrons and gamma-ray onto MIS structures being under high-field Fowler-Nordheim injections of electrons into the gate dielectric by constant current [2, 3]. We discover that ionizing current occurring at the time of radiation of MIS structures being under high-field injection of electrons by constant current can significantly lower density of injection current and decrease electric field in the dielectric film. We demonstrate that from analysis of time dependency of voltage across MIS structure at the time of constant current flowing we can determine an amount of ionization current. The effect can be utilized for sensors of radiations which allow us to control both intensity of radiation and an amount of integral absorbed dose of ionizing radiation. We develop a model describing processes of change of charge state of MIS structures being under high-field injection at radiation influence. This model takes into account an interaction of injected electrons with charges occurring in the dielectric film as a result of ionization radiation.

1. T.P. Ma and P.V. Dressendorfer. *Ionizing Radiation Effects in MOS Devices and Circuits*. Wiley, New York, 1989.
2. V.V. Andreev, V.M. Maslovsky, D.V. Andreev, and A.A. Stolyarov. "Method of Stress and Measurement Modes for Research of Thin Dielectric Films of MIS Structures". Proc. SPIE., International Conference on Micro- and Nano-Electronics, **10224**, pp. 1022429(1-8), 2016.
3. D.V. Andreev, G.G. Bondarenko, V.V. Andreev, V.M. Maslovsky, and A.A. Stolyarov. “Modification of MIS Devices by Irradiation and High-Field Electron Injection Treatments”. Acta Phys. Pol. A., **132** (2), pp. 245-248, 2017.

Generation of surface states in MOS devices by space radiation protons

A.N. Volkov[1], D.V. Andreev[2], V.M. Maslovsky[3]

1. Zelenograd Research Institute of Physical Problems, Zelenograd, Russia, artem.n.volkov@yandex.ru

2. Bauman Moscow State Technical University, the Kaluga branch, Kaluga, Russia, dmitrii_andreev@bmstu.ru

3. Moscow Institute of Physics and Technology (State University), Dolgoprudnyi, Moscow region, Russia, acdmaslovsky@mail.ru

One of the main reasons of electronic devices failure, based on MOS transistors, is generation of surface states at the interface Si/SiO_2 due to Si-H bond breaking [1, 2]. Practice demonstrates that for nanosized field transistors the generation of the surface states also becomes the most significant reason of their failures despite suggestions of the models describing surface state generation for nanosized field effect transistors. The most common models to predict intensity of surface state generation are based on lucky electron model (LEM). Majority of existing models takes into account only intrinsic processes of the surface states generation and does not take into account a possible influence of extrinsic factors as, for example, protons of cosmic radiation. The energy-driven paradigm, being a promising model to predict mechanisms of formation of surface states, make an assumption that for nanosized MOS transistors the electron-electron scattering has dominating influence on process of generation of hot charge carriers and, thus, on generation of the surface states [3].

By analogy with the energy-driven paradigm model, we propose a model of calculating of intensity of surface states generation under influence of cosmic radiation protons. This model is based on two possible processes of surface states generation, which happens as a result of Si-H bond breaking:

a) a process of single excitation of Si-H bond and subsequent cutting of it under influence of proton with sufficient energy (Single Vibration Excitation by proton – SVE);

b) a proton, having insufficient energy to cut Si-H bond, can send sufficient energy to an electron of the channel, which in its turn can initiate dissociation process of Si-H bond (Proton-Electron Scattering – PES).

Utilizing model proposed we obtain an analytical expression for describing the process of formation of surface states in the SVE process under the influence of cosmic-ray protons.

1. V.S. Pershenkov, A.V. Sogoyan, and V.A. Telets. “Conversion model of radiation-induced interface-trap buildup and the some examples of its application”. IOP Conf. Series: Materials Science and Engineering, **151**, pp. 012001(1-6), 2016.

2. V.V. Andreev, G.G. Bondarenko, V.M. Maslovsky, A.A. Stolyarov, and D.V. Andreev. “Modification and reduction of defects in thin gate dielectric of MIS devices by injection-thermal and irradiation treatments”. Phys. Status Solidi C, **12** (1-2), pp. 126-130, 2015.

3. S.E. Rauch and G. La Rosa. “The energy-driven paradigm of NMOSFET hot-carrier effects”. IEEE Transactions on Device and Materials Reliability**,** **5** (4), pp. 701–705, 2005.

The physics-based modeling of TID induced leakage currents atop the buried oxide in SOI MOSFETs

M. Drosdetsky[1], M. Gorbunov[1,2], G. Zebrev[1]
1. National Research Nuclear University "MEPhI", Moscow, Russia. E-mail: m.drosdetsky@gmail.com
2. Scientific Research Institute of System Analysis, Russian Academy of Sciences, Moscow, Russia

The radiation-induced leakage current is one of the main constraints of the CMOS circuit reliability. The leakage current flows through the narrow conductive paths near the isolation oxides. It is well known that the charge trapped in the thick oxides makes a significant contribution to the dose degradation [1]. Despite the relatively low electric fields in thick oxides, they accumulate a large number of positively charged defects near the interface between the isolation oxide and silicon substrate. This, in its turn, causes the occurrence of parasitic electron channels.

The Silicon-on-Insulator (SOI) CMOS process is a promising technology for the development of radiation-hardened integrated circuits, mainly due to it's the single event tolerance. However, the presence of the thick buried oxide (BOX) in the SOI devices leads to increased dose effects sensitivity. This is due to the possibility of a parasitic channel formation near the interface between the BOX and the body. This conductive path is parallel to the gate-voltage controlled channel and this may lead to a complex behavior of radiation-induced leakage current [2].

In this work, we intend to show that the model of the leakage currents in CMOS circuits from [3] can be used to describe dose degradation of SOI transistors. This physics-based model allows for the accurate description of the leakage currents through the parasitic channel atop the BOX. The effect of the threshold dose decrease with a decrease in the channel length was investigated and simulated within the framework of the previously proposed model.

1. H.J. Barnaby *et al.*, "Total-ionizing-dose effects on isolation oxides in modern CMOS technologies". Nucl. Inst. Phys. Res. B, **261**, No. 1-2, pp. 1142-1145, 2007.
2. V. Ferlet-Cavrois *et al*. "Total dose induced latch in short channel NMOS/SOI transistors," IEEE Trans. Nucl. Sci., **45**, No. 6, pp. 2458-2466, 1998.
3. G. Zebrev *et al*. "Physics-based modeling of TID induced global static leakage in different CMOS circuits," Microelectronics Reliability, **84**, pp. 181-186, 2018.

Stabilization methods of V_{SET} and R_{OFF} in cycling process for ReRAM based on hafnium oxide

A.O. Lebedev, S.V. Ivanov, O.M. Orlov
JCS Molecular Electronics Research Institute
1-y Zapadny Proezd 12/1, Zelenograd, Moscow, 124460, Russian Federation
Phone: +7 925 841-93-98, e-mail: alebedev@niime.ru

Development of technologies for non-volatile memory is an important task of microelectronics [1]. One of the main candidates for the replacement of the standard FLASH technology is a resistive memory based on hafnium oxide [2-3]. Its production is associated with some technological problems. One of the big problems is low reproducibility of the main characteristics of memory cells. This work is devoted to the functional [4] methods of stabilizing the characteristics of ReRAM.

These methods can be divided into 2 groups: impulse and DC-methods. The voltage of the transition from the high-resistance state to the low-resistance state and the resistance in the high-resistance state have the greatest scatter. Therefore, all the methods presented in this paper modify the erasure process. The difference between these groups is the principle of work. The first one change the shape or the number or of the erasing pulse, while the second one change the principle of connecting to the cell during erasure - a constant voltage is applied to the upper electrode, while the voltage sweep changes the bias on the gate of transistor to the unlocking value.

Methods from mathematical statistics were applied to analyze the results. The set voltage for both normal cycling and modified erasure cycling is distributed normally, so it can be approximated by a Gaussian curve. It turned out that all methods reduce the scatter of the set voltage, and this can be seen from the analysis of the mean deviations. So for example, the mean value and deviation for the DC GVR method, Reset Verify method and for classical erasure cycling were 1 and 0.06 V, 1.16 and 0.06 V, 0.99 and 0.14 V respectively.

It also turned out that impulse erasing methods show a better result than DC methods. In addition to stabilizing the set voltage, they also lead to a decrease spread in the resistance in high-resistance state. This is a positive result of using the method of Reset Verify, but it is achieved with an increase in the erasure time of about 20 times compared with the usual erasure.

Table 1. Mean Values and Deviation for some methods from both groups: DC-methods and Pulse methods.

Method / Property	Classical Erasure	"Strengthened" Erasure	Application Sweep to BE	SGVR	PGVR	Reset Verify
Mean Value, V	0.99	1.43	0.89	0.98	1	1.16
Deviation, V	0.14	0.14	0.1	0.11	0.06	0.06

Table 1 shows the decrease in set voltage spread during cycling with different erasure methods.

1. *G. Krasnikov, N. Shelepin* State and prospects of development of technologies and element base of VLSI with non-volatile memory // «Designing systems on a crystal: development trends and problems». Book of Abstracts, p. 55, 2010.
2. *J.S. Meena et al*. Overview of emerging nonvolatile memory technologies // *Nanoscale Research Letters,* **9**, 526, 2014.
3. *O.M. Orlov, A.M. Markeev, A.V. Zenkevich, K.V. Egorov, A.G. Chernikova* Research features of FRAM and ReRAM non-volatile memory devices based on ALD processes. // Electronic Engineering. Series 3. Microelectronics, 2015, **4**(160), pp. 62-68.
4. *S. Yu, X. Guan, H.-S.P. Wong* // On the Stochastic Nature of Resistive Switching in Metal Oxide RRAM: Physical Modeling, Monte Carlo Simulation, and Experimental Characterization.

Electroforming-free titanium oxide nanoscale memristor structures for neuromorphic and RRAM elements

V. Avilov[1], V. Smirnov[1], N. Polupanov[1], N. Sharapov[1], O. Ageev[1,2]

1. Southern Federal University, Institute of Nanotechnologies, Electronics and Equipment Engineering, Taganrog, Russian Federation.

2. Southern Federal University, Research and Education Center "Nanotechnologies", Taganrog, Russian Federation. E-mail: ageev@sfedu.ru

One of the most important tasks of nanotechnology and nanoelectronics is the precision manufacture of structures with specified properties. Thus, one of the modern trends in the development of computing technics is the development and implementation of neuromorphic and resistive memory elements RRAM using memristor structures based on titanium oxide [1]. In this case, the local anodic oxidation method is most preferable, since it possesses high accuracy and allows in situ control of the formed electroforming-free titanium oxide memristor parameters [2]. Therefore, the actual task of this work is the formation and investigation of titanium oxide nanoscale memristors for use in neuromorphic and RRAM memory elements using atomic force microscopy.

To carry out the experimental studies, a Si/SiO_2 semi-insulating silicon substrate was used, on which a thin film of titanium with a thickness of about 20 nm was formed by magnetron sputtering. Then, by the method of focused ion beams, the structures of the lower contacts were formed, on which an oxide film with a height of 2.9±0.2 nm was formed by the local anodic oxidation method. Experimental studies of electrical properties have shown that the obtained $Ti/TiO_x/Pt$ structure exhibits a memristor effect without carrying out an additional electroforming operation. The analysis of the obtained characteristics showed a switching of the structure between the high (HRS) and low (LRS) resistance states when applying threshold voltages of ±7.5V, while the HRS structure resistance is about 1.1×10^{10} Ω and in the LRS it is about 6.8×10^{8} Ω (fig 1, ab). Then by the method of ion-assisted deposition, the structures of the upper contacts were formed (fig 1, c).

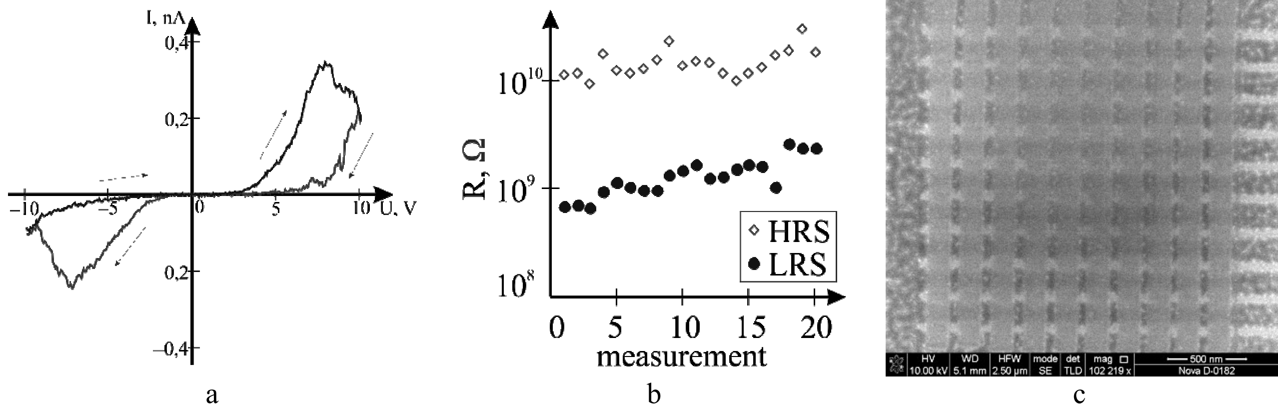

Fig. 1. Current-voltage characteristic (a), values of resistance (b) of titanium oxide and SEM-image of nanoscale memristor structures (c).

The obtained results can be used to develop technological processes for the neuromorphic and RRAM element formation on the basis of oxide nanosized titanium structures formed by the local anodic oxidation method.

This work was supported by RFBR according to the research project № 18-37-00299 and by Grant of the President of the Russian Federation No. MK-2721.2018.8. These results were obtained using the equipment of the Research and Education Center and Center for Collective Use "Nanotechnologies" of Southern Federal University.

1. R.Y. Rozanov, V.A. Kondrashov, V.K. Nevolin, Y.A. Chaplygin, "Characteristics of chloride memristors based on nanothick metal films" Russian Microelectronics, **45**, pp. 26–32, 2016.

2. V.I. Avilov, N.V. Polupanov, V.A. Smirnov et al. " Scanning probe nanolithography of resistive memory element based on titanium oxide memristor structures" Materials Science and Engineering, **256**, p. 5, 2017.

Investigation of size effect on memristive properties of ZnO thin films

R. Tominov[1], V. Avilov[1], V. Smirnov[1], E. Zamburg[2], O. Ageev[1]
1. Southern Federal University, Institute of Nanotechnologies, Electronics and Equipment Engineering, Taganrog, Russia, roman.tominov@gmail.com
2. National University of Singapore, Department of Electrical & Computer Engineering, Singapore

The memristive effect, based on a change in the electrical resistance of thin films of transition metal oxides, is promising for synaptic computer systems manufacturing [1, 2]. Synaptic computer systems offer significant advantages over conventional computers, such as high speed, high-density storage, an effective processing of unstructured data, low-power consumption. One promising oxides for this purpose is zinc oxide (ZnO), which exhibits the effect of resistive switching with increased parameters of speed and energy efficiency. Also, ZnO is compatible with traditional semiconductor technology. ZnO films formed by pulsed laser deposition have unique properties and can be used to fabricate synaptic computer system cells [3]. Today there are insufficiently experimental results to fabricate ZnO synaptic cells. Thus, the aim of this experimental work is investigation of size effect on memristive properties of ZnO thin films.

ZnO films were grown by pulsed laser deposition. Al_2O_3/TiN as a wafer was used. ZnO was used as a target. Deposition performed under the following conditions: wafer temperature: 400°C, substrate–target distance: 50 mm, O_2 pressure: 1 mTorr, pulse energy: 300 mJ, frequency 10 Hz. Number of pulses for sample 1: 1000, for sample 2: 2000, and for sample 3: 3000. AFM images of surface of ZnO films were obtained using Probe Nanolaboratory Ntegra (NT-MDT, Russia). Electrical measurements were carried out using semiconductor characterization system Keithley 4200-SCS (Keithley, USA) with W probes. During experiment, TiN layer was grounded. To prevent thermal breakdown of a thin film of ZnO, a limiting currents 0.5 and 1.0 mA were set. Current-voltage curves were obtained depending on the thickness of ZnO films at the range from -3 to 3 V, -4 to 4 V and from –5 to +5 V voltage sweep. 0.5 V was used as the read voltage. The average statistical current-voltage curve and the dependence of the HRS and LRS resistance on the number of switching cycles at a point are plotted for each ZnO sample. Curves analysis was implemented using Origin 8.1 software. It was shown, that resistive switching from high resistance state (HRS) to low resistance state (LRS) was occurred at 2.6±0.4 V and from LRS to HRS at -2.3±0.6 V for sample 1, at 2.9±0.4 V and at -3.7±0.7 V for sample 2, at 3.9±0.3 V at -5.0±0.7 V for sample 3.

Endurance test shown, that LRS was 3.8±2.4 kΩ and HRS was 27.3±7.3 kΩ for sample 1, LRS was 3.1±1.9 kΩ and HRS was 34.9±6.3 kΩ for sample 2, LRS was 3.5±1.4 kΩ and HRS was 1800.3±200.7 kΩ for sample 3. So, HRS/LRS coefficient was equaled about 7 for sample 1, about 11 for sample 2, and about 514 for sample 3. The increasing of HRS/LRS coefficient can be explained by increasing of the oxygen nanofilament dissolution length on metal/ZnO interface with increasing of ZnO film thickness. The change of LRS and HRS can be explained by the nonuniform distribution of the oxygen vacancy concentration profile in the ZnO volume during switching.

The obtained results can be used for development of technological processes of ZnO film based resistive synaptic computer systems.

This work was supported by Grant of the President of the Russian Federation No.MK-2721.2018.8 and by RFBR according to the research project № 18-37-00299. The results were obtained using the equipment of the Research and Education Center and Center for Collective Use "Nanotechnologies" of Southern Federal University.

1. R.V. Tominov, E.G. Zamburg, D.A. Khakhulin, V.S. Klimin, V.A. Smirnov, Y.H. Chu, O.A. Ageev. “Investigation of resistive switching of $Zn_xTi_yHf_zO_i$ nanocomposite for RRAM elements manufacturing”. Journal of Physics: Conference Series, **917**, pp. 032023, 2017.

2. V.I. Avilov, N.V. Polupanov, R.V. Tominov, V.A. Smirnov, O.A. Ageev. “Scanning probe nanolithography of resistive memory element based on titanium oxide memristor structures”. IOP Conference Series: Materials Science and Engineering, **256**, pp. 012001, 2017.

3. D.A. Khakhulin, Z.E. Vakulov, V.A. Smirnov, R.V. Tominov, J.G. Yoon, O.A. Ageev. “Resistive switching in ZnO/ZnO:In nanocomposite”. Journal of Physics: Conference Series, **917**, pp. 092008, 2017.

Investigations of the resistive switching of the TiN-TiO_2-SiO_2-W memristors in the oxygen atmosphere with varying pressure

E.S. Gorlachev, V.M. Mordvintsev, S.E. Kudryavtsev
Yaroslavl Branch of the Institute of Physics and Technology of the Russian Academy of Sciences, Yaroslavl, Russia, egorlachev@yandex.ru

Currently, memristors are rapidly becoming very prospective for next generation nonvolatile memory development. Memristors based on metal-insulator-metal sandwich structures with SiO_2 (SiO_x) layers present special interest, since they are fully compatible with the traditional Si-based manufacturing and are economically viable. Over the recent years, we have proposed an approach to use sandwich structures with an open SiO_2 layer sidewall (edge) and we have performed an extensive research of such memory elements, including developing their full manufacturing cycles and investigating in detail their functioning [1]. In these elements, the nonvolatile resistivity bistability effects are activated by performing a procedure of electroforming by applying a quasi-static electric pulse of ~10 V to the structure, which results in electron impact and local heating of the SiO_2 open edge, removal of oxygen to the gas phase and, consequently, formation of nanoscale Si-rich conducting phase particles and a conducting filament across the insulator edge between the electrodes. It is obvious that the functioning of such memory element would be strongly influenced by the pressure and composition of the gas phase to which the SiO_2 open edge is exposed. In this work we report the results of the studies of the oxygen influence on the TiN-TiO_2-SiO_2-W sandwich structures, which are a continuation of our first investigations of Si-SiO_2-W functioning in air [2]. For this goal, we have assembled an improved experimental setup, which allowed us to controllably set any oxygen pressure for the sample from 10^{-4} Torr to 1 atm. The resistive switching was performed by pulses of 5 V, 30 ms for the “ON” switching and 8 V, 100 ns for the “OFF” switching. For the sandwich structures studied in this work, the lower TiN electrode was 40–50 nm thick and had a thin TiO_2 oxide layer of ~3 nm; the SiO_2 thickness was 23 nm. We have studied the dependence of the average electric current in the “ON” state on the limitation current and on the oxygen pressure; the results showed the presence of a threshold pressure for which the resistive switching of the memory elements would fail. The obtained dependence of the threshold pressure on the limitation current (fig. 1) had 3 specific sections: a plateau for currents higher that 100 μA, an increase region, which can be approximated by a linear fit in logarithmic scale, thus showing its activation character, and another plateau for low limitation currents, which determined the highest operating O_2 pressure for the studied memory elements. In the report, we will discuss the physical mechanisms behind all these features and also the practical implications of the observed effects.

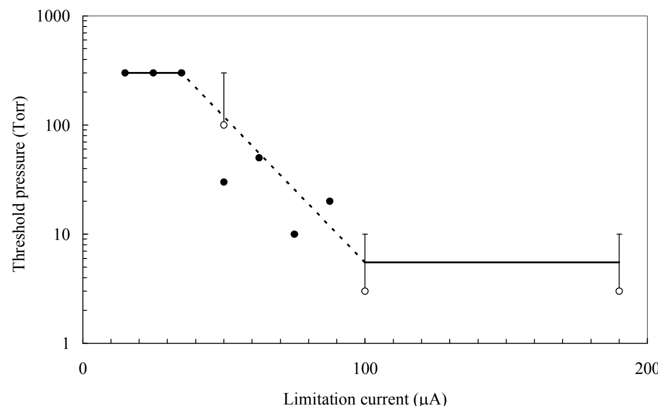

Fig. 1. Dependence of the oxygen threshold pressure on the limitation current.

1. V.M. Mordvintsev, S.E. Kudryavtsev. “Effect of constructional features of the insulating gap of open TiN-SiO_2-W and Si-SiO_2-W “sandwich” structures on the process of their electroforming.” Russ. Microelectron., **46**, pp. 243-251, 2017.
2. V.M. Mordvintsev, S.E. Kudryavtsev, V.L. Levin et al. “Influence of the pressure of the gas medium and duration of controlling pulses on the stability of characteristics of memory cells based on electroformed Si-SiO_2-W structures.” Russ. Microelectron., **39**, pp. 313-322, 2010.

Efficiency of terahertz harmonic generation in GaAs quantum wire structure: a Monte Carlo simulation

A.V. Borzdov[1], V.M. Borzdov[1], V.A. Labunov[2], V.V. V'yurkov[3]
1. Belarusian State University, Minsk, Belarus, borzdov@bsu.by
2. Belarusian State University of Informatics and Radioelectronics, Minsk, Belarus, labunov@bsuir.by
3. Institute of physics and technology, Russian Academy of Sciences, Moscow, Russia, vvyurkov@gmail.com

In present study we ascertain the efficiency of high order harmonics generation in terahertz range in the GaAs quantum wire (QW) structure. To do this we investigate nonlinear electron transport in the QW by means of ensemble Monte Carlo simulation. Size quantization effects in the QW are taken into account via the self-consistent solution of corresponding two-dimensional Schrodinger and Poisson equations. The simulation procedure includes acoustic phonon, polar optical phonon, and surface roughness electron scattering processes [1, 2].

The simulated QW is a rectangular gate-all-around GaAs/AlAs transistor channel as regarded in our previous work [3]. The GaAs is 10 nm×10 nm thick and is surrounded by 5 nm of AlAs barrier layer with aluminum gate. The QW is exposed to the external longitudinal alternating electric field. The field strength E is varying in time according to harmonic law of the form $E(t) = E_0 + E_m\sin(2\pi ft)$, where E_0 is the strength of the constant field component, E_m is the amplitude of alternating field component, f is the frequency, and t is time. The efficiency of kth harmonic generation is defined as the relation of its intensity I_k to the intensity of fundamental one I_1 and calculated according to the model presented in [4].

In the Fig. 1 the efficiency of three higher harmonics is shown for 77 and 300 K versus the value E_0/E_m for 0.5 THz fundamental frequency and $E_m = 10^5$ V/m. The gate bias is zero.

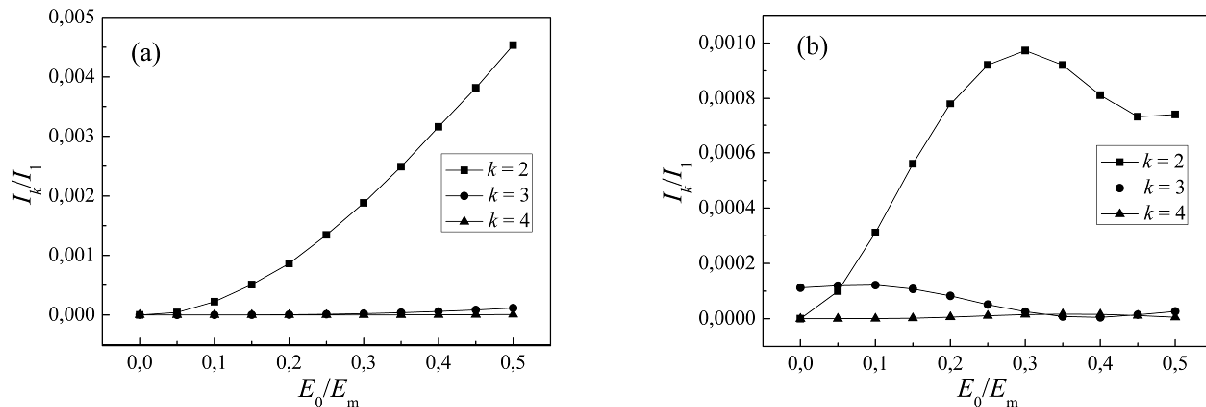

Fig. 1. The efficiency of high order harmonics generation: (a) – 77 K, (b) – 300 K.

The simulation makes it possible to determine optimal conditions for terahertz harmonics generation in the QW. Particularly, in the examined range of E_0/E_m ratio a local maximum of the second harmonic ($k = 2$) generation efficiency (corresponding to 1 THz frequency) is observed for the ratio of approximately 0.3 at 300 K while at 77 K the efficiency has monotonic increase with the growth of the constant field component strength.

1. A.V. Borzdov, D.V. Pozdnyakov, V.O. Galenchik, V.M. Borzdov, F.F. Komarov. “Self-consistent calculations of phonon scattering rates in the GaAs transistor structure with one-dimensional electron gas”. phys. stat. sol. (b), **242**, pp. R134-R136, 2005.
2. A.V. Borzdov, D.V. Pozdnyakov, V.M. Borzdov, A.A. Orlikovsky, V.V. V’yurkov. “Effect of a transverse applied electric field on electron drift velocity in a GaAs quantum wire: a Monte Carlo simulation”. Rus. Microelectronics, **39**, pp. 411-417, 2010.
3. A.V. Borzdov, V.M. Borzdov, V.A. Labunov. “Monte Carlo simulation of terahertz harmonic generation in GaAs quantum wire structure”. International Journal of Materials, **4**, pp. 70-73, 2017.
4. D. Persano Adorno, M. Zarcone, G. Ferrante. “Far-infrared harmonic generation in semiconductors: a Monte Carlo simulation”. Laser Physics, **10**, pp. 310-315, 2000.

THz GaAs/AlAs double barrier nanostructures in the rectification mode with internal amplification

A.A. Aleksanyan, A.L. Karuzskii, Yu.A. Mityagin, V.N. Murzin, A.V. Perestoronin, A.P. Chernyaev[1]

P.N. Lebedev Physical Institute of Russian Academy of Sciences, Moscow, Russia, karuz@sci.lebedev.ru

[1]Institute of Physics and Technology (State University) Moscow District, Dolgoprudny, Russia

The periodical-in-voltage negative differential conductance (NDC) oscillations (Fig. 1, without sub-THz power) [1, 2] in the current-voltage (*I-V)* characteristics of double barrier resonant tunneling diode (RTD), being attributed to LO-phonon-branch polariton excitations stimulated by electrons tunneling through the quantum active region, demonstrate the high-speed performance ($\geq 10^{13}$ Hz) of these terahertz detectors. It features the tunnel, non-metallic type of conductivity [2, 3] in the undoped region of active quantum layers in the resonance nanostructure. The high internal amplification, low-voltage operation, and supplementary functionality, inherently provided by the region of NDC, are rather encouraging for possible implementations of the RTD nanostructure detectors as an alternative for modern high-speed detectors and ultra sensors for various physical quantities (see [4] and references therein). Variations of the RTD dc component in the NDC region, i. e. changes of the *I-V* curve monitoring the external high-frequency signal in the measurement circuit cannot be explained by only the ordinary mechanism of the quadrature rectification proportional to a curvature of the *I-V* curve in the form of second derivative ($\partial^2 I/\partial U^2$). Because of the internal amplification a change of oscillation power begins to be the second affecting parameter [5]. Thus the rectification process in the NDC region should be described by the Ampere/Watt conversion efficiency of a detector in the form $(\partial^2 I/\partial U^2)/(\partial I/\partial U)$. Variations of the dc component of current $I(u(t))$ and of the oscillation power $I(u(t))\cdot u(t)$ after the Taylor series expansion of the function of the current $I(u(t))$ in the variable $u(t)=U_\omega \cos\omega t$ about $u(t)=U_0$ will give, at the expense of the quadratic terms $\sim\cos^2\omega t$, the constant contribution to the change of *I-V* curve $\sim(\partial^2 I/\partial U^2)/(\partial I/\partial U)$. A denominator $\partial I/\partial U$ allows for the change of sign of increments of the current in variations of *I-V* curve and the appearance of discontinuity-type features [2] in the NDC region (Fig. 1, with sub-THz power) caused by the effect of internal amplification.

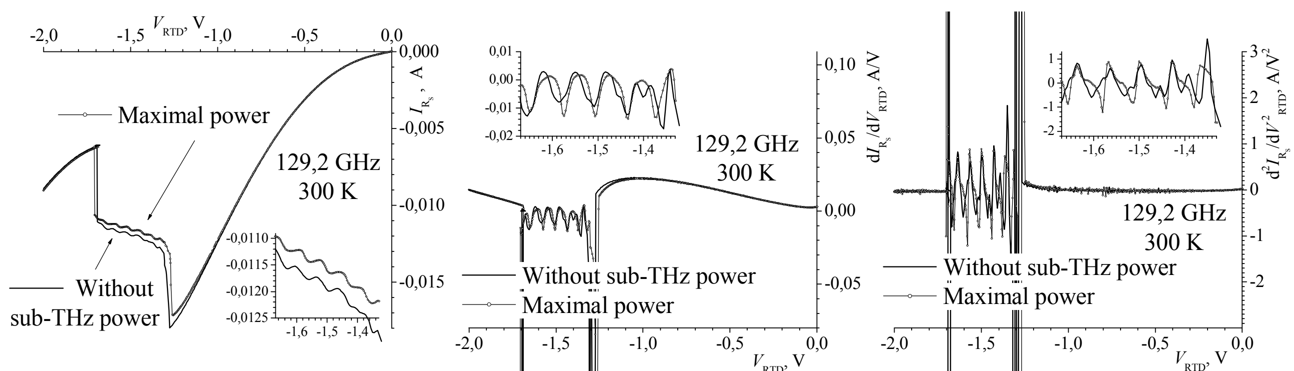

Fig. 1. First (center) and second (right) derivatives of *I-V* curves (left) for a double-barrier RTD with and without incident sub-THz power. *T*=300 K, active layers of AlAs/**GaAs** barriers/**well** 23/**45**/20 Å. Inserts show more details.

This research was supported by RFBR (18-02-00874).

1. A.A. Aleksanyan et al. "Features of the effect of the parameters of resonance systems with different configurations on the current-voltage characteristics of resonant-tunneling nanostructures in a subterahertz frequency range". Vestnik NIYaU “MIFI”, **3**, pp. 671-679, 2014 (in Russian).
2. A.A. Aleksanyan et al. “Electrically stimulated high-frequency replicas of a resonant current in GaAs/ AlAs resonant-tunneling double-barrier THz nanostructures”. Proc. SPIE, **10224**, 102240O, 2016.
3. M.A. Dresvyannikov et al. “The spatially dispersive eigenvalues of permittivity operator and frequency-dependent surface impedance for conductors without the dc dissipation”. Proc. SPIE, **10224**, 1022412, 2016.
4. A. Pfenning et al. “Sensitivity of resonant tunneling diode photodetectors”. Nanotechnology, **27**, 355202, 2016.
5. M.A. Dresvyannikov et al. "Efficiency of the signal detection in RF and sub THz ranges by means of GaAs tunnel diodes". Proc. SPIE, **10224**, 102240N, 2016.

Investigation of the characteristics of relaxation processes in multi-barrier heterostructures based on GaAs

V.A. Gergel[1], N.M. Gorshkova[1], A.S. Sobolev[1,2], M.A. Tarasov[1], V.S. Minkin[1], R.A. Khabibullin[3]

1. Institution of Russian Academy of Sciences Kotelnikov Institute of Radio Engineering and Electronics of RAS, Moscow, Russia, E-mail address: vgergel@mail.ru.

2. Moscow Institute of Physics and Technology, Moscow region, Dolgoprudny, Russia

3. Institution of Russian Academy of Sciences Institute of UHF Semiconductor Electronics of RAS, Moscow, Russia

For tasks of radar-location, technical vision and high-speed communication one of the most convenient is the millimeter wavelength range, in particular, the range of 8 mm with a frequency of about 35 GHz. Good spatial resolution of the waves of this range combined with the high penetration capability through the building construction, as well as a small scattering in fog and dust. Despite a wide variety of integrated microwave circuits in the millimeter range for telecommunication and radar applications presented on the global market, for the domestic industry remains an urgent need in the compact generators in this range that can be integrated on a single crystal of GaAs. The study of the multibarrier heterostructures based on epitaxial layers of AlGaAs/GaAs is promising for use as solid-state generators in millimeter and terahertz ranges. Unfortunately, because of too high heat dissipation, their use at room temperature requires the use of a pulsed power supply with high duty cycle. A detailed study of the dynamics of electrotermometria and relevant thermorelaxation are currently very relevant to extend the functionality of these heterostructures. The closest analogue to the structures considered in the work is resonantly tunnel diodes with an N-shaped volt-ampere characteristic. Individual scientific groups achieve a power of the order of one microwatt at a frequency of 1 THz, not only in cryogenic, but also at room temperature [1, 2]. Nevertheless, the large capacitance of the two tunneling barriers requires a reduction in the area of the diode, which together with the low density of the tunneling current severely limits the radiated power. A multilayer heterostructure based on GaAs/AlGaAs with tunnel-opaque layers was chosen for the study. The novelty of this solution is the use of the specificity of electron drift in doped nanosized superlattices with a finite number of heterobarriers. In this case, a multilayer heterostructure with alternating narrow-band and wide-gap layers is constructed (layer thicknesses, their number, degree of alloying of layers, chemical composition are calculated). The structure has a specific non-linearity of the I-V characteristic. The high-resistance initial section, corresponding to weak heating, passes into the high-current region through the bistability loop. A positive effect in the proposed heterostructures is achieved by realizing in them the thermoinjectional instability, the consequence of which is the S-shape of the static I-V characteristics. This allows us to expect generation frequencies of ~500 ... 1000 GHz in structures with a limited number of hetero-layers of nanoscale thickness. The paper presents a physico-mathematical model of the processes taking place in a multilayer heterostructure from tunnel-opaque layers of nanoscale thickness. The dynamics of electric heating and corresponding thermal relaxation with the use of the developed model is investigated.

The reported study was funded by RFBR according to the research projects 18-07-00743a and No. 18-07-00785a.

1. J. Lee, M. Kim, and K. Yang, "A 1.52 THz RTD Triple-Push Oscillator With a uW-Level Output Power", IEEE Transactions on Terahertz Sci. and Technol., **6**(2), March 2016.

2. K. Okada, K. Kasagi, N. Oshima, S. Suzuki, and M. Asada "Resonant-Tunneling-Diode Terahertz Oscillator Using Patch Antenna Integrated on Slot Resonator for Power Radiation", IEEE Transactions on Terahertz Sci. and Technol., **5**(4), July 2015.

Phase Locking in Josephson High-Q Arrays

N. Kolotinskiy, V. Kornev
Faculty of Physics, Lomonosov Moscow State University, Moscow, Russia, kolotinskij@physics.msu.ru

We consider both Josephson junction and Josephson-junction array coupled to a high-quality tank circuit and present analytical and numerical analysis for Shapiro steps, force and parametric resonances with considering both the spread in parameters and detuning between resonance frequency and frequency of en external signal. Physical mechanisms of these phenomena are discussed.

As far as Josephson junction in resistive state acts as an active element concurrently generating both the *rf* current (and *rf* voltage) and oscillating inductive parameter, both the force and parametric resonances can be observed, when the junction or the junction array are connected to high-*Q* tank circuit. Moreover, when external *rf* signal is applied to such a system, strong nonlinear interaction between the signal and the Josephson oscillations radically changes spectrum of the resultant dynamic process up to the one corresponding phase-locked oscillation state (e.g., see [1]) manifesting itself in formatting Shapiro steps on the resonance peculiarities.

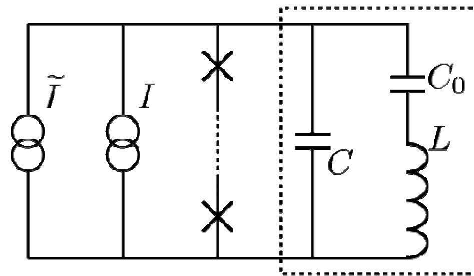

Fig. 1. Equivalent circuit describing a Josephson-junction array coupled to a high-quality parallel resonance circuit (framed by dashed line) under microwave irradiation. Here C and L are the tank capacitance and inductance, and C_0 is a capacitor block; I and $\tilde{I}$ are dc bias current and rf current, respectively.

Fig. 1 shows equivalent circuit which was used to analyze the Josephson junction array coupled to a parallel high-Q resonance circuit under external microwave irradiation, where C and L are the tank capacitance inductance, and C_0 is capacitor block. For analytical consideration of of such a system, the master equation set derived earlier for the one-junction system [2, 3] was generalized to the one capable of describing the array structure as well.

Acknowledgment:
This work is supported by Russian Foundation for Basic Research Grant 18-32-00615.

1. K.K. Likharev, *Dynamics of Josephson junctions and circuits*, ch.8. Gordon and Breach, New York 1986.
2. V.K. Kornev and N.V. Kolotinskiy, "Shapiro Steps Induced by Resonance Irradiation", IEEE Trans. Appl. Supercond., **26**(5), p. 1601605, 2016.
3. V.K. Kornev and N.V. Kolotinskiy, "Resonances and Phase Locking in Josephson High-Q Circuit", IEEE Trans. Appl. Supercond., **28**(4), p. 1500905, 2018.

Spin waves in coupled easy-axis antiferromagnet crystals

A.Yu. Sharaevskaya[1,2], E.N. Beginin[1], D.V. Kalyabin[2,3], S.A. Nikitov[1,2,3], and Yu.P. Sharaveskii[1]

1. Laboratory "Metamaterials", Saratov State University, Saratov 410012, Russia
2. Kotel'nikov Institute of Radioengineering and Electronics, Moscow 125009, Russia
3. Moscow Institute of Physics and Technology, Dolgoprudny, Russia, 408009

During last decade achievements in the fields of spintronics and magnonics have initiated interest to investigations of various antiferromagnetic (AFM) materials [1]. A great number of theoretical and experimental works has been devoted to these materials due to possible applications for new electronic component. The properties of antiferromagnetic structures have been a subject of increasing interest in recent years. Excitations in magnetic films and crystals have been investigated by a number of authors. Main carriers of signals used for information processing in such structures are magnons and, in particular, magnetostatic spin waves (MSW) [1-2].

An additional point is that Antiferromagnet (AFM) structures pay much attention for spintronic devices taking into account their strong exchanged fields [3]. Therefore in current work we investigate MSW propagation in a single AFM film and in a vertically coupled structure of two AFM layers separated by the non-magnetic dielectric layers. In the first part of the paper we state the model under which we consider MSW propagation in AFM films and structures. Here we state the basic equations and the boundary conditions and derive the dispersion equation in case when the external magnetic field is directed in-plane the film. In the second part we present the results of numerical calculations based on obtained results and discuss implementation of these results forwarded from calculations. Conclusion part discusses the main results and possible applications. We demonstrate results of calculating dispersion relation and magnetic potential for such structure. We study spin-wave propagation through AFM layers and compare effect with ferromagnetic (FM) layers.

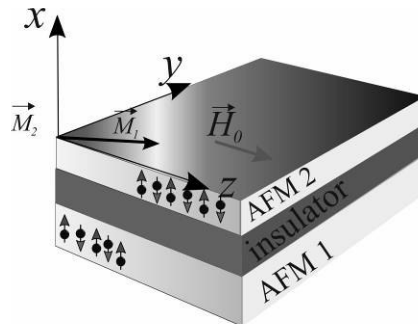

Fig. 1. Scheme of coupled AFM.

We considered a two-sublattice model which describes in [4]. We assume that a static external magnetic field, directed along the easy magnetization axis z, is of such intensity that the antiferromagnetic sublattices are in the antiparallel state. Besides, properties of real FeF2 were used and crystal considered at room temperature. Thickness of films is 3 μm, thickness of dielectric layer is 6 μm. Using coupled mode approach we showed how two modes (FM and AFM) split into symmetric and asymmetric waves compare with similar structure. The scheme of AFM structures with vertical coupling shows on fig. 1.

In general, such model can describe dispersion property of all kind easy-plane AFM with tetragonal symmetry. Effect of splitting modes in AFM and FM crystals can be used for fabrication of the component base of spintronic logic and signal processing devices in THz range.

The support from RFBR (18-57-76001, 18-07-00509) and RSF (14-19-00760) is acknowledged.

1. S.A. Nikitov, D.V. Kalyabin, I.V. Lisenkov, A.N. Slavin, *et al.*, Phys. Usp. **58**, 1099 (2015).
2. V.V. Kruglyak, S.O. Demokritov, and D.Grundler, J. Phys. D: Appl. Phys. **43**, 264001 (2010).
3. E.V. Gomonay and V.M. Loktev, Low Temperature Physics **40**, 17 (2014).
4. A.G. Gurevich*, Magnetic Resonance in Ferrites and Antiferrornagnets*. Nauka, Moscow p. 160 (1973).

Spin waves in 3D magnonic crystals

P. Popov[2,3], A. Sharaevskaia[1,2], E. Beginin[1], A. Sadovnikov[1,2], and S. Nikitov[1,2,3]
1. Laboratory "Metamaterials", Saratov State University, Saratov 410012, Russia
2. Kotel'nikov Institute of Radioengineering and Electronics, Moscow 125009, Russia
3. Moscow Institute of Physics and Technology, Dolgoprudny, Russia, 408009

Today magnetic micro- and nano-scale film structures are widely studied as potential candidates for application in spintronic and magnonic devices, which potentially can replace conventional CMOS electronics due to absence of Joule heating, operational delay and other advantages. Subjects of study in the field of magnonics usually are magnetic structures, which can be utilized as waveguides for spin waves in magnonic devices, such as magnonic crystals, thin films, narrow curved waveguides, two-dimensional arrays of magnetic columns or holes in ferromagnetic films or layered structures, coupled waveguides, etc. Their characteristics as waveguides depend on geometrical and material properties and greatly vary, often introducing effects unpresented in boundless media [1, 2].

Combining such effects in we can effectively manipulate spin wave propagation for creating filters, interferometers, switches for information transfer and storage elements, etc. Recently significant part of studies was focused on three dimensional magnetic structures, similarly to the latest trends in electronics, which develops towards expansion to topologically three dimensional element base. Such transition promises mitigation of the most urgent problems in electronics, related to scaling limits, and can be proved useful in magnonics, effectively decreasing spin wave propagation losses and introducing new effects [1-3].

In our recent work [3] we studied surface magnetostatic spin wave (SMSW) propagation in effectively three dimensional magnonic crystals, composed of isolated or vertically coupled periodic meander-type films. In such structure two different types of VMSW can exist in different areas: forward VMSW (FVMSW) in normally magnetized segments and backward VMSW (BVMSW) in segments, magnetized along direction of propagation.

Using micromagnetic modeling we obtained static internal magnetic field distribution and found conditions for FVMSW and BVMSW coexistence and mutual transformation. We also developed an analytical-numerical method of finding dispersion law for VMSW in an isolated structure. Obtained results indicated presence of band gaps in VMSW spectra, caused by Bragg reflection and inherent for such structures. Next, we developed a similar method for vertically coupled structure, which yielded a split of initial dispersion of isolated into fast and slow coupled modes. Thus, obtained results indicate a possibility of VMSW propagation with controlled group and phase velocity. Such control is possible through geometrical sizes variation. Properties of such structures might be utilized in magnonics as a way of data processing.

The support from RFBR (18-57-00006, 18-07-00509) and is acknowledged.

1. Nikitov S.A., Tailhades P., Tsai C.S.J. "Spin waves in periodic magnetic structures - Magnonic crystals ". Magn. Magn. Mater. **236**, P. 320. 2001.
2. Chumak A.V., Serga A.A., Hillebrands B. J. "Magnonic crystals for data processing ". Phys. D: Appl. Phys. **50**, P. 244001. 2017.
3. Beginin E.N., Sadovnikov A.V., Sharaevskaya A.Y. et al. "Spin wave steering in three-dimensional magnonic networks ". Appl. Phys. Lett. **112**, P. 122404. 2018.

Different magnetooptical properties of metalized nanostructured arrays on silicon surface

A.V. Prokaznikov[1], V.A. Paporkov[2], N.Yu. Zvezdin[2]
1. Yaroslavl Branch of the Institute of Physics and Technology, RAS, Universitetskaya, 21 Yaroslavl, 150007, Russia
2. Yaroslavl Demidov State University, Sovetskaya, 14 Yaroslavl, 150000, Russia
E-mail: prokaznikov@mail.ru

In these investigations we present magneto-optical studies of metal-coated nanostructures formed on a silicon surface. Three-dimensional magnetic nanostructures were created by co-sputtering two targets with the subsequent deposition of a cobalt layer. The performed comparisons of the results of angular dependences and hysteresis loops for the transverse magneto-optical Kerr effect obtained on three-dimensional magnetic nanostructures with the results of measurements performed on nanostructured samples and test samples with a homogeneous nanofilm demonstrate a different behavior. Using the method of micromagnetic simulation, the picture of the topology of magnetic moments in the case of non-magnetic defects due to nanostructuring and in the case of curved surfaces is reconstructed. It is shown that defects contribute to pinning of domain walls. On the spherical surface of nanoobjects a vortex domain structure with a common center for different vortex domains was observed, which was obtained by computer simulation.

The results obtained in this paper make it possible to draw a general conclusion that nanostructuring of samples can essentially affect the magneto-optical properties of the systems formed.

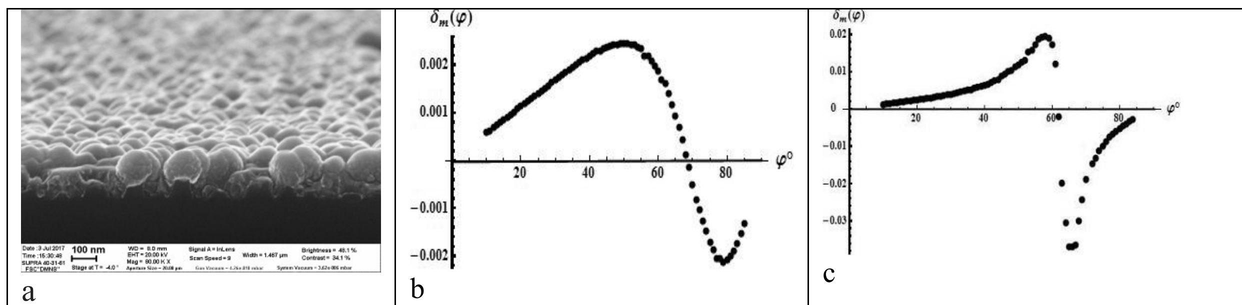

Fig. 1. General view of the formed three-dimensional magnetic nanostructure on a silicon substrate.
(a) - titanium nanostructures with cobalt tops, (b) - the graph of δ_m (φ) for the sample (left) with cobalt tops, λ = 633 nm, (c) - the graph of δ_m (φ) for the nanostructured sample (nanohills), λ = 633 nm.

The method of micromagnetic simulation was used to reconstruct the pattern of the topology of magnetic moments in the case of defects and in the case of curved surfaces. It is shown that defects contribute to pinning of domain walls. The vortex structures formed on spherical and hemispherical surfaces in the presence of the Dzyaloshinskii-Moriya interaction (DMI) in addition to a clearly expressed nucleus exhibit an additional confocal vortex with the original and partially compensating it. The magnetic moments far from the core of the vortex have a vertical component. There was observed a vortex domain structure on a spherical surface obtained by computer simulation with a common center for different vortex domains. The boundaries between different vortex domains with a common center are Bloch ones, even though the width of the domain wall is much larger than the thickness of the film.

Micro-magnetic simulations of states with several magnetic vortices on truncated spheres were obtained, and multivortex states were investigated depending on the conditions for minimizing the energy potential. Let us note that the presence of DMI interaction contributes to the formation of a singular vortex core, which can be a means of storing information. The structures studied in this paper can find application in the development of compact devices operating on spin effects. The observed phenomena find their explanation within the framework of the non-linear sigma model.

Energetics of domain wall in magnetic nanowire

O.S. Trushin[1], E. Granato[2], S.C. Ying[3]
1. Yaroslavl Branch of the Institute of Physics and Technology of RAS, Yaroslavl, Russia, otrushin@gmail.com
2. LAS, National Institute for Space Research, São José dos Campos, SP, Brazil
3. Department of Physics, Brown University, P.O. Box 1843, Providence, Rhode Island, 02912, USA

Magnetic nanowires (MN) have attracted new interest in recent years due to rich physics related to the nucleation and propagation of domain walls (DW) in it. From other side MN is of perspective object for development of racetrack memory [1]. Physics of DW nucleation and motion can be described within framework of micromagnetic theory. Theoretical estimates of energy barriers separating local energy minima can be done using Nudged Elastic Band (NEB) method. We have recently developed home made code implementing NEB within micromagnetics [2]. We focus here on the numerical study of energy landscape of magnetic nanowires. Our model system representing magnetic nanowire consists of rectangular shape single layer Permalloy nanoisland with the following dimensions: length 200 nm, width 20 nmб and thickness 5 nm. The following parameters for permalloy film were used: $A=13,0*10^{-12}$ J/m, uniaxial anisotropy constant K1=0 J/m3, saturation magnetization $Ms=8.0\times10^5$ A/m, damping constant $\alpha=0.5$. Mesh sizes were 2*2*5 nm. Using different initial guess trajectories for NEB minimization we were able to find 3 different Minimal Energy Paths presented in Fig.1. Corresponding energy profiles are shown in Fig.2.

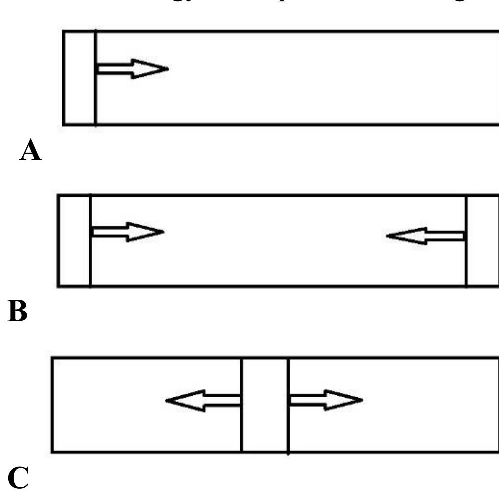

Fig. 1. Alternative transition paths for magnetization switching of magnetic nanowire.

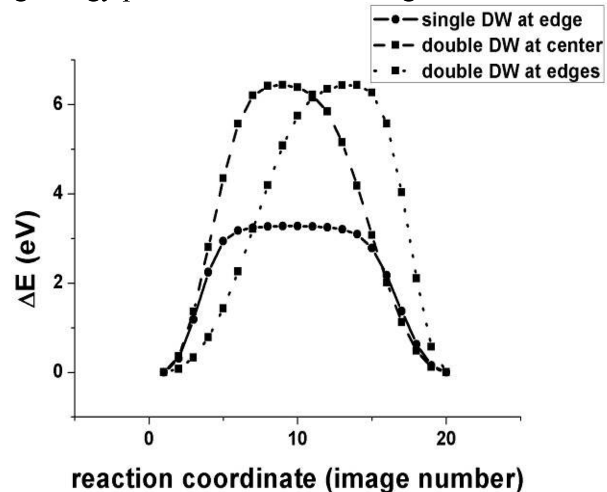

Fig. 2. Energy profiles along 3 alternative transition paths shown in Fig. 1.

The first variant of the transition path (A) starts from initial magnetization directed to the right and involves nucleation of single DW at one end and then propagation of it through the nanowire until the whole sample reaches homogeneous magnetization directed to the left. It is characterized by the lowest energy barrier. The second variant (B) starts from the same state of homogeneous magnetization and involves nucleation of two DWs of opposite chirality at both ends of the nanowire. In that case DWs move towards each other until they meet and annihilate in the middle of the nanowire. The third variant (C) is also involves nucleation of two DWs, but at the center of the nanowire. After that they move in opposite direction until reach ends of the nanowire. The effects of nanowire geometry and presence of notch on long side on the energetics of magnetic switching is also discussed.

1. S.S.P. Parkin, M. Hayashi, L. Thomas "Magnetic Domain-Wall Racetrack memory" Science, **320**, pp. 190-194, 2008.
2. O.S Trushin, N.I. Barabanova "Peculiarities of the Energy Landscape of a Rectangular Magnetic Nanoisland".Russian Microelectronics, **46**, pp. 309-315, 2017.

Edge and defect modes of spin waves in finite chains of ferromagnetic pillars

S. Osokin[1,2], A. Safin[1], S. Nikitov[1,2], D. Kalyabin[1,2]
1. Kotelnikov Institute of Radio-engineering and Electronics of RAS, Moscow, Russia
2. Moscow Institute of Physics and Technology, Dolgoprudny, Russia

Properties of the finite magnetic structures, such as waveguides and resonators, differ from the infinite and semi-infinite structures. Here, we present the theoretical study of the finite waveguide for spin-waves, formed by the linear chain of discrete ferromagnetic pillars. Also, we study properties of edge modes and defect modes of spin waves, existing due to the presence of the boundary in spatially limited structures or introduction of the singular defect in the chain.

Resonance properties of the chain of ferromagnetic pillars in the external magnetic field are considered, with the accounting of the dipole-dipole interaction between pillars in the macrospin approximation. We present the theoretical study of the spin waves in such structures by solving the Landau-Lifshits motion equation. In the proposed mathematical model the interaction between the pillars is taken into account with the help of the multiple-scattering method.

Resonance frequencies are established for different configurations of the chain: unidirectional magnetization of pillars in the chain (ferromagnetic order), two sub-lattices with opposite magnetization direction (antiferromagnetic order), and unidirectional magnetization with singular defects. Resonance frequencies for main cases (FM, AFM) were given from the calculations of eigenmodes of the finite system with estimations from the model with infinite numbers of pillars and. The edge pillars with or without defects have the specific resonance frequency for the edge mode with the excitation localized near the edge.

One of the ways to control the frequency properties of the chain of pillars is the introduction of defects, with magnetization opposite to the chain for example. The defect spin wave mode can be observed when a chain of magnetic pillars has a single defect in the middle of the array. This mode is localized near the defect and its frequency corresponds to one of the resonance frequencies for the AFM case.

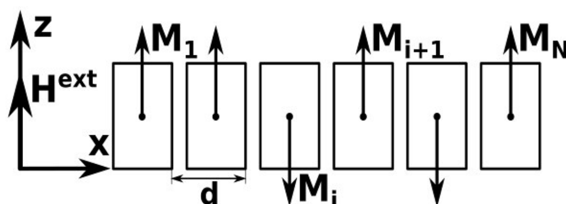

Fig. 1. Cylinrical ferromagnetic pillars placed periodically along the x-axis.

Financial support from Russian Academy of Science via the Program "Terahertz opto-electronics and spintronics", Russian Foundation for Basic Research (Project 18-07-00509) and Russian Science Foundation (Project 14-19-00760) are acknowledged.

1. Y. Barabanenkov, S. Osokin, D. Kalyabin, and S. Nikitov, Physical Review B **91**, 214419, 2015.
2. Y. Barabanenkov, S. Osokin, D. Kalyabin, and S. Nikitov, Physical Review B **94**, 184409, 2016.
3. S.A. Osokin, A.R. Safin, Y.N. Barabanenkov, S.A. Nikitov “Spin waves in finite chain of dipolarly coupled ferromagnetic pillars”, JMMM **465**, pp. 519-523, 2018.

Modeling of characteristics of low-voltage lateral MEMS switch type based on the double fixed beam

K.V. Lebedev
Institute of Physics and Technology, Russian Academy of Sciences, E–mail: kiriklebov@gmail.com

Micro- and nanoelectromechanical system (MEMS and NEMS) is a device that combines micro - and nano-electronic and micro-and nanomechanical components. A wide class of systems of MEMS and NEMS are switches. They find application in RF and microwave systems, such as adaptive antenna switching matrix and the transmitter/receiver units for wireless communication devices [1]. One of the drawbacks of electromechanical keys is a high voltage actuation. Therefore, the development of MEMS/NEMS switches with low voltage operation is an urgent task.

The presentation describes the electrostatic MEMS switch of lateral type with ohmic contacts modeled by finite element method. In the construction of the beam polymer SU-8 is used, so that the beam has a small coefficient of elasticity, allowing us to achieve a relatively low value of the actuation voltage (5 V). Modeling and a theoretical analysis of the basic electromechanical characteristics of the switch, as well as the dependence of the voltage on changes in geometric dimensions are carried out.

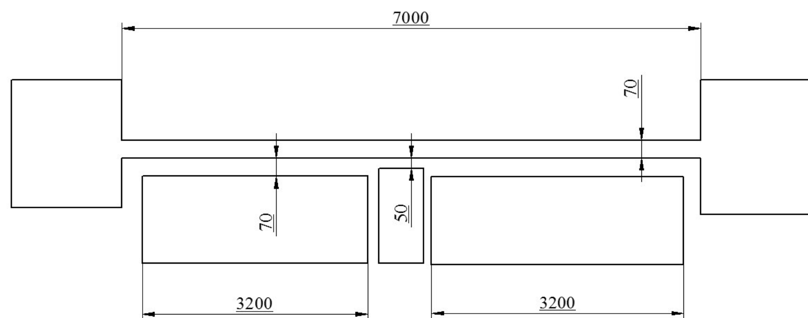

Figure 1. Geometrical sizes of the actuator (in nM).

To verify the simulation results, we calculated the actuation voltage of the MEMS switch using the following formula [2]:

$$V_{\text{Pull-in}} = \sqrt{\frac{8kg_0^3}{27\varepsilon_0 Lt}} \quad (1)$$

It was also the simulation of natural frequencies and resonant frequencies, q factor of oscillation of cantilevers made of different materials. A study of the influence of changes in geometric dimensions on the actuation voltage as well theoretical calculations of various electromechanical characteristics of the MEMS switch and the actuation time are carried out.

The data presented in the author's opinion are of interest to improve the performance of MEMS switches, reducing operation voltage, improving their reliability and reducing their energy consumption.

1. Varadan V.K., Vinoy K.J., Jose K.A. *RF MEMS and their applications*. Chichester. West Sussex: John Wiley & Sons Ltd. 2003. 394 p.
2. Rebeiz G.M. *RF MEMS: Theory, Design, and Technology*. Hoboken, New Jersey: John Wiley & Sons, Inc., 2003. 483 p.

Finite-element predictive 3D modelling and optimization of membrane-based thermoresistive MEMS accelerometers

N.A. Djuzhev, R.V. Lapshin, A.M. Belin, A.I. Ovodov, D.V. Novikov, G.D. Demin
National Research University of Electronic Technology (MIET), Moscow, Russia, andreyovodov@yandex.ru.

The scope of applications of the linear acceleration MEMS sensors is constantly growing. Nowadays each smartphone is equipped with built-in accelerometers and gyroscopes, and, according to Yole Développement estimations [1], the MEMS accelerometer market is about 1.5 billion dollars and will not decrease in the coming years. Unmanned aerial vehicles (drones) and Internet of Things should become the next market drivers and further expand the application areas for MEMS sensors, including accelerometers. In addition to increasing sensitivity and reducing costs, modern accelerometers require high reliability, resistance to dynamic and shock loads and a significant reduction in weight and size. MEMS technology has long established itself in the field of mass production of sensors. There are several types of MEMS accelerometers that measure acceleration using different physical phenomena [2], each of which has its advantages and disadvantages. In this work we propose the thermoresistive MEMS accelerometer, which measures the heat distribution under acceleration instead of measuring the deviation of the moving mass. Avoiding the use of moving parts offers a lot of advantages in terms of sensor reliability, impact resistance and zero-g offset stability.

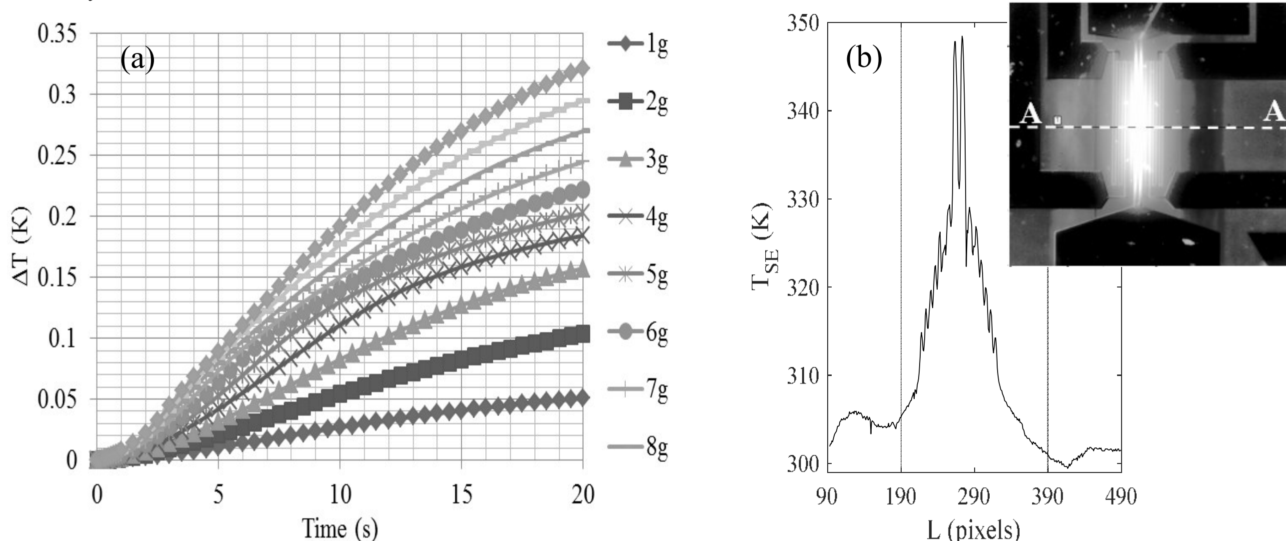

Fig. 1. (a) Time dependence of the temperature drop on the lateral thermistors of the MEMS accelerometer as a function of acceleration. (b) Experimental thermal profile due along the A-A cross-section of the sensitive thermoresistive element due to its current heating in the absence of horizontal acceleration.

Numerical simulation of the characteristics of thermoresistive MEMS accelerometer was carried out using the finite-element three-dimensional model of thermal gas dynamics of the device (Fig. 1a). This model was developed in Comsol MultiPhysics software based on fitting the simulation results to the experimental data of the thermal distribution in the sensing element of MEMS accelerometer [3] in the absence of horizontal acceleration. The presented model can be used in the future to evaluate the performance of various topologies of the thermal MEMS accelerometer in order to increase its sensitivity.

This work was performed on the equipment of MIET Core facilities center "MST and EC ", supported by the Ministry of Education and Science of RF (contract No. 14.581.21.0021, RFMEFI58117X0021).

1. Yole Developpement, "Status of the MEMS Industry 2015", Yole Developpement, France, 2015.
2. V. Narasimhan, H. Li, and M. Jianmin. "Micromachined high-g accelerometers: a review". J. Micromech. Microeng., **25**, p. 033001, 2015.
3. N. Djuzhev et al. "Application of the streamlined body for properties amplification of thermoresistive MEMS gas flow sensor". Solid State Phenomena, **245**(201), pp. 247-252, 2016.

Simulation of the sensitive element of the micro-accelerometer with the software product ANSYS

S.P. Timoshenkov, V.V. Kalugin, S.A. Anchutin, E.S. Kochurina
National Research University of Electronic Technology, Zelenograd, Moscow, e-mail: spt@miee.ru, viktor118@mail.ru

Modern technologies of Russian microelectronics make it possible to manufacture micromechanical sensors with a high level of competitiveness in relation to foreign analogues. The technology of microsystem technology allows the development of individual complex designs and entire complex integrated devices with overall dimensions up to several microns. Advances in the field of microelectronics are associated, among other things, with the use of modern software products, for example ANSYS [1, 2]. At the centre of the software product being used is the object sampling, i.e. the construction of a finite element mesh in order to solve the equations of continuum mechanics under the assumption that these relations are satisfied within the boundaries of each of the elementary regions - the finite element. In our case, the finite element grid for modeling sensor of micro-accelerometer (Fig.1) consists of 113 837 elements and contains 205 392 nodes.

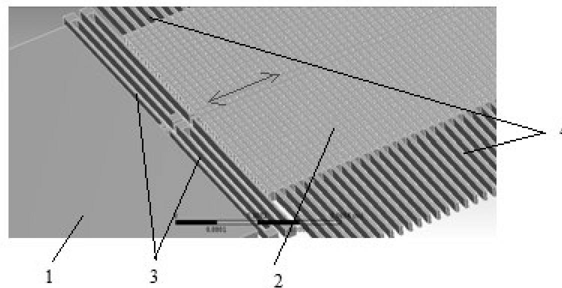

Figure 1. Fragment of geometric model of sensor of micro-accelerometer: 1 - stator, 2 - inertial mass (rotor), 3 - torsions, 4 - electrodes of the removal system.

The design of sensor of micro-accelerometer consists of inertial mass (1), which is suspended on torsion bars (3). When the acting acceleration appears along the sensitivity axis (Fig. 1 the blue arrow), the mass moves, which leads to a change in the capacitance values (4). The great change in capacitance shows what is equal to the acting acceleration.
The modal analysis showed that the working form of the sensor of micro-accelerometer oscillations (the corresponding degree of freedom) is the softest (the natural frequency is of the order of 3.54 kHz). Parasitic waveforms have higher frequencies (more than 7.9 kHz) and therefore practically do not affect the total deformation of the sensor suspension, their contribution to the motion of the sensor is minimal. High values of natural frequencies are a guarantee of the absence of resonance effects under typical external influences (with frequencies up to 2 kHz).
Static analysis was carried out for the model of sensor of micro-accelerometer under the assumption of linearity of deformations of the suspension of the sensor. The calculation showed that the relative displacement of the sensor of micro-accelerometer under the action of gravity along the sensitivity axis is 0.06 μm/g.
Thus, modeling using the ANSYS software allowed modal and static analysis, which showed that the design being developed is operational. The development of the technological process will allow obtaining samples with characteristics at the level of foreign analogues.

1. Kaplun A.B., Morozov E.M., Olferova M.A. *ANSYS v rukah inzhenera: Prakticheskoe rukovodstvo*. URSS, Moscow, 2003 (in Russian).
2. Zotov S.A., Kalugin V.V., Timoshenkov S.P., Morozova E.S., Balychev V.N. “Osobennosti proektirovanija i izgotovlenija chuvstvitel'nogo jelementa mikromehanicheskogo akselerometra”. Pribory i sistemy. Upravlenie, kontrol', diagnostika, **5**, pp. 35-37. 2008 (in Russian).

Magnetometric MEMS manufacture based on magnetoresistive nanostructures

N. Djuzhev, A. Iurov, M. Chinenkov
National Research University of Electronic Technology (MIET), Zelenograd, Moscow, Russia, chinenkov@inbox.ru

The development of contemporary MEMS-sensors, magnetic sensors in particular, aims to improve their sensitivity, thermal stability and compactness. The range of use of magnetoresistive sensors in the technique is extremely wide therefore requirements to sensitivity value are extremely broad. The sensitivity to the magnetic field is determined by the ratio of the signal amplitude imbalance in a magnetoresistive bridge, caused the by influence of the magnetic field, to the value of that field in the linear region of the transfer characteristics of the sensor. It is the most important parameter [1-3], because it determines the use of sensors to address various problems. The sensitivity value is influenced by a number of factors, among which first and foremost design and technology. To ensure a high level of output characteristics of AMR sensors it is needed to improve the magnetic properties of the magnetoresistive material. In particular, it is needed to maximize the AMR effect, which determines the output signal amplitude, and to prevent the strong growth of the coercive force and anisotropy field for maximum sensitivity and minimum hysteresis achievement. However, the magnetoresistive material parameters are determined not only by its internal characteristics, but by the composition and parameters of the film growth, particularly, average grain size.

Experimental samples of permalloy films (80%Ni20%Fe) on the silicon wafer with an insulating layer of Si_3N_4 were manufactured. The value of AMR effect was 2.2%. Then a layer of conductive material (Al) with a thickness of 0.6 μm was formed. Samples with magnetic and non-magnetic layers of a given shape were formed by using photolithography operations. Based on the obtained magnetoresistive nanostructures, magnetometric microsystems (sensors) with even and odd transfer characteristics are developed.

The sensor with an even transfer characteristic consists of four magnetoresistors in the form of a strip of thin magnetic film 0.03 μm thick with contact platforms made from aluminum of ~0.6 μm thick. The magnetoresistors on different shoulders of the bridge are turned 90° from each other, as a result of which a variation in the resistance of all resistors is provided under the action of a planar magnetic field. A prominent feature of this sensor consists in the almost total absence of linear portions. The sensors have a high output signal (~20 mV/V); however, their characteristic is nonlinear, which provides serious difficulties when measuring magnetic fields and prevents determining the magnetic-field polarity.

Sensors with an odd transfer characteristic have wider possibilities. The structure represents a strip of magnetic film 0.03 μm thick on which thin strips of high-conductivity material (aluminum) are located at an angle of 45° to the magnetic-film axis. It enables us to linearize the characteristic and to make it odd. By virtue of these circumstances, sensors with an odd transfer characteristic have received greater circulation in comparison with conventional Hall sensors.

Based on magnetometric MEMS it is possible to develop various sensors of physical quantities.

The work was performed on the equipment of MIET Core facilities center «Microsystem technique and the bases of electronic components», supported by the Ministry of Education and Science of the Russian Federation (state contract No. 14.594.21.0012, unique identifier of the project RFMEFI59417X0012).

1. N.A. Djuzhev, N.S. Mazurkin, V.S. Pozdnyakov, A.S. Iurov, M.Yu. Chinenkov. «Magnetic-field sensors based on anisotropic magnetoresistive thin-film structures for operation in wide temperature range». Semiconductors. Vol. 49, № 13, pp. 1739-1742, 2015.
2. N.A. Dyuzhev, A.S. Yurov, R.Yu. Preobrazhenskii, N.S. Mazurkin, and M.Yu. Chinenkov. «Shape-Coupled Magnetoresistive Structures: a New Approach to Higher Sensitivity». Technical Physics Letters. Vol. 42, No. 5, pp. 546–549, 2016.
3. N. Djuzhev, A. Iurov, N. Mazurkin, M. Chinenkov, A. Trifonov, M. Pushkina. «Effects of average grain size on the magnetic properties of permalloy films». EPJ Web of Conferences, 185, 01003, 2018.

Research and analysis of heat exchange processes of a micromechanical mirror based on a thermal microactuator

S. Evstafiev, V. Samoylikov
National Research University "MIET", Zelenograd, Russia, madcatse@gmail.com

Currently, there is a rapid development of technologies for the creation of microelectromechanical systems around the world. Such systems combine both mobile mechanical structures and electronic control circuits. Micromechanical mirror elements are an important class of such devices. Such mirrors allow one to control the light beam. There are several different physical principles on which such devices could operate, but one could specifically point out the devices based on the thermal principle, which allows to achieve the maximum movement of the element in comparison with the other ones [1].

This paper considers the multi-sectional structure of the thermal micromechanical mirror element, developed and manufactured by the National Research University "MIET". The structure consists of a movable part and a fixed part. The movable part includes a pair of thermal microactuators based on a multilayer structure of silicon oxide and aluminum, and a mirror reflecting element coated with aluminum. The fixed part is the area of attachment of the element to the silicon wafer. Previous studies on the analysis of the thermal state of the moving part of the element allowed us to calculate the average temperature over the length of the multi-section structure of the thermal microactuator [2].

Since the movable part of the micromirror element is a complex structure - two movable beam-heaters connected by a system of transverse thermal conducting structures that were not taken into account by the previous model, it became necessary to analyze the influence of these thermal conductive structures on the temperature distribution of this element.

The temperature distribution along the length of the multi-sectional structure of the thermal microactuator is calculated taking into account the effect of the system of transverse heat-conducting structures under various heating conditions. An essential difference between the calculations, reaching two times, was established. The experimental studies carried out under real conditions showed the adequacy of the calculation results and proved that the calculation of the temperature distribution along the length of the multi-sectional structure of the thermal microactuator should take into account the cooling effect of transverse heat-conducting structures.

Based on the calculations and experimental studies, a technique is proposed for analyzing the thermal state of the microactuator that takes into account the cooling effect of the transverse heat-conducting structures.

1. A. Zarzycki, W. Gambin, S. Bargiel, C. Goreck. *Fabrication of mems devices - a scanning micro mirror case study*. Tecno Lógicas, **20**, pp. 143-157, 2017.
2. S.S. Evstafyev, S.P. Timoshenkov, I.M. Britkov, V.K. Samoilykov, A.M. Tereshhenko. *A bimorph electrothermal actuator for micromirror devices.* Proceedings of SPIE **9467**, Micro- and Nanotechnology Sensors, Systems, and Applications VII, pp. 94672X, 2015.

Silicon nanobridge as high quality mechanical resonator

D. Presnov[1,2], S. Kafanov[3], A. Dorofeev[1], I. Bozhev[1], A. Trifonov[1,2], Yu. Pashkin[3,4], V. Krupenin[1]

1. Quantum Technology Centre, Faculty of Physics, M.V. Lomonosov Moscow State University, Leninskie Gory, 1(2), Moscow, 119991, Russia, adoroff@mail.ru

2. D.V. Skobeltsyn Institute of Nuclear Physics, M.V. Lomonosov Moscow State University, Leninskie Gory, 1(2), Moscow, 119991, Russia

3. Department of Physics, Lancaster University, Lancaster, LA1 4YB, United Kingdom

4. Lebedev Physical Institute, Moscow 119991, Russia

The resonance properties of nanomechanical resonators based on a silicon nanowire fixed at both ends coated with a thin aluminum film are experimentally investigated. A reproducible technology for fabricating such structures from silicon on an insulator (SOI) with a length of 2 to 5 μm, a width of 50 to 150 nm, and a height of 130 nm has been developed (Fig. 1a). The fabricating process is similar to that used for fabrication of field-effect transistors with a nanowire channel based sensors [1].
Using the magnetomotive method, resonant frequencies of the main mode f_0 at a temperature of 20 mK are determined for nanowires of 5.0 μm, 3.0 μm and 2.0 μm lengths: 32.46 MHz, 71.99 MHz and 150.245 MHz (Fig.1b), which corresponds to the estimates obtained from the Euler-Bernoulli theory. The measured quality factor Q of the resonator with a length of 5 μm was 36000, which is higher than the quality factor of similar resonators [2], including those made using SOI technology [3]. The ranges of parameters for which the resonators operate in linear mode are determined. As an example, it is shown that a suspended silicon nanowire 5 μm long, 115 nm wide and 130 nm high, can be used as a mass sensor with a sensitivity of $4*10^{-20}$ g/Hz$^{1/2}$ and a measurement range up to $1*10^{-14}$ g.

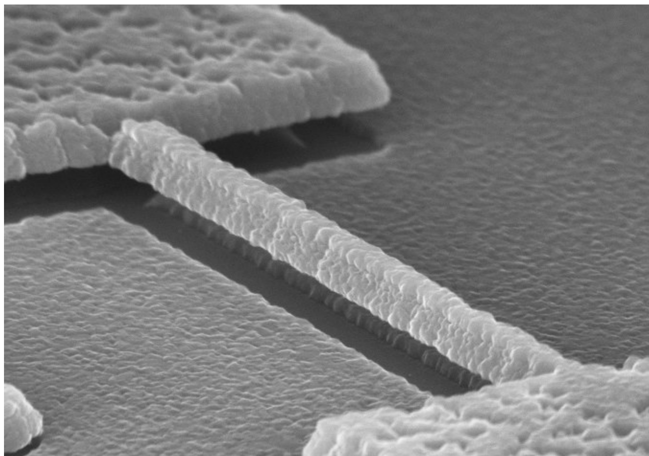

a)

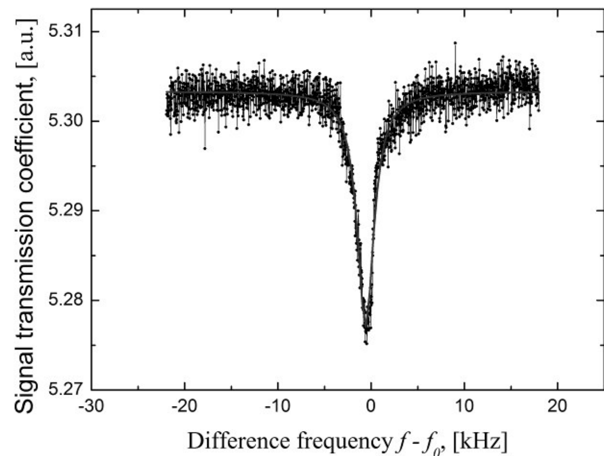

b)

Fig. 1. a) Image of a 2-μm nanomechanical resonator obtained in scanning electron microscope. b) Dependence of the transmission coefficient of the RF signal on the frequency for a suspended nanowire obtained by the magnetomotive method at B = 5 T, T = 20 mK (black), approximation of the experimental plot by the Lorentz distribution (red).

1. Presnov D.E., Amitonov S.V., Krutitskii P.A., et al. "A highly pH-sensitive nanowire field-effect transistor based on silicon on insulator". Beilstein J. Nanotechnol, **4**, pp. 330-335, 2013.
2. Cleland A.N., Roukes M.L. "Fabrication of high frequency nanometer scale mechanical resonators from bulk Si crystals". Appl. Phys. Lett. **69**(18), pp. 2653-2655, 1996.
3. Yu L., Pajouhi H., Nelis M.R., et al. "Tunable, Dual-Gate, Silicon-on-Insulator (SOI) Nanoelectromechanical Resonators". IEEE Transactions on Nanotechnology **11**(1), pp. 1093-1099, 2012.

Determination of vibration axes of a micromachined ring resonator for the modal tuning purposes

O.V. Morozov, I.V. Uvarov
Yaroslavl Branch of the Institute of Physics and Technology RAS, Yaroslavl, Russia, moleg1967@yandex.ru

Axisymmetric structures such as hemispherical shell, cylindrical shell and a ring has been widely used as the sensing elements of various solid-state wave gyroscopes (angular rate sensors). One of the main advantages of the ring-type design is the suitability to miniaturization using MEMS low-cost production principles. An axisymmetric ring detects angular velocity due to the degenerated pairs of the flexural vibration modes. In a perfectly formed ring these modes have identical natural frequencies. Thus, the standing wave precession (gyroscopic) effect can be used. The imperfections of a ring cause a frequency split between the modes and loss of this effect. The general approach to the modal frequency tuning involves the search of the vibration axes and mass trimming at the certain points of the ring by laser ablation [1]. However, the axes location of the ring resonators was not discussed in the literature. The aim of this work is to study the vibration behavior of the micromachined ring resonators by laser vibrometer technique.

We investigated the resonators of the well-known design that is shown in Fig. 1. The resonator comprises a silicon ring of the 6 mm in diameter suspended by eight radially compliant spokes, which are anchored to a support frame with the size of 10×10 mm^2 [2]. A bulk micromachining technique is used to fabricate the devices with 100-μm-thick ring/spokes on the 380-μm-thick silicon wafer. The fabrication process requires only three masks: two masks aligned at both sides of the wafer for silicon etching in a Bosch-process and one mask for metallization.

The experiments were performed at the air pressure of 0.01 mbar. Vibration of the ring was excited by a piezoelectric shaker and registered by a homemade laser vibrometer. A He-Ne laser beam was focused by the 10$^{\times}$ objective lens on the surface of the ring. The reflected beam illuminated the photodetector. The beam was placed on the edge of the ring in such a way that only a part of it was reflected. The cross-sectional area of the reflected beam was varied during the vibration. Thus, an AC voltage was observed at the output of the photodetector allowing estimation the vibration amplitude. Frequency response was measured around the eigenfrequencies of the second order in-plane modes with the step of 0.2 Hz. Resonance curves were taken at several points of the ring, located at an angular distance (φ) of 2.5° from each other in a range of 90° (Fig. 2). In most points of the ring two resonant peaks were observed characterizing a frequency split. At some points only one peak corresponding to one of the modes was detected. These positions were located on the vibration axes to be found (solid lines in Fig. 1).

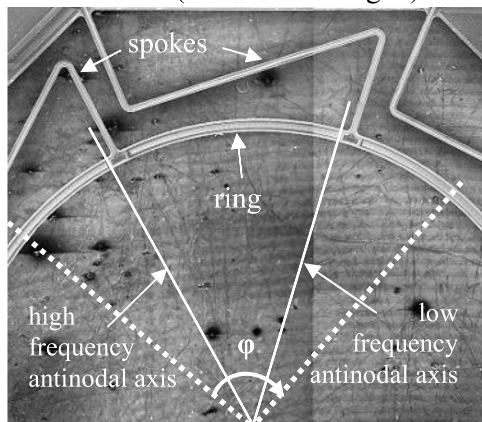

Fig. 1. SEM-image of the resonator.

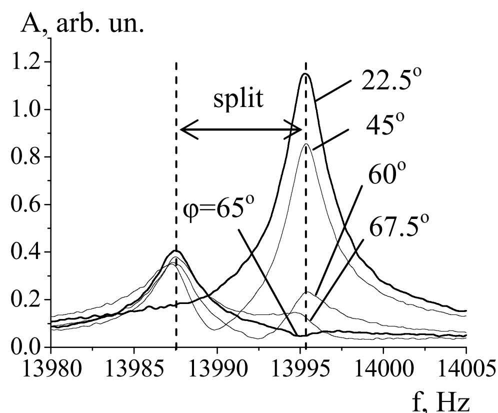

Fig. 2. Resonant curves taken at several points of a ring.

1. B.J. Gallacher et. al. "Multimodal tuning of a vibrating ring using laser ablation". Proceedings of the Institution of Mechanical Engineers, Part C: Journal of Mechanical Engineering Science. **217**. pp. 557-576. 2003. DOI: 10.1243/095440603765226858.

2. B. Chouvion. *Vibration transmission and support loss in MEMS sensors*. Ph.D. thesis. Univ. Nottingham. UK. 2010.

Development of hybrid acousto-nano-biosensors

V. Kolesov[1], V. Anisimkin[1], I. Kuznetsova[1], E. Soldatov[2], S. Dagesyan[2], A. Melnikov[2], V. Kashin[1], A. Smirnov[1]

1. Kotelnikov Institute of Radio Engineering and Electronics of RAS, Moscow, Russia, kvv@cplire.ru.

2. M.V. Lomonosov Moscow State University, Physics Department, Moscow, Russia, esold@phys.msu.ru.

At present development and fabrication of hybrid sensors is actual task. Design of hybrid sensors could be features by different technologies such as electronic, microwave, magnetic, acoustic, optic, chemical, biological ones, etc.

The actuality of the work in this field is connected with fundamental physical investigation of electron and acoustic phonon interaction in electronic devices with nanosize scale as well development of new generation of electronic devices for nanobiosensor elements.

The combination acoustoelectronic technologies with nanoelectronic and molecular devices in frame of hybrid sensor will allow achieve new quality:

- to develop sensor by using acoustoelectronic effect in low dimensional electronic devices;

- to increase the sensitivity of nanoelectronic sensors by using a modulation operating mode based on acoustic pilot signal and the transition from quasi-stationary measurement to measurement at the modulation frequency (decreasing influence of low frequency noise);
- to provide "dilute" the Helmholtz double electrical layer (DEL) (increase in the diffusion coefficients of individual components in the near-surface liquid layer) due to using charge-sensitive nanoelectronic structures in electrochemical and biochemical sensors, for example, in single-molecular DNA sequencers;
- to ensure effective cleaning of the matrix array of nanoelectronic sensors working in combination of devices such as electronic nose and electronic tongue.

Hybrid sensors can be used to registration of biospecific interactions, to detection of various biological objects, to carrying out monitoring of sensitivity of bioobjects to various antibiotics. In work the acoustoelectric chip sensor on the basis of a lithium niobate plate of 0.5 mm thick with system of the interdigital transducers (IDT) is developed for exciting the corresponding acoustic wave. This sensor is inserted into the chip holder with the standard socket of knife type. Acoustoelectronic devices have been calculated for antisymmetric (A0) and symmetric (S0) Lamb waves and a shear-horizontal (SH0) of a zero order in lithium niobate. The following crystallographic orientations for A0, S0 and SH0 waves 128YX, Y-X+50, YX, respectively, have been chosen. The chosen propagation directions are characterized by the greatest electromechanical coupling coefficient. The developed acoustoelectric chip sensor can be used in two modifications: i) the studied object place between IDT at that the sensor can plunge completely into liquid; ii) the hybrid option of a sensor jointed with the nanoelectronic sensor located in acoustically sounded area in the central region the chip sensor is implemented. For producing planar nanostructure of a nanoelectronic transducer the technology of a standard lithograph, various photoresist and reactive ion etching was used. The area of 80x80 microns in size served in the center of the chip for formation of nanostructure which is a prototype of a nanoelectronic transducer. The flare of this area was carried out by an electronic beam in a raster electronic microscope. In the produced nanostructures nanogaps for realization of molecular transistors on the basis of proteins-enzymes can be created.

The work is an initial research step in the development of a hybrid acoustoelectronic nanobiosensor based on an acoustic delay line and a nanoelectronic sensor.

Work is supported by RFBR grants #16-07-00933, 17-57-53101, 18-57-7802.

Prototype of multi-sensor system for gas detection based on effect of adsorption modified resistivity

I. Gasenkova[1], N. Mukhurov[1], S. Denicuk[1], V. Lukichev[2], K. Rudenko[2], A. Miakonkikh[2]
1. State Research and Production Association "Optic, Optoelectronic and Laser technique",
E-mail: n.mukhurov@ifanbel.bas-net.by.
2. Institute of Physics and Technology, 34 Nakhimovsky Ave., Moscow, Russia

Compact and inexpensive gas sensors are widely used in many areas of industry, environmental protection and in everyday life. The designs of modern gas sensors are based on the use of thin films of gas sensitive materials formed by chemical (sol-gel, CVD) or physical (PVD) vacuum deposition methods on dielectric substrates. Current problems for modern gas sensors are reducing of power consumption, increasing sensitivity when detecting trace concentrations, gas selectivity, speed of response, lifetime of device. The extending of the functionality of adsorption-resistive gas sensors made of metal oxide films can be achieved by using both surfaces of the dielectric substrate and introducing additional thin dielectric layers of material which is identical in composition to the dielectric substrate to increase the number of selectively detectable gases [1, 2].

The prototype of an adsorption-resistive gas multi-sensor system contains a dielectric substrate with two sensitive regions that are separated from the dielectric substrate by perforating and connected to it by jumpers at the corners of one of the sides. In the first and second sensitive regions, on top side of the dielectric substrate the heaters and thin film of interdigital data electrodes are formed. Then the films of a sensitive material insulated from the first and second heaters by a dielectric film are deposited on this side. On the back side of the dielectric substrate similar sensitive microstructures with own heaters are manufactured. Both surfaces of the dielectric substrate have the contact areas of the data electrodes system and heating elements which connected by the conductive paths with the corresponding elements of the first and second sensitive areas. Contact pads of the heating elements on both surfaces of the dielectric substrate are connected in parallel circuit through the holes in the dielectric substrate. Thin inserted dielectric films are made of the same material as the dielectric substrate, and their thickness is from 80 to 100 nm.

1. Patent of Republic of Belarus №11057 RB. Adsorption-resistive gas sensor. // N. Mukhurov, I. Gasenkova, V. Lukichev, K. Rudenko, A. Miakonkikh/ АБ, №3(110), 2016. - p. 150.
2. Patent of Russian Federation № 165023 RF. Adsorption-resistive gas sensor. // N. Mukhurov, I. Gasenkova, V. Lukichev, K. Rudenko, A. Miakonkikh / Publ. 27.09.2016. Bull. № 27.

Biosensor with two independent Si NW FETs for cancer biomarker detection

I.I. Tsiniaikin[1], G.V. Presnova[3], V.V. Shorokhov[1], M.Yu Rubtsova[3], I.V. Bozhev[1], A.S. Trifonov[1,2], S.A. Dagesyan[1], M.M. Ulyashova[3], V.A. Krupenin[1], D.E. Presnov[1,2]

1. Faculty of Physics, Moscow State University, 119991 Moscow, Russia, ii.tcinyaykin@physics.msu.ru

2. Nuclear Physics Institute, Moscow State University, 119991 Moscow, Russia, denis.presnov@physics.msu.ru

3. Faculty of Chemistry, Moscow State University, 119991 Moscow, Russia, gpresnova@gmail.com

Nowadays the number of oncological diseases is growing rapidly around all the world and therefore the early prevent diagnostic of specific biomarkers come in to the forefront of research interest. However, the application of the program for early detection of oncomarkers has been affected by the lack of sensitivity and specificity of existing assays.

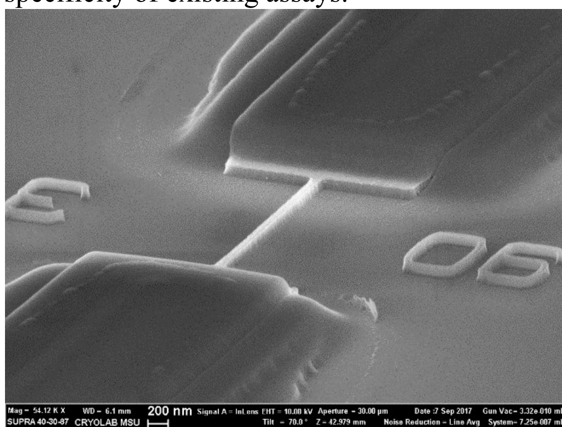

Recent developments of semiconductor nanowire field-effect transistors (NW FET) are extremely promising, especially in a field of bioanalytical applications [1]. Due to high surface-to-volume ratio of the NW, the transistor is capable to detect biomolecular interactions at their surfaces with high sensitivity.

In this work we present a label-free, highly sensitive biosensors based on a silicon nanowire field effect transistor (Si NW FET) with two independent channels for the detection of various cancer biomarkers. Si NW arrays were fabricated on silicon-on-insulator (SOI) substrates with a 110 nm top silicon layer and a 200 nm oxide layer [2]. First, the structure was patterned in positive e-beam resist in a high-resolution EBL system, then, the design was transferred in to the silicon layer through thin aluminium mask by RIE in a fluorine plasma. Next, the titanium metallic contact leads were additionally insulated by a sputtered silicon oxide layer to avoid a current leakage into analyte. The SEM image represents a NW FET with a silicon channel length of 3 μm and a width of 90 nm.

The biomarker detection is based on a highly specific recognition of analytes by antibodies immobilized on nanowire sensor surface. We used an original technique of antibodies covalent immobilization on small-sized gold nanoparticles attached to the Si NW surface [3]. Theoretical estimation of improved the surface-to-volume ratio and an increased the electrical device performance was performed.

The chip design allows modification of nanowire surface with antibodies of different specificity. This allowed us to identify the various cancer biomarkers: prostate specific antigen (PSA), thyroglobulin (Tg) and thyroid stimulating hormone (TSH) in a buffer and artificial human sera. The developed PSA biosensors were successfully applied for monitoring of PSA level in real serum samples. The limit of detection was estimated to be of ~23 fg. Compared with the well-established ELISA methods, this is two orders of magnitude better.

The work was supported by the Russian Foundation for Basic Research (Grant ofi-m 16-29-03266).

1. A. Zhang and C.M. Lieber, Nano-Bioelectronics. *Chem. Rev.,* **116**, 215-257, 2016. http://doi.org/10.1021/acs.chemrev.5b00608
2. D.E. Presnov, S.V. Amitonov, P.A. Krutitskii, V.V. Kolybasova, I.A. Devyatov, V.A. Krupenin, I.I. Soloviev, A highly ph-sensitive nanowire field-effect transistor based on silicon on insulator. *Beilstein journal of nanotechnology*, **4**, 330–335 (2013). http://doi.org/10.3762/bjnano.4.38
3. G. Presnova, D. Presnov, V. Krupenin, V. Grigorenko, A. Trifonov, I. Andreeva, O. Ignatenko, A. Egorov, M. Rubtsova, Biosensor based on a silicon nanowire field-effect transistor functionalized by gold nanoparticles for the highly sensitive determination of prostate specific antigen. *Biosensors and Bioelectronics*, **88**, 283–289, (2017). http://doi.org/10.1016/j.bios.2016.08.054

Basic principles of non-destructive 3-D microtomography in scanning electron microscopy

E.I. Rau, S.V. Zaytsev, V.Yu. Karaulov
Moscow State University, Moscow, Russia, E-mail rau@phys.msu.ru

Obtaining images of hidden under the surface micro and nano structures, that is deep monitoring of three-dimensional objects is a sought after task in nondestructive diagnostics of instrument devices having a planar thin-film structure, for example integrated circuits. In modern nanotechnology, an "ion scalpel" is usually used for monitoring, which produces either successive removal of microstructure layers or the implementation of transverse sections. An alternative non-destructive structure method is the detection of reflected electrons (RE) in a scanning electron microscope (SEM). Electron microtomography has great prospects in the field of non-contact diagnostics of modern 3-D instrument structures of micro and nanoelectronics with the ability to control at all stages of development and production of new devices.

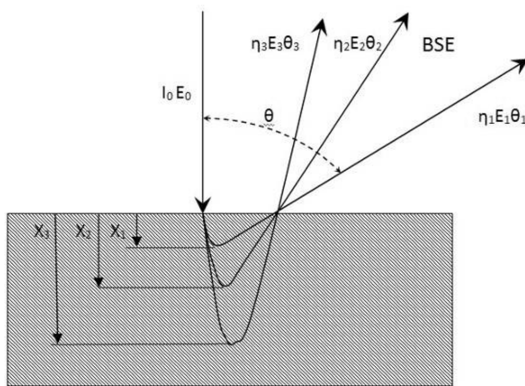

Fig.1a

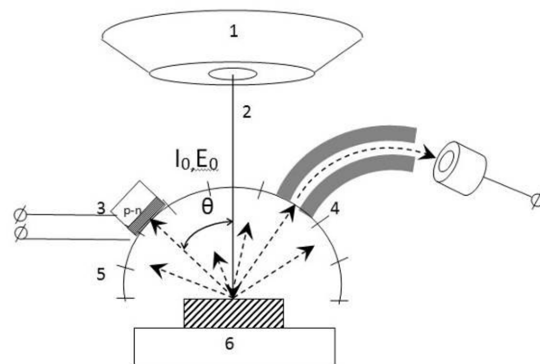

Fig.1b

In this communication, two embodiments of 3-D microtomography are considered - based on the integrated characteristics of BSE and when detecting differential coefficients by means of BSE energy filtering. In both cases, the basic principle is the combination of the three experimental parameters used. The first parameter, the electron energy E_0, determines the depth of the path of the primary electrons, that is, the depth of sounding of the sample, and thus the exit depth x_i of BSE. The second parameter is the exit angle θ_i BSE from a given depth x_i. And, finally, the third parameter is the energy E_i BSE released from the depth x_i at an angle θ_i. The root causes of these characteristics are shown schematically in Fig.1a. Fig.1b shows the scheme for implementing experiments on the proposed algorithms. The electron beam 2 SEM1 scans the sample 6. On the turrel 5, either the semiconductor detector 3 or the electron energy analyzer 4 moves under different selected angles θ_i. In the first case, the energy integral BSE is detected, in the second case, BSE in a certain energy window. The first method is operative and generally available, but gives an insufficiently clear contrast from the selected layers of subsurface structural details. The second method is less accessible, but produces a clearer separation of the layers in the 3-D structure and with a higher image contrast.

Investigation of carbon nanostructures by Photoelectron Spectroscopy

V.P. Afanas'ev[1], A.D. Barinov[1,2], G.S. Bocharov[1], Y.N. Bodisko[1], A.V. Eletskii[1], A.S. Gryazev[1], P.S. Kaplya[3], A.I. Popov[1,2], O.Yu. Ridzel[1,4]

1. National Research University "Moscow Power Engineering Institute", Moscow, Russia, v.af@mail.ru
2. Institute of Nanotechnology of Microelectronic RAS, Moscow, Russia, PopovAI2009@gmail.com
3. Raspletina st. 15, Moscow, Russia, pavel@kaplya.com
4. Vienna University of Technology, Vienna, Austria

Carbon structures such as diamond-like films formed by thermal procession of graphene oxide are studied. Obtained structures are analyzed by X-ray Electron Spectroscopy. Photoemission Electron Spectroscopy (PES) allows determination of allotropic state of a carbon surface by studying photoelectron energy losses and reconstruction of inelastic scattering cross section $x_{in}(\Delta)$. See Fig. 1 for Energy Loss Functions (ELF) of carbon samples with different allotropic states.

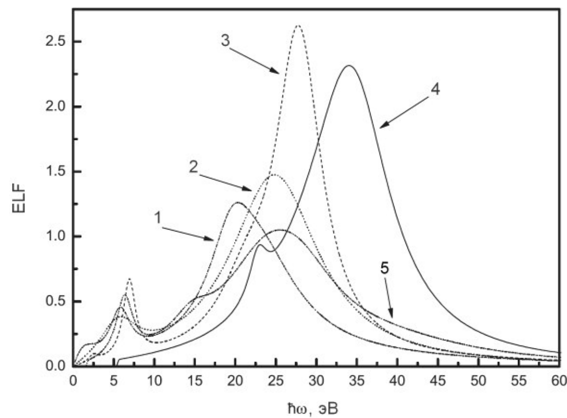

Fig. 1. Energy Loss Functions of electrons for different allotropic states of carbon [1]:
1 – glassy carbon, 2 – amorphic carbon,
3 – graphite, 4 – diamond, 5 – C_{60}.

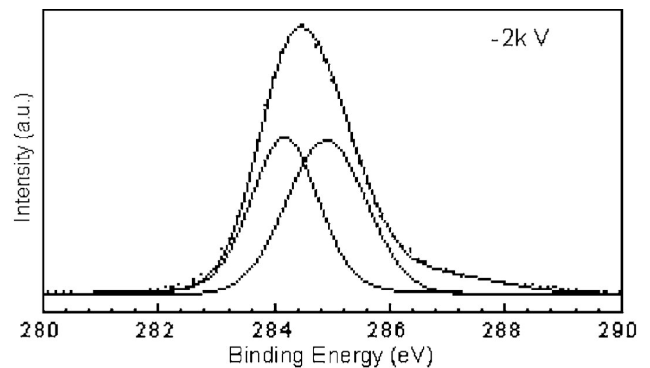

Fig. 2. Peak Shape Analysis (PSA) of carbon 1*s* peak. The peak is formed by the electron emitted from graphite sp^2 bonds and diamond sp_3 bonds [2].

Energy Loss Functions for different allotropic states are clearly distinguishable (see Fig. 1): π-plasmon peak typical for sp^2 hybridization at 7 eV energy loss and $\pi + \sigma$ peak at 28 eV are common for graphite samples. On the other hand, there are characteristic peaks at 23 and 35 eV energy losses for diamonds. See Fig. 2 for an illustration of Peak Shape Analysis (PSA) study of a peak when Rayleigh criterion is offended. The difference between sp^2 and sp^3 energy losses is about 0.7-0.8 eV but the HWHM is greater than 1 eV (Fig. 2).

In the current work PES analysis is done by numerical methods, based on fitting scattering properties and comparing experimental data to the solutions of direct problem of photoelectron scattering [3]. The fitting approach is necessary as the initial problem is mathematically incorrect. It is shown that analysis based on the inelastic scattering cross section reconstruction is well suited for studying thermal induced processes of graphene oxide, but PSA method better performs for diamond-like surface researches.

The work has been performed within the frame of the State Tasks No. 3.1414.2017.

1. N. Pauli, M. Novak, S. Tougaard, "Surface excitation parameter for allotropic forms of carbon". Surf. Interface Anal., **45**, pp. 811-816, 2013.
2. J. Zhu, J. Han, X. Han, H.I. Schlaberg, J. Wang. "*sp*^{3}-rich deposition conditions and growth mechanism of tetrahedral amorphous carbon films deposited using filtered arc". J. Appl. Phys., **104**, pp. 013512, 2008.
3. V.P. Afanas'ev, A.S. Gryazev, D.S. Efremenko, P.S. Kaplya, "Differential inverse inelastic mean free path and differential surface excitation probability retrieval from electron energy loss spectra". Vacuum, **136**, pp. 146-155, 2017.

Formation of the tungsten compound phases in diamond-like silicon-carbon nanocomposites

A.I. Popov[1,3], V.P. Afanas'ev[1], A.D. Barinov[1,3], Y.N. Bodisko[1], A.S. Gryazev[1],
I.N. Miroshnikova[1,3], M.Y. Presniakov[2], M.L. Shupegin[1]

1. National Research University «Moscow Power Engineering Institute», Moscow, Russia, GryazevAS@gmail.com
2. National Research Center «Kurchatov Institute», Moscow, Russia
3. Institute of Nanotechnology of Microelectronic RAS, Moscow, Russia, PopovAI2009@gmail.com

Diamond-like amorphous silicon-carbon films contain the mutual stabilizing structural networks of amorphous carbon with hydrogen and the silicon oxide. Such films have all advantages of traditional diamond-like carbon coating and are free from many drawbacks. It opens the prospects of their widespread using as protective coatings in space technology [1], in optoelectronics [2], etc. Moreover, high stability of silicon-carbon matrix provides the ability to introduce tens atomic percentages of metal into material on retention of its amorphous state. This allows varying properties of nanocomposite materials based on metal-containing silicon-carbon films in a wide range. For example, it is possible to vary the electrical conductivity by 16 orders of magnitude [3].

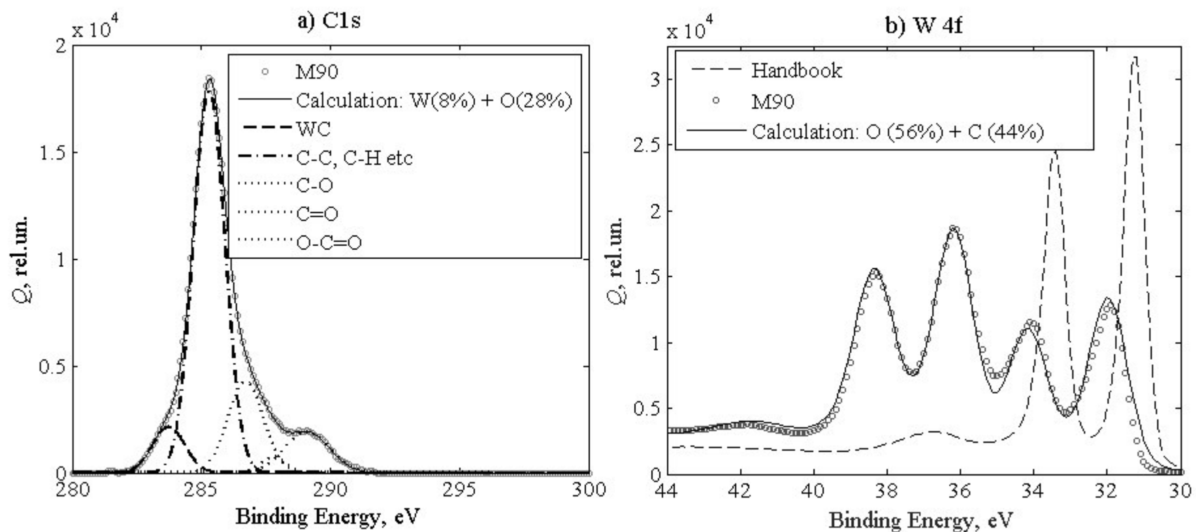

Fig. 1. XPS spectra of tungsten-containing silicon-carbon nanocomposite:
a) C 1*s* peak decomposition, b) tungsten doublet of 4*f*-photoelectron line.

As a rule, the introduction of transition metals into silicon-carbon films leads to the formation of carbides [3]. However, the study of tungsten-containing silicon carbon nanocomposites by the XPS method (Figure 1) showed that along with the carbide phase, tungsten oxide is present in the material. The carbon peak C 1*s* (Fig. 1, a) is indicative of tungsten carbide in the coating. This is also confirmed by Fig. 1, b, from which it also follows that tungsten introduced into silicon-carbon film is divided approximately equally between the nanocrystalline carbide phase and the amorphous oxide phase. The presence of an oxide phase in nanocomposites with transition metals was not observed earlier. On the other hand, this fact must be taken into account for a correct interpretation of the concentration dependences of the properties.

This work has been supported by the Russian Foundation for Basic Research under project No. 16-07-00147.

1. F. Mangolini, B.A. Krick, T.D.B. Jacobs et al. "Effect of silicon and oxygen dopants on the stability of hydrogenated amorphous carbon under harsh environmental conditions". Carbon, **130**, pp. 127-136, 2018.
2. A.I. Popov, A.D. Barinov, M.Y. Presniakov. "Modification of Properties of Silicon-Carbon Nanocomposites". J. Nanoelectronics and Optoelectronics, **9**, pp. 787-791, 2015.
3. A. Popov. *Disordered Semiconductors: Physics and Applications (2nd Edition)*. Pan Stanford Publishing Pte. Ltd., Singapore, 2018.

Photoluminescence of AlGaAs/GaAs quantum well heteroepitaxial structures

M.R. Yuskaev[1], D.A. Pashkeev[1,3], A.V. Nikonov[1,2], V.E. Goncharov[1,3]

1. JSC "Scientific and Production Association "Orion", Moscow, Russia. 2. Moscow Institute of Physics and Technology (State University), Dolgoprudny, Russia. 3. MIREA - Russian Technological University, Moscow, Russia.

The widespread use of promising semiconductor materials in the technology of developing modern photodetectors involves a careful study of the physical properties of both the materials themselves and complex semiconductor compounds they based on [1]. Quantum well photodetectors (QWIPs) based on A^3B^5 compounds have a variety of advantages over traditional narrow-band semiconductor photodetectors. This work is devoted to the investigation of optical characteristics of $Al_xGa_{1-x}As$ compounds and development of a quality control technique for photosensitive elements based on GaAs/AlGaAs multiple quantum wells (MQWs) by analyzing the photoluminescence (PL) spectra.

Investigated samples are multilayer heterostructures with active $Al_{0,3}Ga_{0,7}As$(45 nm) / GaAs:Si(5 nm, $1\cdot10^{18}$ cm^{-3}) layers, grown by molecular beam epitaxy (MBE). Samples were subjected to the exciting radiation of 0.266 μm Nd: YAG Q-switch laser with 6 ns pulse duration and 1.005 mW power.

PL spectra of heterostructures with nanosized layers were measured at various temperatures (300 K & 7 K). The PL characteristics distribution map at 300 K (Fig. 1) is constructed using data collected from spectra of sample's surface.

The results of this study proved that PL mapping is an effective semiconductor structures quality control tool. This technique is used in A^3B^5 and A^2B^6 compounds production.

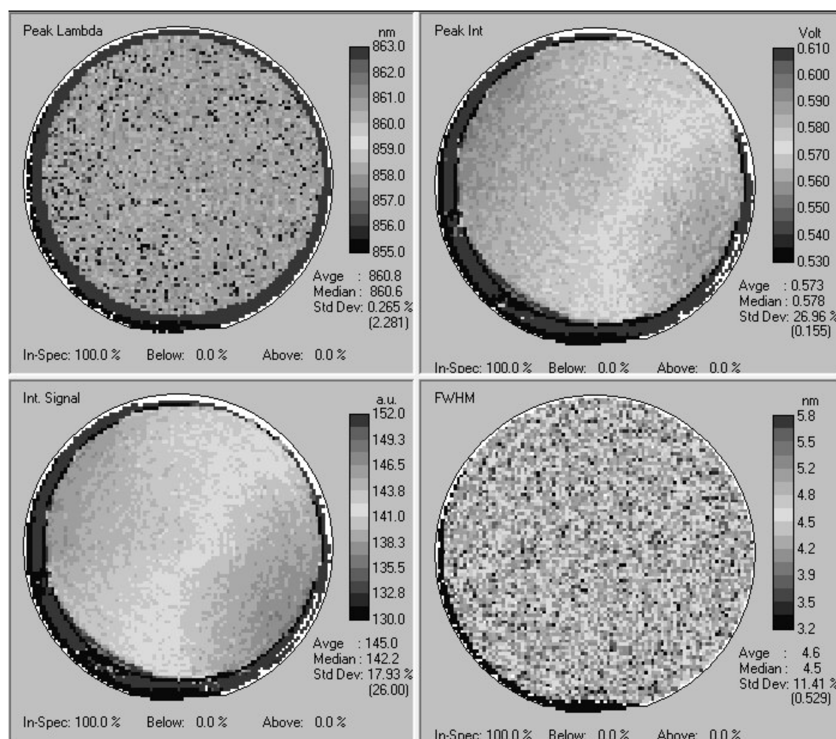

Figure 1. GaAs/AlGaAs MQW sample PL charasteristics distribution map at 300 K.

1. I.D. Burlakov, A.I. Dirochka, V.P. Ponomarenko et al. "Solid state photoelectronics: the current state and new prospects". Journal of Communications Technology and Electronics **61**, pp. 1166- 1174, 2016.

Structural properties of InSb substrates for MBE

A.E. Mirofyanchenko, E.V. Mirofyanchenko
JSC «SPA «Orion», Moscow, Russia, E-mail address: mirofianchenko@gmail.com

Indium antimonide is used for fabrication focal plane arrays (FPA) in the mid- infrared spectral range (3-5 µm) [1]. The structural properties of the samples were investigated by the high-resolution X-ray diffraction method. We used the Bruker Discover D8 X-ray diffractometer in θ/2θ geometry (radiation from the K_{α} line of Cu with a wavelength of 1.54 Å was used).
The samples investigated were 3 (100)–oriented InSb wafers. The values of the full width at half maximum (FWHM) and the shapes of the rocking curves (RC) were used the evaluation of the structural properties. The FWHM plotted as spatial distributions (map). The map of FWHM values was used as indicator of crystalline quality. It can be seen that these samples are locally unperfected over substantial fraction of their area. The fig. 1 show some "hotspot" where the rocking curve width locally is much large than its mean value.

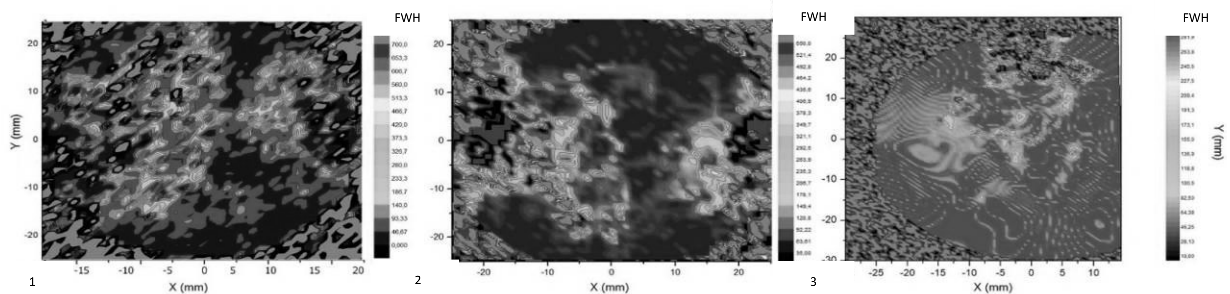

Fig. 1. Maps of FWHM.

At fig. 1 is shown non-uniform distribution of FWHM values. There are regions the average value of the FWHM is 200 arcsec. To determine the influence of dislocations on RC, the samples were investigated by the method of preferential etching [2-6]. Etch pit densities locally are greater than 10^2 cm^{-2}. At the same "hotspot" the value FWHM is much large than its mean value. At fig 2 is shown cellular distribution of the etch pits.

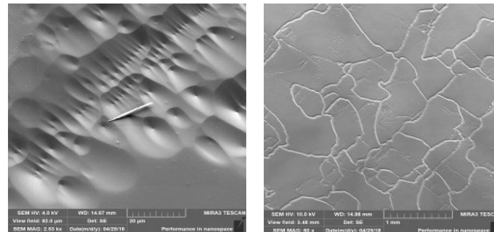

Fig. 2. Preferential etching.

Investigation of structural properties of InSb (100) substrates for molecular beam epitaxy by X-ray diffraction was presented. The relation between rocking curve peak position and full width half maximum (FHWM) with structural imperfections were demonstrated. Crystalline quality maps were created and analyzed.

1. Inaba K. *Rigaku J.* 2014. Vol. 30. P. 7.
2. Ferrari C., Buffagni E., Bonninia E., Korytar D. *J. of Applied Crystallography*. 2013. Vol. 46. P. 1576.
3. Lubbert D., Ferrari C., Mikulık P., Pernot P., Verdi N., Korytar D., Baumbach T. *J. Applied Crystallography*. 2004. Vol. 38. P. 91.
4. Zhao Y., Zhang J. *J. Applied Crystallography*. 2008. Vol. 41. P. 1095.
5. Williamson G.K., Hall W.H. *Acta Metallurgica*. 1953. Vol. 1. P. 22.
6. Yang G., Jones R., Klein F., Finkkelstein K., Livingston K. *Diamond Related Materials*. 2010. Vol. 39. P. 99.

The investigation of the quantum entanglement generation in the process of state transfer along the quantum chain

E.I. Kuznetsova[1], I.D. Lazarev[2]
1. Institute of Problems of Chemical Physics, of Russian Academy of Sciences, Chernogolovka, Moscow region, 142432, Russia, kuznets@icp.ac.ru
2. M.V. Lomonosov Moscow State University, Faculty of Fundamental Physical-Chemical Engineering, 119991, Moscow GSP-1, Russia.

Our work is devoted to a transfer of a quantum state through the chain and the generation of the entanglement between the sender and the receiver in this process. An investigation of such process was begun by Bose [1]. We consider a homogeneous chain with spins s = 1/2, which are coupled by the dipole-dipole interaction (DDI). All spins besides the first one are in the thermodynamic equilibrium state, and the first spin is in a pure state. The system evolution is governed by the flip-flop Hamiltonian. We show that this chain is suitable for a transfer of the quantum state. Especially interesting results were obtained for the entanglement generation. Conditions for emergence of entanglement are different at high and low temperatures. If the parameter β, which is proportional to the inverse temperature, exceeds the quantity

$$\beta_c = 2\ln\left(\frac{|a|}{|b|}\right), \quad (1)$$

than entanglement emerges in the time of the quantum state transfer. If β significantly exceeds β_c we can evaluate the concurrence [2] by the analytical formula

$$C = 2|b|^2\sqrt{FG} \quad (2)$$

where *F* and *G* are the functions of time, *a* and *b* characterize the polarization of the pure transferred state. If the inverse temperature is lower than (1) entanglement does not emerge at the state transfer. However, it emerges later and reaches the maximal value at the condition *F*+*G*=1. Such peaks are repeated periodically. We found that the entanglement can be generated even at temperature

$$\beta \approx \sqrt[2N-4]{\frac{|b|^2}{FG}} << 1. \quad (3)$$

It is necessary to note that the entanglement generation at high temperatures can be predicted using the results of work [3] in the system under consideration. Thus, we investigated the process of the entanglement generation at the quantum state transfer along the linear spin chain.

The work is supported by the Russian Foundation for Basic Research (Grant № 16-03-00056), the Program of the Presidium of RAS No 1.38P “Investigations of fundamental problems of synthesis and the “structure-property” dependence for creation of new compounds and materials”, RFBR and NSFC (Grant No. 18-57-53007).

1. S. Bose, Phys. Rev. Lett., **97**, 207901 (2003).
2. W.K. Wootters. “Entanglement of Formation of an Arbitrary State of Two Qubits”, Phys. Rev. Lett., **80**, 2245 (1998).
3. N. Johnston. “Separability from spectrum for qubit-qudit states”, Phys. Rev. A, **88**, 062330 (2013).

Multi-qubit controlled NOT gates for artificial intelligence natural languages processing

M.F. Ablayev[1], S.N. Andrianov[2], N.S. Andrianova[1], A.A. Kalachev[3], S.A. Moiseev[4], A.V. Vasiliev[1]

1. Kazan Federal University, Kazan, Russia, fablayev@gmail.com

2. Institute for Applied Research of Tatarstan Academy of Sciences, Kazan, Russia, andrianovsn@mail.ru

3. Kazan Physical and Technical Institute of Kazan Scientific Center of Russian Academy of Sciences, Kazan, Russia, a.a.kalachev@mail.ru

4. Quantum Center of Kazan National Technical University, Kazan, Russia, samoi@yandex.ru

Artificial intelligence performs natural language processing using machine learning and evolutionary genetic algorithms. Physical implementation of machine learning for natural language processing via genetic algorithms is perspective with neural nets. In natural language processing, the first layer of neural net often is 1-hot embedding, where each word from M words vocabulary is described by its own dimension in M-dimensional space. Neural net through the interconnections via hidden layer connects this input layer with output layer where each word is in distributed embedding forming space of much smaller dimension and is represented by target and context words. It leads to learning some meaning since words with relating meaning are distributed close to same context words. With that, neural networks are effective in quantum regime using entanglement for narrowing the embedding space.

Quantum neural network based on single-qubit rotation gate and two-qubit CNOT gate was proposed in paper [1] and improved in paper [2]. Learning algorithm with such neural network was considered in paper [3]. It was shown in papers [4-6] that this kind of neural network is efficient with multi-qubit CNOT gate. Multi-qubit CNOT gate allows performing learning algorithm by smaller number of steps. Physical implementation of multi-qubit CNOT gates was considered in papers [7-9]. Multi-qubit CNOT gate of paper [7] is performed in several steps. Gates [8,9] can be realized at extremely low temperatures.

Here, we propose and consider multi-qubit CNOT gate based on multi-wave dynamical holography that can be executed in a single step and at room temperatures. Theory of such multi-qubit gate is constructed using input-output formalism. Parameters matching conditions are found that must be fulfilled for successful gate operation. Recommendations are given for the construction of quantum neural nets that are able to solve various practical problems of natural language processing.

1. N. Matsui, N. Kouda, and H. Nishimura. "Neural networks based on QBP and its performance". Proceedings of the IEEE-INNS-ENNS International Joint Conference on Neural Networks, **3**, pp. 247-252, 2000.
2. J. Li. "Quantum-inspired neural networks with application". Open Journal of Applied Sciences, **5**, pp. 233-239, 2015.
3. P.C. Li and S.Y. Li. "Learning algorithm and application of quantum BP neural networks based on universal quantum gates". Journal of Systems Engineering and Electronics, **19**, pp. 167-174, 2008.
4. M. Cao and P. Li. "Quantum-inspired neural networks with applications". International Journal of Computer and Information Technology, **3**, pp.83-92, 2014.
5. J. Li and S. Zhao. "Neural networks based on quantum gated nodes". International Journal of Computer and Information Technology, **4**, pp.583-589, 2015.
6. P. Li and Y. Zhao. "Model and algorithm of sequence-based quantum-inspired neural networks". Chinese Journal of Electronics, **27**, pp. 9-18, 2018.
7. M. Waseem, M. Irfan, Sh. Qamar. "Realization of quantum gates with multiple control qubits or multiple target qubits in a cavity". Quantum Information Processing, **14**, pp. 1869–1887, 2015.
8. Y.-H. Zhou, X.-Q. Shao, C.-J. Yang, and S. Zhang. "Implementation of non-local multi-qubit CNOT operation with multi-qubit GHZ states". Journal of the Korean Physical Society, **53**, pp. 477-480, 2008.
9. L. Isenhower, M. Saffman, and K. Molmer. "Multibit C_kNOT quantum gates via Rydberg blockade". Quantum Information Processing, **10**, pp. 755-770, 2011.

Robust compact transistor based random number generator

F.M. Ablayev[1], S.N. Andrianov[2], D.V. Vahrushev[1], M.T. Ziatdinov[1], V.S. Romanov[3], A.A. Soloviev[3]

1. Kazan Federal University, Kazan, Russia, fablayev@gmail.com
2. Institute for Applied Research of Tatarstan Academy of Sciences, Kazan, Russia, andrianovsn@mail.ru
3. Kazan Physical and Technical Institute of Kazan Scientific Center of Russian Academy of Sciences, Kazan, Russia, sky-word@mail.ru

Random numbers sequences (RNS) play important role in cryptography. They are using for generation of secrete clues, generation of gamming sequences, formation of control codes etc. Cryptographic demands to using RNS are very strict. RNS are also widely using in statistical sampling, computer modeling and are important in gambling, lotteries where the result of game must be not forecasting.

Random number generators (RNG) are the devices for generation of RNS, which properties are close to the properties of true random sequence. Pseudo random numbers generation (PRNG) is the algorithm for generation of RNS. Such algorithms are able only approximate some properties of true random sequence. True random number generators are the theme of separate development. Such RNG use various physical phenomena for the birth of RNS. When using RNG in embedded electronic cryptographic systems it is reasonable to use RNG on electronic elements. Different such electronic RNG were presented in the previous century and are still developing in last decades. Quantum phenomena can be also used for ensuring randomness. This direction is in the focus of modern quantum technology and is intensively developed in recent decades.

In present paper, we report the creation of RNG based on electron avalanche creation in transistor. Next we present a quantum model of RNG based on quantum effects in a field transistor and discuss its comparative properties with different modern models of quantum RNG.

Optical properties of a microdisk resonator in a diamond substrate with metal contacts

M.S. Rogachev[1,2], I.Yu. Kateev[1], A.V. Tsukanov[1]

1. Institute of Physics and Technology of Russian Academy of Sciences, Moscow, Russia, ikateyev@mail.ru,

2. Moscow Institute of Physics and Technology, Dolgoprudny, Russia, rogachev@phystech.edu

In recent years, several prototypes of hybrid quantum devices have been created in which the spin and orbital states of NV-centers are "dressed" by the photon state of high-quality microresonators (MRs) of the optical range [1]. This is due to the interaction of NV-centers with the optical modes of microdisks [2], microrings [3, 4] supporting whispering gallery modes. By selecting material and geometry of these objects, it is possible to set and control their spectral properties. Usually, diamond disk MRs are manufactured by bonding a single-crystal film to a substrate followed by etching to form a disk pedestal. In [5] the fabrication technique of such MRs on the basis of a bulk diamond single-crystal is developed, where the resulting disks turned out to be surrounded by diamond substrate. To control the electron spin states of NV-centers metal contacts are deposited onto the microdisk surface, which leads to decreasing of the disk Q-factor. In order to avoid this problem one could deposit the contacts on the substrate surface rather than onto the microdisk. Here we study the spectral properties of such system (see inset in fig.2).

The eigen frequencies are found to be practically independent on the size of the gap d between the microdisk and the substrate. At the same time, the substrate has a strong influence on the quality Q (fig. 1). Analysis of the electromagnetic field distribution shows that the oscillations of the Q-factor are determined by the interference of the field in the gap and do not depend on the radius of the microdisk. In addition, the presence of metal contacts can increase Q at small d (fig. 1, R = 3 μm) due to rising of field localization inside the disk.

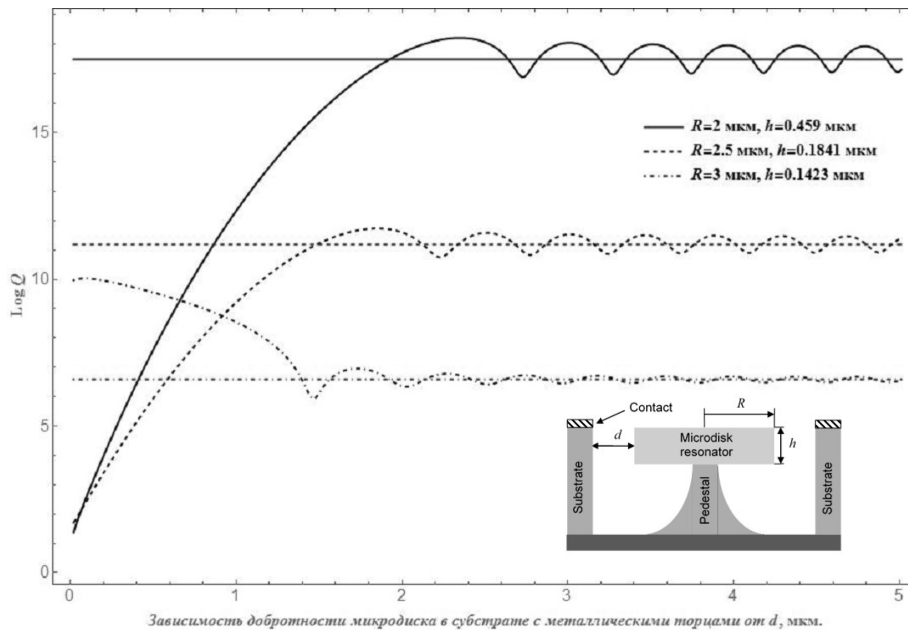

Fig. 1. The dependence of the microdisk Q-factor on the gap size d. Straight lines - Q-factors without substrate. Inset: the diamond microdisk resonator surrounded by substrate.

1. K.J. Vahala. "Optical microcavities". Nature, **424**, p. 839, 2003.
2. P.E. Barclay, K.-M.C. Fu, C. Santori, and R.G. Beausoleil. "Chip-based microcavities coupled to nitrogen-vacancy centers in single crystal diamond". Appl. Phys. Lett., **95**, 191115, 2009.
3. A. Faraon, P.E. Barclay, C. Santori, K.-M.C. Fu, and R.G. Beausoleil. "Resonant enhancement of the zero-phonon emission from a color center in a diamond cavity". LANL E-print. ArXiv:1012.3815, 2010.
4. A.V. Tsukanov, M.S. Rogachev, and I.Yu. Kateev. "Single-Photon Response and Spectroscopy of a Photonic Molecule Based on Diamond Microrings". Russian Microelectronics, **46**, p. 411, 2017.
5. B. Kanaliloo, M. Mitchell, A.C. Hryciw, and P.E. Barclay. "High Q/V monolithic diamond microdisks fabricated with quasiisotropic etching". Nanonolett., **15**, p. 5131, 2015.

The influence of decoherence on the implementation of a C-NOT gate in a double quantum dots-microcavity system under a laser pulse

A.V. Tsukanov and V.G. Chekmachev

Institute of Physics and Technology of the Russian Academy of Sciences, Moscow, Russia, vgchekmachev@mail.ru

In this work, we investigate the possibility of performing a two-qubit controlled-NOT (C-NOT) gate in a structure based on two semiconductor double quantum dots (DQDs) placed in a high-Q optical microcavity (MC) and controlled by a resonant laser field. The influence of a number of relaxation processes on the dynamics of the two-electron system is considered, and the values of dissipation rates for which it is possible to apply algorithms for quantum error correction (QEC) are found. Due to the presence of an additional excitation channel, the laser pulse, it is possible to reduce the impact of the nonideality of the MC on the coherent evolution of quantum states. The selection of optimal values of the electron-field coupling rates makes it possible to achieve C-NOT gate implementation with a high probability over a time of the order of hundreds of picoseconds.

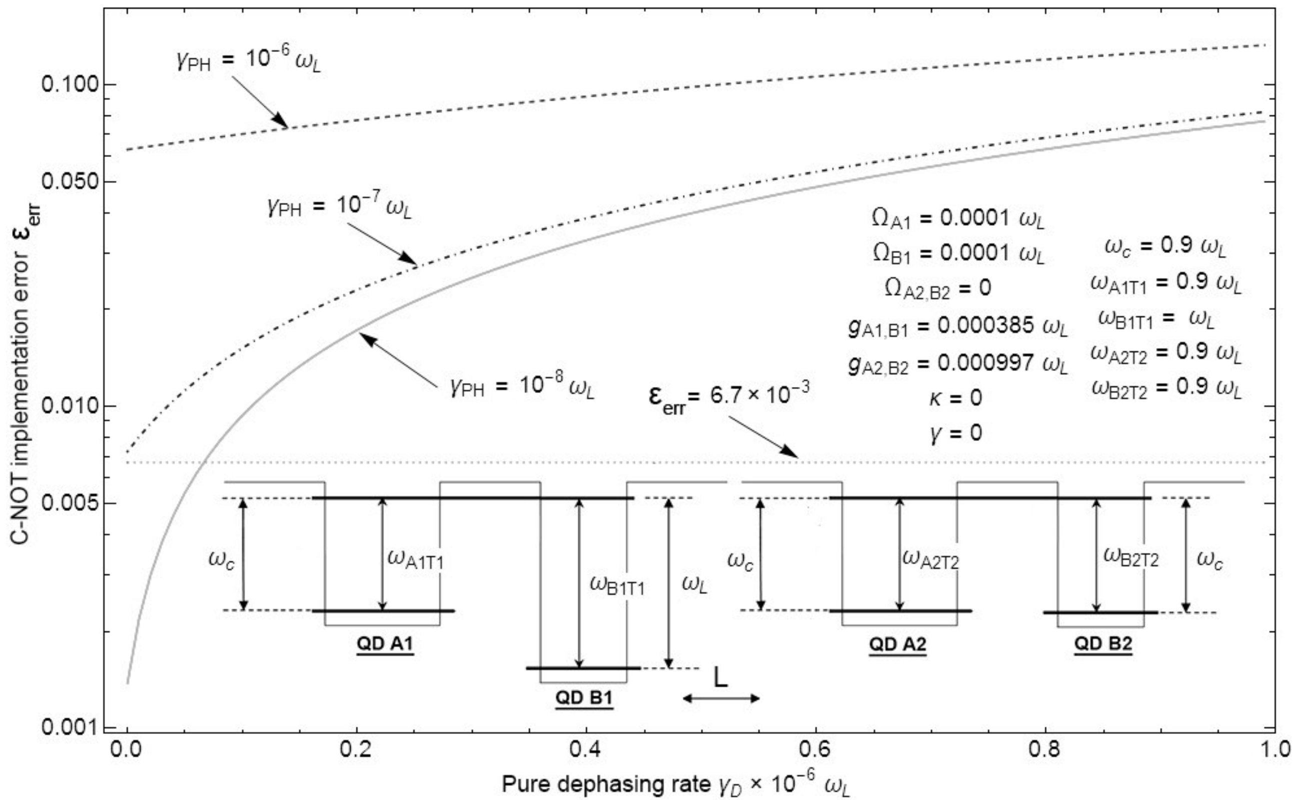

Fig. 1. The dependence of the error of C-NOT gate implementation in a logarithmic scale on the pure dephasing rate of the DQDs levels. Calculations for several combined photon-phonon relaxation rates are shown. The horizontal dotted line indicates the threshold error value for application of QEC algorithms. The diagram of the energy levels of the structure is given at the bottom of the figure. The distance L between DQDs is much larger than the characteristic sizes of objects.

Molecule ground state estimation via continuous-time quantum walks

L. Fedichkin[1,2,3], F. Meshchaninov[2,3]
1. NIX, Moscow, Russia
2. Institute of Physics and Technology, Moscow, Russia
3. Moscow Institute of Physics and Technology, Dolgoprudny, Russia, leonid@phystech.edu

The application of continuous quantum walks of electron on graph of quantum dots subjected to outer noisy environment to the quantum simulation of molecules is studied. The structure of graph used corresponds to the structure of the molecule Hamiltonian. As sources of controllable noise, quantum point contacts are considered. First, the system is set into a state, which has an appreciable overlap with the ground state of the system, then, the evolution starts, and finally, the ground state energy is assessed. The influence of noise, produced by the point contacts, on algorithm performance and fidelity is also investigated.

1. L. Fedichkin, D. Solenov, C. Tamon. “Mixing and decoherence in continuous-time quantum walks on cycles”. Quantum Information & Computation, **6**, pp. 263-276, 2006.
2. A. Melnikov, L. Fedichkin. “Quantum walks of interacting fermions on a cycle graph”. Scientific Reports, **6**, pp. 34226, 2016.
3. L. Fedichkin, F. Meshchaninov. “Quantum-classical crossover in quantum walks mixing time”. International Conference on Micro-and Nano-Electronics 2016, **10224**, pp. 102242M, 2016.

Theoretical and experimental investigation of multi-mode thermal states with subtraction of a random number of photons

Yu. I. Bogdanov[1,2,3], N. A. Bogdanova[1,2], K. G. Katamadze [1,3,4], G. V. Avosopiants[2,4]
1. Institute of Physics and Technology, Russian Academy of Sciences, Russia
2. National Research University of Electronic Technology (MIET), Russia
3. National Research Nuclear University (MEPhI), Russia
4. Faculty of Physics, M. V. Lomonosov Moscow State University, Moscow, Russia

Theoretically and experimentally, we study the statistical distribution of the number of photons, described by the following generating function:

$$G\left(z\middle|k,m,M,\mu_0\right)=\left(G_{th}\right)^m F\left(-k,m,M,1-G_{th}\right) \qquad (1),$$

where F is a hypergeometric function, and $G_{th}=\left(1+\mu_0\left(1-z\right)\right)^{-1}$ is the generating function of a single-mode thermal state.

It is assumed that an M-mode thermal state with an average number of photons μ_0 per one mode was initially prepared, and exactly k photons were subtracted from this state. The generating function (1) describes the statistics of the registered number of photons in the subsystem of the m-modes ($m \le M$).

It is important to note that $G\left(z\middle|k,m,M\right)=F\left(-k,m,M,\left(1-z\right)\right)$ is the generating function of Polya distribution [1]. In our case, it describes the distribution of the random number j of photons ($0 \le j \le k$) subtracted from the m-mode thermal state. The generating function of such a state is $\left(G_{th}\right)^{m+j}$. As a result, taking into account the rules of probability theory [2], we arrive at the following conclusion. The generating function (1) describes the sum of a random number of $m+j$ terms, each of which is a thermal quantity G_{th}. Indeed, the fixed value of m has a generating function z^m, and the random variable j ($0 \le j \le k$) has the Polya distribution, therefore the variable $m+j$ has a generating function $z^m F\left(-k,m,M,\left(1-z\right)\right)$. The last expression is transformed into the generating function (1) if the variable z is replaced by G_{th}.

This work is a continuation of our works [3,4], aimed at engineering different quantum states on the basis of thermal states.

1. Yu.I. Bogdanov, N.A. Bogdanova, and V.L. Dshkhunyan. Statistical Yield Modeling for IC Manufacture: Hierarchical Fault Distributions // Russian Microelectronics, 2003, Vol. 32, No. 1, pp. 51–62.
2. W. Feller, Introduction to Probability Theory and Its Applications, Vol.1 (Wiley, 1950), Vol.2 (John Wiley &Sons, 1966).
3. Yu.I. Bogdanov, N.A. Bogdanova, K.G. Katamadze, G.V. Avosopyants, and V.F. Lukichev. Study of photon statistics with use of compound Poisson distribution and quadrature measurements // Optoelectronics, Instrumentation and Data Processing, 2016, Vol. 52, No 5, pp. 71–83.
4. Yu.I. Bogdanov, K.G. Katamadze, G.V. Avosopiants, L.V. Belinsky, N.A. Bogdanova, A.A. Kalinkin, S.P. Kulik. Multi-photon subtracted thermal states: description, preparation and reconstruction // Physical Review A. 2017 V.96. № 6. 063803.

Quantum approach to the dynamical systems modeling

Yu.I. Bogdanov[1,2,3], N.A. Bogdanova[1,2], D.V. Fastovets[1,2], V.F. Lukichev[1]

1. Institute of Physics and Technology, Russian Academy of Sciences, Russia
2. National Research University of Electronic Technology (MIET), Russia
3. National Research Nuclear University (MEPhI), Russia

We present a general approach to the classical dynamical systems simulation based on its' extension to quantum states. The proposed theory can be applied to analysis of multiple (including non-Hamiltonian) dissipative dynamical systems.
As examples we consider the logistic model, the Van der Pol oscillator, dynamical systems of Lorenz, Rössler (including Rössler hyperchaos) and Rabinovich-Fabrikant.
It is important to note that the quantum dynamical system contains more information than the original classical system. In particular, according to quantum mechanics, we can consider not only the coordinate representation, but also the momentum representation.
We know that the mutually complementary coordinate and momentum representations are linked through the fundamental Heisenberg uncertainty relation. Compression of phase space in a certain direction in the coordinate representation indicates the extension in momentum space in the same direction, and vice versa. We use this property, so to find the Lyapunov exponents in the original coordinate space we perform more simple calculations in momentum space.
From the fundamental point of view, simultaneous consideration of mutually complementary coordinate and momentum frameworks provides a deeper understanding of the nature of chaotic behavior in dynamical systems. From the computational point of view, the new formalism provides a basis for the analysis of complex dynamical systems using quantum simulators.
Present work is a development of our paper [1].
Developed methods and algorithms integrated in quantum simulators will allow one to solve a wide range of problems with scientific and practical significance.

1. Yu.I. Bogdanov and N.A. Bogdanova. The study of Lorenz and Rössler strange attractors by means of quantum theory // Laser Physics 2015. V. 25. 035203. 5p.

The concept of weak measurements and the super-efficiency of quantum tomography

Yu.I. Bogdanov[1,2,3], N.A. Bogdanova[1,2], B.I. Bantysh[1,2], Yu.A. Kuznetsov[1,2], V.F. Lukichev[1]

1. Institute of Physics and Technology, Russian Academy of Sciences, Russia
2. National Research University of Electronic Technology (MIET), Russia
3. National Research Nuclear University (MEPhI), Russia

We estimate the possible advantages of the schemes of weak measurements over traditional sets of projective measurements. We have considered some problems when the feedback provides a real effective control of the quantum system and at the same time the interaction of the probe with the system is quite weak.
The connection between the concept of weak measurements and the theory of Lorentz transformations in quantum measurements was considered. In the simplest case of single-qubit states one can show that in addition to three-dimensional rotations on the Bloch sphere, one can consider four-dimensional pseudo-rotations similar to transformations that are typical for the special theory of relativity. We note that the theory of Lorentz transformations can be applied not only to single-qubit, but also multi-qubits quantum systems.
To estimate the effectiveness of weak measurements, we use the theory of accuracy of quantum measurements, developed in our works. If the measurements are reduced to POVM, then for any given sample size, we can calculate the minimum possible loss of fidelity. On this basis, it is possible to calculate the efficiency of the quantum measurement protocol. For any POVM-protocol, the efficiency cannot be higher than one. The generalized Lorentz protocols and weak measurements are not reducible to POVM, therefore superefficiency is possible for them, i.e. a situation where the efficiency of the protocol is formally higher than one. Thus, the new protocols of measurements can provide higher accuracy than any known standard protocols.
The results of this research are significant for the control of quantum information technology.

Sequences of selective rotation operators to engineer interactions for quantum annealing on three qutrits

V.E. Zobov[1], I.S. Pichkovskiy[2]
1. Kirensky Institute of Physics, Federal Research Center KSC SB RAS, Krasnoyarsk, 660036 Russia;
e-mail: rsa@iph.krasn.ru.
2. Institute of Engineering Physics and Radio Electronics, Siberian Federal University, Krasnoyarsk, 660074 Russia

The most of the work on quantum computation is currently performed in the binary system, and two-level quantum systems, qubits, are taken as elementary units of information. However, the same operations can be performed by taking as elements quantum systems with three levels - qutrites. For example, objects with spin $S = 1$ in the magnetic and the crystal fields are propose to use as qutrit. These include the quadrupole nucleus [1] of deuterium, nitrogen or lithium, as well as NV centers in diamond (paramagnetic color centers formed by an electron on vacancies near the nitrogen atom) [2]. Qutrits promise to increase the efficiency of quantum computing: first, due to the faster growth of the size of the computational basis (Hilbert space) with an increase in the number of elements, and secondly, due to the use of the ternary number system, which is considered more efficient than the binary one. However, theory of qutrit system control is not sufficiently developed.

In the proposed report, such a theory is developed using the example of the realization on three qutrites of the factorization algorithm for the number 15 by means of quantum annealing, i.e. by means of the evolution of a system with a time-dependent Hamiltonian

$$H(t) = (1 - t/T)H_0 + (t/T)H_p, \qquad 0 \le t \le T . \tag{1}$$

where $H_P = \left(15 - \left(6S_1^z + 2S_2^z + 1\right)\left(2S_3^z + 1\right)\right)^2$, and $H_0 = -h\left(S_1^x + S_2^x + S_3^x\right)$. We assume that the spins $S = 1$ are connected by two-spin interactions $b_{ij} S_i^z S_j^z$ and their states can be controlled by means of rotation operators that are selective for transitions between the energy levels of different spins. To simulate the algorithm, continuous time was replaced by a discrete one. When creating single-spin and two-spin interactions of a general form $(S_i^z)^m (S_j^z)^n$ (m, n = 0, 1, 2), we followed the papers [1, 2]. To engineer three-spin interactions in (1), we applied the theory of the averaged Hamiltonian [3], developed to obtain high-resolution NMR spectra in solids. If, with the help of pulses, we average the two-spin interaction in the first order in a small quantity ε, then the dynamics is determined by a term of the next order in the averaged Hamiltonian, i.e. by three-spin interaction. We obtain

$$\begin{aligned} \exp\left[i\varepsilon^2 b_{12} b_{13} S_1^z S_2^z S_3^z\right] &\approx \exp\left[-i\pi S_1^x/2\right]\exp\left[-i\pi S_1^y/2\right]\exp\left[i\varepsilon b_{12} S_1^z S_2^z\right]\exp\left[i\pi S_1^y/2\right]\times \\ &\times \exp\left[i\varepsilon b_{13} S_1^z S_3^z\right]\exp\left[-i\pi S_1^y/2\right]\exp\left[-i\varepsilon b_{12} S_1^z S_2^z\right]\exp\left[i\pi S_1^y/2\right]\exp\left[-i\varepsilon b_{13} S_1^z S_3^z\right]\exp\left[i\pi S_1^x/2\right] \end{aligned} \tag{2}$$

Non-selective rotation operators $\exp\left[\pm i\pi S_1^{x,y}/2\right]$ can be obtained by means of two selective rotation operators acting simultaneously on two transitions [2]. The elimination of unnecessary two-spin interactions is achieved by spin inversion at one of two neighboring evolution intervals. We compiled a sequence of operators of selective rotations and operators of free evolution, which made it possible to implement the algorithm, performed simulation, and investigated the dependence of the accuracy of the result on physical parameters. The results obtained can be applied to the implementation of quantum algorithms on the qutrits represented by other quantum systems.

1. V.E. Zobov and A.S. Ermilov. “Implementation of a Quantum Adiabatic Algorithm for Factorization on Two Qudits”. JETF, **114**, pp. 923-932, 2012.
2. S. Choi, N.Y. Yao, M.D. Lukin. “Dynamical Engineering of Interaction in Qudit Ensembles”, Phys. Rev. Lett., **119**, 183603, 2017.
3. U. Haeberlen and J.S. Waugh. “Coherent Averaging Effects in Magnetic Resonance”. Phys. Rev., **175**, pp. 453-467, 1968.

Fast quantum randomness generation from vacuum fluctuation induced phase diffusion between pulses of laser diode

R. Ermakov[1], V. Sharoglazova[2], A. Losev[1], V. Zavodilenko, V. Kurochkin[1], Y. Kurochkin[1]
1. Russian Quantum Centre, Moscow, Russia, E-mail address: mail@rqc.ru.
2. National Research Nuclear University MEPhI, Moscow, Russia, E-mail address: ONPetukhova@merphi.ru

Random numbers are fundamental resource in science and engineering and are essential for applications ranging from secure communication to numerical simulation and quantitative finance. The inherent randomness in the core of quantum mechanics creates an opportunities to realize different types of random number generators (QRNG). Currently the fastest QRNGs are based on vacuum fluctuations, laser phase noise or amplitude fluctuation in amplified spontaneous emission noise [1].

In the present work we demonstrate a high bit-rate QRNG based on extraction of random bits from vacuum using optical amplification. The proposed device can be realized with highly integrated using commercially available components. The attained bit rate is equal 2.5Gbps and the proposed scheme without any modification can generates up to 10Gbps of raw random numbers.

It is used a distributed feedback (DFB) laser diode as the oscillator, providing single-mode operation and high modulation bandwidth. The DFB laser diode is directly modulated at around 2.5GGz by driver laser as shown at the fig. Electric pulse forming takes place at the FPGA devices. The duration of electrical pulses is equal at around 100 ps. With an aid of driver laser and DFB laser diode the electric pulses transforms in optical pulses. The strong current modulation, well above and below threshold, ensures true randomness from vacuum [2]. This active gain control allows a single device to have a short coherence time for rapid extraction of uncorrelated random bits. Delay of the loop of Michelson interferometer corresponds pulse repetition cycle. Due to the random phase of the different input pulses, the output signals acquire random amplitudes. Due to high signal level it is possible to detect signal by means of PIN diode detector. The amplified signal from the detector falls on the comparator. The reference voltage is adjusted by the FPGA device based on the equality of zeros and ones. Postprocessing is also performed on the FPGA device.

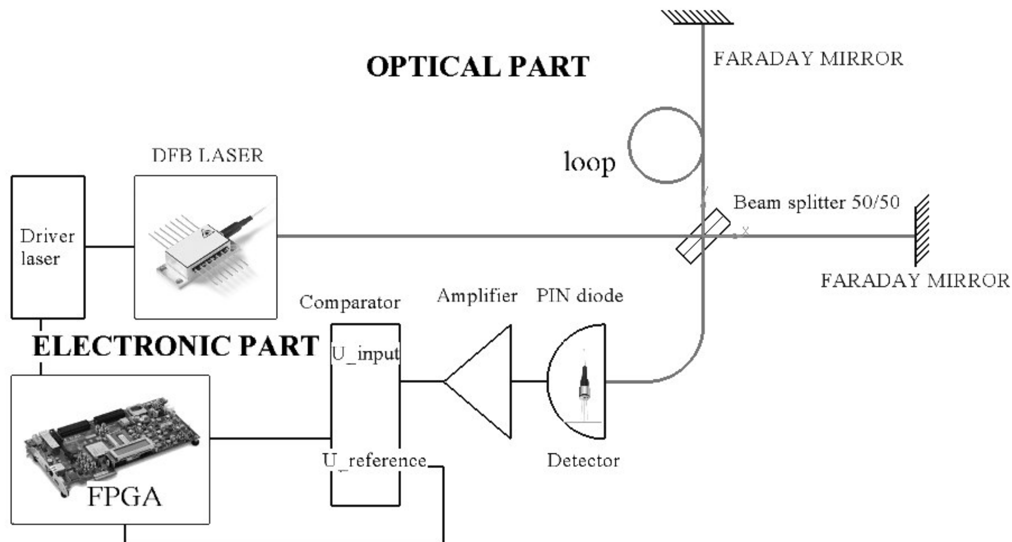

Figure: unbalanced Michelson interferometer with Faraday mirrors. The device produces a raw randomness passing NIST tests.

1. M. Herrero-Collantes and J. Garlos Garcia-Escartin. “Quantum random number generators”, Review of Modern Physics, **89**, 015004(48), 2017.
2. M. Jofre, M. Curty, F. Steinlechner, G. Anzolin, J.P. Torres, M.W. Mitchell, and V. Pruneri. “True random numbers from amplified quantum vacuum”, Optics Express, **19**(21), 20665-20672, 2011.

Bi-SQUID design requirements

N. Kolotinskiy[1], V. Kornev[1], D. Bazulin[1], O. Mukhanov[2]
1. Faculty of Physics, Lomonosov Moscow State University, Moscow, Russia, kolotinskij@physics.msu.ru
2. Hypres, Inc., Elmsford, NY, USA

Bi-SQUID (see schematic in Fig. 1) was suggested with the purpose of attaining a high linearity voltage response to magnetic signal. This is relevant to many high-frequency applications when implementation of standard following feed back loop is not feasible. In bi-SQUID, the linear output is formed over two successive nonlinear signal transformations, which can be tuned to mutually inverse shape within major parts of $\Phi_0/2$ ranges in the Φ_0–periodic voltage response. Numerical analysis shows that the output voltage linearity of the device can amount to 90 to 100 dB.

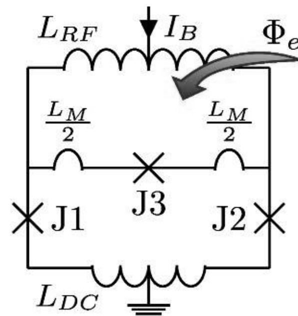

Fig. 1. Equivalent circuit of bi-SQUID; L_{RF} and L_{DC} are inductances of the rf and dc SQUID loops, respectively, and L_m is inductance of the shared part of the loops.

However, the linearity has a peak-like dependence on critical current of the third (added) Josephson junction, and the maximum point depends on normalized values of all inductances of the device: main inductance characterizing one-junction loop, inductance of the three-junction loop, as well as shared inductance part belonging to both loops. All the parameters are specified by design and cannot be changed when the device is used. Therefore, achieving of the needed linearity level requires high accuracy of both the layout design and device fabrication.

Here we present overall multi-parameter analysis of the linearity characteristics. The data have to be used to come to optimal design tradeoff between the voltage response linearity, main inductance value (the higher inductance, the better coupling to the input signal source) and existing design restrictions, on the one hand, and the attainable fidelities of both design and fabrication, on the other hand.

Acknowledgment:
This work was supported by Russian Science Foundation Grant 17-72-10241.

Relaxation of the coherent excited states of a superconductor to a normal metal or superconducting reservoir

I.A. Devyatov[1,2], A.V. Semenov[3,2]

1. Moscow State University, Scobeltsyn Institute of Nuclear Physics, Moscow, Russia, igor-devyatov@yandex.ru
2. Moscow Institute of Physics and Technology, Dolgoprudny, Russia.
3. Moscow State Pedagogical University, Moscow, Russia, av.semyonov@mpgu.edu

Recently [1], there has been shown the presence of coherent excited states in a diffusive s-wave superconductor irradiated by a microwave field. It was demonstrated [1], that the ground state of such superconductor is altered qualitatively, the density of states acquires steps at multiples of photon energy and shows an exponential-like tail in the subgap regime. Theoretical analysis of the influence of inelastic processes on coherent excited states of a superconductor in a convenient tunnel model was done in paper [2]. The model used in [2] is a thin dirty superconducting strip in contact with a diffuse normal metallic reservoir through an opaque tunnel barrier.

In this presentation we consider the case of tunnel relaxation to a diffuse superconducting reservoir. The equations for spectral functions of the superconductor and for non-equilibrium distribution function were obtained.

The obtained results are important in the construction of superconducting parametric amplifiers and superconducting resonators.

We are grateful to a financial support of Russian Foundation for Basic Researches, Grant No. 1702-00757, and of Russian Scientific Foundation, Grant No. 17-72-30036, and of a financial support of Ministry of Education and Science of the Russian Federation, contract No. 14.B25.31.0007.

1. A.V. Semenov, I.A. Devyatov, P.J. de Visser, and T.M. Klapwijk. "Coherent Excited States in Superconductors due to a Microwave field". Phys. Rev. Lett., **117**, p. 047002, 2016.
2. A.V. Semenov, I.A. Devyatov, M.P. Westig, T.M. Klapwijk, “The contribution of microwaves to the Cooper-pair condensate of a superconductor in the presence of inelastic processes”, http://arxiv.org/abs/1801.03311

Superconducting current in heterostructures with a strontium iridate interlayers

Y.V. Kislinskii[a], K.Y. Constantinian[b], A.S. Grishin, G.A. Ovsyannikov, A.M. Petrzhik, and A.V. Shadrin

Kotelnikov Institute of Radioengineering and Electronics RAS, Moscow, Russia,
[a]yulii@hitech.cplire.ru [b]karen@hitech.cplire.ru

Strong spin-orbit interaction in iridium oxides attracts much interest for applications as barrier material in superconducting heterostructures. Iridium has a large atom number and in oxide compounds the energy of the spin-orbit interaction (SOI) is comparable with a Hubbard energy. The SOI has strong influence on electrical and magnetic properties of the iridium compounds [1]. Electrophysical properties of strontium iridates depend on theirs chemical composition: $SrIrO_3$ is a metal with resistivity of 1 mΩ·cm [2], while Sr_2IrO_4 could be described as insulator with a band gap of 100 meV, and as well as variable range hopping conductor with a localization radius $a \approx 0.1 - 0.3$ nm [3]. If Sr_2IrO_4 layer placed between superconductors the strong enhancement of triplet superconducting current due to the SOI has been predicted [4].

Here we report on heterostructures with Sr_2IrO_4 interlayer. For material characterization we have deposited thin films Sr_2IrO_4 on different monocrystal substrates. For particular cases films were insulators with energy gap of 200 meV, in other cases Sr_2IrO_4 films have a hopping conductivity with localization radius $a \approx 0.5$ nm [5].

Heterostructures Nb/Au/Sr_2IrO_4/$YBa_2Cu_3O_{7-\Delta}$ (Nb/Au/SIO 214 /YBCO) were fabricated and studied experimentally. We have observed superconducting current in the Nb/Au/SIO 214 /YBCO samples. Five heterostructures with area A ranged from 10□10 μm^2 to 50×50 μm^2 were placed on a chip. Two type Nb/Au/SIO 214 /YBCO chips with the Sr_2IrO_4 interlayer thickness d 5 nm and 7 nm were made.

In the heterostructures on the chip with d=7 nm superconducting currents had density $I_C/A \approx 0.2 - 0.4$ A/cm^2. The products of I_CR_N were of 30 – 40 μV. Measurements of current-voltage characteristics in a magnetic field were made and dependences of $I_C(H)$ were plotted. Half widths of a central lobe of the $I_C(H)$ dependences were of 0.5 - 1 Oe for heterostructures 50 μm and 40 μm in size.

Heterostructures on a chip with d=5 nm had periods $I_C(H)$ of $10^1 - 10^2$ Oe, that is much larger than for the structures on chip with d=7 nm. Critical current densities for heterostructures with d=5 nm interlayer were of 10 A/cm^2 and products of I_CR_N were of 50 μV.

With the interlayer thickness increase from 5 to 7 nm normal resistivities R_NA increase from 10 up to 100 μΩ·cm respectively. For an exponential dependency $R_NA \sim \exp(2d/a)$, where a is a localization radius of the electron in the interlayer, one can obtain the radius $a \approx 1.5$ nm in the Sr_2IrO_4 interlayer of the heterostructures. This value is large than the radius a in Sr_2IrO_4 films. It could be originates from interface phenomena [6].

The work is partially supported by RFBR and Russian Academy of Sciences.

1. M.A. Zeb, H.Y. Kee. “Interplay between spin-orbit coupling and Hubbard interaction in $SrIrO_3$ and related Pbnm perovskite oxides”. Physical Rev. B, **86**, pp. 085149-1 - 085149-7, 2012.
2. A. Biswas, K.S. Kim, Y.H. Jeong. “Metal isulator transitions in perovskite $SrIrO_3$ thin films”. J. of Appl. Phys., **116**, pp. 213704-1 - 213704-10, 2014.
3. C. Lu, A. Quindeau, H. Deniz, et al. “Crossover of conduction mechanism in Sr_2IrO_4 thin films”. Appl. Phys. Lett., **105**, pp. 082407-1 - 082407-5, 2014.
4. M. Horsdal, G. Khaliullin, T. Hyart. “Enhansing triplet superconductivity by the proximity to a singlet superconductor in oxide heterostructures“. Physical Rev. B, **93**, pp. 220502-1 - 220502-5, 2016.
5. A.M. Petrzhik, G. Cristiani, G. Logvenov, et al. “Grown technology and characteristics of thin strontium iridate films and iridate – cuprate superconductor heterostructures”. Technical physics letters, **43**, pp. 554 – 557, 2017.
6. G.A. Ovsyannikov, K.Y. Constantinian, Yu. V. Kislinskii, et all. “Proximity effect and electron transport on oxide hybrid heterostructures with superconducting/magnetic interfaces”. Supercond. Sci. Technol. **24**, pp. 055012-1 – 055012 -10, 2011.

Quantum magnetic-resistive hc/2em periodic oscillations in a superconducting thin-film aluminum ring

V.I. Kuznetsov

Institute of Microelectronics Technology and High Purity Materials, Russian Academy of Sciences, Chernogolovka, Moscow Region, Russia, E-mail address: kvi@iptm.ru

Superconducting fluxoid [1] changes in steps (is quantized) by the value of the superconducting magnetic flux quantum $\Phi_0=hc/q$ (here q is the effective electric charge $2e$, equal to the charge of the Cooper's pair) in multiply connected superconductor threaded with a magnetic flux Φ. This work suggests a superconducting circulating current in a mesoscopic ring has the effective charge $q=2em$ (m=1, 2, …). We measured $V(B)$ voltage as a function of magnetic field B in a superconducting mesoscopic ring threaded with a magnetic flux Φ and biased by a direct current I_{dc} with at different values higher critical I_c at temperatures T slightly below the critical temperature T_c. A 51 nm thick ring was fabricated by thermal sputtering of aluminum onto a silicon substrate using the lift-off process of electron-beam lithography. The internal and external radii of the ring are equal to 1.79 μm and 2.09 μm, respectively. The ring has the following parameters. $R_{4.2}$=53 Ω, $R_{300}/R_{4.2}$=1.8. T_c=1.339 K was determined from the midpoint of normal-superconducting transition $R(T)$ in zero field. The bottom of the transition was at T_{cd}=1.318 K. At T=1.312 K, like to the Little-Parks oscillations [2], the $V(B)$ oscillates with the period $dB=\Phi_0/S$=1.76G, where $\Phi_0=hc/2e$ is the superconducting flux quantum and S is the effective ring area (the inset of the fig.1). With a decreasing T=1.281-1.282 K and an increasing I_{dc}=9.8 μA, unusual $V(B)$ oscillations are observed in the regions of the negative magnetic resistance (figs.1-2). For a detail analysis, Fourier spectrum of the $V(B)$ oscillations calculated in the fields B=6.1-11.4 G (inset of the fig.2). In addition to the fundamental frequency $f_0=1/dB=0.569\text{G}^{-1}$, the Fourier spectrum contains higher harmonics of the f_0 frequency, $f=mf_0$, (m=2-25) with nearly equal contributions. The higher harmonics are not due to an inharmoniousness of the $hc/2e$ oscillations. Some of the $hc/2em$ oscillations are sufficiently distinguishable on $V(B)$ curves. Moreover, $V(B)$ oscillations were approximated by curves (is not shown here) which are summations of the harmonic oscillations with different amplitudes, frequencies and phases. Earlier, $hc/2em$ oscillations with m>2 were not observed. Unusual oscillations can be

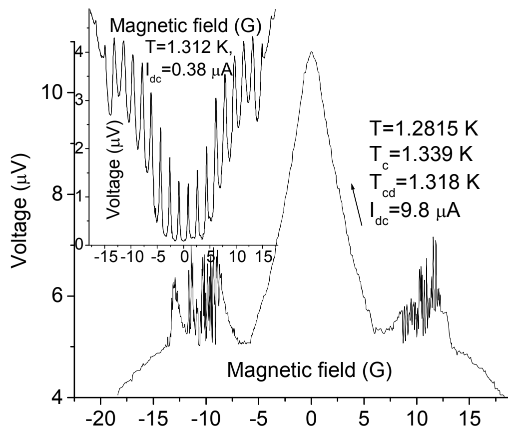

Fig. 1. *V(B)* measured at higher I_{dc} with the parameters given in the figure. Regions of the negative magnetic resistance are seen nearly the zero field and in low fields. The inset: *V(B)* oscillations at lower I_{dc}=0.38 μA.

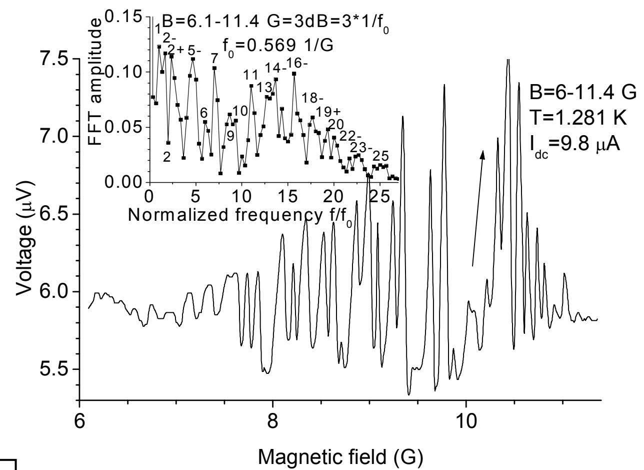

Fig. 2. Right oscillating region of the *V(B*) curve (fig.1) in the fields B=6-11.4 G. The inset: Fourier spectrum of the region of the *V(B*) curve at B=6.1-11.4 G. Values 1/3 are omitted after the symbols "+" and "-".

due to multiple Andreev reflection appearing in nonequilibrium overheat regions (phase slip centers) of the ring if the requirement $V(I_{dc})<2m\Delta(T,B)/e$ ($\Delta(T,B)$ is the superconducting gap and m=1-30) is satisfied [3].

1. A.F. London, Phys. Rev. **74**, 562 (1948).
2. W.A. Little and R.D. Parks, Phys. Rev. Lett. **9**, 9 (1962).
3. V.I. Kuznetsov, A.A. Firsov, JETP Letters, **104**, 709 (2016).

Fundamental difference between the Aharonov-Bohm effects observed in micro- and nano-structures and in the two-slit interference experiment

A.V. Nikulov
Institute of Microelectronics Technology, Russian Academy of Sciences, 142432 Chernogolovka, Moscow District, Russia. E-mail: nikulov@iptm.ru

According to the predominant belief quantum mechanics describes universally all quantum phenomena. But the critical consideration [1, 2] refutes this belief. The creators of quantum mechanics should were using different definitions of the Hamiltonian for the description of different quantum phenomena, for example the Zeeman effect and the Aharonov-Bohm effects [1]. Even the descriptions of quantum effects having the same name - the Aharonov-Bohm effects - differ fundamentally. Y. Aharonov and D. Bohm had predicted that the magnetic flux $\Phi = \oint_l dlA$ should influence on the interference pattern of particles with a charge q because of the connection between the phase φ of the wave function $\Psi = |\Psi|e^{i\varphi}$ and the magnetic vector potential A. This connection is deduced from the canonical definition the gradient operator $p = -i\hbar\nabla$ which corresponds to the canonical momentum $p = mv + qA$ of a particle both with $A \neq 0$ and without $A = 0$ magnetic flux. The canonical momentum equals the phase gradient $\Psi^* p\Psi = |\Psi|^2\hbar\nabla\varphi$ according to this definition and the both $p = \hbar\nabla\varphi = mv + qA$ depend on the magnetic vector potential A when the velocity v does not change. Y. Aharonov and D. Bohm were noting [3] that the phase difference $\varphi_1 - \varphi_2 = \Delta\varphi_0 + 2\pi\Phi/\Phi_0$ along the two paths l_1 and l_2 between a source and any point x of the detecting screen should change with the magnetic flux Φ inside a closed circuit $l = l_1 + l_2$ formed by two paths. They predicted that the arrival probability of particles with the charge q at the point x should change periodically with the magnetic flux Φ with the period equal the flux quantum $\Phi_0 = 2\pi\hbar/q$. The connection between the change of the phase along a closed circuit l, the velocity v and the magnetic flux Φ exists also in the Aharonov-Bohm ring, for example superconducting ring. But all experiments, for example [4-6], testify that the velocity $v = (2\pi\hbar/ml)(n - \Phi/\Phi_0)$ rather than the phase difference $\varphi_1 - \varphi_2$ depend on the magnetic flux Φ in this case. According to the generally accepted explanation [7] of the quantum effects observed in rings, the relation $\varphi_1 - \varphi_2 = 2\pi n$ should be valid due to the requirement that the complex wave function must be single-valued in any point of the closed circuit l. But this mathematical requirement $\Psi = |\Psi|e^{i\varphi} = |\Psi|e^{i(\varphi+2\pi n)}$ is not used at the description of the two-slit interference experiment [3]. The requirement is not valid because of the impossibility to describe this experiment without the collapse of the wave function at observation. This requirement is valid in the case of quantum effects observed in rings since the collapse is not needed for description of all phenomena observed in micro and nanostructures [2]. This fundamental difference must be taken into account since the wonders of quantum mechanics, the EPR correlation, 'spooky action at a distance', contradiction with realism and others are deduced from the collapse.

1. A.V. Nikulov, "Could ordinary quantum mechanics be just fine for all practical purposes?" Quant. Stud.: Math. and Found., **3**, pp. 41-55, 2016.
2. A.V. Nikulov, "The quantum mechanics is a non-universal theory. The realistic Schrodinger's and positivistic Born's interpretation of the wave function" arXiv: 1311.4760.
3. Y. Aharonov and D. Bohm Significance of Electromagnetic Potentials in the Quantum Theory. Phys. Rev. **115**, 485 -491 (1959).
4. N.C. Koshnick, H. Bluhm, M.E. Huber, and K.A. Moler, "Fluctuation Superconductivity in Mesoscopic Aluminum Rings". Science **318**, pp. 1440, 2007.
5. V.L. Gurtovoi, S.V. Dubonos, A.V. Nikulov, N.N. Osipov, and V.A. Tulin, "Dependence of the magnitude and direction of the persistent current on the magnetic flux in superconducting rings". JETP, **105**, pp. 1157-1173, 2007.
6. V.L. Gurtovoi, A.V. Nikulov, and V.A. Tulin, "Aharonov-Bohm effects in nanostructures" Proceedings of 17th International Symposium "NANOSTRUCTURES: Physics and Technology", Belarus, Minsk, Institute of Physics NAS, pp. 87-88, 2009.
7. Tinkham M.: Introduction to Superconductivity, 2nd edn. McGraw-Hill Book Company, New York (1996).

A low actuation voltage MEMS switch with protection against stiction

I.V. Uvarov, A.N. Kupriyanov
Yaroslavl Branch of the Institute of Physics and Technology RAS, Yaroslavl, Russia, i.v.uvarov@bk.ru

In recent decades, the rapid development of wireless communications has sparked a keen interest in microelectromechanical switching devices [1]. Electrostatically actuated MEMS switches combine the advantages of semiconductor switches and electromechanical relays: small size, high switching speed, near zero power consumption and superior RF performance. Such characteristics make them attractive for use in 5G mobile communications, reconfigurable antennas, satellite switching networks and other applications. The main disadvantage of the MEMS switch is the high actuation voltage, which is typically around a few tens of volts. Such switches require external control units generating high-voltage signals, which complicate their use. Therefore, when designing the MEMS switch, much attention is paid to making the actuation voltage as low as possible. The most preferred way is to reduce the elasticity of the micromachined beam. However, in most cases the opening of the switch is carried out by the elastic force arising in the deformed beam. The lower the stiffness, the lower the opening force. As a result, a switch with not sufficiently stiff beam becomes susceptible to stiction and instable operation. In this paper we present a low actuation voltage MEMS switch, which is equipped with the mechanism allowing recovery of the device in case of stiction.

The switch is shown in Fig. 1. It is based on the 1 μm thick aluminum beam attached to the anchors by the torsion suspensions. The beam has a length of 100 μm and a width w of 8, 16, 24 or 32 μm depending on the design. It plays the role of a source electrode. Gate and drain electrodes are made of 100 nm thick Pt film and placed under the each arm of the beam, so the switch has SPDT configuration with two symmetric output channels. Platinum contact bumps are located on the bottom side of the beam. In recent studies we tested the samples with an air gap $g = 1.5$ μm between the beam and the gate electrodes [2]. In the present work two additional batches of switches with the gap of 0.5 and 1.0 μm are investigated.

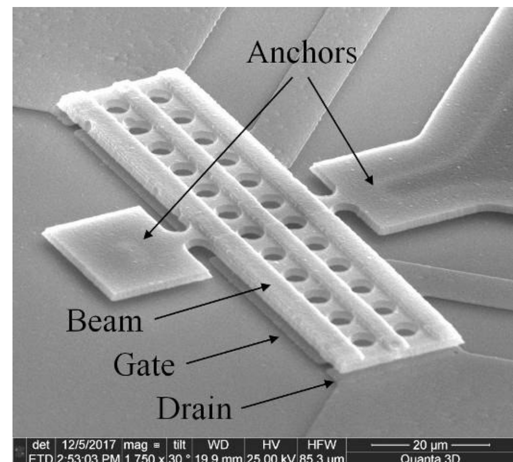

Fig. 1. SEM image of the switch.

The switch operates in the following manner. When the driving voltage is applied to one of the gates, the beam tilts towards the gate under the electrostatic force. At the certain voltage called pull-in voltage (V_{PI}) it touches the drain, and the switch goes to the on-state. When the voltage is removed, the beam returns to the initial state under the elastic force of the suspensions and turns the switch off. In case of stiction, i.e. when the elastic force is insufficient to overcome adhesion forces acting between the bump and the drain, the switch retains the on-state. In order to detach the beam from the drain, the voltage is applied to the opposite gate. At the certain voltage called recovery voltage (V_{REC}) the beam sharply tilts to the opposite direction and comes in contact with another drain, realizing the second on-state.

Performance of the switch is investigated in room air without packaging. Testing is focused on the measurement of V_{PI} and V_{REC}. It is performed in the hot DC mode at the input voltage of 1 V. Switches with $g = 0.5$ μm and $w = 32$ μm have V_{PI} in the range of 4.5÷5.7 V, which is more than ten times lower than the actuation voltage of commercially available devices. V_{PI} gets higher with increasing g and decreasing w. The experimental data is in a good agreement with the results of FEM simulation. Stiction is observed at the input voltage higher than 3 V. V_{REC} of the switches with $g = 0.5$ μm is about 15 V and depends weakly on the width of the beam. Probably, V_{REC} is mainly determined by the adhesion strength of the contact bump to the drain. Resonant frequencies, contact resistance and reliability of the switch are investigated as well.

This work is supported by RFBR research project No. 16-37-60065 mol_a_dk and performed using the equipment of Facilities Sharing Centre “Diagnostics of Micro- and Nanostructures”.

1. G.M. Rebeiz. *RF MEMS: Theory, Design, and Technology.* John Wiley & Sons, New Jersey, 2003.
2. I.V. Uvarov, V.V. Naumov, A.N. Kupriyanov, O.M. Koroleva, E.I. Vaganova, and I.I. Amirov. "Resistive contact MEMS switch in a “hot” operation mode". J. Phys.: Conf. Ser., **917**, 082001, 2017.

Research of the microelectromechanical switch with different materials of metal membrane

I.E. Lysenko, A.V. Tkachenko, O.A. Ezhova

Southern Federal University, Institute of Nanotechnology, Electronics and Electronic Equipment Engineering, Taganrog, Russian Federation, msqk@mail.ru

Microelectromechanical (MEMS) switches are used in communication devices due to their miniature size, low weight and high efficiency high isolation, low self-power consumption, low insertion losses. However, the vast majority of MEMS switches require large values of pull down voltage and hold the metal membrane in the lower position, which significantly reduces the scope of their application, excluding wireless communication devices, which involve the use of low-voltage power supplies, as the life expectancy and reliability depends on the magnitude of the applied pull down voltage. Consequently, a decrease in the bias voltage can not only expand the range of possible applications, but also significantly increase the life expectancy of MEMS switches.

In this study the design of MEMS switch with capacitive principle of switching signals is proposed a special feature of the proposed design of MEMS switch is additional electrodes of displacement of the suspended movable metal membrane, which allows to implement the mechanism of membrane release in the case of its adhesion to the dielectric film, as well as the exclusion of arbitrary operations when switching high-frequency (HF) signals of high power (over 100 mW) and sensitivity to vibrations, external accelerations in the positive and negative direction of the axes X, Y, Z. In addition, the technological manufacturing route proposed by MEMS switch is compatible with integrated circuit technology.

Within the framework of this work, the mechanical and electrical parameters of the proposed device with different materials of the metal membrane were investigated (Fig. 1).

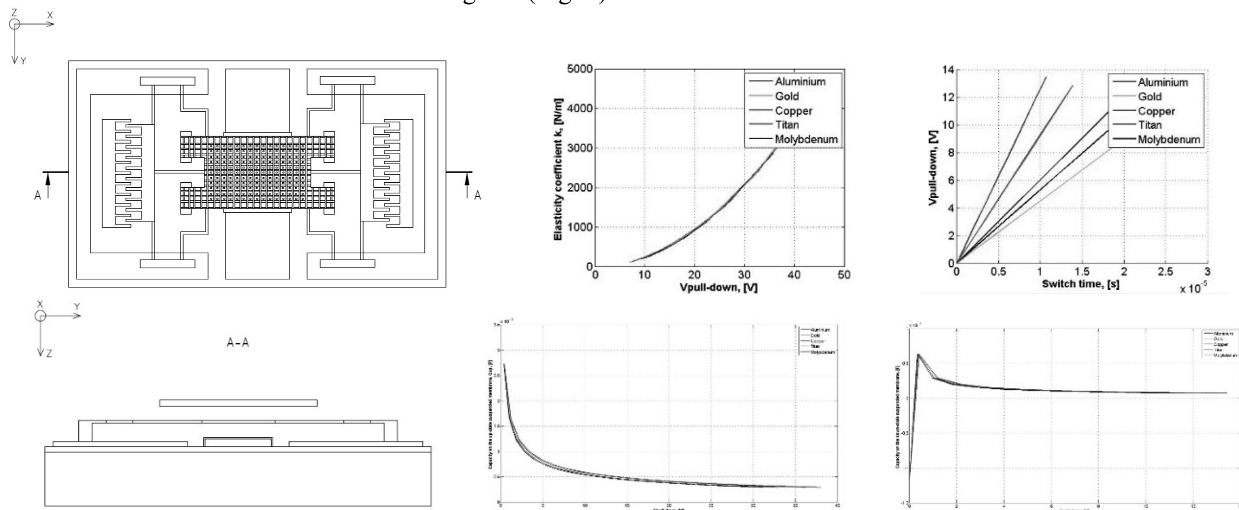

Fig. 1. Topology and structure of the proposed MEMS switch design, study of mechanical and electrical parameters with different materials of metal membrane.

As a result of the study of the proposed design of the MEMS switch, the coefficient of elasticity of the metal membrane fastening, the pull down voltage, the hold voltage of the metal membrane in the lower position, the capacity formed by the variable capacitor in the upper and lower position of the metal membrane, taking into account the perforation, was calculated. The resonance frequency of the switch is 14.7 GHz. Losses when passing the RF signal through the switch when the membrane is raised (on state) -1.12 dB, when the membrane is lowered (off state) -53.015 dB. Based on the data obtained the proposed MEMS switch can be used for switching RF signals of the *Ku*-range (12-18 GHz.). In addition, this study showed that aluminum and gold are appropriate materials for the design of MEMS switches with the required mechanical and electrical parameters. However, gold is an expensive material, which imposes restrictions on the mass production of MEMS switches. In this regard, it is proposed to use aluminum as a material of the metal membrane of capacitive MEMS switches.

The results were obtained using the equipment of the student design bureau "Elements and devices of inertial navigation systems of robotics" of the Institute of Nanotechnologies, Electronics and Electronic Equipment Engineering, Southern Federal University (Taganrog, Russia).

This research is supported by the "Program for the Development of the Southern Federal University until 2021" (project VnGr-07/2017-10).

Computer Simulation of Heavy Charged Particles Damage on Distributed Microsystems

A. Glushko, V. Makarchuk, L. Zinchenko, V. Terekhov, S. Mikhaylichenko, D. Paliy
Bauman Moscow State University, Moscow, Russia, E-mail address: lyudmillaa@mail.ru

Microelectromechanical systems (MEMS, microsystems) are widely used in space missions, and radiation is one of crucial factors in systems design for space missions. Radiation damage on MEMS functionality is not well investigated, but experimental radiation damage tests are expensive and dangerous. Therefore, simulation of radiation damage for different systems is preferable, and our paper [1] was devoted to computer simulation of heavy charged particles damage on individual microsystems. Our investigation of single and multiple ion penetration into capacitive elements has shown that stepped capacitive elements are more tolerant to heavy charged particles in both cases, even when ions trajectories are perpendicular to plates surfaces [1].

The results obtained were collected and stored in a database. The database is used in our tool to estimate distributed microsystems damage.

Distributed microsystems, that include dozens of microsystems, are more important in modern devices used in space missions. In the paper, we present our approach to estimate distributed microsystems damage by heavy charged particles with different parameters (angle of penetration, walkthrough distance and a number of ions). We use SRIM and TCAD Sentaurus software [2] for distributed microsystems simulation. SRIM tool has been used to evaluate the energy loss function and parameters of spatial distribution of generated charge using the predefined energy of ions, and TCAD Sentaurus has been applied for transient processes simulation [2].

In the paper, we summarize our results for computer simulation of radiation damage on distributed electrostatic MEMS, which are the most sensitive devices to radiation effects. It can cause a change in device calibration and even device failure. To compare radiation tolerance of distributed microsystems we use two test capacitive elements: a parallel plate capacitor and a stepped capacitor based on the Cantor set. We have chosen silicon capacitor plates; a dielectric spacer is made of silicon dioxide. Coordinates of a test capacitive element in a distributed plane microsystem is generated randomly. Radiation tolerance to heavy charged particles are estimated by analyzing properties changes of test elements and then the corresponding mean and the standard deviation are calculated.

Our analysis of multiple penetration of ions in microsystems has shown that distributed microsystems of capacitive elements, based on the Cantor set, demonstrate lower value of the mean of current peak in comparison with microsystems of parallel plate capacitive elements.

Finally, conclusions about radiation sensitivity of fractal electrostatic distributed MEMS are envisaged. It seems, self-similarity design for distributed microsystems can be a good way to increase its tolerance to heavy charged particles fluxes.

L. Zinchenko, V. Makarchuk, A. Glushko, V. Terekhov, and S. Michaylichenko acknowledge a support by the RFBR (grant RFBR No. 16-07-0676-a).

1. V. Shakhnov, A. Glushko, V. Makarchuk, L. Zinchenko, V. Terekhov, S. Mikhaylichenko. “Simulation of heavy charged particles damage on MEMS”, Proc. of SPIE Vol. 10224, 2016.
2. A.A. Glushko, *Device and Process Simulation in TCAD Sentaurus System*. BMSTU Press, Moscow, 2015.

A novel approach to model high-speed microelectronic switch on the basis of hydrodynamic approximation

E. Ryndin, A. Al-Saman
Southern Federal University, Taganrog, Russia, e-mail address: earyndin@sfedu.ru, al-saman@sfedu.ru

As the integration of high-speed microelectronic devices is becoming deeper and deeper, the problem of their modeling is also arising. For instance, reported in [1] ultrafast microelectronic switch based on the tunnel-coupled quantum wells (QWs) has a specific structural feature, which is the combination of both vertical and horizontal integration of the quantum areas. Therefore, its modeling will involve the consideration of both the longitudinal and the transverse transport of electrons along with the tunnelling processes between QWs. For this purpose, three-dimensional numerical models based on quantum-hydrodynamic approximation were proposed. Nevertheless, they are impractical in term of using them for circuit designing due to their time and computational expenditure. The latter is a solid argument to develop a new approach that provides an adequate physics-based simulation of the microelectronic switch and at the same time; it is so straightforward to be employed for the practical circuit design. In [1] we have suggested an equivalent circuit for microelectronic switch based on the implication that the switch can be represented as two HEMT-like structures linked by a tunnel barrier. This assumption allows us to perform the modeling issue in two separate steps: 1) longitudinal electron transport modeling for each channel separately; 2) transverse electron transport modeling. The latter can be modelled using two serial-joined RC-circuits with a current source in the middle between them. Here the RC-circuits model the transit time, while the current source models the current flow between the QWs. What is related to the longitudinal electron transport modeling, it can be more challenging, as it is vital to provide an accurate calculation of the spatial distributions of potential, electrical field, mobility, drift velocity and electron concentration within the QW. Utilization of the drift-diffusion approximation for this end may lead to a miscalculation. That miscalculation associated with neglect of two significant factors: the overshoot effect and current density resulting from the gradient of electrons temperature. To overcome these shortcomings, we have developed the quasi-two-dimensional hydrodynamic model, where the calculation of spatial distributions of velocity and energy was carried out using modified balance equations:

$$v_n\left(\tau_{p_n}\frac{\partial v_n}{\partial y}+1\right)=-\mu_n(T_n)E; \qquad \frac{\partial W_{tn}}{\partial y}+\frac{W_{tn}}{\tau_{W_n}v_n}=-qE\,, \tag{1),(2}$$

where v_n is the drift velocity, τ_{p_n} is the momentum relaxation time, μ_n is the electron mobility, E is the electrical field within the QW, T_n is the electron temperature, W_{tn} is the difference between non-equilibrium and equilibrium energies of electrons, τ_{W_n} is the relaxation time of energy and q is the elementary charge.

Apparently, to solve equations (1) and (2) self-consistently, one should calculate the potential distribution within QW. Therefore, we imply that the QW of HEMT-like structure could be subdivided into (J - 1) sections with similar dimensions. So, the potential drop on j-section may be defined as follows:

$$U_{j+1}=U_j+U_{\mathrm{d}}\frac{R_j}{\sum_1^{J-1}R_j}; \qquad R_j=\frac{U_{j+1}-U_j}{I_{\mathrm{d}}}; \tag{3}$$

$$I_{\mathrm{d}}=W\left[\mu_n(y)E(y)Q_n(y)+\frac{k_B}{q}\mu_n(y)T_n(y)\frac{\partial Q_n(y)}{\partial y}+\frac{k_B}{q}\mu_n(y)Q_n(y)\frac{\partial T_n(y)}{\partial y}\right], \tag{4}$$

where U_{d} is the drain voltage, U_j is the potential at j-node of the coordinate grid, U_{j+1} is the potential at (j+1)-node of the coordinate grid, $Q_n(y)$ is the surface charge density of electrons within QW, W is the gate width and k_B is the Boltzmann constant. The equations (1) and (2) with allowance for equations (3) and (4) have been solved self-consistently using finite difference method. The outcomes of this procedure were the above-mentioned spatial distributions along with current-voltage curves taking into account the overshoot effect and ballistic transport as well.

This research is supported by the Russian Foundation for Basic Research (Grant № 16-07-00018).

1. E.A. Ryndin, A.A. Al-Saman. “A Circuit Model of High-Speed Integrated Switch with Controlled Re-Dislocation of the Electrons Density in Tunnel-Coupled Quantum Wells”, Izvestiya SFedU. Engineering Sciences, **3**, pp. 178-88, 2017.

Improving the selectivity of carbon nanotube-based gas sensors to ammonia and nitrogen dioxide via UV irradiation

N. Nekrasov[1], V. Nevolin[1], F. Fedorov[2], A. Nasibulin[2], I. Bobrinetskii[1]
1. National Research University of Electronic Technology, Russia, 8141147@gmail.com.
2. Skolkovo Institute of Science and Technology, Russia, f.fedorov@skoltech.ru

The detection of ppm (parts per million) and sub-ppm concentrations of gas vapors is necessary in the fields of safety, air pollution control and health monitoring. Solid-state gas sensors use complex oxide materials to detect ammonia or nitrogen dioxide molecules, but usually require activation at elevated temperatures up to 300-400 °C [1]. Carbon nanotube-based gas sensors can detect sub-ppm concentrations of ammonia and nitrogen dioxide molecules while working at room temperature without heating [2]. However, large cross-sensitivity of carbon nanotubes requires accurate approaches to tune the selectivity of these sensors. Here we report the results on UV assisted functionalization of carbon lattice for selectivity improvement toward ammonia and nitrogen dioxide gas vapors.

In our work, we used CVD grown single-walled carbon nanotube (SWCNT) films transferred onto polyethylene terephthalate substrates and individual SWCNTs grown on silicon substrate [3] as sensor platforms. Ultraviolet irradiation at 194 nm wavelength with irradiation power of 20 W was applied to functionalize SWCNTs [4]. We varied the time and gas environment in the chamber during UV irradiation. We observed that the atmosphere and air conditions such as temperature and humidity highly affect the functionalization process. The defect concentration in SWCNTs was tracked by Raman spectroscopy and atomic-force microscopy before and after UV illumination. The changes in transfer current-voltage characteristics reveal the growth of the hole doping for individual SWCNTs along with the rise of processing time. Gas sensing measurements were performed at concentrations varying from 1 to 50 ppm and at different humidity. The irradiated samples show a good selectivity to ammonia while the response to nitrogen oxide decreases when compared with pristine SWCNT films (Fig. 1). We associate it with the increased amount of grafted functional groups on the SWCNT surface, which enlarge the effect for electron donor gas and reduce the sensitivity for electron acceptor gas.

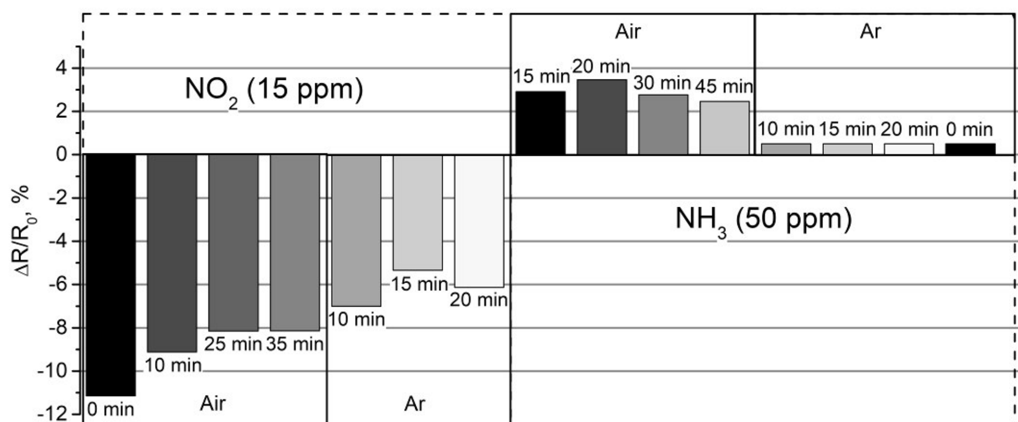

Figure 1. The response to nitrogen oxide and ammonia gases of SWCNT films irradiated with different time via UV light in air and in argon atmosphere.

1. Z. Qiu, et al. “NH_3 sensing properties and mechanism of Ru-loaded WO_3 nanosheets”. Journal of Materials Science: Materials in Electronics, **29**, pp. 11336-11344, 2018.
2. F. Rigoni, et al. "Humidity-enhanced sub-ppm sensitivity to ammonia of covalently functionalized single-wall carbon nanotube bundle layers" Nanotechnology, **28**, p. 255502, 2017.
3. A. Moisala, et al. "Single-walled carbon nanotube synthesis using ferrocene and iron pentacarbonyl in a laminar flow reactor", Chem. Eng. Sci., **61**, p. 4393, 2006.
4. N. Nekrasov, A. Emelianov, and I. Bobrinetskiy. “UV functionalization of carbon nanotubes on plastic substrates”. 2018 IEEE Conference of Russian Young Researchers in Electrical and Electronic Engineering (EIConRus), pp. 2000-2002, 2018.

Deep Silicon Plasma Etching: Selection of Processes for Different Applications

A.V. Miakonkikh, S.N. Averkin, K.V. Rudenko, V.F. Lukichev
Institute of Physics and Technology of RAS, Nakhimovsky av. 34, 117218, Moscow, Russia, miakonkikh@ftian.ru

Deep silicon plasma etching (DSE) processes are in-demand for fabrication of a variety devices including capacitors in DRAMs and capacitors in RF ICs, isolation trenches for HV devices, TSV in interposers for 3D-integration, MEMS devices, Silicon elements of X-ray optics. Each case requires own specification for etched structures but general condition for DSE technologies is relatively high anisotropic etch rate (3 – 20 um/min) of Si and process selectivity to mask > 50:1. Structures for microelectronic application require clean sidewalls to minimize leakage currents and vertical or tapered etching profiles. On the other hand the surface contamination is not such critical for MEMS devices where the possibility of etching up to hundreds microns depth features with high aspect ratio and vertical profile is main issue. In many applications the low values of sidewall roughness is crucial.

Present paper overviews existent and newly developed DSE technologies offering optimal choice for specific demands. Under consideration there are four types of deep silicon etching processes: cyclic original Bosch process [1] and modified one, continuous cryoetch process [2], cyclic STiGer process [3], and new Ox-Etch process [4] developed in IPT RAS. All processes designed with fluorine chemistry of SF_6 based plasma that provides fastest etch reaction with Silicon enhanced by ion bombardment from plasma. The differences are in approach used to suppress the isotropic etching of the structure sidewalls to achieve required anisotropy and of etch process.

Bosch process consisting of sequential alternating steps of etching and polymer sidewalls passivation gives typically scalloping profile and polymer contamination of sidewalls (Fig. 1a). The SF_6 plasma step etches the Silicon, and the C_4F_8 plasma steps deposits protection layer. By choice of step durations in cycle and wafer bias during etch step it is possible significantly reduce scalloping up to nanoscale size (Fig. 1b) but with reducing of average etch rate also. More clean cryogenic DSE processes utilizes $Si_xF_yO_z$ passivation layer stable only at cryogenic temperature (<-80 ^{o}C). First version is continuous regime with SF_6+O_2 plasma, and the second one is gas chopping process SiF_4+O_2/SF_6 which is patented as STiGer etch process. The first gives minimal sidewall roughness (< 5 nm) (Fig. 1c) with control of profile angle, and the second is more fast, also clean but gives scalloping profile similar Bosh process. An alternative clean process was proposed [4] where the layer of stable SiO_x formed as a result of the oxidation of the silicon surface in oxygen plasma is used as a passivant; the etch step is then carried out in SF_6 plasma. As a result new DSE process with clean low roughed sidewalls was designed (Fig. 1d).

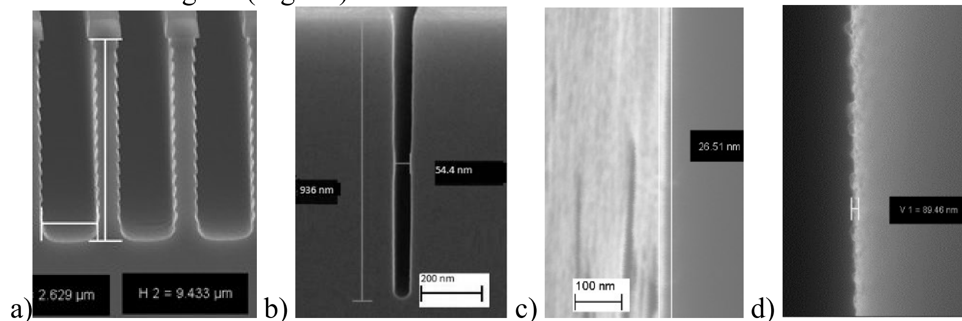

Fig. 1. Etched structures for (a) original Bosh process; (b) nanosized Bosch process; (c) sidewall for cryo DSE 5 nm roughness; (d) sidewall roughness in Ox-Etch process.

Observed technologies were used to etch trenches for microelectronic applications, TSVs, capacitors, MEMS. Reported study was carried out under Program of FASO of Russia and partially supported by RFBR, research project # 18-07-01190.

1. Laermer F. and Schilp A. 1996 U.S. Patent 5501893.
2. Tillocher T., Dussart R., Mellhaoui X., et al. Microelectronic Engineering **84 (**2007) 1120-1123.
3 Tillocher T., Dussart R., Overzet L.J., et al. J. Electrochem. Soc. **155 (**2008) D187.
4. Miakonkikh A.V. et al. “Anisotropic plasma etching of Silicon in gas chopping process by alternating steps of oxidation and etching” J. of Phys. Conf. Series (IOP) 2018 (in press).

Model-based approach for optimization of plasma etching processes in non-oxygenated fluorocarbon plasmas

A. Efremov[1], D. Murin[1], K.-H. Kwon[2]
1. Ivanovo State University of Chemistry & Technology, Ivanovo, Russia, amefremov@mail.ru.
2. Korea University, Sejong, South Korea, kwonkh@korea.ac.kr

Fluorocarbon gases with a general formula of $C_xH_yF_z$ are widely used in the microelectronic device technology for the dry patterning of silicon and silicon-based materials (SiC, SiO_2, Si_3N_4). Among these, the CF_4 is characterized by the highest F/C ratio and provides the domination of etching over the surface polymerization process under the typical reactive ion etching conditions. The gases with low F/C ratio (C_4F_6, C_4F_8, CHF_3 and CH_2F_2) exhibit much higher polymerization ability and are normally used for the etching processes which require the maximum SiO_2/Si etching selectivity. The mechanism of last effect is connected with relative increase in the SiO_2 etching rate due to the lower fluorocarbon polymer film thickness on the oxygen-containing surface. At the same time, a decrease in absolute Si and SiO_2 etching rates as well as an increase in etching residues take place. As such, the choice of an appropriate fluorocarbon gas for the given etching process needs the deep understanding of plasma chemistry in order to determine types of plasma active species as well as their fluxes to the treated surface.

In this work, we performed the combined (experimental and model-based) comparative study of CF_4+Ar, CHF_3 + Ar and C_4F_8 + Ar inductively coupled plasmas under one and the same operating conditions. The main goals were 1) to compare the formation/decay kinetics for plasma active species, steady-state plasma compositions and efficiencies of both chemical and physical etching pathways; and 2) to determine the gas-phase-related parameters characterizing the etching/polymerization balance, including etching rates for target material and fluorocarbon polymer film, polymer deposition rate and polymer film thickness.

The experiments were carried out in a planar inductively-coupled 13.56 MHz plasma reactor. The process conditions were: total gas flow rate (q) of 40 sccm, gas pressure (p) of 6 mTorr, input ICP power (W) of 700 W and bias power (W_{dc}) of 200 W. Langmuir probe diagnostics provided the data on electron temperature (T_e), ion current density (J_+) and total positive ion density (n_+). Compositions of feed gases were set by adjusting the partial gas flow rate of the components within p = const. In order to determine the absolute densities and fluxes of plasma active species, we used the simplified global (zero-dimensional) plasma model. The input model parameters were experimental data on T_e and n_+ while the outputs include volume-averaged plasma parameters, densities and fluxes of neutral and charged species.

It was found that the main feature of CHF_3 + Ar plasma compared with the CF_4+Ar one is the effective gas-phase reactions $CHF_x + F \rightarrow CF_x + HF$, $CHF_x + H \rightarrow CHF_{x-1} + HF$ и $CF_x + H \rightarrow CF_{x-1} + HF$. This reasonably results in 1) domination of HF over other fluorine-containing species; 2) low density and flux of F atoms; and 3) high density and flux of polymerizing CF_x (x = 1, 2) radicals. In fact, this explains numerous published data that CHF_3 -based plasmas provide the higher SiO_2/Si etching selectivity. The C_4F_8 + Ar gas system is characterized by higher values of both F atom flux (by ~ 1.9–1.4 times for 0–75% Ar) and polymerizing radical flux (by ~ 3.2–3.8 times for 0–75% Ar) compared with those in CHF_3 + Ar. The first effect is caused by the higher F atom formation rate from CF_x (x = 1, 2, 3) in electron impact reactions while the second one follows by direct formation of CF_2 from the original C_4F_8 molecules. Therefore, since the C_4F_8 + Ar plasma is also characterized by lower ion flux in the range of 0–60% Ar (in fact, by the lower polymer etching rate), it exhibits the higher polymerization ability compared with CHF_3 + Ar gas system.

The model-based analysis of both etching and polymerization kinetics allowed one to compose the set of formal parameters (in a form of flux-to-flux ratios) characterizing the efficiencies for various heterogeneous reaction pathways. This provides the ability to compare the features of various fluorocarbon gases (and thus, to evaluate their applicability for the given etching process) based on plasma diagnostics data and simple plasma chemistry calculations.

This work was supported by the RFBR grant, project № 18-37-00064 mol_a.

Effect of terminal methyl group concentration on plasma resistance of spin-on low-k dielectric films

A. Rezvanov[1,2,*], A. Miakonkikh[3], A. Vishnevskiy[4], D. Seregin[4], U. Baislamova[1], K. Vorotilov[4], K. Rudenko[3], M. Baklanov[5]

1. Moscow Institute of Physics and Technology, Dolgoprudny, Russia
2. Molecular Electronics Research Institute, Zelenograd, Moscow, Russia
3. Institute of Physics and Technology of Russian Academy of Science, Moscow, Russia
4. MIREA – Russian Technological University, Moscow, Russia
5. North China University of Technology, Beijing, China
* rezvanov@phystech.edu

For several decades, scaling the dimensions of the elements in the integrated circuits (ICs) is the driving factor for the continuously evolving microelectronics industry [1, 2]. The steady scaling to smaller and smaller feature sizes led to a significant increase in the density of functional elements on the Si wafer area, resulting in an increased RC delay and cross-talk, which adversely affect device performance. Therefore, the introduction of new materials is necessary to improve the device performance. The RC scaling in damascene technology is enabled by introducing Cu and porous low-k materials instead of Al and SiO_2, respectively [3]. The present work investigates the effect of terminal group concentration on low-k damage during plasma etching.

The spin-on glass low-k dielectrics were deposited on Si wafer with different TEOS/MTEOS (0/100-100/0) ratio and the similar porogen Brij®30 content (19.3%) [4]. The main properties of deposited low-k films were analyzed by ellipsometry, porosimetry, FTIR, water contact angle and nanoindentation. For study the plasma induced damage, prepared low-k films were treated in SF_6 plasma – to simulate the dielectric damage from F radicals, in Ar plasma – to simulate damage from VUV photons, and in Ar/SF_6 (1:1) mixture – to study the joint effect. Plasma treatment was performed in ICP cluster tool Plasmalab (OIPT) without applying bias to the sample (pressure 5 mTorr, power 1500 W). Sample temperature was about 20°C during the process. Plasma parameters (electron density, positive ion density, electron temperature and density of F* radicals) were measured by Langmuir probe and OES. Reduce in film thickness was measured by ellipsometer. The etch rate (ER) in case of pure Ar plasma is very small for all studied films that explained the surface densification/sputtering by ions. In case of SF_6 and Ar/SF_6 plasmas the ER increases as a function of methyl group concentration. According to ellipsometry measurements the refractive index (RI) of low-k films goes up significantly after etching in SF_6 and Ar plasmas (lower effect for Ar/SF_6 mixture). However, additional annealing at 300°C in atmosphere ambient during 30 min leads to decreasing of RI that can be explained by etch by-products or polymer desorption. FTIR analyzes shows that the low-k plasma damage decreases with increasing the methyl content for all plasmas. Equivalent damaged layer (EDL) calculation (Eq.1), which based on Si-CH_3/Si-O-Si peaks ratio before and after plasma treatment, shows significant reduction for high methylated samples, especially in case of Ar plasma. For instance, damage from F radicals decreases with change in composition (TEOS/MTEOS) by 60% comparing the samples with TEOS/MTEOS composition from 80/20 to 0/100. Plasma damage from VUV photons reduces more than 70% for the same samples.

$$EDL = d_{etch} \cdot \left(1 - \frac{I_{etch}[Si - CH_3]/I_{etch}[Si - O - Si]}{I_{pristine}[Si - CH_3]/I_{pristine}[Si - O - Si]} \right) \quad (1)$$

As a conclusion, the increasing of the terminal methyl group concentration leads to the significant reduction of EDL, especially in case of VUV photons. According to the material properties analyzation and plasma damage study, the best TEOS/MTEOS ratio 40/60 was chosen for the future integration in IC schemes.

1. K. Maex, M.R. Baklanov, D. Shamiryan, F. Iacopi, S.H. Brongersma, and Z.S. Yanovitskaya. “Low dielectric constant materials for microelectronics”. J. Appl. Phys., **93**, p. 8793, 2003.
2. A.S. Valeev, G.Y. Krasnikov, V.A. Gvozdev, and P.I. Kuznetsov. “The method of producing a multi-level copper metallization with ultra-low dielectric constant”. **RU 2548523**, 17 December 2013.
3. H. Struyf *et al*. “Low damage damascene patterning of SiCO(H) low-k dielectrics”. In Proc. IITC, 2005.
4. C. Liu *et al.* “Effect of terminal methyl groups concentration on properties of organosilicate glass low dielectric constant films”. Jpn. J. Appl. Phys., **57**, p.07MC01, 2018.

Formation of metallic nanowire and nanonet structures on the surface of SiO_2 by combine plasma etching processes

I.I. Amirov, E.S. Gorlachev, L.A. Mazaletsky, M.O. Izyumov

Yaroslavl Branch of the Institute of Physics and Technology of RAS, Yaroslavl 150007, Russia, ildamirov@yandex.ru

Nanowires and nanonet (NW and NN) metallic structures are promising materials of nanoelectronics, optoelectronics [1]. There are different methods of obtaining them. Earlier, we developed a method for the formation of nanoscale structures (NSS) from fluorocarbon nanowires on the Si surface using a plasma etching process [2]. In this work it is shown how on its basis it is possible to obtain NW and NN metallic structures on the oxidized Si surface.

The method of the nanostructure formation consisted of two stages. In the first stage, NSS were obtained on the SiO_2 surface. For this purpose, a nanowire fluorocarbon film (NFCF) of nanometer thickness was formed on the surface of a film of amorphous Si (500 nm) deposited on SiO_2 by etching in C_4F_8 / 80% Ar plasma at an ion energy of ~200 eV. NSS on the SiO_2 surface were obtained by complete etching of the a-Si layer in the SF_6 / 50% Ar plasma. As a result of the higher etching rate of a-Si than NFCF, the latter remains on the SiO_2 surface in the form of NSS consisting of carbon-fluorinated nanowires with the thickness of ~10 nm. The NSS formation was controlled by a sharp change in the reflection signal of the laser beam from the sample surface. The dimensions of the formed nanocells depended on the etching time of the NFCF and were 100-300 nm. In the second stage, a metal film (Pt) with a thickness of 7 nm was deposited by a magnetron method on the SiO_2 surface with the formed NSS. Then, the metal film was sputtered in Ar plasma at a low ion energy (E_i ~100 eV). The sputtering of the metal film was monitored by a change in the reflection signal of the laser beam. The metal on the surface of NSS structures (Fig. 1) remained as a result of a redeposition and formed NN and NW metallic structures. Thus, using this method, it is possible to obtain various metallic NSS.

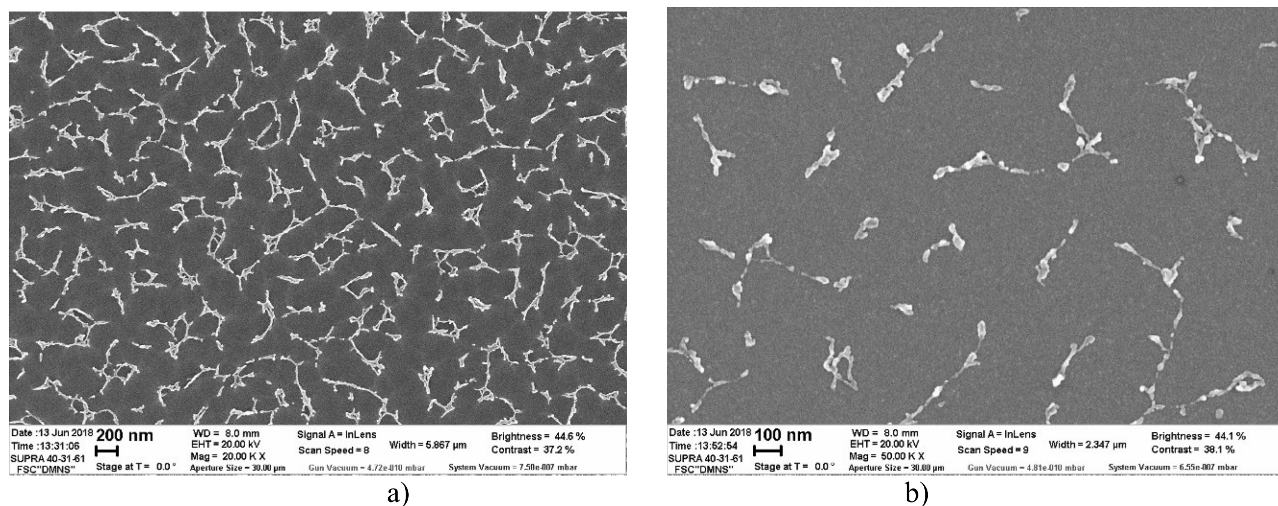

a) b)

Fig. 1. Nanonet (a) and nanowire Pt (b) structures on the SiO_2 surface.

The reported study was funded by RFBR according to the research project № 17-07-00657.

1. S. Ye, A.R. Rathmell, Z. Chen, I.E. Stewart, B.J. Wiley. “Metal nanowire networks: The next generation of transparent conductors”. Adv. Mater. **26**, pp. 6670-6687, 2014.

2. I.I. Amirov, E.S. Gorlachev, L.A. Mazaletsky, M. O. Izyumov, N.V. Alov. “Self-formation of a nanonet of fluorinated carbon nanowires on the Si surface by combine etching in fluorine-containing plasma. J. Phys. D: Applied Physics, **51**, p. 11LT01, 2018.

Effect of Ar ion-plasma treatment on residual stress in thin Cr films

A. Babushkin, R. Selyukov, I. Amirov
Yaroslavl Branch of the Institute of Physics and Technology RAS, Yaroslavl, Russia, artem.yf-ftian@mail.ru

The reliability and durability of MEMS can be reduced due to residual stress in the films used. Excessive stress can cause film cracking, peeling and bulging. Also the MEMS failures can be caused by the device elements deformations induced by both mean stress and stress inhomogeneity along the film thickness (stress gradient). On the other hand stress allows the self-assembly of MEMS components, tensile stress in bridges and membranes leads to increase in their resonant frequencies. Thus, the regulation of film stress is important. One of the methods to modify the stress in films after their deposition is the bombardment with inert gas ions. Most researchers are focused on the ion energy in the range 0.5 keV-1 MeV. However, bombardment with that ion energy results in the sputtering of the film material. This can be avoided by using ion energy below the sputtering threshold. The aim of our work was to investigate the evolution of the mean stress and stress gradient in thin polycrystalline Cr films exposed to bombardment by ions with energy below the Cr sputtering threshold in the Ar plasma.

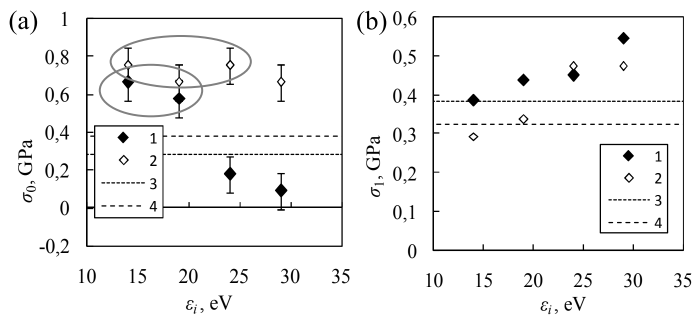

Fig.1. (a) – $\sigma_0(\varepsilon_i)$ and (b) – $\sigma_1(\varepsilon_i)$. Treatment duration – 30 min. 1, 3 – batch #1. 2, 4 – batch #2. 3, 4 – as-deposited films. The regimes in which there were local film delamination marked by ellipses.

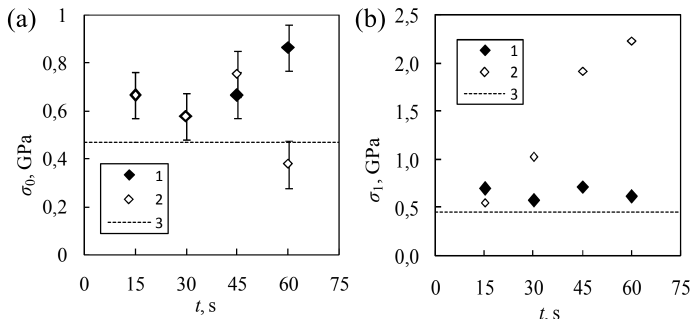

Fig.2. (a) – $\sigma_0(t)$ and (b) – $\sigma_1(t)$. ε_i = 14 eV (1) and 29 eV (2). Batch #3. 3 – as-deposited film.

300 nm Cr films were deposited on Si(100) substrates by magnetron sputtering. Three batches Cr/Si were fabricated at identical conditions. After deposition Cr films were exposed to Ar ion-plasma treatment. The ion energies ε_i were 14-29 eV and treatment times t were 15-60 min. Ion current density was 6.4 mA/cm^2. In polycrystalline films the stress state is biaxial, the out-of-plane stress σ_z, as a rule, equals to 0 and in-plane stress is isotropic and independent of in-plane coordinates x, y, but dependent of out-of-plane coordinate z: $\sigma_x = \sigma_y = \sigma(z)$. Usually the linear approach for $\sigma(z)$ is used: $\sigma(z) = \sigma_0 + \sigma_1 \cdot 2z/h$. The mean stress σ_0 and stress gradient σ_1, were determined using X-ray diffractometry and test microcantilevers, respectively. It was found that as-deposited films had compressive stress and positive gradient, i.e. film is more compressed near the interface then near the surface. Treatments of Cr films at ε_i = 14-24 eV, t = 15-45 min, as a rule, lead to the increase of compressive stress to the value sufficient to induce the local film delaminations (Fig. 1a, 2a). Delaminations have the form of hollow hemispherical bulges. Treatments at ε_i = 24-29 eV, t = 60 min, lead to the decrease of compressive stress, and at ε_i = 29 eV lead to the decrease of compressive stress at even lower treatment time. The stress gradient increases after ion-plasma treatments with ε_i > 14 eV (Fig. 1b, 2b). The higher ion energy or the longer treatment time the larger stress gradient. Treatments at ε_i = 14 eV don't change the stress gradient. We assume that stress changes after ion-plasma treatments are due to surface and grain boundary diffusion of atoms and vacancies that are generated during ion bombardment. According to the existing theory of stress origin in films the atom diffusion into grain boundaries results in compressive stress. Vacancy diffusion into grain boundaries should lead to the recombination of atoms and vacancies. Recombination results in the reducing of compressive stress. Usually the activation energy of vacancy diffusion is larger than that of atom diffusion. So, atom diffusion leads to the increasing of compressive stress at lower ion energy and shorter treatments. At higher ion energy and longer treatments vacancy diffusion becomes significant and leads to the decreasing of compressive stress.

Interprocess quality control of critical dimensions in MEMS manufacturing

N. Izrailev[1,2], A. Kazachkov[2], I. Rod[1,2], A. Isachenko[2], D. Shamiryan[2]
1. LLC Mapper, Moscow, Russia, mapperllc@mapperllc.ru.
2. Moscow Institute of Physics and Technology, Moscow, Russia, info@mipt.ru.

Modern high-tech MEMS manufacturing is not able to function without developed system of quality monitoring. Well-managed quality monitoring system enables to predict production risks and minimize them effectively. Control for the critical dimensions (CD) of MEMS structures after different production steps such as optical lithography, oxide etching, deep silicon etching and film deposition makes possible not only to establish and track the dependencies between the parameters of the above processes, but also to monitor inconsistencies in results and to correct these deviations.

Our research is devoted to such quality management tool as monitoring of product's geometrical parameters between different MEMS manufacturing stages. It presents the results of the script development for the optical images analysis. There are several advantages of our solution is presented inside paper such as low cost, automaticity and avoidance of human factor in quality control. Our technique enables to obtain critical dimensions of micro-sized structures captured by an automated optical system with required accuracy. Full optical inspection along with image processing takes less than 10 minutes per wafer while fully manual inspection can take hours. Despite huge size of images to be processed (2 GB), processing time is quite short due to image segmentation and the use of Deriche edge detection [1] method with optimal $\alpha = 0.5$.

1. Deriche R. Using Canny's criteria to derive a recursively implemented optimal edge detector // Int. J. Computer Vision. April 1987. V.1. P. 167–187.

The opportunities of Rutherford backscattering spectroscopy for analysis of multilayer nanometer thin film structures

V. Bachurin, A. Churilov, N. Melesov, E. Parshin, A. Rudy, O. Trushin
Yaroslavl branch of the Institute of Physics and Technology of the Russian Academy of Sciences, Yaroslavl, Russia
E-mail: vibachurin@mail.ru

The results of study of multilayer thin film structure using Rutherford Backscattering Spectroscopy (RBS) are presented. The spin-tunnel structure of the following composition: 5(nm)Ta/30CuN/5Ta/3NiFe/16IrMn/2.0CoFe/0.9Ru/2.5CoFeB/2MgO/2.5CoFeB/10Ta/7Ru on SiO_2 was used as a test sample. This kind of structure is used for MRAM fabrication. For chemical analysis of multilayer structures Secondary Ion Mass Spectroscopy (SIMS) is usually used. While being more sensitive this method has serious drawbacks. Cascade mixing due to ion bombardment leads to the distortion of actual picture near borders of layers, especially with going deeper inside the structure. Besides that, the converting from time scale to the depth leads to large errors for such structures. Both those factors lead to the results, which significantly differ from the data of the deposition process [1].

Alternative to SIMS in layer by layer analysis in some cases might be the method of RBS. However the analysis of such samples might appear significant difficulties during measurement and interpretation of RBS spectra because of small thickness of layers and overlay of peaks of elements with close masses. The experiments were done on the installation K2MV. The best experimental conditions were chosen for measurement and subsequent processing of spectra using SIMNRA software. The part of RBS spectrum obtained at surface bombardment with double charged He^{++} ions with energy of 3 MeV, current of 2 nA and scattering angle of 165° is presented in fig. 1 together with the results of SIMNRA simulations.

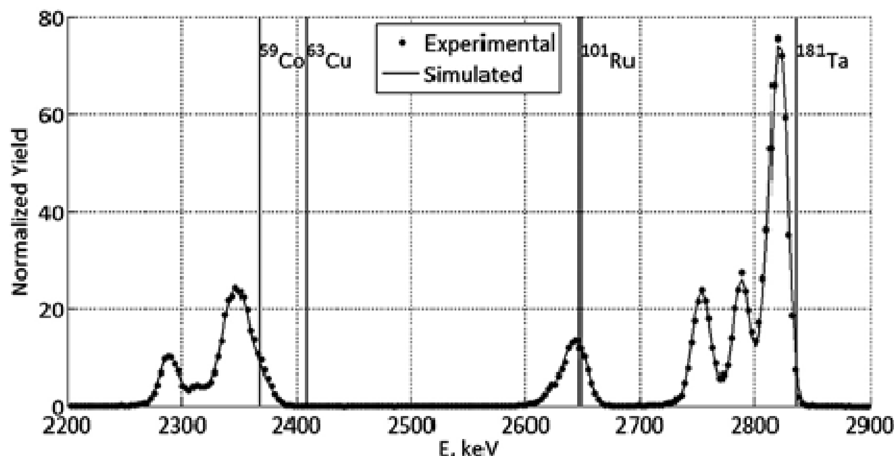

Fig. 1. Fragment of experimental RBS spectrum (dots) and the results of SIMNRA simulation (solid line).

Analysis of RBS data shows clear signature of the existence of 3 layers containing Ta (~2800 кэВ) in studied multilayer structure. High energy peak of Ta constitutes the sum of signals from Ta and Ir. Separate peak corresponding to Ru has also been resolved. The spectrum in the range from 2250 up to 2400 keV represents the composition of peaks (ordered by the growth of energy of scattered ions) Mn, Fe, Ni, Cu, and Co. The RBS method due to its own limitations does not allow to obtain layer by layer depth distribution of those elements, but let us to estimate integral thicknesses of layers in specific for RBS units of depth (atom/cm^2), which might be converted in nm at certain assumptions. The results obtained show that analysis of such samples using RBS method might be useful supplement to the results of SIMS and TEM.

1. O.S Trushin, S.V. Vasiliev, S.G. Simakin, E.A Smirnov. "Quality control of multilayer spin-tunnel structure using combination of methods of analysis". Russian Microelectronics, accepted for publication in 2018.

Fast local IC delayering using high energy BIB

E. Kelm, D. Zubov, S. Sokolov, R. Milovanov
Institute of Nanotechnology of Microelectronics, Russian Academy of Science, Russia, 119991 Moscow, Leninsky Prospekt, 32A, kelm87@yandex.ru.

Within the confines of failure analysis technique is often necessary to study the 3d-structure of the integrated circuit in the area of the intended failure. That is, analyzing all the conductive and interconnection layers for damage or defects. Standard delayering technique involving dry plasma etching, wet chemical etching and mechanical polishing in various combinations allows fully analyze all IC layers, however requires a complex of equipment and a lot of time [1]. New IC delayering approaches based on using Focused Ion Beam (FIB) have a number of limitations – different etching rate of various materials and electric charging of surface make it difficult to use this technique for elaborate multilayer (number of layers more than 5) IC and IC based on copper metal layers consisting low-k interlayer dielectric[2]. Broad Ion Beam (BIB) serial section tomography allows us to restore 3d structure of the investigated object, however, the low resolution of this method in the direction of the series sections and a lot of time makes this technique is unpromising for IC failure analysis.

In our work we investigate using low angle (4-15°) BIB milling for local IC delayering. Main differences between low energy BIB (up to 2 kV) and high energy BIB (4-15 kV) sources for low angle milling also were determined. From our experiments it can be concluded that increasing of beam energy leads to increasing of removal rate of material, and decreasing differences of different materials removal rate with respect to each other. Thus, using high-energy beam (10-15 kV) for an a selective layer removal and a low energy beam (0-2kV; 4-5kV) for opening a conductive layer can be considered a promising direction for rapid local IC failure analysis (field of application is about 100 mkm).

Ultrafast (several minutes per layer) local IC layers analysis also can be achieved by using only 15 kV BIB (fig.1).

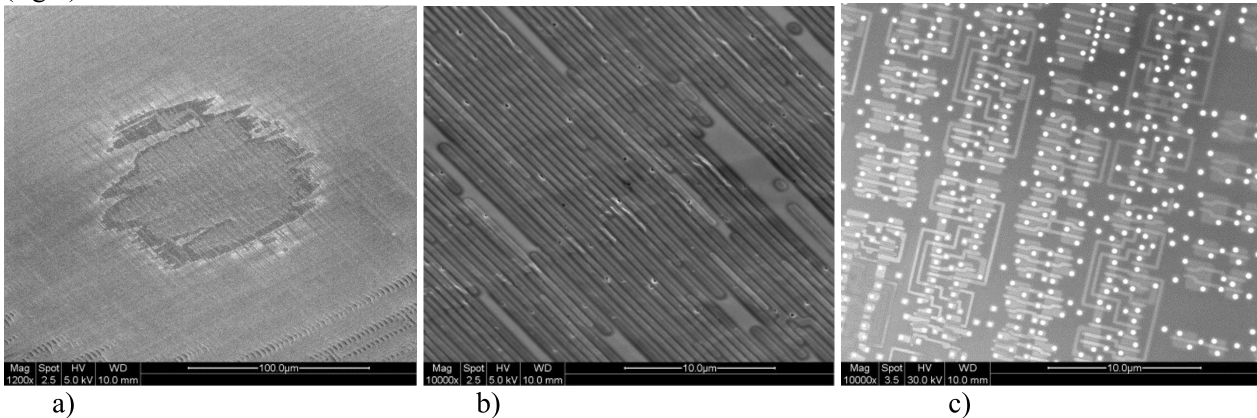

a) b) c)

Fig. 1. SEM image of IC surface after BIB milling. a) – field of plane surface b) – second aluminum layer c) – 6th polysilicon layer.

As you can see from these images – IC passivation surface profile doesn't affect the layer milling planarity, however using only high energy BIB is not possible to estimate damage of thin barrier sublayers, such as Ti, TiN and Ta. Thus, combination BIB and SEM in single equipment allows locally analysis all IC layers for about an hour.

1. F. Beck. *Integrated Circuit Failure Analysis: A Guide to Preparation Techniques.* John Willey & Sons *1998*.

2. D.D. Wang, Y.M. Huang, P.K. Tan, H. Feng, G.R. Low, H.H. Yap, R. He, H. Tan, M.K. Dawood, Y.Z. Zhao, J. Lam, and Z.H. Mai "Two planar polishing methods by using FIB technique: Toward ultimate top-down delayering for failure analysis". AIP Advances **5**, 127101, 2015.

3. B. Winiarski, A. Gholinia, K. Mingard, M. Gee, G.E. Thompson, and P.J. Withers. "Broad ion beam serial section tomography". Ultramicroscopy Volume 172, January 2017, Pages 52-64.

Local IC delayering using FIB technology

R. Milovanov[1,2], D. Abdullaev[1,2], S. Sokolov[1,2], E. Kelm[1,2]
1. Institute of Nanotechnology of Microelectronics, Russian Academy of Science, Russia, 119991 Moscow, Leninsky Prospekt, 32A, milovanov_r@inbox.ru
2. MIREA - Russian technological university, 119454 Moscow, Vernadsky Prospekt, 78, abdullaev@mirea.ru.

Delayering is one of the most common approaches to IC failure analyses. Then location of an IC failure is identified on the IC die surface it is necessary to find its certain position. Usually, such finding are done with help of delayering - sequential remove of all die layers (layer by layer) and further surface inspection of all layers with electron or optical microscopy. Now days, for delayering often use dry and wet etching or/and mechanical lapping/polishing [1-3]. The advantage of mentioned approaches is usability for large areas and whole IC dice. However, the application of these methods takes several days and some number of equipment (plasma etcher, lapping machine, chemistry laboratory, microscopes etc.).
In recent time has been performed a few new IC delayering approaches which base on FIB technology and require only one system (FIB system) [4, 5]. The main difficulty of FIB IC delayering is different rate of milling die materials which located in one plane, and non-uniform milling in the field of electrical breakdown between surface and underneath metallization (Fig. 1). Modern FIB IC delayering approaches based on alternated gas assisted etching of dielectric (XeF_2) and metal (H_2O) layers or simultaneously nonstop milling of all dies materials in the presence of special gas "D_x" [4, 5].

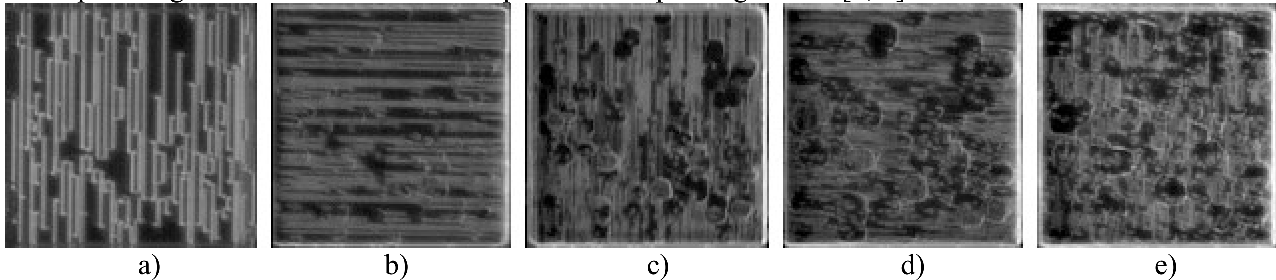

a) b) c) d) e)

Fig. 1. IC die surface during focused ion (Ga^+) milling.

In our work we research possibility of planar FIB IC delayering with help of focused ion (Ga^+) milling alternated with gas assisted deposition. Delayering was done by the dualbeam FIB system with source of gallium ions, deposition was assisted with gas (platinum and silicon oxide) injection system. Non-conformal deposition reduce surface relief and gives possibility of planar IC delayering (Fig. 2)

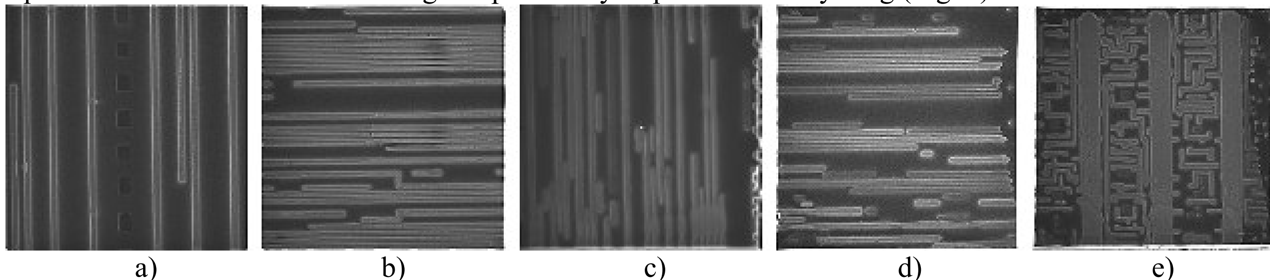

a) b) c) d) e)

Fig. 2. IC die surface during focused ion (Ga^+) milling alternated with gas assisted deposition (InDep).

1. Wills K.S., Perungulam S. Delayering techniques: dry processes, wet chemical processing and parallel lapping // Microelectronics Failure Analysis Desk Reference, Sixth Ed., p.p. 397-416, 2011.
2. Beck F. Integrated circuit failure analysis // John Wiley & Sons. 1998.
3. Burobin V.A., Milovanov R.A., Shchuka A.A. Importance of Layer-to-Layer Deprocessing of Chips for the Failure Analysis of State-of-Art Integrated Circuits. Science Intensive Technologies **14**(11), pp. 45-49, 2013 (in Russian).
4. Carleson P., Donnet D., Sidorov O., Rue Ch. Delayering on advanced process technologies using FIB // Proceeding of 40th International symposium for Testing and failure analysis, 2014, pp. 430-435.
5. Wang D.D. et al. Two planar polishing methods by using FIB technique: Toward ultimate top-down delayering for failure analysis // AIP Advances **5**, 127101, 2015.

Excitation spectra and magnetic dynamics of antiferromagnetic and ferrimagnetic nanoparticles revealed in Mössbauer spectroscopy

M.A. Chuev
Institute of Physics and Technology of Russian Academy of Sciences, Moscow, Russia, chuev@ftian.ru

A wide application of materials containing nano-sized antiferromagnetic particles in different branches of nanotechnology is primarily due to a number of specific structural, magnetic and thermodynamic properties of these materials found within long-term fundamental studies. However, these real materials are still characterized by different experimental techniques on the basis of phenomenological Néel approach describing a superposition of antiferromagnetism and superparamagnetism of uncompensated magnetic moments on two magnetic sublattices [1]. However, the ground state for antiferromagnetic nanoparticles should be much more complicated as compared to that for a bulk sample, which is evidenced from the atomic-scale magnetic modeling [2] that in its turn is hardly possible to be used for analyzing experimental data in practice due to computational expenses followed by an uncontrollable accuracy of calculations. Meanwhile, a quantum-mechanical model for describing thermodynamic properties of an ensemble of antiferromagnetic nanoparticles is recently developed [3, 4]. This model clarifies principally the difference in thermodynamic behavior of ferromagnetic and antiferromagnetic particles revealed in spectroscopic measurements as well as describes qualitatively macroscopic quantum effects earlier observed repeatedly in experimental Mössbauer absorption spectra of antiferromagnetic and even ferrimagnetic nanoparticles [5]. However, the macroscopic quantum effects are treated within the quantum-mechanical model only in terms of wave functions and mean values of macrospins of sublattices for different energy levels with no a phenomenological explanation. The latter can be found only in the macroscopic limit.

In the present contribution I will discuss the corresponding macroscopic model of magnetic dynamics of a Néel ensemble of antiferromagnetic nanoparticles with uncompensated magnetic moment recently developed [6, 7]. The excitation spectrum of the ensemble is deduced in the two-sublattice approximation following from the exact solution of equations of motion for magnetizations of sublattices. This excitation spectrum represents four excitation branches corresponding to the normal modes of self-consistent regular precession of magnetizations of sublattices and the continuous spectrum of nutations of magnetizations accompanying these normal modes. Nontrivial shape of the excitation spectrum as a function of the value of uncompensated magnetic moment corresponds completely to the quantum-mechanical calculations earlier performed. This approach allows one to describe also Mössbauer absorption spectra of slowly-relaxing antiferromagnetic and ferrimagnetic nanoparticles and to give a phenomenological interpretation of macroscopic quantum effects observed earlier in experimental absorption spectra and described within the quantum-mechanical representation.

The reported study was partially supported by RFBR, research project No 17-00-00443.

1. L. Néel. "Superposition de l'antiferromagnétisme et du superparamagnétisme dans un grain très fin". Compt. Rend., **253**, pp. 9-11, 1961.
2. R.H. Kodama and A.E. Berkowitz. "Atomic-scale magnetic modeling of oxide nanoparticles". Phys. Rev. B, **59**, pp. 6321-6336, 1999.
3. M.A. Chuev. "On the thermodynamics of antiferromagnetic nanoparticles by example of Mössbauer spectroscopy". JETP Lett., **95**, pp. 295-301, 2012.
4. M.A. Chuev. "The role of an uncompensated spin in the formation of a hyperfine structure of the Mössbauer spectra of antiferromagnetic nanoparticles". Doklady Physics, **57**, pp. 421-426, 2012.
5. W. Kündig, H. Bömmel, G. Constabaris, and R.H. Lindquist. "Some properties of supported small α-Fe_2O_3 particles determined with the Mössbauer effect". Phys. Rev., **142**, 327-333, 1966.
6. M.A. Chuev. "Nutations of magnetizations of sublattices and their role in the formation of Mössbauer spectra of antiferromagnetic nanoparticles". JETP Lett., **103**, pp. 175-180, 2016.
7. M.A. Chuev. "Excitation spectrum of the Néel ensemble of antiferromagnetic nanoparticles as revealed in Mössbauer spectroscopy". Advances in Condensed Matter Physics, **2017**, 6209206, pp. 1-15, 2017.

Determination of Al content in Al/Si thermomigration fabricated structures by X-ray diffraction

A. Lomov[1], A.Yu. Belov[2], B. Seredin[3], A. Tatarintsev[1], S. Simakin[4]
1. Institute of Physics and Technology of RAS, Moscow, Russia, E-mail lomov@ftian.ru
2. FSRC "Crystallography and Photonics" of RAS, Moscow, Russia, E-mail belov@crys.ras.ru
3. Platov South Russian State Polytechnic University, Novocherkassk, Russia, E-mail seredinboris@gmail.com
4. Institute of Physics and Technology of RAS, Yaroslavl Branch, Yaroslavl, Russia.

One of the initial steps in forming both planar and channel silicon p-n junctions consists in injection of dopant impurity. Boron and phosphorus diffusion is widely used to fabricate power high-voltage devices. But blurring of the p-n interfaces leads to device degradation. As an alternative, zone-gradient melting (thermo-migration technique) can be used. An advantage Al/Si thermomigration process [1] is its high rate which exceeds by two or three orders the rate of conventional diffusion based techniques. It is one of the promising approaches to overcome the disadvantage and increase the efficiency of devices. In addition, by means of Al/Si thermomigration one can fabricate a micro silicon matrix composed of connected photocells with p-n junction channels on faces normal to the working surface of conventional Si wafers [2]. For metrological control of the dopant concentration and structural defects (Al_xO_y precipitates and so on) generated by thermomigration process X-ray diffraction techniques can be applied. Here, using a combination of the X-ray diffraction data and first-principles density functional calculations with ABINIT code [3], we determined the Al content in different structures produced by Al/Si thermomigration, in particular, in planar layers and channels. In DFT calculations Al was assumed to occupy substitutional positions. Additional calculations of lattice distortion due to Al in a number of interstitial positions were carried out on the basis on a many-body interatomic potential [4]. Results of spectroscopic (SIMS) and microscopic (EDX) investigations were used for comparison. It was found that the aluminum content in the Al/Si thermomigration channel and film is (0.95÷1.05) 10^{19} cm^{-3} .

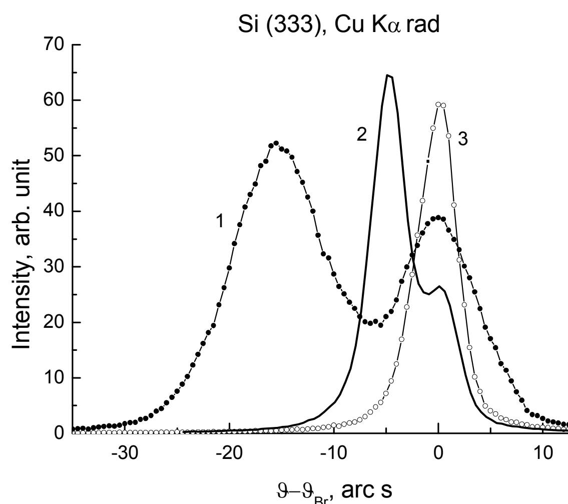

Fig. X-ray double-crystal diffraction rocking curves (reflection 333, copper rad.), from thermomigration Si(Al)/Si(111) structures: channel (1), film(2) and conventional substrate Si (P, 4×10^{14} cm^{-3}) (3). The channel width and the film thickness was 120 and 25 mkm respectively. The process was done at 1050-1200 °C.

Investigation was carried out under Program of FASO of Russia.

1. V.N. Lozovskii, L.S. Lunin, and V.P. Popov. *Temperature- Gradient Zone Recrystallization of Semiconductor Materials.* Metallurgiya, Moscow, 1987 [in Russian].
2. V.N. Lozovskii, A.A. Lomov, L.S. Lunin, B.M. Seredin, and Yu.M. Chesnokov. "*Crystal Defects in Solar Cells Produced by the Method of Thermomigration*". Semiconductors, **51**, n.3, pp. 285–289, 2017.
3 X. Gonze, J.-M. Beuken, R. Caracas et al. "*First-principles computation of material properties: the ABINIT software project*". Comp. Mater. Science, **25**, pp. 478-492 (2002).
4. B. Jelinek, S. Groh, M.F. Horstemeyer, J. Houze, S.G. Kim, G.J. Wagner, A. Moitra, M.I. Baskes. "*Modified embedded atom method potential for Al, Si, Mg, Cu and Fe alloys*". Phys. Rev. B, **85**, pp. 245102-1(18), 2012.

The depth distributions of crystalline structure parameters in thin textured films and the method of their determination

R. Selyukov, V. Naumov
Yaroslavl Branch of the Institute of Physics and Technology, Yaroslavl, Russia, E-mail: rvselyukov@mail.ru

The structure parameters of polycrystalline films such as the fraction of crystalline phase δ and the degree of preferred orientation (in textured films the latter parameter is quantified as the FWHM of corresponding rocking curve designated here as $\Delta\gamma$) have non-uniform depth distributions. Determination of these distributions $\Delta\gamma(t)$ and $\delta(t)$ is necessary for the investigation of residual stresses in films [1]. Existing methods don't provide the direct measurement of $\Delta\gamma(t)$ and $\delta(t)$ in films thinner than ~100 nm [2]. In present work we propose the method of obtaining $\Delta\gamma(t)$ and $\delta(t)$ comprising the deposition of thin films with various thicknesses at identical conditions and their rocking curve (RC) analysis. This method is applicable for textured films in case of negligible grain boundary motion during deposition because this motion changes $\Delta\gamma(t)$ and $\delta(t)$ in growing film. Proposed method was used to investigate thin textured Pt films.

Pt films with thickness h=20, 40, 60, 80 nm were deposited on oxidized Si(100) wafers by magnetron sputtering at room temperature. θ-2θ diffraction patterns, pole figures Pt (111) and Pt (200) and RCs Pt (111) were recorded. It was found that all films have fiber (111) texture but texture sharpness are different for different h. Firstly, we assumed that distributions $\Delta\gamma(t)$ and $\delta(t)$ are uniform and calculated the average values $\Delta\gamma_{\mathrm{eff}}(h)$ and relative $\delta_{\mathrm{eff}}(h)$ (highest $\delta_{\mathrm{eff}}(h)$ was set equal to 100%). For δ_{eff} calculation it was assumed that the quantity of crystalline phase in film is proportional to the area under RC. The calculation of δ_{eff} using RC allows to take into account crystalline phase in the grains of all orientations. To calculate $\Delta\gamma_{\mathrm{eff}}(h)$ and $\delta_{\mathrm{eff}}(h)$ accurately the RCs were corrected to account for background, absorption and scattering volume variation during sample rotation. Secondly, we calculated distributions $\Delta\gamma(t)$ and relative $\delta(t)$ for 80 nm film. For this purpose film was considered as consisting of four layers with equal thickness Δh=20 nm. Within every layer $\Delta\gamma(t)$ and $\delta(t)$ were set as constants. The values $\Delta\gamma$ и δ for layer located between t-Δh and t (it's accepted that t=0 at film-substrate interface) were calculated analogously to $\Delta\gamma_{\mathrm{eff}}$ и δ_{eff} using RC obtained by subtraction of RC for film with thickness $h=t-\Delta h$ from RC for film with thickness $h=t$ along with RC correction. The simple model of film structure was proposed and analyzed to compare $\delta(t)$ obtained experimentally with theoretical evaluations. The results are presented in Fig. 1. It is shown that $\Delta\gamma(t)$ and $\Delta\gamma_{\mathrm{eff}}(h)$ exponentially decay with t and $\Delta\gamma(t)\leq\Delta\gamma_{\mathrm{eff}}(h)$ for all t. $\delta(t)$ increases with t in 20-60 nm region and saturates at larger t. This result, in general, agrees with the theoretical prediction made on the basis of the proposed model.

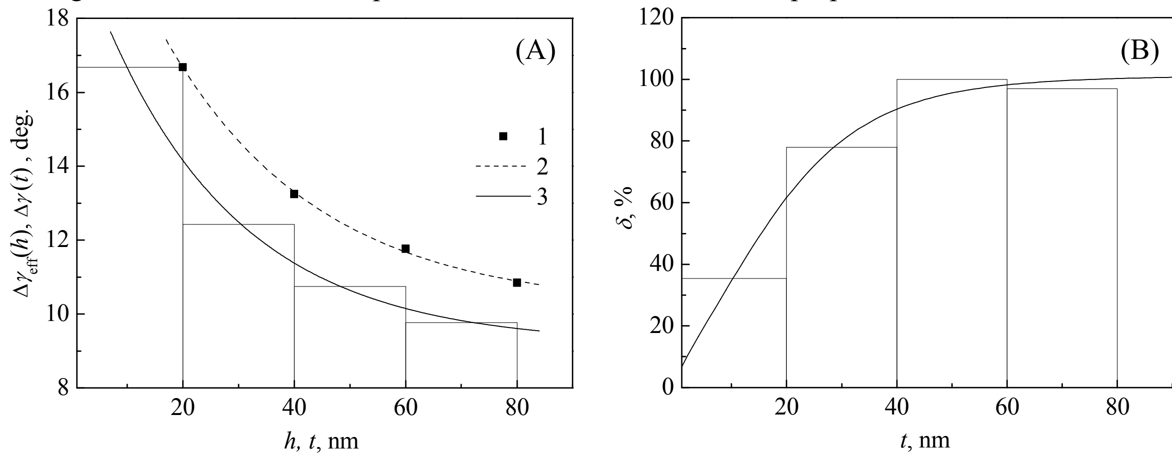

Fig. 1. A - $\Delta\gamma(t)$ (column chart), $\Delta\gamma_{\mathrm{eff}}(h)$ (1) and their approximations by exponential decay function (2, 3). B - $\delta(t)$ (column chart) and its theoretical evaluation (line).

1. Y. Kuru, U. Welzel, and E. J. Mittemeijer. "Coexistence of colossal stress and texture gradients in sputter deposited nanocrystalline ultra-thin metal films". Appl. Phys. Lett., **105**, 221902, 2014.
2. M. Stefenelli et al. "X-ray analysis of residual stress gradients in TiN coatings by a Laplace space approach and cross-sectional nanodiffraction: a critical comparison". J. Appl. Cryst., **46**, pp. 1378–1385, 2013.

Investigation of ALD initial stage and precursor kinetic by spectroscopic ellipsometry

I. Clemente[1,2], A. Miakonkikh[1,2]
1. Institute of Physics and Technology, Russian Academy of Sciences, Moscow, Russia.
2. Moscow Institute of Physics and Technology, Dolgoprudny, Russia.

Understanding of the processes occurring on the surface of substrate during atomic layer deposition is necessary to optimize existing and develop new ALD processes. The initial stages of film growth, nucleation delay and control are of interest in the task of developing area selective atomic layer deposition processes.
Spectroscopic ellipsometry (SE) [1] was applied as nondestructive optical technique capable of *in situ* measurements. The sample does not require special preparation for SE measurement. High sensitivities of SE to film thickness and optical properties of material allows to measure thickness with monolayer precision and to distinguish films of different materials. So that, ellipsometry makes it possible to observe in situ the film growth [2-4] and precursor desorption kinetic during ALD process which could be crucial for deposition of films on the sidewalls of high aspect trenches.
In present work initial stage of Al_2O_3, Hf_2O_3, TaN deposition processes were studied in plasma enhanced and thermal ALD process with metalloorganic precursors TMA, TEMAH, TBTDET dosed to the reactor chamber by fast valves from heated vessels.
Films were deposited in FlexAl ALD tool (Oxford instruments plasma technology, UK). SE measurements were carried out in 245–998 nm wavelength range at angle of incidence of 71° by M2000X spectral ellipsometer (Woollam Co., USA) with temporal resolution of 1 s. Although optical constants of monolayer could not be derived in the same measurements, the optical parameters of underlying layer were used, giving “apparent thickness” of monolayer of adsorbed precursor. Using the temperature dependence of Silicon optical constants the temperature of sample could be estimated. The desorption of TMA, TEMAH and TBTDET from film surface were investigated (Fig. 1). Desorption rate and its dependence on wafer temperature in 100–400 °C range were estimated.

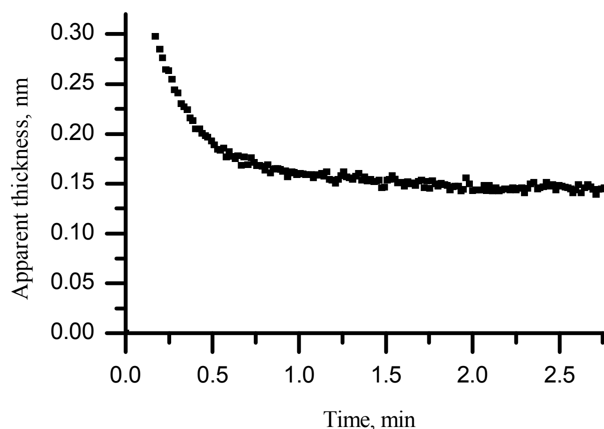

Figure 1. TEMAH desorption at 200 °C.

The reported study was carried out under Program of FASO of Russia and was partially supported by RFBR, research project # 18-37-00354.

1. Fujiwara H. *Spectroscopic Ellipsometry: Principles and Applications*. John Wiley & Sons, Chichester, England; Hoboken, NJ, 2007.
2. Clemente I.E., Miakonkikh A.V. "Application of spectral ellipsometry to in situ diagnostics of atomic layer deposition of dielectrics on Silicon and AlGaN", Proc. of SPIE, **10224**, pp. 1022425-1-7, 2016
3. Langereis E. et al. "In situ spectroscopic ellipsometry as a versatile tool for studying atomic layer deposition", Journal of Physics D: Applied Physics, **42**, pp. 73001-1-19, 2009.
4. Muneshwar T., Cadien K. "Probing initial-stages of ALD growth with dynamic in situ spectroscopic ellipsometry". Applied Surface Science, **328**, pp. 344–348, 2015.

Optical emission spectrum of BF_3 plasma: Identification of lines and bands belonging to boron-contained species

V.P. Kudrya
Institute of Physics and Technology (RAS), Moscow, Russia;
E-mail address: kvp@ftian.ru

It is known only small number of articles in which optical emission spectra of BF_3- or BF_3/Ar-plasma are given and analyzed. They are Refs. 1 and 2 (240-800 nm), Ref. 3 (200-900 nm), and Ref. 4 (300-855 nm). If the B- and B^+-lines are known well enough, then this cannot be said about the electron-vibrational bands of the BF radical. The aim of the study is to analyze the B and B^+ emission lines and to identify the BF emission bands in BF_3-plasma optical spectrum from [4]. The emission lines are fitted by Gaussian functions whose parameters are searched by the least square method. In addition to the strong line 345.1 nm (B^+), a weak line 563.31 nm (B) observed in BCl_3/Ar plasma [5] was extracted. Identification of the BF electron-vibrational bands observed in [1, 4] was carried out taken into account the BF Franck-Condon factors calculated in [6]. No other boron-contained species are observed in the emission spectra [1-4].

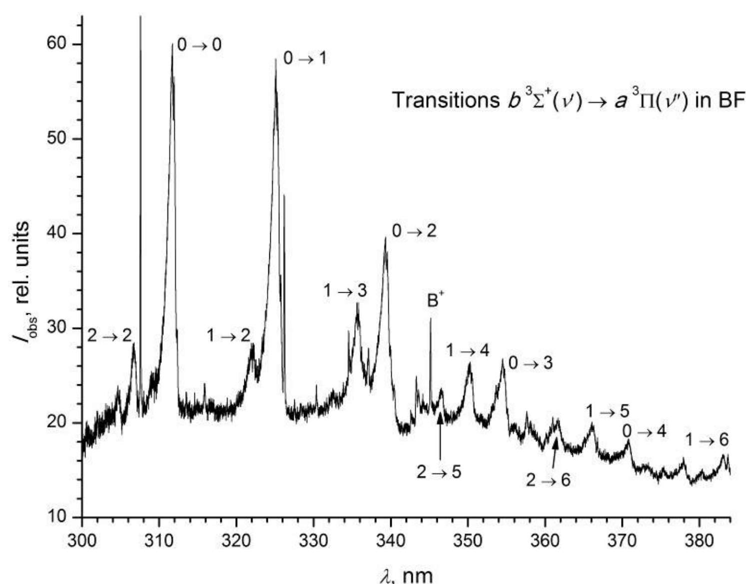

Figure. The BF_3 plasma spectral region published in [4] with the BF band identification.

1. Stejic G., Graf M.A. "Monitoring of plasma constituents using optical emission spectroscopy". European Patent Application EP 0 942 453 A2 (1999).
2. Graf M.A., Benveniste V. "Real-Time Monitoring of Ion Source Plasma Using Optical Emission Spectroscopy". Proceedings of the 12th International Conference on Ion Implantation Technology, Vol. 1, pp. 304-307 (1999).
3. Hays D.C. et al. "Comparison of F_2-Based Gases for High-Rate Dry Etching of Si". J. Electrochem. Soc., **146**, pp. 3812-3816 (1999).
4. Rudenko K. et al. "Ultra Shallow p^+-n Junctions in Si Produced by Plasma Immersion Ion Implantation". Proceedings of SPIE, 2005, V. 6260 "Micro- and Nanoelectronics 2005", P. 626003.
5. Pierson J.F. et al. "Kinetics of boron atoms in Ar-BCl_3 flowing microwave discharges". Plasma Sources Sci. Technol., **7**, pp. 54-60 (1998).
6. Pathak A.N., Maheshwari R.C. "Franck-Condon Factors & r-Centroids for ($b\ ^3\Sigma^+ \rightarrow a\ ^3\Pi$) System of Boron Monofluoride Molecule". Indian J. Pure and Appl. Phys., **5**, pp. 138-139 (1967).

Experimental study of a broadband vacuum photosensor with tunnel emission of a metal nanoscale blade

D.A. Zimnyakov[1,2], N.P. Aban'shin[1], G.G. Akchurin[1],
Yu.A. Avetisyan[1], A.P. Loginov[3], S.A. Yuvchenko[1,2], A.N. Yakunin[1]
1. Institute of Precision Mechanics and Control, Saratov, Russia, anyakunin@mail.ru
2. Yury Gagarin State Technical University of Saratov, Saratov, Russia, zimnykov@mail.ru
3. Volga-Svet Co. Ltd, Saratov, Russia, aploginov@gmail.com

In this work, we describe the technology and design of planar multilayer structure. It is used as a sensitive element of the vacuum photosensor shown in Fig. 1. Metal and dielectric layers are of nanoscale thickness. It is shown that the use of a thin molybdenum blade in the structure ensures the localization of the electrostatic field [1] and increases the photosensitivity of the vacuum sensor. Submicron interelectrode gaps provide a short transit time of the electron beam caused by the action of a light pulse. The ballistic transport of electrons in a vacuum is characterized by high speed.

Figure 1. The vacuum device with the nanostructure under study.

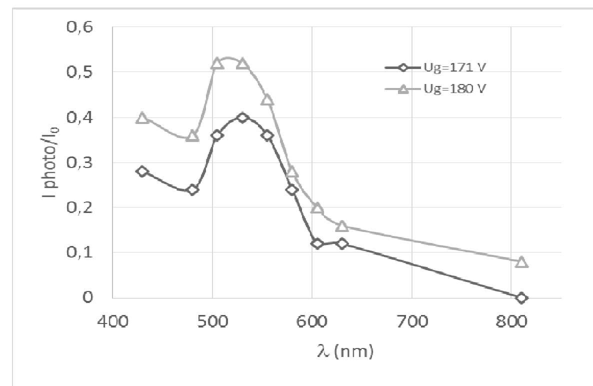

Figure 2. Normalized photocurrent, depending on the wavelength of light of equal pulse energy.

The red threshold of the classical photoelectric effect for molybdenum is slightly above λ=300 nm. However, we observe in Fig. 2 tunnel photocurrent in a wide range of wavelengths beyond the indicated limit. The localization of the electrostatic field arises when a gate potential U_g is applied, and the deformation of the potential barrier on the Mo surface occurs. Analysis of curves of spectral photosensitivity indicates an increase in the level of response by increasing U_g. The range of wavelengths with non-zero photosensitivity progresses to the IR region (compare curves U_g=171 V and U_g=180 V in Fig. 2). This trend is broadly consistent with the theoretical model [2]. The features of the mechanism of tunneling from molybdenum into vacuum under strong-field conditions are discussed. The estimated time of flight of electrons is not more than 10 ps. The achieved results make the photosensor based on nanoscale molybdenum blade promising in the development of ultrafast vacuum micro- and nanoelectronic devices.

The research was supported by the Russian Scientific Foundation, project No. 16-19-10455.

1. N.P. Aban'shin, Y.A. Avetisyan, G.G. Akchurin, A.P. Loginov, S.P. Morev, D.S. Mosiyash, A.N. Yakunin. "A Planar Diamond-Like Carbon Nanostructure for a Low-Voltage Field Emission Cathode with a Developed Surface". Tech. Phys. Lett., **42**, pp. 509–512, 2016.
2. G.G. Akchurin, N.P. Aban'shin, Yu.A. Avetisyan, G.G. Akchurin, (Jr), V.I. Kochubey, A.N. Yakunin. "Investigation of the spectral characteristics of a tunnel photodiode based on DLC nanofilm". Proc. of SPIE. **10716**, p. 1I (8 pp.), 2018.

Vacuum photoemission diode and triode based on ultraviolet detector

E. Il'ichev[1], V. Khaustov[1], A. Kuleshov[1], R. Nabiev[1], G. Petrukhin[1,2], E. Teverovskaya[1], G. Rychkov[1]
1. National Research University of Electronic Technology, Zelenograd-Moscow, Russia, start_94@mail.ru
2. LLC "CNEL Devices", Zelenograd-Moscow, Russia, cneldevices@gmail.com

Detectors of vacuum ultraviolet (VUV) are in great demand in medicine, microelectronics, biophysics and other fields of science and technology [1, 2]. A major drawback of VUV detectors is their sensitivity to solar radiation and especially to its ultraviolet component. Diamond detectors attract the attention of electronic equipment developers due to its solar radiation "blindness". A number of discrete solid-state VUV detectors were obtained on the natural and artificial diamond. However in solid-state detectors the ultimate sensitivity is limited by dark currents which are not less than 10^{-12} A/cm^2. Such current values are obtained on discrete detectors formed on single-crystal diamond films. Solid-state detectors can have a large external quantum efficiency EQE = 10^3 - 10^4 with a low performance (due to the persistent photocurrent) and low sensitivity. Therefore the most sensitive detectors are photoemission detectors with a diamond film as a photocathode. To exit on the other side of the film the photoelectrons produced on the film's surface by the UV radiation must pass through the entire film. It requires a strong electric field which would ensure the photoelectrons time-of-flight through the film less than the recombination time. There must be used single-crystal film with thickness does not exceed 3 - 5 μm which is practically impossible.

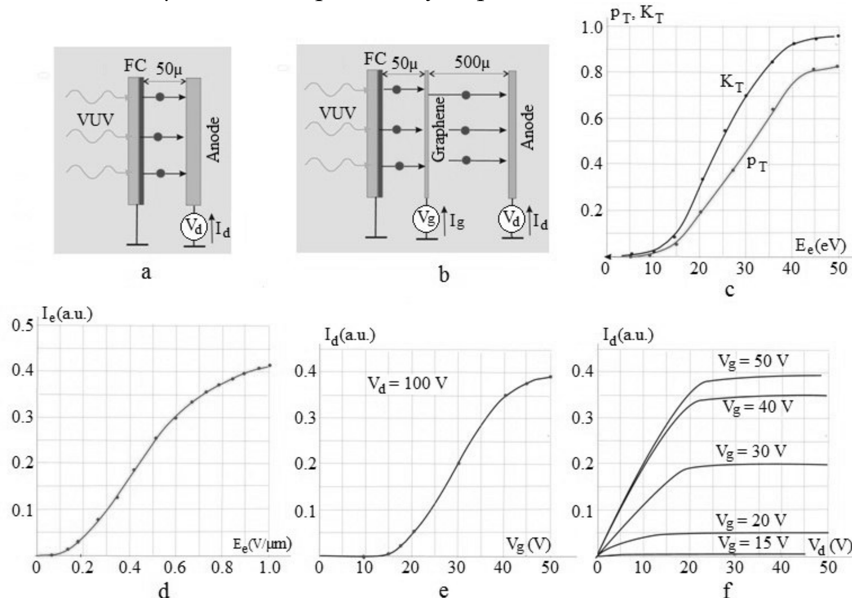

Fig. 1.

The problem can be solved if a thin layer of diamond (~ 1 - 2 μm thick) is formed on the substrate transparent for VUV. We used sapphire Al_2O_3 substrate for this case. Deuterium DDS-30 lamp was used as a VUV source which provided radiation in the range 180 - 225 nm. The ideal diamond has a negative electron affinity so the electron under the light quanta affection must leave into vacuum. However a real diamond has a potential barrier of height ~ 0.5 eV which prevents the electron from entering the vacuum. A weak field near the surface of the diamond film will effectively control the transparency of this barrier. Fig. 1a shows the scheme of the experimental setup and Fig. 1d the results measured. A field-emission diode is practically obtained. It can be transformed into the field emission triode (Fig. 1b) with electron-transparent graphene used as a control grid. Graphene transparency on electron energy presented in Fig. 1c. The dependence of the anode current on the graphene grid voltage is shown in Fig. 1e. Anode currents on the anode voltage are shown in Fig. 1f. There can be seen a pentode character. Electronic circuits based on this emission triode (memory cells, generators, amplifiers, etc.) with a high radiation resistance might be produced.

1. I. Artyukov et al. "Detectors of ultraviolet radiation". Photonics, **5**, pp. 26-33, 2008.
2. M.P. Ulmer et al. "Future detectors for space applications". Proc. SPIE, **6189**, p. 61890, 2006.

Theory and numerical modeling of nanoresonators, discrete waveguides, and modulators of planar radio-photonic assemblies

M. Barabanenkov[1,2], A. Italyantsev[1], M. Makarov[1], A. Sapegin[2,3], R. Minnullin[3]

1. Molecular Electronics Research Institute, Zelenograd, Moscow, Russia

2. Institute of Microelectronics Technology, Russian Academy of Sciences, 142432 Chernogolovka, Moscow Region, IMT RAS, barab@iptm.ru

3. Moscow Institute of Physics and Technology, Dolgoprudny, 141700, Moscow Region, Russia

Among the most remarkable units of planar integrated radio-photonic assemblies are conventional strip like waveguides on the optical buffer layer, their modern discrete counterparts composed of a linear chain of nanoparticles, discrete optical nanoresonators composed of a few nanoparticles or even a single nanoparticle. The conventional waveguides can be loaded as with diffraction gratings for their optical coupling to external electromagnetic (EM) radiation as with a modulator for guiding mode. Calculated EM properties of the above mentioned units are presented in this report.

We provide calculations on the basis of general system of equations formulated in [1] for self-consistent currents excited inside dielectric and conducting particles by an incident EM wave field derived from the rigorous approach of quasi–separable T-scattering operator to the problems of multiple scattering of EM waves by ensembles of dielectric and conducting nonmagnetic particles. Physically, the T-scattering operator is directly related to electric currents excited in the particles by an incident EM wave. First, frequency dependences of the eigenmodes, their widths, Q-factor of discrete resonators consisting of a few spherical or cylindrical nanoparticles with their different mutual arrangement are calculated on the basis of complete analytic solution for the eigenmode and eigenvalue problem for a chain of small particles under transverse polarization and electric dipole coupling. Analytic formulas are derived for fundamental and overtone modes in a circular chain, i.e. in a few particles cluster. Second, we demonstrated that the equations for self-consistent currents excited in the particles together with collective extinction factor for particle chains are very fruitful for seeking narrow transparency band with relative width of 10^{-6}- 10^{-5} in the spectra of free standing long particle chains, with only first particle of the chain being irradiated by incident narrow EM wave beam. In particular, we revealed 200 MHz transparency band in the visible frequency range in the spectra of straight chain of closely spaced Au nanospheres with radius of 76 nm with the length of a few centimeters and investigated frequency filtering properties of a finite linear chain of Au nanoparticles in the visible wavelength range. At the same time we established that there is no long-range EM energy transfer along linear chain of Si particles. We give the explanation of this dissimilarity in terms of the resonant condition for the particle coupling parameter and dielectric permittivity frequency dispersion. Third, we analyzed Mach Zehnder phase modulator and an intensity modulator with a Bragg mirror on the basis of numerical simulations. The principle of operation of these devices is based on the plasma dispersion effect which allows varying the refractive index of the waveguide. Both devices are assumed to be integrated at Silicon-On-Insulator (SOI) structure and p-i-n diode with the undoped region as a waveguide. The intensity modulator with a Bragg mirror shows a higher frequency near 0.6 GHz with the same doping parameters and dimensions. It should be noted, that our research takes place at voltages less than unity volt according to the limitation of the integrated circuits maximum voltage. Fourth, we numerically investigated resonant effects in lamella diffraction gratings incorporated into Si strip line waveguides of SOI structures on the basis of the Riccati equations [3].

1. Yu.N. Barabanenkov and M.Yu. Barabanenkov, “Quasi-separable T-scattering operator approach to local field direct calculations in multiple scattering problems”. J. Radioelectronics, Is.4, 2013.
2. Yu.N. Barabanenkov, M.Yu. Barabanenkov, “Radiation losses and dark mode at light guiding by a liner chain of nanoparticles”. JOSA A, **34**, pp.321 – 330, 2017.
3. Yu.N. Barabanenkov, V.L. Kouznetsov, M.Yu. Barabanenkov, “Transfer relations for electromagnetic wave scattering from periodic dielectric one-dimensional interface”, Electromagnetic waves, v. 24, Progress in Electromagnetic Research, ed. J.A. Kong (EMW Publishing, Cambridge, Massachusetts USA) 1999, pp. 39-75.

Quasi-Hydrodynamic Numerical Model of High-Speed On-chip Photodetectors for Optical Interconnections

I. Pisarenko, E. Ryndin, B. Konoplev
Southern Federal University, Institute of Nanotechnology, Electronics and Electronic Equipment Engineering, Taganrog, Russia, ivan123tgn@yandex.ru, earyndin@sfedu.ru, kbg@sfedu.ru

The high-speed on-chip $A^{III}B^{V}$ photodetectors designed for optical interconnecting of integrated circuit elements are considered [1]. To estimate their performance, we propose the quasi-hydrodynamic model, finite difference numerical simulation technique and applied software in the GNU Octave program. The model is based on the following formulation of the semiclassical quasi-hydrodynamic equations for semiconductors [2]:

$$\frac{\partial n}{\partial t} = \frac{1}{q} \cdot \nabla \overrightarrow{j_n} + G - R; \tag{1}$$

$$\frac{\partial p}{\partial t} = -\frac{1}{q} \cdot \nabla \overrightarrow{j_p} + G - R; \tag{2}$$

$$\overrightarrow{j_n} = -q\mu_n n \nabla(\varphi + V_n) + \mu_n k \nabla(n T_n); \tag{3}$$

$$\overrightarrow{j_p} = -q\mu_p p \nabla(\varphi - V_p) - \mu_p k \nabla(p T_p); \tag{4}$$

$$\nabla(\varepsilon \cdot \nabla\varphi) = -\frac{q}{\varepsilon_0}(p - n + N_D - N_A); \tag{5}$$

$$\frac{\partial W_n}{\partial t} = -q\upsilon_n E_n - \frac{W_n - W_{n0}}{\tau_{wn}}; \tag{6}$$

$$\frac{\partial W_p}{\partial t} = q\upsilon_p E_p - \frac{W_p - W_{p0}}{\tau_{wp}}; \tag{7}$$

where n, p are the electron and hole densities; t is time; $\overrightarrow{j_n}$, $\overrightarrow{j_p}$ are the electron and hole components of current density; q is the elementary charge; G, R are the generation and recombination rates of electron-hole pairs; μ_n, μ_p are the electron and hole mobilities; φ is the electrostatic potential; V_{n}, V_{p} are the heterostructure potentials in conduction and valence bands; k is the Boltzmann constant; T_n, T_p are the electron and hole temperatures; ε is the dielectric permittivity of semiconductor; ε_0 is the permittivity of vacuum; N_D, N_A are the concentrations of the ionized donors and acceptors; W_n, W_p are the mean energies of electrons and holes; υ_n, υ_p are the average velocities of electrons and holes; E_n, E_p are the gradients of electron and hole imrefs; W_{n0}, W_{p0} are the mean energies of electrons and holes at the equilibrium state; τ_{wn}, τ_{wp} are the energy relaxation times for electrons and holes. We performed one-dimensional quasi-hydrodynamic numerical simulation of conventional p-i-n photodetectors and uni-travelling-carrier photodiodes. According to the simulation results, the effect of charge carrier heating in AIIIBV semiconductors leads to the significant change of photodetector performance.

The research is supported by the funds of “The Development Program of Southern Federal University up to 2021” (Project VnGr-07/2017-10).

1. I.V. Pisarenko and E.A. Ryndin. "Numerical Drift-Diffusion Simulation of GaAs p-i-n and Schottky-Barrier Photodiodes for High-Speed $A^{III}B^{V}$ On-Chip Optical Interconnections". Electronics, **5**, 52, 2016.
2. A. Jüngel. *Quasi-hydrodynamic Semiconductor Equations.* Springer Basel AG, 2001.

Study of complex reflectivity of ultrathin metal films at frequencies 9-11 GHz

V. Vdovin[1], V. Andreev[2], S. Pronin[2], I. Khorin[3]
1. Kotel'nikov Institute of Radio Engineering and Electronics of RAS, Moscow, 125009 Russia.
2. Moscow State University, Moscow, 119991 Russia.
3. Institute of Physics and Technology of RAS (IPT RAS), Moscow, 117218 Russia, ivan-khorin@mail.ru

In [1], the optical coefficients of metallic nanometer-thick films were studied at a fixed frequency of 10 GHz. It was shown that the measured transmission and reflection coefficients differ significantly from the theoretical values for films 1-5 nm thick. In this paper, the amplitude and phase dependences of the reflection coefficient of nanometer films in the frequency range 9-11 GHz are studied.
Copper and platinum films with thicknesses from 0.5 nm to 30 nm, synthesized on quartz substrates 22.9 mm x 9.9 mm in size and 2 mm thick, are studied. The metal films were deposited on substrates in vacuum by magnetron sputtering at room temperature. Cu films were formed in a Leybold Z-550 deposition system, and Pt films were formed in a Balzers SCD 050 deposition system. The thickness of the films was determined by the deposition time.
Measurements of the amplitude and phase of the reflection coefficient were performed in the waveguide using a matched load, which made it possible to eliminate the effect of the re-reflected waves [2]. Radiation and registration of the reflected wave was carried out by the vector analyzer of electrical circuits R & S ® ZVA 24, operating in the range up to 24 GHz.
It was shown that at a copper film thickness of 3-5 nm, the phase of the reflected wave was changed abruptly. The measured phase jumps were about 20 degrees. For platinum films, such jumps were not detected. Analysis of the morphological structure of the films by electron microscopy showed that at thicknesses of 3-5 nm, a completely conducting copper surface was formed. Platinum films retained the islet structure to thicknesses of the order of 20 nm.
The reported study was funded by RFBR according to the research project N° 16-07-01246 and 16–29-09581.

1. I. Khorin, N. Orlikovsky, A. Rogozhin, A. Tatarintsev, S. Pronin, V. Andreev, and V. Vdovin. "Experimental study of optical coefficients of nanometer-thick copper and gold films in microwave frequency range". Proceedings of SPIE - The International Society for Optical Engineering. 2016. Vol. 10224. P. 1022407–1–1022407–7.
2. V.G. Andreev, V.A. Vdovin, S.M. Pronin, I.A. Khorin. "Measurement of the optical coefficients of nanometer metal films at a frequency of 10 GHz". Journal of radio electronics. [online journal]. 2017. №11. (In Russian).

New families of quantum hash functions

F.M. Ablayev, M.F. Ablayev
Kazan Federal University, Kazan, Russia, fablyaev@gmail.com

The formalization of quantum hashing was recently defined and is investigated in our research group. Informally speaking quantum hash function is a function that maps numbers or (equivalently) sequences of characters to quantum states. Such mapping should be collision robust and should be one-way. These two properties provide cryptographically reliable quantum function. We call such function quantum hash function. During last years we developed a construction of quantum hash functions based on a combinatorial construction known as epsilon-biased sets. We proved an optimality of such quantum hash function in respect to the computational time and number of qubits needed for such function realization.

In this talk we present families of quantum hash functions. Such quantum hash functions are combination (superposition's) of the epsilon-biased function and functions based on classical universal-hash families. In particular one can take classical universal-hash families based on linear error-correcting codes (for example Reed-Solomon codes). We prove that such constructions are optimal.

Hitting time for quantum walks of identical particles

A.A. Melnikov[1], L.E. Fedichkin[1,2,3]
1. Institute of Physics and Technology, Russian Academy of Sciences, Moscow, Russia, melnikov@phystech.edu
2. NIX, Moscow, Russia, leonid@phystech.edu
3. Moscow Institute of Physics and Technology, Dolgoprudny, Moscow Region, Russia

Quantum particles are known to be faster than classical when they propagate stochastically on certain graphs. An average time needed for a particle to reach a target vertex, the hitting time, can be exponentially less for quantum walks than for classical random walks. For some graphs the speed-up is polynomial, e.g., for lines and cycles, as also shown in Ref. [1]. Here we present our results on hitting times for quantum walks of identical particles, and relate the results to our previous findings on the usage of identical particles in quantum information theory.

Quantum walks of identical interacting particles, such as electrons with Coulomb repulsion, can be used to develop new tools for quantum information theory. These tools include, e.g., new algorithms for quantum computation and new quantum-enhanced machine learning methods. We consider a quantum system of two indistinguishable particles in a cycle graph. The quantum walk dynamics of this system can lead to entanglement given some physical interaction between particles, e.g., mutual repulsion. Here we show how one can define qudits by using the freedom of dividing the graph into two subgraphs [2]. The studied quantum walk dynamics of two indistinguishable particles can hence be used for the preparation of a two-qudit entangled state of two distinguishable subsystems [3]. Moreover, using different dimensions of the cycle graph one can expect a diverse structure of two-particle entanglement of high dimensions [4]. These highly entangled states of qudits can be obtained by only using the free quantum evolution of identical particles, without relying on any additional manipulations with particles.

1. D. Solenov and L. Fedichkin. "Continuous-time quantum walks on a cycle graph". Phys. Rev. A, **73**, 012313, 2006.
2. A.A. Melnikov and L.E. Fedichkin. "Quantum walks of interacting fermions on a cycle graph". Sci. Rep., **6**, 34226, 2016.
3. A.A. Melnikov and L.E. Fedichkin. "Fermionic entanglement via quantum walks in quantum dots". AIP Conference Proceedings **1936**, 020025, 2018.
4. A.A. Melnikov and L.E. Fedichkin. "Continuous-time quantum walk of two interacting fermions on a cycle graph". Proceedings of SPIE **10224**, 102242L, 2016.

Exponential bound on heating rate in periodically driven spin systems

V.E. Zobov[1], M.M. Kucherov[2]
1. Kirensky Institute of Physics, Federal Research Center KSC SB RAS, Krasnoyarsk, 660036 Russia;
e-mail: rsa@iph.krasn.ru.
2. Institute of Space and Information Technologies, Siberian Federal University, Krasnoyarsk, 660074 Russia

According to R. Feynman, a promising way for studying complex quantum systems is to model them on other quantum systems. The studies of topological states and discrete time crystals are modern illustrations. To obtain the effective Hamiltonian for modeling, powerful periodic actions are applied to the system such as sequences of RF or microwave pulses, for example, in the case of spin systems. The necessary evolution of the system under the influence of the average Hamiltonian is accompanied by its parasitic heating by higher harmonics [1, 2]. The duration of the modeling stage and, therefore, the effectiveness of the method depends on the rate of heating. Qualitative estimates for the heating rate bound were found in [2, 3], which showed its exponential slowing with increasing frequency of oscillations. In the proposed report, we indicated a rigorous bound for the exponent. The calculations are performed in the approximation of a self-consistent fluctuating field (SFF). Its basis was founded in the 50s by Anderson and Kubo, who suggested for the solids, that fluctuating local field at the spin is represented by the Gaussian random process due to the large number of independent contributions to the field from the neighboring spins. Later, it was proposed to express the correlation functions of the Gaussian field in a self-consistent manner through the time autocorrelation functions (ACF) of an individual spin. Because of non-commutative property of spin rotations about different instantaneous field directions, a very complicated equation is obtained for ACF. A study of the equation [4] showed the existence of ACF singular points on the axis of imaginary time, the coordinate of which τ_0 determines the desired exponent of high-frequency asymptotics $g_x(\omega) \approx |\omega| \exp(-\tau_0|\omega|)$. We have shown that the lower bound τ_{c0} for this exponent is given by the solution of the equation obtained for ACF in the cumulant approximation

$$D(t) = \exp\{-B^2 \int_0^t \int_0^{t'} D(t'')dt'dt'' - W^2 t^2 / 2\},$$

where W^2 is variance of the Gaussian inhomogeneous field and B^2 is the mean square of local fields due to the spin-spin interactions. The coordinate τ_{c0} of the singular point has been calculated by us through the radius of convergence of the series in powers of time for ACF. Its dependence on parameters is well approximated by the function

$$M_2 \tau_{c0}^2 = 2{,}35 \ln\{2M_2 / B^2\} + 3{,}05,$$

where $M_2 = B^2 + W^2$. The SFF-approximation applied above does not consider the correlations between the contributions to the field from different environmental spins in real spin lattices. The correlation effects weaken the effect of the fields and lead to an increase in τ_0. Therefore, the Fourier transform of the ACF of the cumulant approximation: $g_{cx}(\omega) \cong (2/B^2)|\omega| \exp(-\tau_{c0}|\omega|)$, multiplied by the square of the amplitude of the corresponding harmonic of the periodic action, is the rigorous upper bound on the heating rate in real spin systems.

1. B.N. Provotorov, E.B. Fel'dman. “Thermodynamic effects in multi-pulse NMR experiments”. Sov. Phys. JETP, **52,** pp. 1116-1127, 1980.
2. W.W. Ho, I. Protopopov, and D.A. Abanin. “Bounds on energy absorption, and prethermalization in quantum systems with long-range interactions”. Phys. Rev. Lett., **120**, 200601, 2018.
3. V.E. Zobov, M.M. Kucherov. ”On the effect of an inhomogeneous magnetic field on high-frequency asymptotic behaviors of correlation functions of spin lattices”. JETP Letters, **107**, pp. 553–557, 2018.
3. V.E. Zobov. “Autocorrelation functions of an anisotropic Heisenberg paramagnet in the self-consistent fluctuating field approximation”. Sov. J. Theor. Math. Phys., **84**, pp. 751-759, 1990.

On the fidelity of quantum gates under T1 and T2 relaxation

A.Yu. Chernyavskiy
Institute of Physics and Technology, Russian Academy of Sciences, Russia

Decoherence is one the main obstacles on the way of quantum computer realization, that is why the analysis of its impact on quantum gates and circuits is very important. It is convenient to use the mathematical formalism of quantum operations for such analysis: the fidelity of Choi-Jamiolkowski states may be taken as the accuracy of noisy gates. We research the behavior of accuracy of different gates under T1 and T2 relaxation. The main result of the computations is the very small dependence of the accuracy on the chosen gate. As an extension of this result we present the approximation of the arbitrary gate fidelity and numerically analyze the best and worst cases of the fidelity decreasing.

Quantum dynamics induced by selective measurements

S.N. Filippov[1,2]
1. Institute of Physics and Technology of the Russian Academy of Sciences, Moscow, Russia.
2. Moscow Institute of Physics and Technology, Dolgoprudny, Moscow Region, Russia.
E-mail: sergey.filippov@phystech.edu

Repeated projective measurements on a quantum system in the limit of infinitesimal duration τ between the measurements naturally lead to freezing of system — the famous Zeno effect [1]. If the rank of projector P is greater than 1, then quantum dynamics in the corresponding subspace is effectively decoupled from other degrees of freedom, which results in the unitary Zeno subspace dynamics [2]. Suppose γ is the characteristic frequency of system Hamiltonian H, then the unitary dynamics in the measurement subspace takes place in the limit $\gamma\tau \to 0$, with PHP being the effective Hamiltonian. The first goal of this report is to consider higher order contributions of small parameter $\gamma\tau$ to the system evolution. We consider so-called stroboscopic limit $\gamma\tau \to 0$, $\gamma^2\tau \to \Omega$ and find the deviation from unitary evolution with characteristic frequency Ω [3]. The considered scenario is not exceptional and occurs, e.g., when the system in interest interacts with the auxiliary one, and the latter is repeatedly measured with rank-1 projector $|\varphi\rangle\langle\varphi|$. Auxiliary system is effectively frozen and remains in the state $|\varphi\rangle\langle\varphi|$, whereas the system in interest evolves non-trivially. If $H = \gamma \sum_j A_j \otimes B_j$ is the system-ancilla Hamiltonian, then the normalized dynamics of system density operator in the stroboscopic limit reads

$$\frac{\partial \rho_{\mathrm{sys}}}{\partial t} = -i[H_1, \rho_{\mathrm{sys}}] - \{H_2, \rho_{\mathrm{sys}}\} + 2\mathrm{tr}(H_2 \rho_{\mathrm{sys}})\rho_{\mathrm{sys}}, \tag{1}$$

$$H_1 = \gamma \sum_j \langle\varphi|B_j|\varphi\rangle A_j, \qquad H_2 = \frac{\Omega}{2}\sum_{j,k}\left(\langle\varphi|B_j B_k|\varphi\rangle - \langle\varphi|B_j|\varphi\rangle\langle\varphi|B_k|\varphi\rangle\right) A_j A_k. \tag{2}$$

Suppose the initial state $\rho_{\mathrm{sys}}(0)$ is pure, then the dynamics (1) preserves purity of the initial state and the evolution of the state vector $|\psi\rangle$ satisfies

$$i\frac{\partial|\psi\rangle}{\partial t} = (H_1 - iH_2)|\psi\rangle + i\langle\psi|H_2|\psi\rangle|\psi\rangle. \tag{3}$$

The obtained non-unitary dynamics can be used in practice, e.g., it can significantly affect lowly populated energy level in such a way that the increased population can be effectively measured. The developed theory can be also modified to cover the case of nonselective measurements [3, 4].

The second goal of the report is to present new results in tomography of quantum states via using the same measurement device repeatedly. In this case, possible evolutions of the system form a tree, with branches encoding measurement outcomes. Under certain circumstances, the sufficiently deep tree is able to provide enough information to reconstruct the quantum state.

The study is supported by the Russian Foundation for Basic Research under Project No. 16-37-60070 mol-a-dk.

1. B. Misra and E.C.G. Sudarshan. "The Zeno's paradox in quantum theory". J. Math. Phys., **18**, 756-763, 1977.
2. P. Facchi and S. Pascazio. "Quantum Zeno subspaces". Phys. Rev. Lett., **89**, 080401, 2002.
3. I.A. Luchnikov, S.N. Filippov. "Quantum evolution in the stroboscopic limit of repeated measurements". Phys. Rev. A, **95**, 022113, 2017.
4. S.N. Filippov. "Quantum dynamics intervened by repeated nonselective measurements". Int. J. Quantum Inform., **15**, 1740027, 2017.

Quantum tomography based on principles of completeness, adequacy and fidelity

Yu.I. Bogdanov[1,2,3], N.A. Bogdanova[1,2], B.I. Bantysh[1,2], D.V. Fastovets[1,2], V.F. Lukichev[1]

1. Institute of Physics and Technology, Russian Academy of Sciences, Russia

2. National Research University of Electronic Technology (MIET), Russia

3. National Research Nuclear University (MEPhI), Russia

In this report we present a general approach for estimating quantum circuits by means of measurements. We apply the developed general approach for estimating the quality of superconducting and optical quantum chips. Using the methods of quantum states and processes tomography developed in our previous works, we have defined the adequate models of the states and processes under consideration.

Our approach to tomography of quantum states and quantum operations is based on three principles: completeness, adequacy and fidelity. Completeness means that the quantum measurement protocol allows us to reconstruct any quantum state and any density matrix. To test the completeness property, we introduce a special matrix, based on the operators of quantum measurements. Completeness is valid if and only if the considered measurement matrix is a matrix of full rank. Adequacy means consistency between the obtained experimental data and the developed quantum model. Usually we conduct a verification of adequacy through a chi-square test. Precision of quantum tomography can be defined by a parameter called fidelity. Fidelity shows how close the reconstructed state is to the ideal theoretical state. Our method based on purification procedure allows us to formulate a generalized statistical distribution for fidelity. This distribution is a natural generalization of the chi-squared distribution.

For the analysis of incomplete measurement protocols we introduced the concept of adjusted fidelity. The concept of adjusted fidelity gives us a way to estimate only those parameters of state, information about which is contained in the experimental data. In this case, we ignore the parameters, information about which is not contained in the measurement protocol at all. To find adjusted fidelity, we use the matrix of complete information for the purified state introduced in our works.

The results of this research are of practical value for the tasks of provision of quality and effectiveness of quantum information technologies.

Adaptive quantum tomography of high-dimensional bipartite systems

G.I. Struchalin, E.V. Kovlakov, S.S. Straupe, and S.P. Kulik
Faculty of Physics, M.V. Lomonosov Moscow State University and
Quantum Technologies Centre, M.V. Lomonosov Moscow State University, 119991, Moscow, Russia.

Adaptive measurements have recently been shown to significantly improve accuracy of quantum state and process tomography compared to conventional techniques. By definition in adaptive protocols future measurements depend on the data previously obtained. The measurements are chosen in an optimal way according to some criterion. Tomography of high-dimensional systems itself is a computationally involved problem, therefore adaptive criterion should be simple enough to allow fast measurement selection. On the other hand, measurement choice should result in high reconstruction accuracy of the true state. Moreover, an adaptive scheme should be flexible, i.e. it can be easily tailored to use only some subset of experimentally available measurements. A selected subset in high-dimensional multipartite tomography is factorized measurements, namely, local measurements of subsystems. We mainly focus on the simplest case of bipartite systems.

In our opinion there is lack of computationally fast protocols for high-dimensional tomography that utilize only factorized measurements. For example, Bayesian optimal experimental design is a versatile approach with high reconstruction accuracy, but it is computationally involved [1]. A prominent class of protocols includes measurements in the eigenbasis of the current estimate [2]. The problem is that the eigenbasis will almost certainly contain entangled vectors, and therefore these protocols require general type of measurements, which is a severe experimental limitation. There is no straightforward generalization of these protocols to include solely factorized measurements.

We propose a novel adaptive protocol [3], which is both computationally fast and relies only on factorized measurements, and still improves reconstruction accuracy. The protocol is especially advantageous for true states that can be treated as low-rank ones (this includes the important for applications case of pure states). The idea behind the protocol is to select measurements with nearly zero outcome probability, whenever it is possible. We provide arguments that such measurements, called orthogonal measurements, are necessary to qualitatively improve the estimation accuracy compared to non-adaptive protocols.

We investigate the performance of the proposed protocol in both numerical simulations and real experiments for the states with dimension up to 36. In experiments the true state is encoded in spatial degrees of freedom of photon pairs produced by a spontaneous parametric down conversion. We compare our protocol with random measurement strategy (experiment and simulations) and protocols based on measurements in the eigenbasis (simulations). We use a maximum likelihood estimation (MLE) for data processing, however, our protocol is independent of the choice of a statistical estimation procedure. We observe an improvement of reconstruction accuracy for our protocol, compared to the non-adaptive random measurements.

1. K.S. Kravtsov, S.S. Straupe, I.V. Radchenko, N.M.T. Houlsby, F. Huszar, and S.P. Kulik. "Experimental adaptive Bayesian tomography". Phys. Rev. A, **87**, 062122, 2013.
2. D.H. Mahler, L.A. Rozema, A. Darabi, C. Ferrie, R. Blume-Kohout, and A.M. Steinberg. "Adaptive Quantum State Tomography Improves Accuracy Quadratically". Phys. Rev. Lett., **111**, 183601, 2013.
3. G.I. Struchalin, E.V. Kovlakov, S.S. Straupe, and S.P. Kulik. "Adaptive quantum tomography of high-dimensional bipartite systems". arXiv:1804.05226 [quant-ph], 2018.

High-fidelity quantum tomography with imperfect measurements

B.I. Bantysh[1,2], D.V. Fastovets[1,2], Yu.I. Bogdanov[1,2,3]
1. Institute of Physics and Technology, Russian Academy of Sciences, Russia
2. National Research University of Electronic Technology (MIET), Russia
3. National Research Nuclear University (MEPhI), Russia

The quantum tomography is a very important tool for quality control of real quantum information technologies as it provides the complete description of quantum states and processes. This possibility plays a crucial role for the verification of quantum computers element base as well as for analysis of quantum algorithms subjected to decoherence.

However, in real physical experiments the measurement setup is not ideal which creates a challenge for performing a precise quantum tomography. The presence of measurement errors results in two significant problems. On the one hand, the estimation of a quantum state (process) becomes non-consistent which limits the achievable fidelity of quantum tomography. On the other hand, it introduces additional errors in the resulting quantum state that it does not contain.

The most efficient way to overcome these problems is to modify the state reconstruction procedure to consider measurement errors within the reconstruction model. However, to achieve this one should possess the complete information about the measurement imperfection. This information could be obtained by the thorough theoretical analysis of physical processes behind the measurements. If this can’t be done in a precise way this information could be also obtained from the direct tomography of the measurement setup.

The present work considers the analysis of possibilities to perform the tomography of measurement setup imperfections without having any information about the physical processes behind the measurements. Using the numerical analysis it will be shown that the result of this estimation could significantly increase the quality of quantum states and quantum processes tomography. The efficiency of the proposed approach will also be demonstrated experimentally using the IBM quantum process.

Precision guaranteed quantum process tomography

E. Kiktenko[1,2], D. Norkin[1,3], D. Kublikova[3], A. Karazeev[1,3], A. Fedorov[1]
1. Russian Quantum Center, Skolkovo, Moscow 143025, Russia
2. Steklov Mathematical Institute of Russian Academy of Sciences, Moscow 119991, Russia
3. Moscow Institute of Physics and Technology, Dolgoprudny, Moscow Region 141700, Russia

Quantum tomography appears to be one of the most important ingredients for efficient quantum information processing. In Ref. [1] a method for quantum state tomography was proposed, which gives a bound δ on a distance between reconstructed density matrix ρ^{rec} and true density matrix ρ for a given confidence level CL. Consequently, after the implementation of the tomography protocol one can be sure that the following relation holds:

$$\mathrm{Prob}(\|\rho^{\mathrm{rec}} - \rho\| < \delta) \geq \mathrm{CL}. \quad (1)$$

Here for distance measures $\|\cdot\|$, three types of measures, Hilbert-Schmidt distance, trace distance, and infidelity, have been considered.

In our contribution, we obtain more accurate estimations for δ using Gaussian approximations and extend this approach to quantum process tomography. We employ the Choi-Jamiolkowski channel-state duality [2] $\Phi[\cdot] \leftrightarrow \rho_{\Phi}$ in order to match a completely positive trace preserving map $\Phi[\cdot]$ to a positive semi-definite unit trace matrix ρ_{Φ}. We obtain a method for calculating a bound Δ on a Hilbert-Schmidt distance between reconstructed Choi-Jamiolkowski matrix $\rho_{\Phi}^{\mathrm{rec}}$ and true Choi-Jamiolkowski matrix ρ_{Φ} for given confidence level CL as follows:

$$\mathrm{Prob}(\|\rho_{\Phi}^{\mathrm{rec}} - \rho_{\Phi}\|_{\mathrm{HS}} < \Delta) \geq \mathrm{CL}. \quad (2)$$

We note that Δ depends on precision of reconstructing output states from input states.

This approach allows finding an optimal set of probe states $\{\rho_{\mathrm{in}}^{(j)}\}$ whose tomography after passing them through the channel $\Phi[\cdot]$ gives the best reconstructing accuracy. We employ the considered approach to quantum process tomography of the teleportation circuit implemented with the use of IBM quantum processor [3] based on superconducting qubits.

This work is supported by the RFBR.

1. T. Sugiyama, P.S. Turner, M. Murao, “Precision-guaranteed quantum tomography”. Phys. Rev. Lett. **111**, pp. 160406, 2013.
2. M. Jiang, Sh. Luo, and Sh. Fu, “Channel-state duality”. Phys. Rev. A **87**, pp. 022310, 2013.
3. https://quantumexperience.ng.bluemix.net

The manifestation of rising of the impurity density of states after the field stress in increasing of the effective electron mobility in the inversion channel at the silicon-oxide contact

G. Chucheva[1], E. Goldman[1], A. Nabiev[2], V. Naryshkina[1]
1. Fryazino branch of the Kotel'nikov Institute of Radioengineering and Electronics of Russian Academy of Sciences Moscow region, Fryazino, Russia, E-mail: gvc@ms.ire.rssi.ru
2. Azerbaijan State Pedagogical University, Baku, Azerbaijan, E-mail: asaf.fizik@mail.ru

The ionic polarization of insulating layers is an important tool for modifying of electronic properties of interfaces in metal-oxide-semiconductor (MOS) structures. Consequences of the polarization are not only shifts in threshold voltages of opening of inversion channels due to the accumulation of the built-in charge, but also deep changes of the band structure of conducting paths in connection with the formation of a high concentration of impurity localized states at the semiconductor-insulator interface. Earlier [1] it was found, that the ionic polarization of Si-MOS structures leads to an anomalously high (several times) increase of the effective electron mobility of μ in the inversion channel at the Si-SiO_2 interface. In this paper, an explanation of the nature of this phenomenon is given on the basis of an analysis of the large volume of experimental data on current-voltage (I-V) characteristics of a transistor in states after the polarization and the depolarization at different temperatures. The polarization of the oxide was carried out at the gate voltage V_g = 10 V and at the drain voltage V_d = 0.01 V for one hour at a temperature T = 420 K, the depolarization for the same T, but at V_g = -10 V. I-V measurements were carried out at $T \leq 200\,K$, since under room conditions in strong electric fields of the ion drift can change of the state of samples. At least $6 \cdot 10^{13}$ cm^{-2} of ions flows over in the oxide with a polarization. The transition from a depolarized to a polarized state is relatively weak compared to the flowed ion charge, shifts the threshold of channel opening ranges from 0.05 V for 200 K to 0.5 V for 100 K. This fact confirms the well-known fact about a high degree of the neutralization of ions at the silicon-oxide interface. Temperature dependences of $\mu(T)$ for the polarized and depolarized states are accompanied by an increase of the effective mobility, and that in the temperature interval of 100–200 K $\mu \propto T^{-0.7}$. The μ value passes through a maximum and then falls sharper, than a power law with a further decrease in temperature. This mobility behavior does not correspond to the conductivity of free electrons in the inversion channel along the silicon surface. The negative magnetoconductivity is observed: the μ value decreases with increasing of the magnetic induction from 1.07 to 4.28 T after both the polarization and after the depolarization by an average of 1.3 times. This fact indicates about the hopping nature of the conductivity in both the polarized and the depolarized states. Pepper group [2] was found, that concentrating relatively small concentrations of sodium ions at the Si-SiO_2 interface on the order of $3.7 \cdot 10^{11}$ cm^{-2} leads to the formation of the upper and lower impurity Hubbard bands. In our experiments, after the polarization at the Si-SiO_2 interface impurity centers turns out at least two orders of magnitude greater than in samples, studied in the paper of [2]. This means that impurity Hubbard bands are substantially broadened and overlapped both with each, other and with the conduction band of the inversion channel near the silicon surface. The density of states sharply increasing, as a result, of the polarization and, accordingly, the conductivity along delocalized states, ultimately explain the increase of μ.

The study was supported in part by the Russian Foundation for Basic Researches (projects 16-07-00666) and by the Programs of Basic Researches of the Presidium of the Russian Academy of Sciences: Nanostructures: Physics, Chemistry, Biology: Engineering Principles.

1. Yu.V. Gulyaev, A.G. Zhdan, and G.V. Chucheva. "Increase in the Electron Mobility in the Inversion Channel of a Si-MOS Transistor in the Case of Ion Polarization of the Gate Oxide". Semiconductors, **41**, pp. 357-360, 2007.
2. T. Ferrus, R. George, C.H.W. Barnes, N. Lumpkin, D.J. Paul, and M. Pepper. "Evidence for multiple impurity bands in sodium-doped silicon MOSFETs". Phys. Rev. B, **73**, Rapid Communication, pp. 041304 1-4, 2006.

Features of the field damage of ultra-thin insulating layers of the silicon oxide

G. Chucheva, E. Goldman, Yu. Gulyaev
Fryazino branch of the Kotel'nikov Institute of Radioengineering and Electronics of Russian Academy of Sciences
Moscow region, Fryazino, Russia, E-mail: gvc@ms.ire.rssi.ru

Results of experimental studies of the stability of metal-oxide-semiconductor (MOS) structures with an oxide thickness of less than 40 Å to the effect of strong, but before breakdown electric fields are analyzed. Experiments were carried out on n-Si-MOS structures with an Al-n^+Si:P field electrode (donor concentration of ~10^{20} cm^{-3}, an area of S = $1.6 \cdot 10^{-3}$ cm^2), isolated from a silicon substrate (free electron concentration of $2 \cdot 10^{15}$ cm^{-3}) by a layer of a pyrogenic oxide with an optical thickness h = 40 Å. The field effect was carried out in the following way: samples were kept in room conditions for up to 30 min at a gate voltage V_g = 3.1 V (the accumulation of the substrate), or up to 120 min at V_g = -3.8 V (the depletion of the substrate). Different holding times and absolute values of V_g make it possible to achieve almost identical in the value and the duration of the action of fields in the oxide and, thereby, to compare of results of stress with different polarities of the gate voltage. In the Figure is a general view of graphs of dynamic current-voltage (DCVC) and ideal C-V characteristics. The current of I in the gate-substrate circuit was registered.

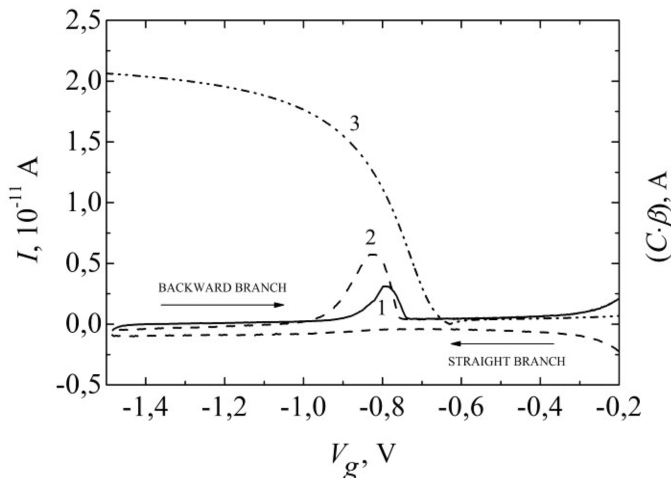

Figure. General view of the dynamic current-voltage characteristics of Si-MOS structures: 1 – before stress, 2 – after field stress, 3 – equilibrium C-V-characteristic of an ideal Si-MOS structure with the same parameters as for experimental samples. The value of V_g varied with time t at a constant rate $\left|dV_g/dt\right| = \beta = 16\,\mathrm{mV/s}$: on the direct characteristic of the state of the flat band to V_g = -1.5 V, and on the reverse – from V_g = -1.5 V to the initial value. The value of the capacitance C was multiplied by the field sweep rate β.

The process of the accumulation of minority charge carriers ends with a "stepped" decrease in the rate of generation of electron-hole pairs and a sharp transition to equilibrium. After reaching the equilibrium in the region of the strong or weak inversion, the inverse branch of DCVC goes into the quasi-equilibrium curve of the C-V characteristic of the Si-MOS structure falling off with the voltage. Thus, the graph of DCVC has a sharp maximum, which practically lies on the ideal C-V characteristic of the sample. The increase of the number of generation centers of minority charge carriers in Si-MOS structures was determined from the shift of dynamic current-voltage characteristics after the field stress. The direct information about the band bending in a semiconductor, the change in the charge of boundary states and concentration of minority charge carriers at the silicon-oxide interface was obtained from the form of high-frequency capacitive characteristics of MOS-structures. It turned out, that objects with an ultra-small thickness of SiO_2 are much more "submissive" to the field stress – they are more easily damaged by external influences, but they are much more quickly restored to their original state at the room temperature. In the process of aging structures in a strong electric field, additional localized electronic boundary states with a concentration exceeding 10^{13} cm^{-2} at the silicon-oxide contact are formed. Recharging of newly formed centers with increasing field voltage certainly ensures the accumulation of an excess charge at the silicon-oxide interface, sharply increasing field in the insulating layer. This phenomenon should have a decisive influence on the change in tunnel current-voltage characteristics of Si-MOS structures after the field stress.

The study was supported in part by the Russian Foundation for Basic Researches (projects 16-07-00666) and by the Programs of Basic Researches of the Presidium of the Russian Academy of Sciences: Nanostructures: Physics, Chemistry, Biology: Engineering Principles.

Synergistic effects of deformation and solid-state reactions in Si with buried glass layer initiated by annealing in non-isothermal reactor

Yu.I. Denisenko
Yaroslavl Branch of the Institute of Physics and Technology, Institution of Russian Academy of Sciences, Yaroslavl, Russia, E-mail: den-yur55@mail.ru

The key task of modern semiconductor materials science is the production of new materials with a given set of physical, mechanical, electrical, optical and other properties. The concept of "defect engineering" allows manipulating the type, concentration and spatial distribution of defects within a crystalline substrate. The artifacts of modifying the defective subsystem of a (001)-oriented silicon substrate, which co-implanted by high doses of P^+ and O_2^+ ions and subjected to 2-stage annealing process, continues to be studied [1].
At the first stage of annealing process, a substrate was exposed to the 5-minutes lamp heat treatment in the non-isothermal reactor at average temperature 900 °C and at two signs (directions) of grad *T*. With that, temperature difference between "cold" and "hot" sides of the substrate was about 1.5˚C. At the second stage, a substrate was subjected to annealing procedures in usual isothermal furnace (1150 ˚C, 2.5 - 4 h). Then, the cleaved specimens were studied using SEM and SIMS techniques. Depending on the sign of grad *T* at the first annealing stage, the time evolution process led to the formation of two distinct in kind dislocation dissipative structures. In the case of sign (grad *T*) > 0, it is important to note, the continuous capsulated layer of SiP_zO_y phase was synthesized. Formation of the layer originates in the vicinity of maximum concentration of O_2^+ ions (R_p=100 nm), and corresponding changes in phosphorus concentration profile illustrates it (Fig. 1). The specimen surface had mirror-like quality without any traces of pitting process or dislocation tracks. Below the SiP_zO_y layer, the classic artifacts of the process of plastic flow in crystalline substrate as the evolution of an active medium in an open system far from thermodynamic equilibrium were exposed. The regular structure of mixed dislocations contained both edge and screw components with hollow nanotubes that were orienting along axes of the screw components. With that, the nanotubes were covered with SiO_x phase from within. Probably, nanotubes formation was accompanied by pipe diffusion of vacancies and their coagulation in the dislocation core followed by inserting of free oxygen from the top layer. In the case of sign (grad *T*) < 0, no continuous layer of SiP_zO_y phase was synthesized. The periodic dislocation structure was based on dislocations multiplication at sites of SiO_x phase localization. At these sites, formation of microcracks was taking place too. In the control specimens without non-isothermal "prehistory" (grad *T* = 0), no formation of any irreversible dissipative defect structures was observed.

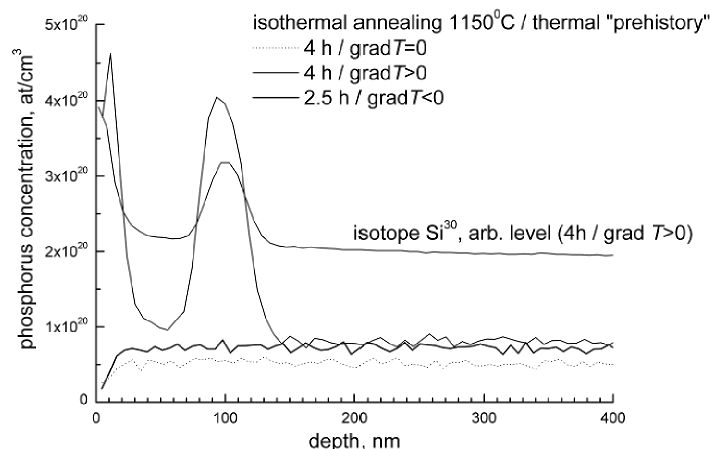

Figure 1. The changes in phosphorus concentrations of SIMS profiles after two-stage annealing.

1. Y.I. Denisenko and V.I. Rudakov, "Formation of nanoporous structure in silicon substrate using two-stage annealing process", Proceed. SPIE, 10224, International Conference on Micro-and Nano-Electronics, Moscow-Zvenigorod, Russia, 2016, 1022401.

Structural and morphological properties of Ga(Al)N grown by MBE on 3C-SiC/Si (111) templates with off-axis and on-axis substrate orientation

K.A. Tsarik[1], S.D. Fedotov[1,2], V.K. Nevolin[1], V.N. Statsenko[2]
1. National Research University of Electronic Technology, Moscow, Russia, tsarik_kostya@mail.ru
2. Epiel JSC, Moscow, Russia, fedotov@epiel.ru

Ga(Al)N compounds was expected to be a new materials for next generation high-power electronics (HPE) due to the unique properties of GaN-based devices: high breakdown strength, thermal and radiation resistance, faster switching, lower on-resistance and power dissipation [1]. Extremely high price of GaN bulk substrates impede to the wider spread of III-nitride HPE while the utilization of low-cost and large-diameter Si substrates with CMOS integration ability is very important nowadays. However, the unconformity of lattice parameters and coefficients of thermal expansions (CTE) between the Ga(Al)N and Si lead to cracks and traps formation besides then Si surface are damaged by Ga and N sources at the initial growth [2]. Recently, numerous of breakthrough had been created with SiN_x and AlN buffer layers but another way to obtain high-quality GaN with simpler epitaxy process is using 3C-SiC buffer layer on Si, since the lattice parameters and CTE of SiC are more appropriate for hexagonal Ga(Al)N growth [2, 3].

In the present investigation, we used the molecular beam epitaxy (MBE) which is part of nanotechnology facility Nanofab-100 [4]. High purity Ga and Al metals and NH_3 were used as source materials for MBE growth of Ga(Al)N compounds. High-quality 3C-SiC/Si 6 inch templates (manufactured by Advanced Epi Materials and Devices Ltd, UK) were utilized with 4° off-orientation (type 1) and on-orientation (type 2) (111) Si substrates. The templates were cut to 2 inch sample wafers and investigated before the growth by FTIR, AFM, XRD and bow measurements. 3C-SiC epi-layers (both types) is measured to be 300 ± 10 nm thickness with RMS about 1.5 ± 0.2 nm, ω-2θ scan confirms monocrystalline 3C-SiC(111) with FWHM below 0.1°. Wafer bow was measured across the diameter 2 inch wafers which shown tensile strain with bow about 1.2-1.5 μm. Epitaxial process consisted of standard stages which typical for GaN-on-Si: AlN was used to initiate growth and avoid the Ga/Si eutectic (on the polished wafer edge), according to a strain relief stack we exploited dynamic AlGaN/AlN superlattice and step-graded $Al_xGa_{1-x}N$ (with $x \approx 0.3$ to 0.1), then the channel GaN layer with thickness 560-1500 nm was grown with classic AlN spacer and $Al_{0.2}Ga_{0.8}N$ cap on top. Initial AlN-layer and complete 2 inch epi-wafers were examined by AFM, SEM, XRD, Raman and wafer bow measurements.

The surface morphology investigation of III-nitrides epi-layers had shown increasing of the microrelief height by several times after the initial AlN-layer deposition. RMS values had increased up to ~5 nm for type 1 and to ~7 nm for type 2 after 560 nm deposition of GaN. AFM and HR-SEM measurements revealed the presence of the through growth defects on epi-surface which probably could be sprouting from AlN/3C-SiC interface. Epi-surface with GaN thickness 1500 nm had the morphology as crystal grains on the scale of one micrometer which possibly due to the poor nucleation on 3C-SiC buffer. Crystallinity of Ga(Al)N layers was verified through ω-2θ scan and ω-rocking curve measurements which confirmed the monocrystalline AlN (0002) with FWHM of about 1.5° (both types), GaN (0002) with FWHM of about 0.55-0.65° for type 1 and GaN (0002) with FWHM of about 0.61-0.76° for type 2. It was observed that scanning offset geometry $(\theta + 3.8°)/2\theta$ gives the most intense diffraction reflection from GaN (0002) what might probably mean that on 3C-SiC with 4° off-orientation the crystalline nuclei of AlN (0002) grown perpendicular to the surface. The measurement of the wafer bow shown the ascending of the bow values up to ~8 μm after AlN deposition and >10 μm for epi-layers (both types) and tensile strain for all samples which had been confirmed by XRD and Raman strain analysis.

This work was carried out with the partially financial assistance of the Ministry of Education and Science in the framework of state task 16.2056.2017/4.6.

1. H. Amano, Y. Baines, E. Beam, M. Borga et al. J. of Phys. D: Appl. Phys., **51**, No. 16, pp. 1-48, 2018.
2. Y. Abe, N. Ohmori, A. Watanabe, J. Komiyama, et. al. J. Cryst. Growth, **318**, pp. 460-463, 2011.
3. G. Colston, M. Myronov, S. Rhead, D. Leadley. Semicond. Sci. Technol., **30**, pp. 1-6, 2015.
4. A.N. Alekseev, S.I. Petrov, V.K. Nevolin, et al. Russ. Microelectron., **41**, pp. 400-404, 2012.

Dependence of dielectric constant of hydrocarbon bridged low-k films on porosity

A. Palov[1], M. Baklanov[2], Sh. Wei[2]
1. Skobeltsyn Institute of Nuclear Physics, Lomonosov Moscow State University, Moscow Russia, a_palov@mail.ru
2. North China University of Technology, Beijing, China

The porous hydrocarbon bridged low-k films are now considered as the perspective materials for advanced interconnectors technology because of their exceptional elastic stiffness predicted by molecular dynamics calculations [1]. To the moment, there are no theoretical calculations of dielectric constants (DC) for such materials in literature and we decided to predict these values on base of our numerical approach developed recently [2].

The approach is based on the classical Clausius-Mossotti equation considering distribution of molar concentrations of fragments like bonds/atoms/molecule/groups and their polarizability. This method has demonstrated an excellent agreement of calculated dielectric constants of organosilicate glass (OSG) films with corresponding experimental data [2]. The basic difference between OSG and hydrocarbon bridged (HB) low-k films seems to be the matrix of HB materials has methylene, ethylene or benzene bridges incorporated in silicon dioxide. Thus, our idea to predict the DC values for HB films is to consider the input of such bridges in silicon dioxide matrix in addition to methyl groups on the pore surface. Technically this can be done by random replacement of silicon dioxide cells by methylene, ethylene or benzene ones in 3D map of silicon dioxide matrix.

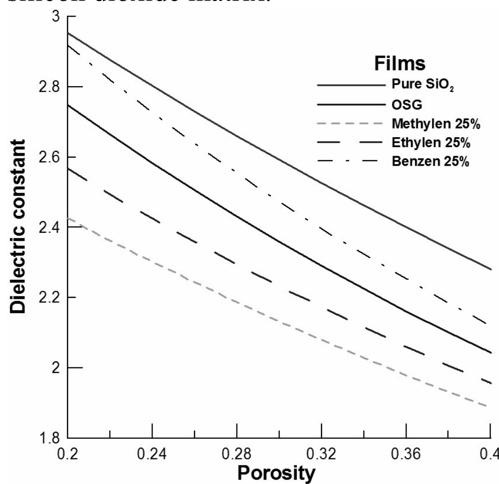

Fig. 1. Dependence of dielectric constant of hydrocarbon bridged low-k films on porosity.

To analyze numerically dependence of the dielectric constant on porosity in the range of 0.2-0.4 we chose the pore and interconnectivity radii as 1.5 nm and 1.35 nm, correspondingly.

Fig. 1 presents DC values of porous pure silicon dioxide, OSG film and HB films at ratio of 25% of methylene, ethylene and benzene bridges. It is clearly seen the predicted DC values of HB films based on benzene bridges are always higher than pure SiO_2 and OSG ones while DC values calculated for methylene and ethylene bridges are lower.

Thus, the numerical analysis of the DC dependence on porosity for HB films shows it is similar and close to OSG one but in addition we can expect the benzene-based HB films should have DC values higher than OSG films while ethylene and methylene bridges-based films have notably lower DC than OSG ones.

A. Palov thanks the RFBR (Grant № 18-52-53017) and Sh. Wei thanks the NSCF (Grant №81811530114) for financial support.

1. J.A. Burg, M.S. Oliver, T.J. Frot, M. Sherwood, V. Lee, G. Dubois, and R.H. Dauskardt, Nature Comm. **8**, pp. 1019, 2017.
2. A. Palov, T.V. Rakhimova, M.B. Krishtab, M.R. Baklanov, J. Vac. Sci. Technol. **B33**, pp. 020603, 2015.

Hydrocarbon bridged low-*k* films

D. Seregin[1], A. Vishnevskiy[1], N. Kotova[1], K. Vorotilov[1], A. Sigov[1],
Yingjie Wang[2], Jing Zhang[2], Jim Leu[3], M. Baklanov[1,2]

1. MIREA – Russian Technological University, Moscow, Russia, d_seregin@mirea.ru
2. North China University of Technology, Beijing, China
3. National Chiao Tung University, Hsinchu, Taiwan

Semiconductor industry calls for new generation of low k materials for 7 nm technology node and beyond. Some specific features of chemical solution deposition (CSD) make possible to consider it as a promising approach for subtractive integration (alternative to damascene: metal patterning first) [1] in BEOL process, including possibilities for molecular self-assembly-, inorganic-organic hybrids, and gap filling performance [2, 3]. Hydrocarbon bridges are also allowing significant improvement of mechanical properties of low-k material [4].

The goal of this research is to explore the main properties of CSD organosilicate films in which a part of silicon-oxide network is replaced by silicon-hydrocarbon bonds. Different types and content of -Si-*X*-Si- bridging groups (where *X* is methylene, ethylene or benzene group) are studied.

The film-forming solutions were prepared by co-hydrolysis of methyltrimethoxysilane (MTMS, 98%, Fluka) and alkylenesiloxane with a distinct type of -Si-*X*-Si- group. Hydrolysis and polycondensation of the first one results in formation of silicon oxide network with the terminal -CH_3 groups, whereas the second one creates structure with different organic bonds between silicon atoms. Evaporation induced self-assembly with nonionic surfactant Brij 30 (30 wt.%) is used to provide porous structure. The films were spin-on deposited on silicon wafers and annealed at T_a = 150°C, 30 min on the hot plate; at T_a = 200°C 30 min, and finally at T_a = 430°C, 60 min. Table 1 shows main properties of the films with different content of methylene, ethylene and benzene groups: refractive index *n*, dielectric constant *k*, network/cage ratio estimated by FTIR, porosity and pore radius estimated by ellipsometric porosimetry (adsorption and desorption modes), and Young's modulus (YM) obtained by nanoidentation.

Table 1. Measured properties of studied films

-Si-*X*-Si- (mol.%)	*n*	*k*	$I_{network}/I_{cage}$	Porosity (%)	Radius (nm) Ads/Des	YM (GPa)
Methylene 25%	1.297	2.35	1.9	38.3	1.84/1.94	5.0
Ethylene 25%	1.297	2.37	2.2	32.2	1.57/1.67	6.6
Benzene 25%	1.312	2.39	1.4	35.1	1.3/1.35	7.0
Methylene 45%	1.316	2.48	2.2	29.2	0.79/0.92	8.5
Ethylene 45%	1.294	2.6	2.2	36.4	1.52/1.67	8.3
Benzene 45%	1.361	2.95	1.5	30.3	0.81/0.87	11.2

The YM values increase with the increase of carbon chain as benzene > ethylene > methylene. Concentration of bridge content also increases the YM values. However, the *k*-value also increases especially in the case of a benzene bridge. The reasons are related to higher polarizability of chemical bonds in the case of a benzene bridge and higher silanol content due to steric effect as confirmed by FTIR. It is interesting that the pore radius drastically decreases with the increase of the bridge content, except of the case of 45 mol.% ethylene bridge.

The obtained results suggest that molecular self-assembly of organosilicate low-*k* films with hydrocarbon bridges is a promising approach for the next generations of technology node in semiconductor manufacturing technology.

The study was supported by the Ministry of Education and Science (project No. 11.2259.2017/4.6), and RFBR 18-52-52010.

1. L. Zhang et al. Appl. Phys. Letters, **109**, pp. 232901, 2016.
2. R. Nenashev et al. ECS J Sol St Sci Techn, **6** (10), pp. 182-188, 2017.
3. Patent 2530534 Russian Federation, IPC H01L 21/768, Valeev A.S. et al.
4. H. Li, J.M. Knaup, E. Kaxiras, J.J. Vlassak, Acta Mater., **59** (1), pp. 44-52, 2011.

Evaluation of technology for obtaining sol-gel Al_2O_3 film for organic field-effect transistors

S. Avdeev[1], E. Gusev[1,2]

1. Southern Federal University, Institute of Nanotechnology, Electronics and Equipment Engineering, Taganrog, Russia, savdeev@sfedu.ru

2. Southern Federal University, Research and Educational Centre "Nanotechnologies", Taganrog, Russia, eyugusev@sfedu.ru

One of the applications of sol-gel Al_2O_3 films in micro- and nanoelectronics technology is using the films as a gate dielectric in organic transistors, which are now increasingly attracting developers of matrixes for displays, sensors, etc.

Promising methods for obtaining a homogeneous composition and powder properties are liquid-phase technologies, in particular, sol-gel. The sol-gel technology of forming an aluminum oxide film has unique technological capabilities that are not fully understood.

Aluminum isopropoxide $Al(C_3H_9O)_3$ is used as an initial material for the sol-gel synthesis of oxide layers in the technology of nano- and microelectronic components. During the formation of the Al_2O_3 film, obtained by sol-gel method from aluminum isopropoxide, a number of polymorphic transformations are observed. It is known, first, the xerogel film of aluminum is heated (100-150 °C), non-stoichiometric water, contained in the pores and between the crystallite boundaries, will be removed first. Then, the temperature rises above 300 °C, the stabilizer acids are sublimed from the film, and above 450-500 °C the film is dehydrated by passing to γ-Al_2O_3. Finally, carbohydrate organic compounds contained in xerogels at a temperature above 600°C are burn out. Further modification of the film with increasing temperature can be described by xerogel sintering processes.

The strength properties of the produced films (sol-gel film Al_2O_3) proportionally affect the change in the refractive index. The electrical properties of Al_2O_3 films have been studied by the formation of MDS structures (fig. 1).

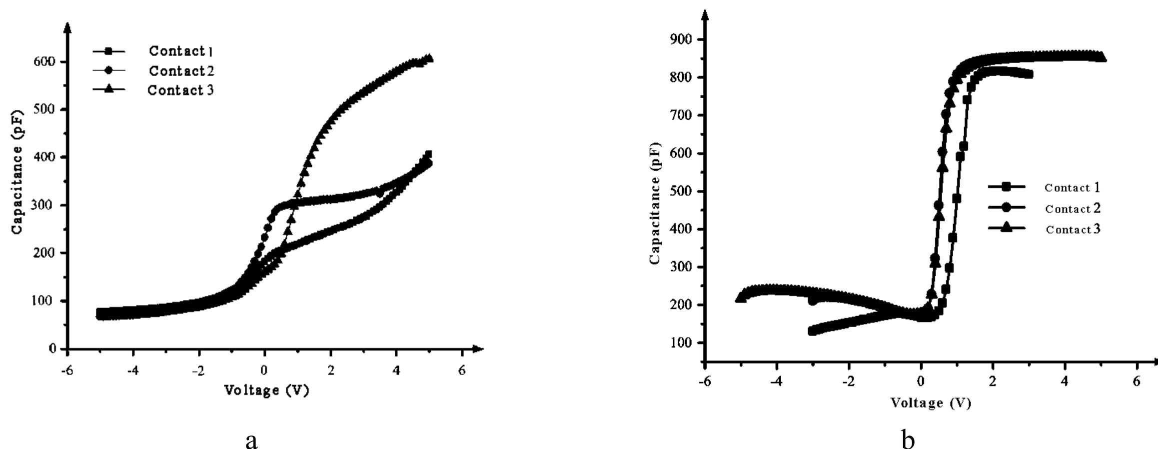

Figure 1. C-V characteristics of the structures annealed at a) 600 °C and b) 1000 °C.

The research was financially supported by Southern Federal University, grant VnGr-07/2017-02. The results were obtained with the equipment of the Research and Education Centre "Nanotechnologies" of the Southern Federal University.

1. A.I. Belous, V.A. Soloduha, S.V. Shvedov. *Space electronics (Kosmicheskaya electronika)*. Technosphera, Moscow, 2015. (in Russian).

2. K.R. Murali, P. Thirumoorthy. "Characteristics of sol-gel deposited alumina films". J. Alloy. Comp., **500**, pp. 93-95, 2010.

3. L.A. Majewski, R. Schroeder, M. Grell. "Flexible high capacitance gate insulators for organic field effect transistors". J. Phys. D, **37**(21), pp. 21-24, 2004.

Nanoscale domain growth dynamics of lead-free ferroelectric BST thin films

M.S. Afanasiev[1], G.V. Chucheva[1], D.A.Kiselev[1,2]
1. Fryazino Branch of the Kotel'nikov Institute of Radioengineering and Electronics of Russian Academy of Sciences, Vvedensky Square 1, Fryazino, Moscow region, Russia
2. Department of Materials Science of Semiconductors and Dielectrics, NUST "MISiS", Leninskiy pr. 4, Moscow, Russia (dm.kiselev@gmail.com)

Previous and today's dynamic random access memories (DRAMs) have been advanced by mainly focusing on how to make memory cells small to realize high density DRAMs. The most critical challenges in gigabit density DRAMs are yield loss due to large die size and small feature size, standby current failure caused by large chip size and small data retention times owing to reduced charge packet in the memory cell. In the recent years thin film perovskite materials with high dielectric constant such as PZT, $SrTiO_3$ and (Ba, Sr)TiO_3 (BST) have been investigated as dielectric materials for future DRAMs [1].
In this work, we report a voltage-induced domain growth kinetics in ferroelectric BST 80/20 films (thickness 150 nm) fabricated by RF magnetron sputtering measured via piezoresponse force microscopy (PFM) [2]. The surface of the sample shows small grains which diameter ranges from 50 to 75 nm and roughness is less than 5 nm. Using the PFM mode to detect the out-of-plane polarization, the domain sizes were measured as a function of the applied writing voltage and the pulse time. As example Figure 1 show the result the local polarization effect via PFM. For the investigation of written domains on as-grown surface of the BST film the negative voltage pulses were applied to fixed locations within this area, thus we have an array of 23 stable domains created by applying voltage pulses of fixed height (V_{tip} = -20 V ÷ -60 V with step 10V) and various durations ranging from 1 to 100 s. The dynamics of domain growth is analyzed experimentally taking into account the strong inhomogeneity of the external electric field in the film. Using the approximation, we can calculate the coercive field (E_C) and natural curvature radius of the cantilever used in the experiment. Therefore, we have obtained the value E_C = 3 kV/cm and d = 75 nm [2]. The obtained results point to the fact that the BST ferroelectric thin films are promising materials for using as the memory elements.

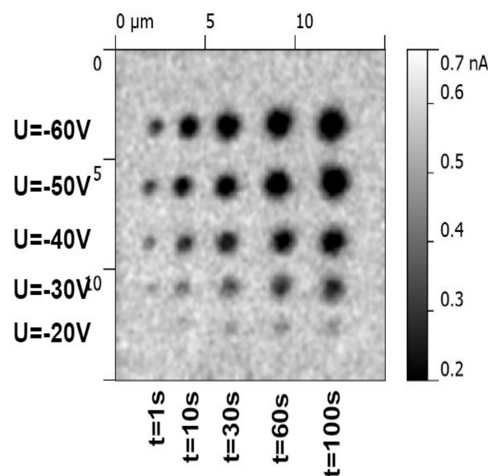

Figure 1. PFM image of dot patterned domains formed by negative voltage pulses to tip on as-grown BST 80/20 film.

The study was supported in part by the Russian Foundation for Basic Researches (projects 16-07-00665, 16-07-00666, 18-29-11029).

1. J.F. Scott. *Ferroelectric Memories*, Springer, 255 pp., 2000.
2. D.A. Kiselev, M.S. Afanasiev, S.A. Levashov, and G.V. Chucheva, "Growth kinetics of the induced domains in ferroelectric BST 80/20 thin films". Phys. Solid State, **57**, pp. 1151-1154, 2015.

Forming methods research and electrophysical properties of ferroelectric films ZnO study

A. Zotov, A. Perevalov, V. Shevyakov
National Research University of Electronic Technology, Moscow, Zelenograd, Russia, ardents@bk.ru

Zinc oxide possesses an interesting combination of physical and chemical properties: a high melting point and thermal conductivity, photosensitivity, piezoelectric and pyroelectric effects, the adsorption of gases on the surface. This material is widely used in microelectronics, chemistry and medicine. ZnO crystals, thin films and diode structures based on it are the subjects for scientific studies and applications [1-2].
Today, thin films structures are playing a big role in micro and nanoelectronics development. They are used in electronic and optical devices fabrication and as reinforcing and decorative coatings. Materials combination allows us to get new properties of structures that could have completely new physical and electrical properties [3].
An anisotropic crystal structure, a non-stoichiometric composition, semiconductor properties with a large band gap and other properties make this material not only interesting but also quite complex object for study. The dependence of the characteristics of ZnO thin film on the preparation conditions and various external factors is currently of great interest, for example in the semiconductor sensor technology. In connection with the aforementioned, in the present work has been investigated a technological regimes of deposition, the conductivity and dielectric properties of structure contained a thin layer of zinc oxide.
In this paper shown series of experiments focused on electrical properties study in ZnO ferroelectric films in composition of Al/ZnO/Al heterostructure, which was produced by several methods: sol-gel method, magnetron sputtering of ZnO target and atomic layer deposition. It has been found a specific volume resistivity by measuring surface resistivity (four-point probe method) and film thickness (atomic force microscopy). Film thickness was determined via SEM. SEM image of the formed ZnO film is on fig. 1. Elemental composition was controlled using EDX (energy dispersive x-ray) analysis. Films structure was determine by X-ray diffraction.

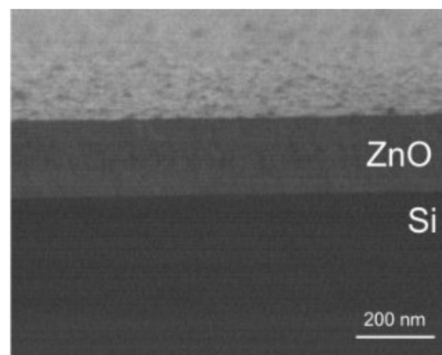

Figure 1. SEM image of the formed ZnO film.

It has been found that a sol-gel method is forming an amorphous ZnO films without ferroelectric properties. Thermal annealing of films in 300-800 °C range changed a film structure from amorphous to polycrystalline. The films have shown low ferroelectric properties. Films that produced by magnetron sputtering were dielectrics and they had polycrystalline structure and showed ferroelectric properties. Films that formed by atomic layer deposition method had polycrystalline structure and showed enhanced ferroelectric properties.

1. Kilinc et al. *"Fabrication of 1D ZnO nanostructures on MEMS cantilever for VOC sensor application".* Sensors and Actuators B: Chemical, **202**, pp.357–364, 2014.
2. V. Coleman and C. Jagadish "*Zinc Oxide Bulk",* Thin Films and Nanostructures ed. By Jagadish C. and Pearton S. (Elsiever), pp. 1-3, 2006.
3. A.O. Zotov, A.A. Perevalov, A.N. Belov. "Electrical conductivity of Cu/ZnO/Si heterostructure" *IOP Conf. Series: Journal of Physics: Conf. Series,* **816,** p. 012013, 2017.

Features of ferroelectric charging process and switching of the domains under electron beam irradiation

A.A. Tatarintsev[1,2], E.I. Rau[1], K.E. Markovets[1]
1. Moscow State University, 119991, Moscow, Russia, rau@phys.msu.ru.
2. Institute of Physics and Technology of RAS, 117218, Moscow, Russia, tatarintsev@ftian.ru

In recent years integration of polar dielectric materials such as ferroelectric, piezoelectric and pyroelectric in microelectronic technology has been increased. For a example, creating a regular domain structures (RDS) configuration required in ferroelectric crystals is a practically important problem in microelectronics. One of the most convenient ways to create the RDS is irradiation of a sample by focused electron beam with different energies in the electron beam lithography setup [1, 2]. However, the associated mechanism of ferroelectric charging under electron beam irradiation is not fully investigated and understands.

This work is aimed to a comprehensive study of all the main parameters of the charging process of ferroelectrics $LiTaO_3$ and $LiNbO_3$ namely: surface potential V_s, secondary electron emission current I_σ, sum of the displacement current (the accumulated charge Q) and the leakage current $I_{L+D.}$ Experiments were carried out in wide energy range from 200 eV to 10 keV and on both sides of the Z-cuts: plus and minus. Value of the primary e-beam current was I_0=100 pA and the irradiation area was 100x100 μm^2. This complex approach [3] allows us to establish the main features of the process of charging ferroelectrics and the accompanying switching of the domain structure.

Anomalous behavior of the secondary electron emission current was established (see fig.1). The change of sign of current which is registered by hemispherical collector is observed in the obtained results. This fact is explained by the determining influence of the displacement current on the collector caused by the appearance of the surface positive charge of large density by reason of the polarization switching for –Z-cut or the screening charges exit at +Z-cut. The possibility of such scenario is confirmed by the model experiment and the evaluation of surface positive potential gives values about 20 kV. Along with this the change of sign of current which is registered by hemispherical collector is observed on account of capacitance coupling.

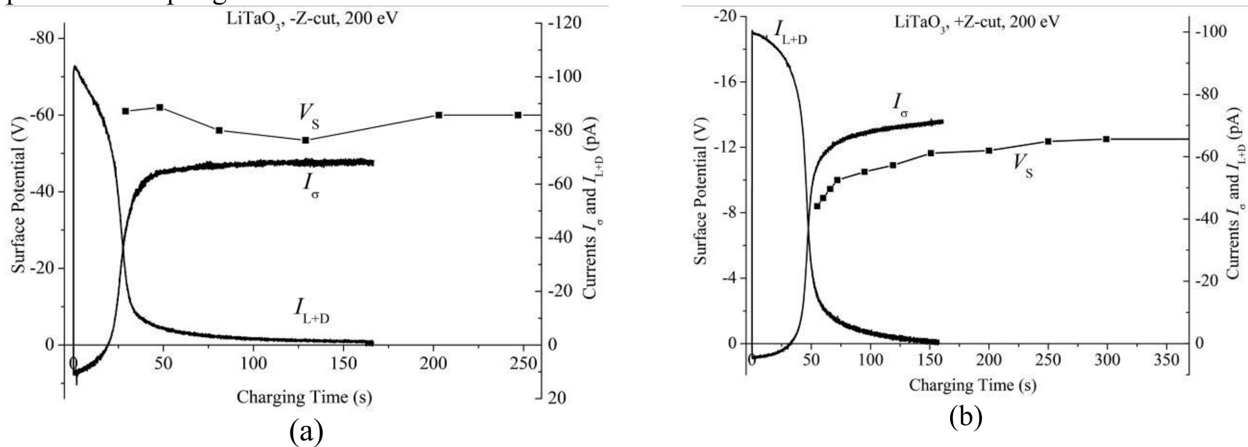

Fig. 1. Surface potential V_S, secondary electron emission current I_σ, sum of displacement current and the leakage current I_{L+D} versus time of ferroelectrics irradiation for –Z-cut (a) and +Z-cut of $LiTaO_3$. Charging parameters: primary electron beam energy E_0= 200 eV and current density $j_0=10^{-6}$ A/cm^2.

1. E.V. Emelin, A.I. Il’in, and L.S. Kokhanchik, “Recording of domains by an electron beam on the surface of +Z cuts of lithium niobate”, Fizika Tverdogo Tela, **55**(3), pp. 489-493, 2013.
2. L.S. Kokhanchik and D.V. Irzhak, “Formation of regular domain structures and peculiarities of switching of the spontaneous polarization in lithium tantalate crystals during discrete electron irradiation”, Fizika Tverdogo Tela, **52**(2), pp. 285–289, 2010.
3. E.N. Evstaf’eva, E.I. Rau, and A.A. Tatarintsev, “An explanation of certain contradictions in the treatment of the charging dynamics of dielectric targets under the effect of electron irradiation”, Moscow University Physics Bulletin, **68**(2), pp. 128-131, 2013.

Influence of Power and Pulsed Regime of Low Frequency Discharge on Clusters Incorporation in Dielectric Films for ReRAM Application

A.A. Popov, A.E. Berdnikov
Yaroslavl Branch of Institute of Physics & Technology of Russian Academy of Sciences, 150007, Russia, Yaroslavl;
e-mail: imiraslab4@yandex.ru

We investigated effect of nanoclusters formation during deposition of dielectric by low frequency PECVD method. These dielectric films may be used for formation metal–insulator–semiconductor structures (MIS) with conductive switching effect for ReRAM application [1]. For downsizing MIS structures with this effect volume concentration of clusters in deposited film must be increased.

Clusters formed in gas phase and incorporated in growth film. We supposed that power increasing lead to chemical active particles concentration in gas phase increased and probability of gas phase's polymerization increased. As a result cluster flow increased in more degrees then the deposition rate of film.

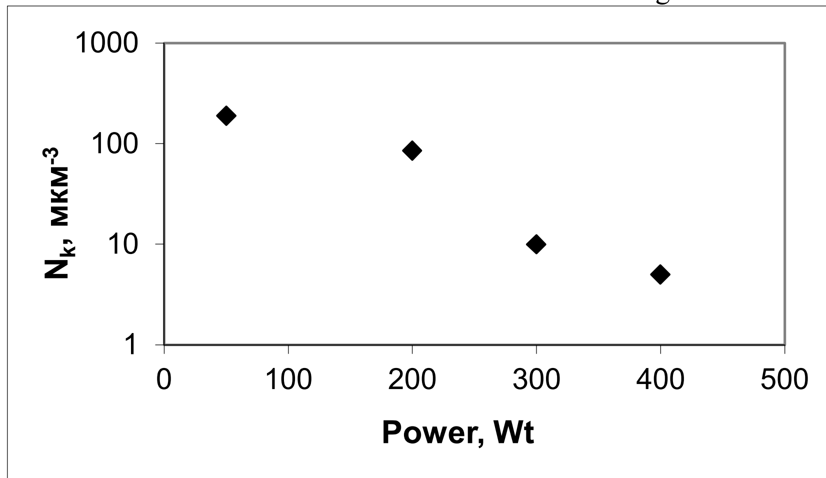

Fig. 1. Dependents volume density of clusters from low frequency power of discharge.

Experimental researches showed opposite results, presented in Fig. 1. Numbers of incorporated in film clusters decrease, but there size increased. Power increasing lead to acceleration of charged particles connection to clusters formed in gas phase. As a result these clusters removed in interelectrode space by plasma potential, and dropped on the reactor sidewall.

Other way of control low frequency discharge is using of pulsed regime of electric power supply. During time T_{on} power supplied to electrodes system and during other time T_{off} power is turn off, and in plasma chemical reactor take place relaxation process.

Experimentally observed, that using pulsed regime with $T_{on}=T_{off}$ instead continues regime, total volume cluster density decrease and incorporation of big size cluster increase. This effect connected with absent of plasma potential during T_{off}. Charged particles diffused during this time on growth surface and incorporated in deposited material.

Then $T_{on} \ll T_{off}$ total clusters volume concentration drastically decreased. It means that during T_{off} gas faze clusters nucleation's interrupted, gas phase concentration of chemical active particles dropped to negligible value and biggest part of clusters removed from gas phase.

So, simultaneous control of supplied low frequency power and parameters T_{on} and T_{off} of pulsed regime of discharge allowed change volume density of nanoclusters formed in gas phase and its distribution by size. But managing relationship between technology parameters and structural properties is not obvious and rather sophisticated.

1. A.E. Berdnikov, V.N. Gusev, A.A. Mironenko, A.A. Popov, A.V. Perminov, A.C. Rudy, V.D. Chernomordick, "Conductivity switching effect in MIS structures with silicon-based insulators, fabricated by low-frequency plasma-enhanced chemical vapor deposition methods" Semiconductors, **47**, pp. 641–646, 2013.

Effect of mechanical deformations on absorption spectrum of metallic films of nanometer thickness

K.M. Tsysar[1], E.M. Smelova[1], V.S. Zelensky[1], V.G.Andreev[1], V.A.Vdovin[2]
1. Lomonosov Moscow State University, Faculty of Physics, Moscow, Russia, smelova_k_m@mail.ru
2. Kotel'nikov Institute of Radio Engineering and Electronics of RAS, Moscow, Russia

Recently the problem of electromagnetic field interaction with low-dimensional structures is of special interest. The most interesting is the study of the interaction of electromagnetic field with thin metal films which may be used as substrates for nanocircuits. In the recent studies the thickness dependent energy loss function was observed in ultrathin metal nanofilms [1, 2], also the optical and conducting properties strongly depend on the elasticity of a film. Present study is focused on dependence of conducting and optical properties of Ag nanofilms on its thickness and mechanical deformations in infrared and terahertz range.

First longitudinal elastic deformations of thin Ag films are studied by the methods of classical molecular dynamics realized in LAMMPS code [3]. Dependence of the elastic properties of Ag films on the thickness was found (Fig. 1(a)). The critical values of the longitudinal stresses on the rapture and the limiting values of the elastic deformations at which irreversible defects in the atomic structure appear in the film are determined (Fig. 1(a)). 9% elongation is crucial for 6 monolayer (ML) Ag films (12A) leads to appearance of atomic dislocations in its surface (see Fig. 1(a)). The dependence of critical stresses on the film thickness was found. The data on elasticity of Ag nanofilms obtained from classical calculation were used for further investigation of their optical and conducting properties. The Vienna Ab-initio Simulation Package (VASP) code which is based on the density functional theory [4] was used for optical calculations.

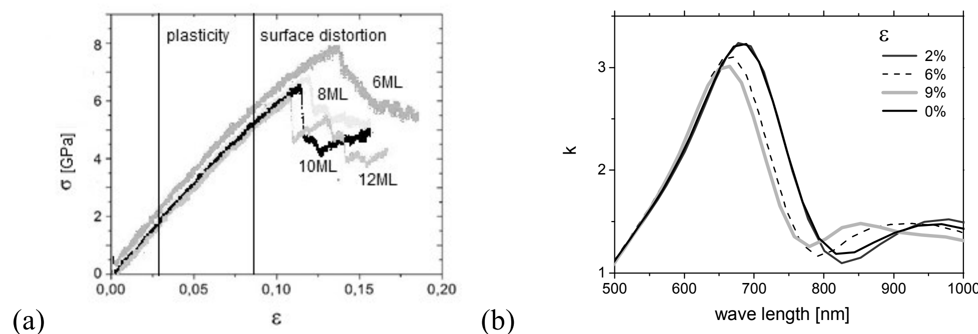

Fig. 1. Total stress (s) as function of elongation (e) of Ag nanofilms 6ML width (12A) (a); extinction coefficient (k) as function of wave length for visible diapason and infrared (300nm-1000nm) (b).

For 6ML Ag nanofilms the dependence of the optical properties on mechanical strain was found. The study showed a shift of the absorption peak in the region of the optical wavelength range with increasing external longitudinal stresses. At 9% (the limit of plasticity for 6ML Ag nanofilm,) elongation of silver film, the absorption peak shifts by 25nm to the optical range. The height of the peak decreased from 3.4 to 3.0 (Fig. 1(b)).

Thus our study predict the changes in optical and conducting properties of deformed metal nanofilms in plasticity region before mechanical destructions of nanofilm surface which also leads possible to the changes of physical properties supported nanocircuits and nanodevices.

This work was carried out using high-performance computing resources of federal center for collective usage at NRC “Kurchatov Institute” and Joint Supercomputer Center of the Russian Academy of Sciences. Work is supported by RFBR grants 16-07-01246, 16-29-09581, 17-07-00745

1. J. Gong et al., Scientific Reports, **5**, p. 9279, 2015; Tsysar K.M. et al., Proceedings of SPIE - The International Society for Optical Engineering, **10224**, p. 1022408-1-1022408-6, 2016.
2. D. Kwon et al., Nature Nanotechnology, **5**, pp.148-153, 2010.
3. S. Plimpton, J. Comput. Phys. **117**, pp. 1–19, 1995.
4. G. Kresse and J. Furthmuller, Phys. Rev. B, **54**, p. 11169, 1996.

Modeling of the effective ion charges in grain boundaries of polycrystalline interconnects

T. Makhviladze, M. Sarychev
Institute of Physics and Technology of RAS, Moscow, Russia, sarych@yandex.ru .

When electrical current runs through a conductor the effective charge of an ion or vacancy characterizes the combined effect of the applied electrical field and the electron wind on the ion [1]. Values of effective charges strongly influence on characteristic times of conductor failures due to electromigration, i.e. they determine the microcircuit reliability [2.3]. Thus calculation of effective charges of ions is an important problem for adequate modeling reliability of microelectronic interconnects.

An approach to calculate effective ion charges and vacancies in bulk of monocrystalline metals and alloys was suggested in [4]. However, real microelectronic conductors are polycrystalline. As known [3], in such conductors electromigration is generally along grain boundaries (in aluminum) or on the conductor surface (in copper). Therefore, the effective charge values calculated in [4] cannot be used for practical simulation of microcircuit reliability.

In the present work we suggest a model, which is capable to calculate *ab initio* effective ion charges in tilt grain boundaries. In the developed model we consider tilt grain boundaries of infinite length, and a grain boundary is considered as the monocrystalline layer with the atomic density depending on a misorientation (tilt) angle of the grain boundary. This dependence is obtained by modeling the grain boundary as a dislocation sequence. At the same time the atomic density enter into the expressions for the wave numbers of conduction electrons and phonons, and, according to [4], just these quantities determine the values of effective ion charges. Thus it turns out that an effective charge has to depend on a tilt angle and a texture of the grain boundary as well as on temperature.

Using the model we calculated the dependences of the form-factors of copper and aluminum ions as a function of an conduction electron momentum q at different tilt angles θ for the textures (100) and (111) of the grains forming the grain boundary. Then we also calculated the resistivity of the aluminum grain boundary as a function of temperature at different values of θ. Then we used the results obtained to calculate the effective charges of copper and aluminum ions in an aluminum grain boundary as a function of temperature at different tilt angles for the texture (100) and (111). Our results also show that in the case of a grain boundary they are lower than in the metal bulk, and these results are in good agreement with the phenomenological considerations and experimental data. Besides, this difference increases if the temperature decreases. As it follows from our numerical results, in an aluminum grain boundary having the texture (100) and the tilt angle 45^0 the effective charge of copper ions vanishes at $T \approx 770$ K. This effect can be validated experimentally.

According to the obtained results one can decelerate the electromigration of the copper ions by fitting the tilt angle and texture of grain boundaries. It would give a possibility to control the metallization reliability at the stage of microcircuit manufacture.

1. V. B. Fiks. *Ion conductivity in metals and semiconductors*. Nauka, Moscow, 1969 (in Russian).
2. K.A. Valiev, R.V. Goldstein, Yu.V. Zhitnikov, T.M.Makhviladze and M.E.Sarychev. "Nano- and micrometer-scale thin-film-interconnection failure theory and simulation and metallization lifetime prediction, Part 2: polycrystalline line degradation and bulk failure". Russian Microelectronics, **39**, pp.145-157, 2010
3. R.V. Goldstein, T.M.Makhviladze and M.E.Sarychev. "Electromigration-unduced instability between solid conductors". Phys. Mesomechanics, **19**, pp.19-26, 2016.
4. R. S. Sorbello. "A pseudopotential based theory of the driving forces for electromigration in metals". *J. Phys. Chem. Sol.*, **34**, pp. 937-950, 1973.

Swift heavy ion stimulated formation of the Si quantum dots in Si/SiO_2 multilayer heterostructures

G. Kamaev[1], S. Cherkova[1], A. Gismatulin[1], V. Volodin[1,2], V. Skuratov[3,4,5]

1. A.V. Rzhanov Institute of Semiconductor Physics SB RAS, Novosibirsk, Russia, E-mail address: kamaev@isp.nsc.ru
2. Novosibirsk State University, Novosibirsk, Russia
3. Joint Institute for Nuclear Research, Dubna, Russia
4. National Research Nuclear University MEPhI, Moscow, Russia
5. Dubna State University, Dubna, Russia

Silicon nanocrystals (nc-Si) as new elements of micro- and optoelectronics are of significant interest.The ability of systems containing such nanoclusters to emit light or retain the charge depends on the cluster characteristics (size, spatial distribution) and interface nature. The necessity of high-temperature treatment for Si nanostructures formation and modification stimulates the search for methods of thermal budget reduction. Therefore the methods which allow a local stimulation of the structural transformations would be of great interest.

Here we present studies of the formation of nc-Si in multilayer structures with alternating ultrathin layers of SiO_2 and amorphous hydrogenized silicon (α-Si:H) varied layer thickness, irradiated with 167 MeV Xe ions in the dose range of $10^{12}\div3\bullet10^{14}$ cm^{-2} and then annealed in the temperature region of $500\div1100$ ^0C for 30 min in N_2 ambient. The Si/SiO_2 multilayer nanoscale structures consisting of alternating α-Si:H and SiO_2 layers were deposited on Si substrates on a inductively coupled plasma chemical vapour deposition setup with a wide-aperture source. A silicon oxide layer 30–35 ˚Å thick was first formed on the Si substrate by means of direct processing in an oxygen plasma. Then the PECVD procedure was applied to deposit an amorphous silicon film of a required thickness from monosilane. After that, the α-Si:H film was oxidized to a prescribed depth in an oxygen plasma. The multilayer structure was formed in consecutive processes of plasma-enhanced chemical vapor deposition of α-Si:H films and their oxidation. As a result, Si/SiO_2 multilayer structures containing up to six α-Si:H layer sandwiched between SiO_2 were obtained.

The effect of swift heavy ions (SHI) irradiation and annealing on the transformation of the structure of the α-Si:H layers is studied by methods of high-resolution transmission electron microscopy (HREM), Raman spectroscopy in the back-scattering geometry, and photoluminescence (PL). HRTEM studies have shown that SHI irradiation disintegrates partly the α-Si:H layers in PECVD Si/SiO_2 heterostructures and leads to the formation of individual silicon nanoclusters into the nm-size inclusions. At the same time, the layered structure of Si/SiO_2 has not broken, but one can see the vertically ordering of Si nanocrystals/nanoclusters along ion tracks. The post-irradiation annealing at 1100^oC led to an appearance of intensive PL peak at about 780 nm, typical for the nc-Si, and its intensity was growing with the dose. Mechanism of formation of silicon nanoclusters in oxide matrix under the impact of SHI irradiation treatments is discussed.

The electrical properties of Si/SiO_2 multilayer heterostructures were studied by the measurements of their capacitance-voltage (C-V), conductance-voltage (G-V), and current–voltage (I–V) characteristics. The memristive effect with bipolar switching is demonstrated. The introduction of Si nanoclusters into the dielectric reduces the randomness of formation of a conducting channel. Intermediate metastable states are observed in the I–V characteristics in the process of switching on and off. This may prove to be important for the generation of intermediate resistance values (multibit data storage) and for the development of adaptive neuromorphic systems.

The work is supported by RFBR, contract number 18-07-01278.

Luminescent properties of GeO_x thin films and GeO/SiO_2 heterostructures modified with swift heavy ions

S.G. Cherkova[1], V.A. Volodin[1,2], V.A. Skuratov[3,4,5], M. Stoffel[6], H. Rinnert[6], M. Vergnat[6]

1. Rzhanov Institute of Semiconductor Physics, Siberian Branch, Russian Academy of Sciences, Novosibirsk, Russia, E-mail: cherkova@isp.nsc.ru

2. Novosibirsk State University, Novosibirsk, Russia

3. Joint Institute for Nuclear Research, Dubna, Russia

4. National Research Nuclear University MEPhI, Moscow, Russia

5. Dubna State University, Dubna, Russia

6. Université de Lorraine, CNRS, IJL, Nancy, France

Germanium nanocrystals and defects in germanium/silicon oxide films have gained an increasing interest because of their luminescent properties. Defects in such films act as traps for charge carriers, which can be exploited in either flash memories or memristors. Irradiation with swift heavy ions (SHI) may modify the film properties. When SHI penetrate in solid-state targets, their stopping in near-surface layers occurs predominantly by the electronic (ionization) losses. If the energy density exceeds ~1 keV/nm, tracks may be formed with nm-scale diameters and the temperature inside the tracks may exceed 5000 K for 10^{-13}–10^{-11} s in silica [1]. For example, SHI irradiation of Si/SiO_2 multilayers is known to lead to the formation of vertically ordered Si nanoclusters due to phase separation in ion tracks [2].

In this work, we modify the structure of both GeO_x films and GeO/SiO_2 multilayers using SHI irradiation to form light-emitting Ge-related (oxygen deficient) defects. The films were obtained by evaporation of GeO_2 powder or by alternating evaporations of GeO_2 and SiO_2 powders in high vacuum (10^{-8} Torr) onto Si(001) substrates heated up to 100°C. The 100 nm thick GeO_x film was capped by a 100 nm thick SiO_2 layer. The multilayer sample, which contains 20 periods of GeO_x(5nm)/SiO_2(5nm) layers, was capped by a 40 nm thick SiO_2 layer. The samples were irradiated with 167 MeV Xe^{+26} ions at fluences varying from 10^{11} cm^{-2} to 10^{13} cm^{-2}, using the cyclotron at FLNR JINR, Dubna. Within the studied layers, stopping power of the ions was nearly completely (~99%) due to the ionization losses, according to the SRIM calculations (www.srim.org). The projected range of the ions was about two orders of magnitude larger than the films thicknesses. Fourier transform infrared (FTIR) absorption spectroscopy, photoluminescence (PL) and Raman measurements were used for the characterizations.

According to Raman spectroscopy data, the swift heavy ion irradiation does not lead to the expected decomposition of germanium suboxide in germanium nanoclusters and GeO_2. We have shown that SHI irradiation with 167 MeV Xe^+ ions and fluences as high as 10^{13} cm^{-2} does not lead to the formation of a noticeable amount of Ge-Ge bonds in 100 nm thick GeO films and GeO(5nm)/SiO_2(5nm) multilayered heterostructures. Infrared absorption spectroscopy measurements show that under irradiation the GeO/SiO_2 layers were intermixed with formation of Ge-O-Si bonds. We report strong photoluminescence in the visible range at room temperature, which is most probably due to Ge-related defect-induced radiative transitions. Moreover, two infrared luminescence bands (at ~0.8 eV and ~1.1 eV) were observed at low temperatures in irradiated structures. The observed PL may be caused by defects located either in the silicon substrate or in the GeO_x films. In order to identify the origin of the two PL bands, we have considered a SHI irradiated Si substrate as a reference sample. In this case we have observed a broad PL peak centered at ~0.8 eV. It is known, that A-centers in ion implanted Si modified by carbon are characterized by a broad PL peak centered at ~0.79 eV [3]. In our SHI irradiated films the huge PL signal close to 1.1 eV may thus be due to defects in GeO_x films. The intensity of this peak decreases, with increasing temperature but was even observed at room temperature, which may be of interest for future optoelectronic applications.

The work was supported by the state research program of ISP SB RAS project № 0306-2016-0015.

1. M. Toulemonde, C. Dufour, A. Meftah, E. Paumier. “Transient thermal processes in heavy ion irradiation of crystalline inorganic insulators”. Nucl. Instr. and Meth. B, **166-167**, pp. 903-912, 2000.

2. S.G. Cherkova, V.A. Volodin, A.G. Cherkov, A.Kh. Antonenko, G.N. Kamaev, V.A. Skuratov. “Light-emitting Si nanostructures formed by swift heavy ions in *a* - Si:H/SiO_2 multilayer heterostructures”. Mater. Res. Express, **4**, p. 085001, 2017.

3. C.G. Kirkpatrick, J.R. Noonan, B.G. Streetman. “Recombination luminescence from ion implanted silicon”. Radiation Effects, **30**, pp. 97-10, 1976.

Growing on silicon multilayer heterostructures of Ge/SiGe for optoelectronics

T.M. Burbaev, Yu.G. Sadofyev, M.A. Akmaev[1], V.Ya. Aleshkin[3], Yu.A. Aleshchenko[1,2], A.V. Klekovkin[1,4], A.V. Muratov[1], A.V. Novikov[3], V.V. Ushakov[3], P.A. Yunin[3], D.V. Yurasov[3]

1. P.N. Lebedev Physical Institute RAS, Moscow, Russia, e-mail: aklekovkinbox@gmail.com

2. National Research Nuclear University "MEPhI", Moscow, Russia, e-mail: YAAleshchenko@mephi.ru

3. Institute for Physics of Microstructures RAS, 603950, Nizhny Novgorod, Russia, e-mail: director@ipmras.ru

4. Institute of Ultrahigh Frequency Semiconductor Electronics RAS, Moscow, Russia, e-mail: mail@isvch.ru

With the undoubted dominance of silicon as the main material of microelectronics, the problem of creating photonics elements (emitters, photodetectors, modulators) integrated on Si-substrates, which is necessary for improving the speed of integrated circuits, still not solved. Solution of this problem is the development of photonic elements based on silicon-germanium heterostructures. The heterosystem "buffer layer $Si_{1-z}Ge_z$ / active layer $Si_{1-x}Ge_x$" over a wide range of composition changes x and z forms II-type heterostructures. Transitions in such systems are indirect in real space. This fact leads to a decrease in the absorption coefficient and an increase of the lifetime. In work [1], it is proposed to use a multilayer $Ge/Si_{1-x}Ge_x$ superlattice with quantum wells (QWs) formed by Ge layers and $Si_{1-x}Ge_x$ barriers enriched with germanium to create monolithically integrated with silicon photonic devices. Such structures are I-type heterostructures and can be used to create modulators whose operation principle is based on the Quantum-confined Stark effect (QCSE) for direct-band transitions in a QW formed by a Ge layer.

In the present work, multi-layer heterostructures of the I-type (strained superlattices) with QWs (Ge layers) and barriers ($Si_{1-x}Ge_x$ layers) are developed and grown on silicon substrates by molecular-beam epitaxy. The Si (001) / buffer $Si_{1-z}Ge_z$ / ($Si_{1-x}Ge_x$ / Ge) × n / $Si_{1-z}Ge_z$ -cap structures with a high germanium content in the layers (x, z ~ 1, z> x) are grown on a completely relaxed Si buffer layer (001) / buffer $Si_{1-z}Ge_z$, with a low density of germinating dislocations. Parameters of repeating layers of the superlattice ($Si_{1-x}Ge_x$ /Ge) × n in composition and thickness provided compensation of elastic strains (n repetitions).

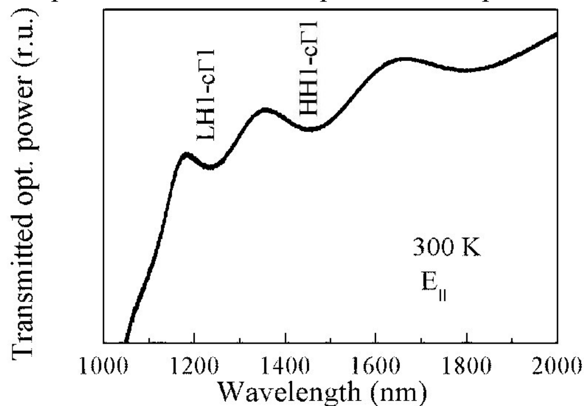

Fig. 1. Normalized transmission spectrum of a $Ge/Si_{1-x}Ge_x$ heterostructure. T = 300 K, the vector E of transmitted light is parallel to the planes of the layers.

The transmission spectra of multilayer $Ge/Si_{1-x}Ge_x$ heterostructures were measured by infrared spectroscopy. Figure 1 shows the transmission spectrum of one of the structures. The spectrum clearly shows the minima associated with absorption on the direct-band excitonic transitions between the valence band and the conduction band in the center of the Brillouin zone (Γ -point). The position of the lines corresponds to transitions between the levels of size quantization for electrons in the conduction band and for holes (heavy HH and light LH) in the valence band in the QW.

Thus, the obtained I-type heterostructures with a direct-band energy spectrum give a chance, after improving the growth technology (reducing the number of dislocations), to use such structures for monolithic integrated silicon nanophotonics elements in the telecommunications range.

In the IR measurements, was used the equipment of the Centre of Collective Usage FIAN.

Yu.A. Aleshchenko thanks for the support of the Program for Enhancing the Competitiveness of the NRNU MEPhI.

The work was supported by the Russian Foundation for Basic Research, project No. 16-02-00986, No. 16-29-03352 ofi_m and the RAS Presidium Program.

1. Marris-Morini D., Chaisakul P., Rouifed M.-S. et al. "Towards low energy consumption integrated photonic circuits based on Ge/SiGe quantum wells", J. Nanophotonics, **2**, pp. 279-288, 2013.

Concept of glass formation in chalcogenide systems and the possibility of predicting new compounds for micro- and nanoelectronics

N. Korobova, S. Timoshenkov, V. Minaev

Institute of Nano-MicroSystem Technique, National Research University of Electronic Technology (MIET), Zelenograd, Moscow, Russian Federation. korobova0210@gmail.com

An important place among semiconductors belongs to chalcogenide vitreous semiconductors (CVS) of heavy metals. For decades due to the unique complex of electronic and optical properties CVS are the basic materials of micro- and optoelectronics.

General principles of the structural and energy concept of glass formation and interpretation of glass properties as one of the varieties of a non-crystalline substance have been developed [1]. Concrete concept of glass formation in chalcogenide systems has been developed and experimentally tested, which made it possible to establish a number of new regularities. Analysis of glass formation in the binary chalcogenide systems A^{IA}-B^{VI}, A^{IB}-B^{VI}, A^{IIB}-B^{VI}, A^{IIIA}-B^{VI}, A^{IVA}-B^{VI}, A^{VA}-B^{VI}, A^{VIIA}-B^{VI} was previously carried out separately for each group of the periodic table. On the basis of the data systematized in this way throughout the periodic system, the glass-forming ability of the binary alloys was calculated, the patterns of glass formation were determined, and the prognostic calculation of the glass formation regions for systems in which glasses were not known (A^{IA}-B^{VI}, A^{VIIA}-B^{VI}) was made.

The experimental search for all glass formation regions was carried out with our modified simplex method, which minimizes the number of experimental points when a complete glass-forming mass is detected on a concentration triangle with the accuracy of determining the glass formation boundaries equal to the simplex size [2].

Calculation using a modified glass formation criterion, which takes into account the liquidus temperature showed that the glass-forming ability in the binary Ga-Te system increases with increasing distance from the eutectic towards an increase in the gallium concentration and has a maximum 0.279 kJ/(mol·K) at 24-25 at.% Ga. It was confirmed experimentally. Accounting for the energy of covalent ionic (chemical) bonding and liquidus temperature gives a more objective assessment of the glass-forming ability. In this paper we estimated the amount of covalent - ion binding energy E_{cib} in order to predict (quantify) glass properties. This value reflects the dependence of composition properties and glass structure. Quantitative ratio of glass transition temperature T_g and E_{cib}, it means $T_g/E_{cib} = (2.3 \pm 0.3)$ $K \cdot kJ \cdot mol^{-1}$ on the basis of glass softening temperature analysis data (at the cooling melt rate around 180 $K \cdot s^{-1}$) has been obtained for over than twenty binary telluride systems. Maximum deviation from the average value was ± 14.0%. Obtained relation allows predicting T_g for telluride glasses. All synthesized new binary telluride glasses (in accordance with the forecast) were semiconductors with p-type conductivity and $\sigma = \sigma_0 \exp(-E_\sigma/kT)$. Glasses had resistivity from 1.3 to $1.0 \cdot 10^7$ Ohm·cm and activation energy of conductivity E_σ from 0.1 to 1.0 eV.

The forecast of glass formation in more than 30 binary and hundreds ternary chalcogenide systems was carried out. The experimental approbation of the forecast in 2 binary and more than 20 ternary chalcogenide systems has been done. On the basis of new glass-forming systems many original compositions have been synthesized. Their properties have been studied and recommended for electrical switches, memory elements, and optical information recording.

1. V.S. Minaev, *Semiconducting Chalcogenide Glass. Series Semiconductors and Semimetals*. Elsevier Academic Press, NY, 2004.

2. V.S. Minaev, S.P. Timoshenkov, V.P. Vassiliev, E.V. Aleksandrovich, V.V. Kalugin, N.E. Korobova. “The concept of polymer nano-heteromorphic structure and relaxation of the glass-forming substance by chalcogenides, oxides and halides example. Some results and perspective”, Journal of Optoelectonics and Advanced Materials, **18** (1-2), 10-23, 2016.

Crystallization and amorphization of Ge-Sb-Te thin films by ns-laser pulses

P. Lazarenko[1], Y. Vorobyov[2], M. Savelyev[1], A. Yakubov[1], A. Sherchenkov[1], S. Kozyukhin[3], A. Gerasimenko[1], V. Glukhenkaya[1], A. Polohin[1]

1. National Research University of Electronic Technology, Zelenograd, Russia, alexsey007@mail.ru
2. Ryazan State Radio Engineering University, Ryazan, Russia, juriy.vorobjov@gmail.com
3. Kurnakov Institute of General and Inorganic Chemistry of RAS, Moscow, Russia, sergkoz@igic.ras.ru

Currently, phase change materials, in particularity compositions of Ge-Sb-Te (GST) system, is intensively investigated. This is due to the perspectives of using GST thin films in the different integrated optical waveguide devices (Mach-Zehnder modulators, ring resonators, full optical memory) [1]. The fast reversible phase transition between amorphous and crystalline states is the basis of their operation. However, phase transformation mechanisms in Ge-Sb-Te thin films under the short laser irradiation is not well investigated. In this work we investigated phase transition induced by nanosecond laser pulses for the most promising $Ge_2Sb_2Te_5$ compound, which has already wide used in the rewritable optical disks.

Investigated thin films were deposited by dc-magnetron sputtering. The thicknesses of the films were estimated by the atomic force microscopy (AFM NT-MDT SolverPro) and were 130 nm. Investigations of the composition by Auger spectroscopy (Perkin Elmer PHI-660) showed that the deposited films had compositions close to $Ge_2Sb_2Te_5$. According to the X-ray diffraction (XRD, Rigaku Smart Lab) as-deposited films were amorphous. The exposure of the samples by nanosecond laser pulses was performed at the wavelength of 532 nm with 16 ns duration. The polarizing Glan-Taylor prism was used in the optical scheme to adjust the fluence of the beam. Scanning electron microscope (SEM Helios NanoLab 650) and profilometer were used for the investigation of the film morphology. The Horiba LabRAM HR Evolution spectrometer (He-Ne laser, (633 nm, 10 mW) was used for Raman study. Conductive AFM (C-AFM, NT-MDT Ntegra) at 0.5 V bias voltage was used to map electrical conductance across the modified areas of the experimental samples.

The effect of excitation by pulses of different energy fluence (from 57 to 125 mJ/cm^2) and their number (from 1 to 6) for the $Ge_2Sb_2Te_5$ thin film was analyzed. Four different ranges of irradiation parameters causing crystallization, amorphization, re-amorphization and ablation of the $Ge_2Sb_2Te_5$ thin films by nanosecond laser pulses were identified. Results of investigations showed that these processes in $Ge_2Sb_2Te_5$ thin films were accompanied by the significant changes in the optical reflectivity, Raman spectra and electrical conductivity. Computer simulation of the temperature distribution in the irradiated regions correlates with the obtained experimental results.

This work was supported by the Russian Science Foundation (project number 17-79-10465).

1. M. Wuttig, H. Bhaskaran, and T. Taubner. “Phase-change materials for non-volatile photonic applications”. Nat. Photon, **11**, pp. 465–476, 2017.

Mechanical properties and adhesion of $Ge_2Sb_2Te_5$ thin films obtained by different deposition methods

A. Yakubov[1], A. Sherchenkov [1], I. Bdikin[2], P. Lazarenko[1], D. Terekhov[1], A. Babich[1]

1. National Research University of Electronic Technology, Zelenograd, Russia, alexsey007@mail.ru

2. Department of Mechanical Engineering & Centre for Mechanical Technology & Automation, University of Aveiro, Portugal, bdikin@ua.pt

Electrical phase change memory (PCM) is candidate for the new generation of memory devices, and is actively developed now. The most promising compound used for the PCM devices fabrication is $Ge_2Sb_2Te_5$ (GST225) composition lying on the quasi-binary line GeTe-Sb_2Te_3.
However, despite the progress PCM technology needs to be improved. One of the tasks is to ensure adhesion of the GST225 layer in the multilayered PCM cell heterostructure. In addition, the contacts between materials are highly dependent on their mechanical properties, which can play important role in the formation of the boundary characteristics of the heterostructures. At present, the mechanical properties of the GST225 layer are weakly studied.
So, the aim of this work is investigation of the mechanical properties and adhesion of $Ge_2Sb_2Te_5$ thin films obtained by various deposition methods on different substrates and layers.
Thin films of GST225 were obtained by thermal evaporation in vacuum (TEV) and magnetron sputtering (MS). The synthesized material and the monolithic target of GST225 were used for the TEV and MS, respectively. The thicknesses of the films were estimated by the atomic force microscopy (AFM NT-MDT SolverPro) and were 130 nm for both methods.
Investigations of the composition by Energy Dispersive X-ray analysis (EDX, CAMEBAX, Cameca) and Auger spectroscopy (Perkin Elmer PHI-660) showed that the deposited films had compositions close to GST225.
The nanoindentation (nanoindentor B-J53) measurements were performed using a three-sided pyramidal Berkovich diamond indenter having a nominal edge radius of 20 nm (faces 65.3° from vertical axis) attached to a fully calibrated nanoindenter (TTX-NHT, CSM Instruments). During the measurements maximum indentation load was varied in the range of 0.1 – 50 mN.
Atomic force microscopy (AFM Multimode Nanoscope (IV) MMAFM-2) was used for evaluation of the adhesion properties. To determine the adhesion properties during the measurement, the normal force was varied from 0.88 to 80 μN.
The mechanical and adhesive properties were investigated for GST225 thin films deposited on silicon and oxidized silicon substrates and various sublayers (TiN + W, W, TiN, Al, NiCr) formed by magnetron sputtering. The thicknesses of Al, W and TiN layers were 300 nm, of TiN+W layer was 250 nm and of NiCr layer was 200 nm.
The measurements by nanoindentor allowed to determine such mechanical properties as hardness, stiffness, and Young's modulus. In general, the hardness, stiffness and Young's modulus increase with the depths of the groove. However, the hardness and Young's modulus in most cases demonstrate saturation, while the stiffness monotonically increases with the depth. The deposition method has a significant effect on the mechanical properties. The hardness and Young's modulus of GST225 thin films deposited by the MS method are higher compared to TEV.
The highest hardness was determined for TiN layers (5292 and 5937 MPa for TEV and MS, respectively), TIN + W (4732 and 5254 MPa for TEV and MS, respectively) and the lowest for Al layer (3041 and 4040 MPa for TEV and MS, respectively).
Investigation of the adhesion showed that the GST225 thin films deposited on the NiCr and Al sublayers have the highest adhesion, while the lowest adhesion is characteristic for the films fabricated on the Si substrate.
So, mechanical properties and adhesion of GST225 layers were investigated. It was revealed that the deposition methods of $Ge_2Sb_2Te_5$ thin films affects the mechanical properties and adhesion of the layers.
This work was supported by the Russian Federation President's grant (MK-6347.2018.3).

Influence of annealing on nanocrystalline $LiNbO_3$ films properties

Z.E. Vakulov[1], R.V. Tominov[1], Yu.N. Varzarev[1], E.G. Zamburg[2], I.E. Clemente[3], A.V. Miakonkikh[3], K.V. Rudenko[3], O.A. Ageev[1]

1. Institute of Nanotechnologies, Electronics and Equipment Engineering, Taganrog, Russia, zvakulov@sfedu.ru.

2. National University of Singapore, Singapore, Singapore, zamburg.evgeniy@gmail.com

3. Institute of Physics and Technology of Russian Academy of Sciences, Moscow, Russia, miakonkikh@ftian.ru

Currently, the development of piezoelectronics is characterized by fabrication of a large number of functional devices, while ferroelectric films application in micro- and nanoelectronics is substantially limited due to the lack of compatible fabrication technology of thin ferroelectric films. High Curie temperature of lithium niobate ($LiNbO_3$) makes it a promising candidate for using in devices for collecting energy from mechanical vibrations at high temperatures [1].

Prospective fabrication technique of ferroelectric films is pulsed laser deposition (PLD), which allows controlling a large number of technological parameters and provides the possibility of obtaining films with controlled properties [2, 3].

The purpose of this work is a study of the effect of annealing in an oxygen atmosphere on the properties of nanostructured $LiNbO_3$ thin films fabricated by PLD technique.

For the fabrication of the $LiNbO_3$ thin films, we used nanotechnological cluster complex NANOFAB NTK-9 (NT-MDT, Russia), comprising PLD module Pioneer 180 (Neocera Co., USA). Ablation of the $LiNbO_3$ target (Kurt J. Lesker Co., USA) was carried out by KrF excimer laser (λ = 248 nm) under energy density on the target surface of 2.5 J/cm^2 and the number of laser pulses of 80 000. The target-substrate distance was 70 mm. The formation of the films was carried out on silicon substrates. The repetition rate of the laser pulses was 10 Hz. Annealing of the films was accomplished under a temperature of 600 ° C and pressure of $1 \cdot 10^{-1}$ Torr, for 1 hour. The morphology of obtained films was studied using the Ntegra probe laboratory (NT-MDT, Russia) by atomic force microscopy technique (AFM).

Under the influence of annealing, the surface roughness of obtained $LiNbO_3$ films decreases from 63 to 47 nm, and average grain diameter decreases from 110 to 64 nm. In addition, annealing influence the shape of the grains. For non-annealed $LiNbO_3$ films formations of triangle grains and as well as large drops on the film surface are characteristic. Decreasing in surface roughness of the films and droplet density under the influence of annealing in an oxygen atmosphere can be associated with the activation of solid-state interactions in the near-surface layer and the processes of niobium oxidation.

Using of annealing procedure during the formation of $LiNbO_3$ films made it possible to reduce the maximum value of absorption rate from 1.12 to 0.29 due to a decrease in the surface roughness of the films.

Thus, the influence of the annealing of $LiNbO_3$ films in an oxygen atmosphere on their morphological properties was studied. It is shown that the surface roughness of $LiNbO_3$ films (from 63 to 47 nm) and the density of droplets on the surface of $LiNbO_3$ can be substantially reduced by using annealing. Obtained results can be used to create energy converters for use in electronics and medicine, as well as acousto-optics devices.

This work was financially supported by the Russian Foundation for Basic Research № 18-29-11019_mk. The work was done on the equipment of the Research and Education Centre «Nanotechnology» and Collective Use Centre «Nanotechnology», Southern Federal University.

1. R.W.C. Lewis, D.W.F. Allsopp, P. Shields, A. Šatka, S. Yu, V.Yu. Topolov, and C.R. Bowen. "Nano-imprinting of highly ordered mano-pillars of lithium niobate ($LiNbO_3$)". Ferroelectrics, **429**, pp. 62–68, 2012.

2. A. Tumuluri, M.S.S. Bharati, S.V. Rao, and K.C.J. Raju. "Structural, optical and femtosecond third-order nonlinear optical properties of $LiNbO_3$ thin films". Mat. Res. Bul., **94**, pp. 342–351, 2017.

3. Z.E. Vakulov, E.G. Zamburg, D.A. Golosov, S.M. Zavadskiy, A.V. Miakonkikh, I.E. Clemente, K.V. Rudenko, A.P. Dostanko, O.A. Ageev. "Effect of substrate temperature on the properties of $LiNbO_3$ nanocrystalline films during pulsed laser deposition". Bull. Rus. Acad. Sci.: Phys., **81**, pp. 1476–1480, 2017.

Materials based on $AgGaS_2$ for X-ray Detection

S. Asadov[1], S. Mustafaeva[2], V. Lukichev[3]
1. Institute of Catalysis and Inorganic Chemistry, Baku, Azerbaijan, E-mail: salim7777@gmail.com
2. Institute of Physics, Baku, Azerbaijan, E-mail: solmust@gmail.com
3. Institute of Physics and Technology (RAS), Moscow, Russia, E-mail:lukichev@ftian.ru

The aim of this study was to obtain optically homogeneous based $AgGaS_{2x}Se_{2-2x}$ (x = 0, 0.5, 1) single crystals with high X-ray sensitivity. Single crystals were grown by the Bridgman–Stockbarger (BS) technique [1] and also using the method of chemical transport reactions (CTR) [2].
$AgGaS_{2x}Se_{2-2x}$ was synthesized from its elementary components: Ag (high purity grade), Ga (5N grade), S (high purity grade, TU 609254677), and Se (TU 6-09-2521-77). The initial synthesis components were taken in a stoichiometric ratio. The synthesis was performed in a horizontal furnace with the temperature within it increasing at a rate of 50 K/h to 1275 K. The reaction between the components proceeded for 4 h.
The synthesized material was transferred to an ampule into a dual chamber vertical furnace for growth. $AgGaS_2$ single crystals were grown using the Bridgman–Stockbarger technique. The $AgGaS_2$ melting temperature was $T_m = 1271 \pm 3$ K. The thermal conditions in the furnace were maintained using VRT-3 high-precision temperature controllers. The temperature gradient at the crystallization front in the furnace was 3 K/mm. The ampule with molten material was lowered vertically and cooled at a rate of 0.5 mm/h. Following crystallization, the furnace was turned off and cooled to room temperature together with the sample.
The growth of $AgGaS_{2x}Se_{2-2x}$ (x = 0; 0.5 и 1.0) single crystals was performed by the CTR method. $AgGaX_2$ (X – S, Se) are taken together with the transporting agent iodine in the ampoule for the crystal growth. They react to form the gaseous binary iodides and selenium at high temperature. All these gaseous species diffuse to the colder growth zone due to the drop-in temperature. At the growth zone they react back to form the ternary chalcogenide with the release of iodine. The iodine liberated diffuses back to the source end to form the metal iodides once again. The chemical reaction for $AgGaSe_2$ may be given as

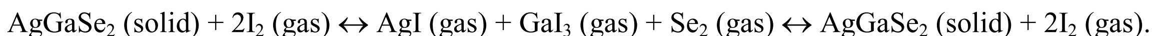

$$AgGaSe_2\ (solid) + 2I_2\ (gas) \leftrightarrow AgI\ (gas) + GaI_3\ (gas) + Se_2\ (gas) \leftrightarrow AgGaSe_2\ (solid) + 2I_2\ (gas).$$

The main advantage of growing single crystals using the CTR method is the ability to conduct the process at lower temperatures and pressures.
The results of X-ray studies at room temperature showed that single crystals based on the $AgGaS_2$ compound crystallize in the chalcopyrite structure with the lattice parameters a = 5.7571–5.7572 Å and c = 10.3110–10.3036 Å for $AgGaS_2$ and a = 5.992; c = 10.883 Å for $AgGaSe_2$.
It was established that $AgGaS_{2x}Se_{2-2x}$ single crystals grown by chemical transport reactions method (CTR) method are characterized by high values of X-ray sensitivity coefficients (K) at room temperature. The roentgendosimetric characteristics of $AgGaS_{2x}Se_{2-2x}$ single crystals of different composition are compared. Of all the compositions studied, $AgGaSe_2$ single crystals had the highest X-ray sensitivity. For example, at an effective radiation hardness of 30 keV and a dose rate of E = 10 R/min $K = 5.4 \times 10^{-13}$ (A·min)/(V·R) for $AgGaS_2$ and $K = 15 \times 10^{-13}$ (A·min)/(V·R) for $AgGaSe_2$. It was demonstrated that for $AgGaS_2$ (BS - Bridgman–Stockbarger) $K = 1.3 \times 10^{-11}–1.4 \times 10^{-10}$ (A·min)/(V·R) at an effective radiation hardness of V_a = 25–50 keV and dose rate of E = 0.75–78.05 R/min.

Acknowledgements. This work was supported by the Science Development Foundation under the President of the Republic of Azerbaijan, grant EİF-BGM-3-BRFTF-2+/2017-**15/05/1,** project AzRus1/2018 and RFFI Az_a_2018**.**

1. S.N. Mustafaeva, M.M. Asadov, and D.T. Guseinov, "X-ray dosimetric properties of $CdGa_2S_4$ single crystal grown from the gas phase". Inorg. Mater., **46** (6), pp. 587-293, 2010.
2. M.M. Asadov and S.N. Mustafaeva, "X-ray Dosimetry of an $AgGaS_2$ Single Crystal". Bul. Rus. Acad. Sci. Physics, **79** (9), pp. 1113-1119, 2015.

Comparative study of the dependence of line edge roughness of resists patterns on its molecular structure

A. Sharapov[1,2], G. Baranov[1,2], A. Shishlyannikov[1,2], A. Tatarintsev[3], O. Gushin[1], K. Rudenko[3]
1. Molecular Electronics Research Institute, Zelenograd, Russia, asharapov@niime.ru
2. Moscow Institute of Physics and Technology, Dolgoprudny, Russia, andrey.sharapov@phystech.edu
3. Institute of Physics and Technology Russian Academy of Sciences, Moscow, Russia, rudenko@ftian.ru

Permanent development of CMOS integrated microchips manufacturing technologies means in the first place the scaling of transistors critical dimensions. However, dispersion of these values is not scaled [1]. This leads, in particular, to the fact that the relative roughness of linear structures edges increases.

The key quantitative parameter to be controlled is the line-edge roughness (LER). There are a number of methods to measure LER, such as scanning electron microscopy (SEM), atomic force microscopy, scatterometry which provide also the information on spatial distribution of roughness. The most well-known methods of LER calculation from SEM images are examined for the stability in [2]. Using the self-developed 'LER&LWR Calculator' to process all the SEM images we obtained the results both for the average value of LER and the power spectral density (PSD). The spatial complexity and the frequency distribution were studied to detect the sources of roughness among various microscopic factors.

Based on comparison of modern resists in [3], we conducted the experiment within this research using 1 negative and 5 positive resists:

1. Dow Corning XR–1541
2. JSR MES EP555JE
3. OEBR CAN038AE
4. OEBR 112
5. OEBR 164
6. ZEP-520A

Using the product information provided by the resist manufacturers we identified the components with the highest relative weight proportion for each resist. We analyzed the behavior of these components during the processes of lithography, post-exposure baking and etching based on previous reports.

We studied the chemical reactions and the products during each technological procedure. Based on the conclusion [4] that there is no straight relationship between LER and molecular weight of resist components, we also studied within this research the aggregate structures formed by the polymers molecules during the development phase. At each stage we estimated the sizes of the nonuniform structures at the molecular level and their contribution to the spatial complexity of roughness.

Finally, we compared the resulting LER on the structures with the lowest pitch we could achieve on all of the resists (30 nm). The results suggest that despite the observation that low-molecular-weight resists are not necessarily advantageous in reducing LER, the size of aggregates formed by them is lower, hence it is theoretically possible to achieve the lower resulting LER specifying certain parameters of technological procedures.

1. International Technology Roadmap for Semiconductors, 2011.
2. A. Sharapov and G. Baranov. "Comparative analysis of measurements methods of the nanoscale roughness quantitative characteristics". Proceedings of MIPT, **10**(2), pp. 72-79, 2018.
3. G. Krasnikov, O. Gushin, A. Shishlyannikov, E. Gornev, N. Orlikovskiy, and A. Tatarintsev. "Investigation of process parameters of modern electronic resists". El. Eng. Ser. 3. Microelectronics, **3**(167), pp. 33-52, 2017.
4. T. Yamaguchi, K. Yamazaki, and H. Namatsu. "Influence of molecular weight of resist polymers on surface roughness and line-edge roughness". J. Vac. Sci. Technol. B, **22**(6), pp. 2604-2610, 2004.

Dry&Wet Hybrid Electron Lithography

M.A. Bruk[1], E.N. Zhikharev[2], A.E. Rogozhin[2]
1. L.Ya. Karpov Institute of Physical Chemistry, Moscow 105064, Russia
2. Institute of Physics and Technology of RAS, Moscow 117218, Russia

Earlier [1, 2], we proposed Dry E-beam Etching of Resist (DEBER) technology, which allows: 1) to form an image directly during exposure (without additional development stage); 2) significantly (in tens and hundreds of times) to reduce the required dose of exposure; 3) in a single-stage process, to form micro- and nanostructures with a well rounded section profile of a given shape, including sinusoidal; 4) to form 2D and 3D structures with high accuracy of vertical dimensions (about 1 nm). However, the proposed method has significant drawbacks, the main ones of which are low lateral resolution (not better than 100 nm) and low contrast of the image. The traditional wet EL technology is known to obtain an image with a high lateral resolution and high contrast. It seems to us that the hybrid method (mix of ordinary e-beam lithography and DEBER) is of great interest. According to the method, in the first stage large regions are formed that do not contain small critical elements by the DEBER method. This is much faster than ordinary e-beam lithography. In the second stage after sample cooling to room temperature and additional e-beam focusing correction, (if necessary), the critical relief elements could be formed with ordinary high-resolution e-beam lithography. Such a "hybrid" process can open up new possibilities for the use of EL, for example, in optics, photonics, 3D structuring, and other fields.

In this paper, the first results of developing a hybrid EL are presented. Using the PMMA resist as an example, it was shown that the formation of an image in resist layer by the DEBER method does not prevent the subsequent formation of drawing in the same layer by the wet-technology. "Hybrid" samples were obtained in which on the relief in PMMA, obtained by the DEBER method, arrays of lines, frames, "wells", pillboxes were formed by the standard wet EL. The image on the wet stage can be formed both in the unexposed in the first stage, and in the exposed areas of the resist. The possibility of implementing a hybrid technology in our opinion is due to two main factors: the smallness of the doses received by the sample at the DEBER stage, and the self-developing of the image during the exposure of the sample at this stage.

1. M.A. Bruk, E.N. Zhikharev, D.R. Streltsov, V.A. Kalnov, A.V. Spirin. The new dry method of mask (relief) formation by direct electron-beam etching of resist. Microelectron. Eng., **112**, pp. 1-4, 2013.
2. M.A. Bruk, E.N. Zhikharev, A.E. Rogozhin, D.R. Streltsov, V.A. Kalnov, S.N. Averkin, and A.V. Spirin. Formation of micro- and nanostructures with well-rounded profile by new e-beam lithography principle. Microelectron. Eng., **155,** pp. 92-96, 2016.

Formation of nanosized elements by ion beam lithography for multiple fin field effect transistor prototyping

K.A. Tsarik[1], A.I. Martynov[1], S.D. Fedotov[1,2], V.K. Nevolin[1]
1. National Research University of Electronic Technology, Moscow, Russia, tsarik_kostya@mail.ru
2. Epiel JSC, Moscow, Russia, fedotov@epiel.ru

Currently, the leading companies in the semiconductor industry in the creation of new field nanotransistors with minimum topological dimensions of 32 nm and below work in the direction of creating transistors with a three-dimensional gate structure in the form of fin (FinFET). The topology in the form of a "fin" or "crest" allows creating a volumetric nano-sized channel on a dielectric substrate, which helps to avoid serious short-channel effects [1]. For small-scale production of micro- and nanoelectronic devices, it is desirable to use a lithographic method that does not require the production of templates (without a mask) and characterized by a relatively high performance. This method is lithography with a focused ion beam (FIB), which has a number of advantages over electron beam radiation. The ions have a larger mass in comparison with the electrons and therefore give up their energy more efficiently, and the scattering of the beam is smaller in this case [2]. The diffraction limit is practically absent because of the extremely small de Broglie wavelength of the ions. In addition, the effect of masking by gallium ions the near-surface region in silicon for resistance to plasma-chemical etching (PCE) is known [3].

In this paper, the developed technique for the formation of nanoscale silicon fins on silicon-on-sapphire structures based on FIB and PCE was demonstrated. The stability of the obtained mask to PCE was investigated depending on the dose of ionic exposure. It was found that the Si fin 150 nm in height and a width of less than 40 nm was obtained by implantation of Ga ions with a dose of 4×10^{17} до 5×10^{17} $см^{-2}$. The FIB module, which is part of the nanotechnology facility Nanofab-100, was used. The ion beam current should be 30 pA, the exposure time 0.1 microseconds, the number of passes is 56000. The minimum exposure time for etching absence was chosen. After the ion beam exposure, the substrates were treated with plasma in a Corial 200IL unit for 30 seconds, where gases were supplied: SF_6 (25 sccm) and O_2 (1.5 sccm). Geometric dimensions of silicon structures were investigated by the atomic force microscopy (AFM). Sixty fins with a length of more than 15 microns were created in groups of 10 fins in each. Alignment marks in the form of crosses of 15x15 μm were created near each group.

The creation of contacts to the extended fin form silicon nanostructures was carried out by FIB exposing the electronic resist 950-PMMA-A2. After development, this resist served as a mask for lift-off resist (LOR).The development depth of this resist in methyl isobutyl ketone was studied at different values of FIB exposure time. The required thickness of LOR was 300 nm, thickness of PMMA - 40 nm and the exposure time in each pixel was 22 μs, with beam current of 1pA and ion beam size of 7 nm and no overlap between neighboring points in exposure process. Control of lithographic processes was carried out by optical microscopy, an AFM, and a visualization of a FIB. In the created prototypes of the transistor, the length of each channel was 1.2 μm, and the gate - 100 nm. The drain and source contacts were made of nickel 50 nm thick. Measurements were in the range from -2 to 2 V and the current-voltage characteristic (VAC) was in the form of a slightly increasing exponent. The gate dielectric Al_2O_3 2-3 nm thick was deposited by the ALD method. The controllability of the channel which is created by nano-sized silicon fin was investigated. The current-voltage characteristic Id (Uds) was measured and analyzed by applying the Uds voltage from 0 to 3 V for the range of the voltage Ugs applied to the gate from 0 to +0.7 V. Also the current-voltage characteristic Id(Ugs) was measured by applying the gate voltage of Ugs from -2.5 to 2 V for the Uds = 3 V. The obtained I-V characteristics prove the good controllability of the channel in the nanosized fin and demonstrate the operability of the devices.

This work was carried out with the financial assistance of the Ministry of Education and Science in the framework of state task 16.2056.2017/4.6.

1. R.W. Keyes. Rep. Prog. Phys., **68**, pp. 2701–2746, 2005.
2. K.K. Lavrentyev, V.K. Nevolin et al. Russian Microelectronics, **45**, pp. 451-454, 2016.
3. M.D. Henry, M.J. Shearn, B. Chhim, A. Scherer. Nanotechnology, **21**, paper № 245303, pp.1-8, 2010.

Mask formation on GaAs substrate by focused ion beams of Ga^+ for plasma chemical etch

I.N. Kots[1], V.S. Klimin[1,2], V.V. Polyakova[1], A.A. Rezvan[1], O.A. Ageev[2]
1. Southern Federal University, Institute of Nanotechnologies, Electronics, and Equipment Engineering, Department of Nanotechnologies and Microsystems, Taganrog, Russia, E-mail address: inkots@sfedu.ru
2. Southern Federal University, Research and Education Center "Nanotechnology", Taganrog, Russia, E-mail address: ageev@sfedu.ru

At the present time, optical lithography has reached its limit in the field of deep ultraviolet, and in connection with this, the study of new methods for the nanoscale structures formation is an urgent task. In the field of nanoelectronics, electronic components are actively developing. Their size decreases, which is accompanied by a decrease in energy consumption and increased productivity. A promising method of nanoscale profiling is the combination of focused ion beam and plasma chemical etching methods. The method of focused ion beams is based on the interaction of accelerated gallium ions with the sample surface. This method allows us to modify the material without using a mask. The purpose of this work is to obtain nanoscale structures on the surface of A_3B_5 materials without the optical lithography use. One of the tasks posed is to study the surface of gallium arsenide modification by a focused ion beam for subsequent plasma-chemical treatment.

At the initial stage of the experimental studies, we have formed templates in the .bmp format for formation the irradiated Ga^+ region on the sample surface. Next, the test structures formation was performed on the generated template on a scanning electron microscope with an ion column Nova NanoLab 600 (FEI Company, Netherlands) at accelerating voltages from 10 to 30 keV, ion beam current of 1 pA and the ion beam passes number from 10 to 100. In the next stage of the experimental studies, the samples were etched in the chlorine-containing plasma in the Semiteq STE ICPe68 unit at a power of W_{ICP} = 200 W, W_{RIE} = 10 W at an etching time from 15 to 180 seconds. For experimental studies, we take gallium arsenide with an orientation of 100. We have carried out modification of the gallium arsenide surface substrates on 5x5 μm regions. We have investigated the morphology study was carried out on a scanning probe microscope Ntegra Vita (NT-MDT, Russian Federation).

As a result of investigations it was established that after plasma chemical etching the area irradiated by the focused ion beam method was higher than the level of the remaining substrate. With an increase in the accelerating voltage from 10 to 30 keV and the etching time from 15 to 180, the height of the resulting structures increased from 15 to 140 nm.

It can be seen from the results obtained that when the accelerating voltage is increased and the etching time is increased, the height of the resulting structures increases. This can be explained by a more intense tanning of the material with an increase in the accelerating voltage and an increase in the actual etching depth in the plasma with increasing etching time. The tanned layer in turn acts as a mask for chlorine containing plasma. With an increase in the ion beam passes number, the modified regions exhibit large masking properties. In the course of the work, the structure height as a function of the number of passes and the time of etching in the plasma were obtained. These dependences show that with 100 passes of the ion beam, with an increase in the etching time from 15 to 180 seconds, the height of the resulting structures will increase from 15 to 140 nm. The number of passes also affects the height of the structures, but with a longer etching time in the plasma, the difference in height is greater. With a short etching time in the plasma, with a small number of ion beam passes through the surface, etching is stimulated.

This technology can be used to form the structures and functional layers of quantum and optical nanoelectronics devices that require high resolution.

The results were obtained using the equipment of the Research and Education Center and the Center of Collective Use "Nanotechnology" of the Southern Federal University. This work was supported by the Russian Science Foundation Grant No. 15-19-10006

Nanoscale profiling of A_3B_5 surface by the local anodic oxidation and plasma chemical etching

V.S. Klimin[1,2], M.S. Solodovnik[1,2], R.V. Tominov[2], A.A. Rezvan[1], O.A. Ageev[2]
1. Southern Federal University, Institute of Nanotechnologies, Electronics, and Equipment Engineering, Department of Nanotechnologies and Microsystems, Taganrog, Russia, E-mail address: klimimnvs@sfedu.ru
2. Southern Federal University, Research and Education Center "Nanotechnology", Taganrog, Russia, E-mail address: ageev@sfedu.ru

The current pace of electronics development leads to a magnification in the density of elements arrangement on a single crystal, as well as a significant reduction in their technological dimensions. Due to this fact, there is a toughening of requirements to precision methods of forming elements of micro- and nanoelectronics. Thus, the main problem of technology of forming devices based on gallium arsenide is to find and improve methods of surface treatment. Moreover, it must possess the resolving power and high accuracy of the process, which directly corresponds to given parameters. In addition, surface of structures obtained by this technology should be characterized by a high degree of quality [1].

The combination of local anodic oxidation with subsequent chemical etching in low temperature plasma is a promising technology for formation of a complex surface relief of nanoscale structures, their modification and profiling. The main feature of this method is possibility of high precision variation of nanoscale processing. In addition, extra operations of surface cleaning of residual reaction products and various impurities from the starting reagents are not required for this technology.

The substrate material was plates of peculiar gallium arsenide. Geometric parameters of surface were improved by standard liquid polishing. Further, substrate's surfaces were subjected to modification by the method of local anodic oxidation, and, as a result, a layer of oxide nanostructures was formed. These oxide nanoscale structures were obtained at the following formation parameters: relative humidity RH = 90%, probe travel speed V_P = 2.5 μm/sec, feedback current of the microscope I_F = 1 nA, and formation voltage varied from 7 to 10 V. Studies and the formation of local oxide regions were carried out on a scanning probe microscope Ntegra Vita (NT-MDT, Russia) [2].

The formed oxide layers were used as negative masks for subsequent plasma chemical etching by the SemiTEq STE ICPe68 unit. BCl_3 was chosen as the chlorine containing gas, which differs from analogs in some parameters for the effect of etching of nanostructures based on gallium arsenide in the low temperature plasma. The gas mixture of reaction chamber consisted from a buffer gas N_{Ar} = 100 cm^3/min and a chlorine containing gas N_{BCl3} = 15 cm^3/min at a pressure P = 2 Pa. The power of source consisted from induced-associated plasma W_{ICP} = 400 W, resistive-associated plasma W_{RIE} = 35 W and bias voltage U_{bias} = 102 V. The processing time in the plasma ranged from 0.5 to 2 minutes. Rectangular oxide structures with dimensions of 0.3x0.3μm were formed. In the crystallographic direction [110], the deviation their angle from the vertical was from 10° to 28°, for the crystallographic direction [111] - from 7° to 33°.

In this experimental work, studies were made of the effect of formation regimes of oxide masking layers obtained by the local anodic oxidation method on the anisotropy of the plasma chemical etching process. It is also shown that the surface of the obtained structure, after removal of the oxide layer and plasma chemical etching, has a roughness and a relief comparable to the surface of the initial GaAs plate. Due to this fact, it allows us to conclude that this technology can be introduced into standard processes of micro- and nanoelectronics for production of modern optical and quantum devices nanoelectronics based on GaAs structures.

This research has been supported by the Results obtained using the Research and Education Center and Center for Collective Use "Nanotechnology" South Federal University. This work was supported by the Russian Science Foundation Grant No. 15-19-10006.

1. A.M. Korsunsky, E. Salvati, A.G.J. Lunt, T. Sui, M.Z. Mughal, R. Daniel, J. Keckes, E. Bemporad, M. Sebastiani. *J. Matdes* **145** 55–64, 2018.
2. V.S. Klimin, M.S. Solodovnik, V.A. Smirnov, A.V. Eskov, R.V. Tominov, O.A. Ageev. *Proc. of SPIE* **10224** 102241Z-1, 2016.

Investigation of modes profiling of silicon surface by the method of local anodic oxidation to create promising elements of nanoelectronics

V. Polyakova[1], I. Kots[1], O. Ageev[2]
1. Southern Federal University, Institute of Nanotechnologies, Electronics and Equipment Engineering, Taganrog, Russia, vik5702935@yandex.ru
2. Scientific and educational center of nanotechnology of Southern Federal University, Taganrog, Russia, ageev@sfedu.ru

Today, one of the promising elements of nanoelectronics is one-dimensional filamentary silicon nanostructures that can be used to create not only field-effect transistors and photonics, but also to create THz biosensors that increase sensitivity to adsorbed atoms and molecules [1-2]. One of the problems of creating filamentary nanostructures is their oriented localization on the surface of the material. We propose the solution of these problems by using the method of local anodic oxidation (LAO) in combination with liquid chemical etching in HF. The method of LAO has high resolution and reproducibility, and also allows modification of the substrate surface without additional operations characteristic of photolithography [3].
At the first stage of the investigation, by the method LAO on silicon surface in the contact mode of atomic force microscopy (AFM) by the tip was carried out on the surface of silicon 5 (111), using the Ntegra probe nanotechnology laboratory (NT-MDT, Russia) using tip NSG 10 with a conductive coating of Pt. Various parameters were used to study the LAO mode: voltage pulse amplitude, duration of voltage pulses, probe oscillation frequency, feedback current, relative humidity. As a result, matrices of 49 oxide nanoscale structures (ONS) were formed on the surface of the silicon substrate. Then, the ONS was removed by liquid etching in aqueous HF (1:3) solution at room temperature. As a result, profiled nano-sized (PNS) structures were formed on the silicon surface. Based on the results obtained, plots of the height and diameter of the ONS and PNS were plotted for various applied voltage pulses (Fig. 1).

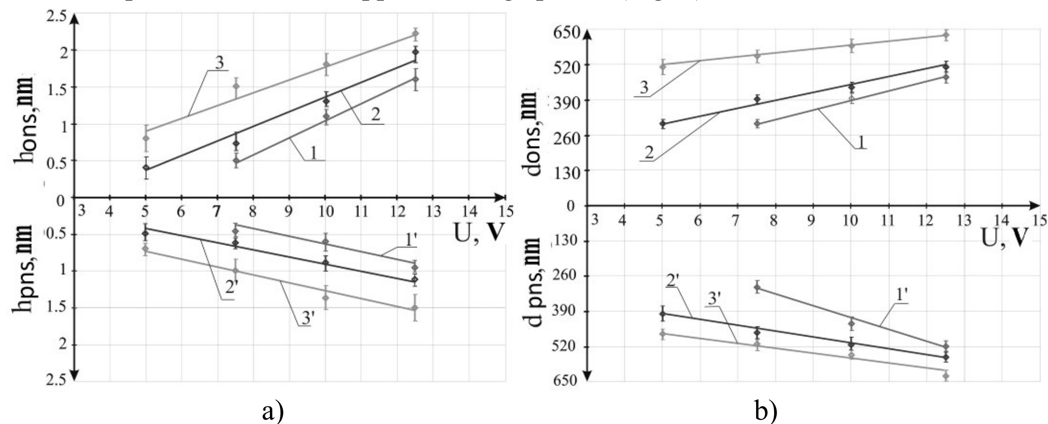

Fig. 1. Dependences of the geometric parameters of nanostructures on the voltage amplitude for LAO at different relative humidity (1, 1 / - 30 ± 1%, 2, 2 / - 50 ± 1%, 3.3 / - 70 ± 1%): a) (1-3) and the depth of the PNS (1 / -3 /); b) the diameters of ONS (1-3) and PNS (1 / -3 /).

This method allows the formation of oriented filamentary nanostructures that can be used to create nanowires, sensor sensors and transistors, as well as can be use for the development of silicon-based nanoelectronics.

1. A.V. Miakonkikh, A.A. Tatarintsev, A.E. Rogozhin, K.V. Rudenko. Technology for fabrication of sub-20 nm Silicon planar nanowires array.The International Conference on Micro- and Nano-Electronics 2016.
2. A.I. Khrebtov, V.G. Talalaev, Yu.B. Samsonenko, P. Werner, V.V. Rutskaya, M.V. Artem'ev, and G.E. Tsyrlin. A Hybrid System of GaAs Whisker Nanocrystals and PbS Quantum Dots on Silicon Substrate Technical Physics Letters, Vol. 40, No. 7, pp. 558–561, 2014.
3. Y.K Ryu1 and R. Garcia. Advanced oxidation scanning probe lithography. Nanotechnology, **28**, pp. 1-17, 2017.

Sidewall defects in deep cryogenic Si etching in SF_6/O_2 plasma: numerical simulation

M. Rudenko, A. Miakonkikh, D. Kurbat, V. Lukichev
Institute of Physics and Technology of RAS, Moscow, Russia, mikhail.rudenko@ftian.ru

Cryogenic plasma etching of silicon is a common type of deep reactive ion etching (DRIE) process, used in the fields of X-ray microscopy, DRAM and MEMS fabrication and 3D ICs integration. These applications impose stringent requirements on the surface quality (low roughness and absence of polymer contamination) of the structures created, giving rise to the need for careful optimization of the process.
A special feature of cryogenic etching is the high sensitivity of the results to the changes in the parameters of the process, such as particle fluxes from the plasma, the temperature of the sample, the bias power and the pressure in the chamber. In such a situation, the experimental procedure for determining the optimal parameters of the etching process becomes very time-consuming [1]. This makes numerical simulation an important tool for optimizing cryogenic etching processes. Special attention should be given to simulation of the development of sidewall defects during high aspect ratio etching.
Methods such as the method of cellular automata [2] and the string / integral equations method [3] are generally employed for the simulation of cryogenic etching. In this paper, the method of macroscopic cells based on the Monte Carlo method is developed. Its distinctive features are the detailed accounting of the state of all silicon atoms in the macrocell and the interaction of the reflected ions with the surface. It allows one to adequately simulate etching modes, in which the stochastic nature of the flow of plasma particles plays a significant role, such as the formation of wall roughness, “nanograss” and subtrenching, and etching with high aspect ratios.
Fig. 1 shows a comparison of some simulation results with experimental data. On the Fig. 1a and Fig. 1b, the development of roughness in the upper part of the wall profile with insufficient oxygen content in the plasma is demonstrated (experimental and modeled respectively). Fig. 1c and Fig. 1d show the experimental and simulated illustration of the effect of the formation of subtrenches while high aspect ratio feature etching in the case of excess of oxygen. Comparison of other types of simulated defects with the experimental results will be given for various parameters of plasma.
Based on the results of numerical simulation, we arrived at assumptions about the mechanisms of formation of sidewall defects of various types. The obtained results can be used to optimize the processes of cryogenic plasma etching of trenches.

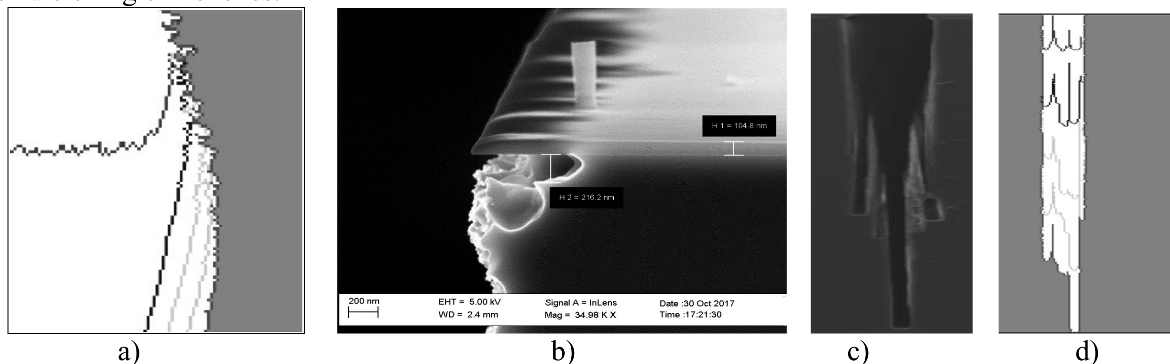

Fig. 1. Defects arising from cryogenic etching: undercut with caverns formation (a - simulated, b - experimental) and formation of subtrenches (c - simulated, d - experimental).

1. H.V. Jansen, M.J. de Boer, S. Unnikrishnan, M.C. Louwerse, and M.C. Elwenspoek. “Black Silicon Method: X. a Review on High Speed and Selective Plasma Etching of Silicon With Profile Control”. Journal of Micromechanics and Microengineering, **19,** p. 033001, 2009.
2. Y. Haidar, A. Rhallabi, A. Pateau, A. Mokrani, F. Taher, F. Roqueta, and M. Boufnichel. “Simulation of Cryogenic Silicon Etching Under $SF_6/O_2/Ar$ Plasma Discharge”. Journal of Vacuum Science & Technology A: Vacuum, Surfaces, and Films, **34**, p. 061306, 2016.
3. V. Lukichev, V. Yunkin. “Scaling of silicon trench etch rates and profiles in plasma etching”. Microelectronic engineering, **46**, pp. 315-318, 1999.

Cyclic discrete etching of Silicon oxide in deposition-sputtering cycles: towards to ALE

V. Kuzmenko[1,2], A. Miakonkikh[1,2], K. Rudenko[1,2]
1. Moscow Institute of Physics and Technology, Dolgoprudny, Russia, kuzmenko.vo@phystech.edu.
2. Institute of Physics and Technology of RAS, Moscow, Russia, miakobnkikh@ftian.ru

High demands to etching selectivity and atomic precision attract attention to atomic layer etching (ALE). One of possible approaches to achieve cyclic discrete etching (CDE) is two step routine: (1) deposition of monolayer film containing reactive particles which do not interact with substrate in a self-limiting process; (2) activation of surface reaction of deposit with substrate by means of accelerated ions from beam source of plasma. It was realized for Silicon oxide etching by alternating polymer deposition from C_4F_8-based plasma and Oxygen ion bombardment from plasma [1]. Oxygen etches deposited film and stimulates formation volatile SiF_4 and CO_2. Actually this process is closer to CDE than ALE.
In presented work, etching was performed on samples of Silicon with deposited CVD films of SiO_2 with initial thicknesses of 350 nm. Thicknesses of oxide were measured before and after etching by spectral ellipsometer on J.A. Woollam Co M-2000X.
Presented cyclical ALE process was carried out in PlasmaLab 100 Dual (OIPT) two-chamber RIE cluster. A cycle consist of 2 steps: 1) deposition of a polymer film C_xF_y from C_4F_8 plasma at pressure 10 mTorr, which was excited by applying of RF bias (10W, DC bias of 47V) at 13.56 MHz to the wafer chuck with zero ICP power, 2) etching step by O_2 Inductively Coupled Plasma (ICP) which was excited in 2 stages: a) 2 second strike with 25 Watt RF bias at 13.56 MHz to the wafer chuck and 2500 Watt (2 MHz) of ICP power, b) 10 second etching with decreased to 15 W RF bias to the wafer chuck and 2500 W of ICP power. During the main etch step DC bias was about 22V. Oxygen ions transfer energy to activate reaction between C_xF_y film and SiO_2 also it etch the carbon-rich film formed on the SiO_2 surface from polymer film residues.
Each process consisted of 20 cycles. ALE properties of this process were studied by variation of deposition and etching step durations and by measurements of etch rate per cycle. As *ex situ* ellipsometry shows, deposition rate in C_4F_8 plasma for given process parameters is about 0.15 nm/sec at first 10 seconds of deposition. Fig. 1 shows dependence of average etch rate for SiO_2 on deposition time. It can be seen that the process is saturated with average etch rate about 0.22 nm/cycle which is much closer to monolayer thickness then previously reported 1 nm/cycle in [1].

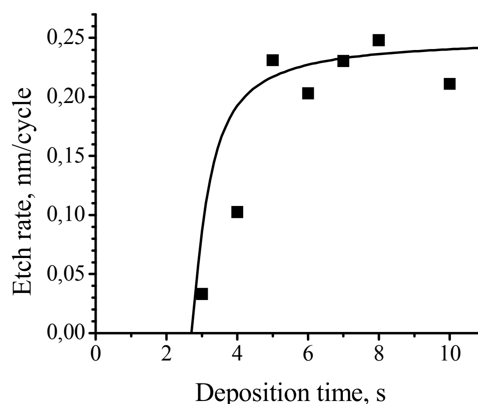

Fig. 1. The average per cycle etch rate of SiO_2 (nm/cycle) as a function of duration of deposition step(s).

Additionally it was shown that Oxygen plasma etch step could be replaced with the step of argon plasma with the same etch rate which proves that plasma in this process provide enhancement for surface reaction.

1. T. Tsutsumi et al. "Atomic layer etching of SiO_2 by alternating an O_2 plasma with fluorocarbon film deposition". J. Vac. Sci. Technol. A, **35**, pp. 01A103-1 - 01A103-4, 2016.

Study of synergy phenomena for atomic layer etching of Silicon, Aluminum, and Hafnium oxides

V. Kuzmenko[1,2], A. Miakonkikh[1,2], K. Rudenko[1,2]
1. Moscow Institute of Physics and Technology, Dolgoprudny, Russia, kuzmenko.vo@phystech.edu.
2. Institute of Physics and Technology of RAS, Moscow, Russia, miakobnkikh@ftian.ru

Plasma enhanced atomic layer etching (ALE) is cyclic process generally consisted of 2 surface processes: 1) chemical modification of surface layer of material, 2) removal of modified layer. It is important for ALE that both these steps should be self-limiting [1]. ALE is supposed to be promising for fabrication of different nanoscale devices for which high selectivity of plasma etch processes is required.

In the present work the ALE experiments were designed in PlasmaLab100 Dual (OIPT) two-chamber RIE cluster tool. The cycle were performed with sequential steps: 1) BCl_3 was adsorbed from gas phase, during adsorption step, 2) excess of BCl_3 was pumped out for 30 sec, 3) the reaction of surface etching was activated by Ar ions bombardment from plasma, during etch step (t_{plasma}). This step was performed at 30 mTorr pressure of Ar. Plasma was excited by applying of RF bias (10 W) at 13.56 MHz to the wafer chuck without inlet of ICP power. Average DC bias was about 100 V. Wafer temperature was kept at -20°C÷+20°C with He backing to insure thermal contact. Each process consisted of 20-50 cycles. Chamber walls and gas line were heated up to 40°C to prevent condensation of BCl_3.

Etching was carried out on samples of Silicon with deposited films of 1) HfO_2 (ALD), 2) Al_2O_3 (ALD), 3) SiO_2 (CVD) with thicknesses of 40-450 nm. Thicknesses of oxides were measured before and after etching by the spectral ellipsometer J.A. Woollam Co M-2000X tool.

The quantity of BCl_3 adsorbed to the surface could be characterized by dose of BCl_3 which is calculated as integral of pressure over the time of BCl_3 residence in the chamber during stages of BCl_3 feeding and pumping:

$$Dose = \int p \cdot dt \,,$$

where p is chamber pressure. Dose measurement unit is Langmuir ($1L=10^{-6}$Torr·sec). Pressure was measured by capacitor gauge. Fig. 1 shows dependence of average etch rate for Al_2O_3 and HfO_2 on dose of BCl_3. It can be seen that the etch rate saturates with dose. The points, which correspond to zero doses, refer to process without exposure to BCl_3 in which etching should be attributed only to sputtering by Ar.

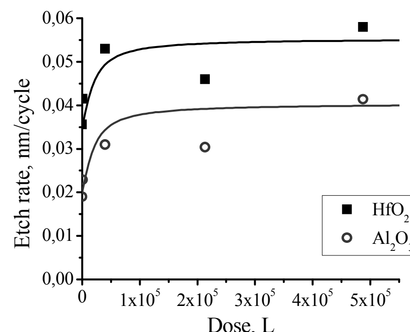

Fig. 1.The etch rate of Al_2O_3 and HfO_2 (nm/cycle) as a function of BCl_3 dose (L) at -20°C.

Etch rate dependence on sample temperature were measured too. It was shown that etch rate decrease with temperature growth dramatically, becoming close to zero at temperature +20°C at studied doses of BCl_3, which proves that we observe true ALE process. Silicon oxide mean etch rate exceed rate for hafnium and aluminum oxide for two times due to higher adsorption of BCl_3.

Performed study allows measuring ALE etching synergy [2] which is about 50% for Al_2O_3 and is about 30% for HfO_2 for the considered process of adsorption BCl_3 and argon bombardment.

1. K.S. Min et al."Atomiclayer etching of Al_2O_3 using BCl_3/Ar for the interface passivation layer of III-VMOS devices". Microel.Eng., **110**, pp.457-460, 2013.
2. K.J. Kanarik et al. "Predicting synergy in atomic layer etching". J.Vac.Sci.Technol. A, **35**(5), 05C302-1-05C302-7, 2017.

Features of silicon deep plasma etching process at 3D-TSV structures producing

A.A. Golishnikov, D.A. Kostyukov, M.G. Putrya, V.I. Shevyakov
National Research University of Electronic Technology, Russia, Shev@dsd.miee.ru

Nowadays the 3D TSV-technology is one of the promising solution for system-in-package production since it allows to increase an active component packing density, improve device performance, decrease power consumption and protect the circuits from copying [1]. One of the crucial technological operations in 3D TSV-technology is through silicon vias (TSV) plasma etching which determines TSV profile and subsequent metal filling operations [2, 3]. Since TSV production to the large extend depends on the formed through vias critical sizes (which are currently approaching Ø 1 μm and less) with high aspect ratio ≥ 10:1 and TSV density on a substrate [4], in this work deep plasma etching process for TSV in monocrystalline silicon for 3D-ICs is researched.

In the work the Bosch-process for the Si deep plasma etching performed in the high-density inductively coupled plasma source was applied. For Si deep plasma etching process the following working gases were used: sulfur hexafluoride in etching cycle, octafluorocyclobutane or trifluoromethane – in polymerization cycle. Experimental samples were 100 mm diameter monocrystal silicon substrates with 1 μm thickness photoresist mask deposited on their surfaces and vias with diameter varying from 1.5 to 2.5 μm. The geometric sizes of Si structures before and after deep plasma etching were measured by scanning electron microscopy and optical spectroscopy.

In the work the influence of the operating parameters in Si etching cycle (inductor RF-power, process pressure, rate SF_6, RF-power bias) on the process characteristics (Si etching rate, selectivity S(Si/PR) and etching profile) was researched. At the passivation stage, the operational parameters were not changed.

During TSV deep plasma etching process the following correlation parameters as a functions of the ion energy and radical density in plasma were obtained: silicon etching rate, etching selectivity S(Si/PR), etching structure profile.

The values of the inductor RF power at which the photoresist mask is decomposed, what in turn leads to the change of the observed structures configuration and their linear sizes, are determined. In addition, it was identified the values of the inductor RF power at which the Si etching rate become insignificant (less than 2 μm/min), microroughness such as microneedles and rod structures at the bottom of structure are observed and the situation of the full-stop of silicon etching process might occurs.

During deep plasma etching of Si-structures with different linear sizes so-called “aperture effect” related to mechanism of “RIE lag” was observed. The reasons of this mechanism are in detail considered in Buie's works.

During the polymerization stage it has been observed an increase in the fluoride-carbon film deposition rate on inclined surface compared to the deposition rate on vertical surface. At the same time the fluoride-carbon film deposition rate is higher on the bottom of the vias in comparison with the inclined surface of the structure. These results demonstrate an ion-stimulated mechanism of the fluoride-carbon film deposition process and show that the ion trajectory angle influences on the fluoride-carbon film deposition rate.

Additionally the fluoride-carbon film adhesive capacity in respect to silicon and silicon oxide was researched on the test samples. For investigated samples it has been shown that adhesion is not observed or insignificant.

Thus in this work the critical aspects in the through silicon vias plasma etching technology were determined. These aspects have to be taken into consideration for 3D-TSV structure development.

1. A. Topol et al. 3D Integrated Circuits // IBM Journal of Research and Development. 2006. P. 491.
2. X. Wu, W. Zhao, M. Nakamoto, et al. Electrical characterization for intertier connections and timing analysis for 3-D ICs. // IEEE Trans. Very Large Scale Integr. Syst. 2012. Vol. 20, №. 1. P. 186–191.
3. A.A. Golishnikov, D.A. Kostyukov, M.G. Putrya. Research and Development of Deep Anisotropic Plasma Silicon Etching Process to Form MEMS Structures. // Russian Microelectronics. 2012. Vol. 41, №. 7. P. 9–13.
4. W.-W. Shen, K.-N. Chen. Three-Dimensional Integrated Circuit (3D IC) Key Technology: Through-Silicon Via (TSV) // Nanoscale Research Letters. 2017. Vol. 12, №. 1. P. 1-9.

Radicals and molecules on the wafer surfaces after plasma activation for direct bonding

V.A. Antonov, L.N. Safronov, E.D. Zhanaev, V.P. Popov
Institute of Semiconductor Physics, Novosibirsk, Russia, popov@isp.nsc.ru

Hydrophilic surfaces of (100) silicon and thermal silicon dioxide surfaces are used for direct bonding (DB) processes. These surfaces are coated with a monolayer of hydroxyl radicals – OH, on top of which, depending on the humidity, several monolayers of H_2O molecules are adsorbed. Recently, a method of plasma-activated bonding (PAB) has been proposed and is rapidly developing. Main feature of the PAB is creating a large number of active bonds and radicals on the surfaces to be connected. By the method of hydrophilicity control by wettability angle it is impossible to obtain information about the presence of Si-O, Si-H, hydrocarbons and carbides on the surface. Moreover they determine the electronic and optical quality of the heterojunction after the manufacture of the structures. Spectroscopy of multiple frustrated total internal reflection (multiple ATR), based on the absorption evanescent modes with exponentially damped intensity away from the surface of the waveguide field is used to measure the absorption cubonavicular layers (Fig. 1)

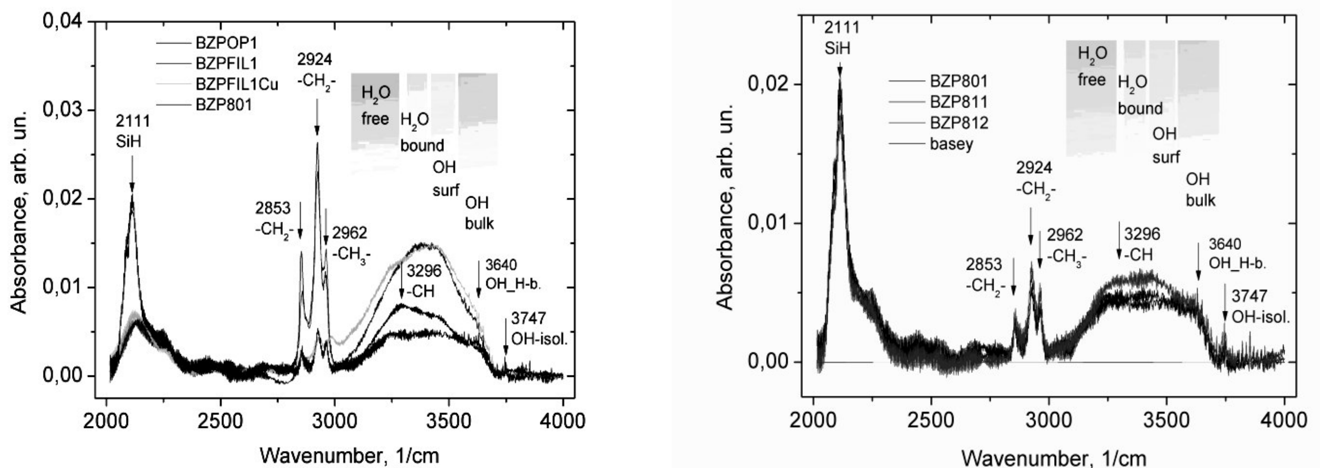

Figure 1 a) Spectra of the multiple ATR unit of the silicon wafer after treatments: BZPOP1 – hydrophobic surface after removal of a thermal SiO_2 in the HF aqueous solution; BZPIL1 – hydrophilic surface after chemical treatment in RCA-1; BZPIL1Cu – hydrophilic surface after treatment with "Plasma-600"; BZP801 hydrophobic after treatment in "BA8 Suss Microtech"; b) the same after aging in vacuum for 6 (801), 60 (811) and 120 (812) min after DBD plasma treatment.

The method of multiple ATR was placed on the Fourier-spectrometer Bruker-66/s for the analysis of adsorption processes by bonded radicals and molecules on the surface of high-resistance silicon produced in ISP SB RAS by floating zone process (BZP) after chemical and plasma treatments in radio frequency oxygen plasma (13.5 MHz) at the low pressure (10^{-2} Pa) on the "Plasma-600" unit and in atmosphere with dielectric barrier discharge (DBD) plasma on the DBD module of "BA8 Suss Microtech" unit. It is shown that in addition to the transformations of Si-OH and Si-H bonds well described in the literature, there are radicals -CH, $-CH_2$ and $-CH_3$. Their total concentrations weakly depend on the type of chemical treatment, but significantly decrease after plasma treatment of the silicon surface (Fig. 1a). The storage of the treated wafers in the vacuum at the low pressure (10^{-2} Pa) slowly decreases the density of the SiH bonds but increases the chemically and physically adsorbed water molecule content on the wafer surfaces after PAB. Hydrocarbons during such storage grow also slowly. The surface treatment in the atmospheric DBD plasma provides more hydrophobic surface of (100) silicon wafers than RF oxygen plasma treatment (Fig. 1a).

Growing of $Si/Si_{1-x}Ge_x/Si$ (x < 0.1) quantum wells by modulation of the Ge flow

A.V. Klekovkin[1,2], I.P. Kazakov[1], V.A. Tsvetkov[1], M.A. Akmaev[1], O.V. Uvarov[3]
1. Physical Institute. P. N. Lebedev RAS, Moscow, Russia, e-mail: aklekovkinbox@gmail.com
2. Institute of ultrahigh frequency semiconductor electronics RAS, Moscow, Russia, e-mail: mail@isvch.ru
3. Prokhorov General Physics Institute RAS, Moscow, Russia, postmaster@gpi.ru

The obtaining of Si / $Si_{1-x}Ge_x$ / Si quantum wells (QW) with x < 0.1 by molecular beam epitaxy (MBE) is difficult due to the instability of Ge flow at low values of Ge gun electron beam current.
In the present work, the layer of the solid alloy of the $Si_{1-x}Ge_x$ QW was obtained as a result of periodic overlapping (modulation) of the Ge molecular flow with continuous Si flow. This method allows to operation of the molecular source in a stable mode at higher values of the electron beam current. This method was used, for example, in [1, 2], for growing Si / Ge quasi-direct-gap materials with a high Ge content (x > 0.4).
The samples were made on the MBE system Siva 21 (Riber). The preparation of Si (100) substrates used in this work described in [3]. The assumed sequence of the layers $Si_{1-y}Ge_y$ / Si / $Si_{1-y}Ge_y$ /..., with the effective thicknesses d_{SiGe} and d_{Si} (Table 1) varied in samples in the range 0.14 nm to 1.4 nm (~1 to 10 monolayers (ML)) and dSi in the range 0.14-0.28 nm (~1-2 ML), respectively. The number of periods in the supposed sequence $Si_{1-y}Ge_y/Si/Si_{1-y}Ge_y/$... was from 3 to 17.

Table 1. Parameters of the layers of the solid solution $Si_{1-x}Ge_x$ in the quantum well.

Structure №	Effective layer thickness, nm		Number of periods, N	The averaged composition of the layer $Si_{1-x}Ge_x$, x
	d_{SiGe} ($Si_{1-y}Ge_y$)	d_{Si} (Si)		
A	14	1.4	3	0.08
B	3.14	1.4	10	0.06
C	2.1	2.1	11	0.09
D	1.4	1.4	17	0.01
E	2.8	1.4	11	0.08

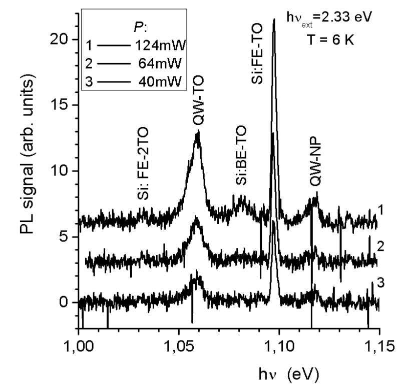

Fig. 1. The PL spectrum for the "E" structure.

The structures were studied by the photoluminescence (PL) method at temperatures from 6 to 15 K and excitation levels up to 150 mW. Figure 1 shows the spectra of the photoluminescence of the investigated QW, taken at different pump powers. Observed intensive lines of the TO-phonon components of the spectrum from the QW (line QW-TO) and the Si substrate (Si: FE-TO line). The line of the bound exciton Si: BE-TO is visible in the emission of Si substrate at high pump power. The phononless components of the spectrum from the QW (line QW: NP) much weaker than phonon.
To compare technologies, samples $Si_{1-x}Ge_x$ QW with constant composition x, equal to the average composition of the samples described above, were grown. The position of the emission lines on PL spectra practically coincide.
Thus, in this paper we demonstrate the possibility of obtaining quantum wells $Si_{1-x}Ge_x$ with x < 0.1 by modulation of the Ge flow.
The work was supported by the Russian Foundation for Basic Research, project No. 16-02-00986 a, No. 16-29-03352 ofi_m and the RAS Presidium Program.

1. T.P. Pearsall et al. "Structurally induced optical transitions in Ge-Si superlattices". J. Phys. Rev., **58**. pp. 729-732, 1987
2. E. Kasper et al. "Symmetrically strained Si/Ge superlattices on Si substrates". J. Phys. Rev., **38**, pp. 3599-3601, 1988
3. Yu.G. Sadofyev, V.P. Martovitsky, M.A. Bazalevsky. "Silicon-germanium nanostructures with high germanium concentration". Bull. Russ. Acad. Sci. Phys., **78**, pp. 29-33, 2014.

Formation of In/AlGaAs nanostructures by droplet molecular beam epitaxy

M.S. Solodovnik[1,2], S.V. Balakirev[1], M.M. Eremenko[2], I.A. Mikhaylin[2], O.A. Ageev[2]
1. Southern Federal University, Institute of Nanotechnologies, Electronics and Equipment Engineering, Department of Nanotechnologies and Microsystems, Taganrog, Russia, solodovnikms@sfedu.ru
2. Southern Federal University, Research and Education Center "Nanotechnologies", Taganrog, Russia, ageev@sfedu.ru

Recently many techniques to produce high-quality arrays of quantum dots (QD) have been developed, but a number of problems are still urgent such as a limited set of materials suitable for the QD formation, dislocations and strain-induced growth, etc. However, droplet epitaxy technique allows non-strain-induced formation of various nanostructures with independent control of their size, surface density and chemical composition [1]. As a consequence, droplet epitaxy can be used to obtain high-quality QD arrays, although many aspects of this technology still need clarification.

The goal of this work was study of effect of epitaxial layer composition on the In/AlGaAs nanostructures formation processes during the droplet epitaxy. Experimental studies were carried out using SemiTEq STE 35 MBE system. GaAs (001) epi-ready wafers were used as substrates. The surface temperature (T) varied from 150 to 300°C. The results of experimental studies showed that an increase in the substrate temperature led to an increase in the average droplet size with a simultaneous decrease in their density. The high mobility of the In adatoms leads to the fact that with the same main control parameters, the droplet size in the In/AlGaAs system is larger compared to Ga/AlGaAs [2]. The size dispersion of In tends to decrease from 30% to 5% when the T increases from 150°C to 300°C, whereas for Ga it varies from 78% to 55% at the same T.

The increase in Al content in the epitaxial layer leads to an expansion of the range of variation in the density of arrays. At T below 200°C, the droplet density varies from 2.2×10^{9} cm^{-2} to 2.1×10^{10} cm^{-2} with an increase of Al content. However, increasing the temperature to 300°C leads to a decrease in density from 1.8×10^{8} cm^{-2} for GaAs to 3.7×10^{7} cm^{-2} for AlAs, while the average diameter of droplets increases from 98 nm to 177 nm, respectively.

In addition, it is worth mentioning, that the thickness of the indium wetting layer on the GaAs substrate is much stronger dependent on the growth temperature than that on the AlAs substrate. In the latter case, its thickness practically does not change being 1.0-1.25 ML, which is approximately corresponds to surface arsenic layer thickness. Apparently, this unusual behavior of the system is due to the difference in the chemical interaction between adatoms and the surface when the composition of the functional layer changes.

This work was supported by the Russian Science Foundation Grant No. 15-19-10006 and by Grant of the President of the Russian Federation No. MK-2629.2017.8. The results were obtained using the equipment of the REC and CCU "Nanotechnologies" of Southern Federal University.

1. N. Koguchi, S. Takahashi, and T. Chikyow. "New MBE growth method for InSb quantum well boxes". J. Cryst. Growth, **111**, pp. 688–692, 1991.
2. M.S. Solodovnik, S.V. Balakirev, M.M. Eremenko, I.A. Mikhaylin, V.I. Avilov, S.A. Lisitsyn, and O.A. Ageev. "Droplet epitaxy of GaAs nanostructures on the As-stabilized GaAs(001) surface". J. Phys. Conf. Ser., **917**, pp. 032037, 2017.

Droplet epitaxy of indium on nanopatterned GaAs(001) substrate studied by kinetic Monte Carlo simulations

S.V. Balakirev[1], M.M. Eremenko[2], I.A. Mikhaylin[2], M.S. Solodovnik[1,2], O.A. Ageev[2]
1. Southern Federal University, Institute of Nanotechnologies, Electronics and Equipment Engineering, Department of Nanotechnologies and Microsystems, Taganrog, Russia, sbalakirev@sfedu.ru
2. Southern Federal University, Research and Education Center "Nanotechnologies", Taganrog, Russia, ageev@sfedu.ru

Control over the interaction between active elements of nanodevices is an outstanding problem in quantum science and engineering. Semiconductor quantum dots fabricated by droplet epitaxy are particularly attractive for the realization of quantum computers and photonic integrated circuits, as they can be controllably positioned and varied in geometrical characteristics [1].
In the present work, the processes of droplet epitaxy of In on the nanopatterned GaAs substrates are studied by the kinetic Monte Carlo model which was previously validated by the experiments on the flat surface [2]. The simulations show that the growth by droplet epitaxy can be selectively positioned by collecting the deposited material within the triangular holes (Fig. 1a, 1c). A sufficient distance between holes should be provided to prevent nucleation of nanostructures outside the holes (Fig. 1b). To ensure the best selectivity of the growth, an appropriate combination of parameters of patterning and growth conditions should be chosen.

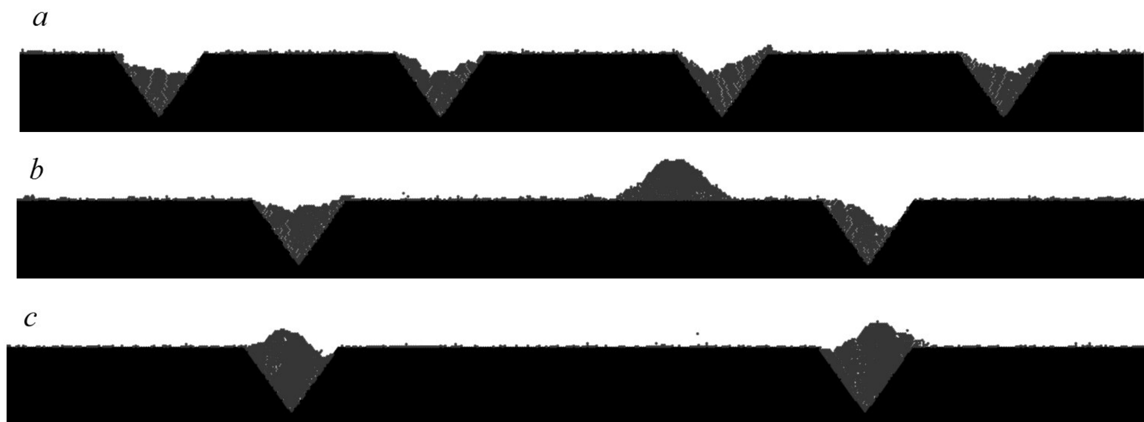

Figure 1. Morphology of the array of In/GaAs(001) nanostructures after deposition of 5 ML of indium on the Ga-stabilized nanopatterned substrate with $d = 16$ nm, $h = 12$ nm and a) $r = 50$ nm at $T = 100$°C, b) $r = 100$ nm at $T = 100$°C, c) $r = 100$ nm at $T = 200$°C ($L = 200$ nm).

For the formation of In droplets with dimensions limited by a hole diameter (d) of 16 nm and a height (h) of 12 nm, an interhole distance (r) of 50 nm is sufficient to achieve localization of nanostructures in holes at $T = 100$ °C (Fig. 1a). However, an increase of this distance to 100 nm at the same T leads to the nucleation outside holes on the flat region of the substrate (Fig. 1b). T must be increased up to at least 200 °C to achieve the better localization keeping the same r to provide a smaller surface density of nanostructures (Fig. 1c).
Our study also shows that varying deposition thickness enables an independent control of nanostructure sizes, while maintaining the surface density unchanged. When 5 ML of In is deposited at $T = 200$°C, the holes are completely filled with the deposited material exceeding the substrate level. Reducing the deposition thickness to 4 ML results in a decrease in the height of nanostructures relative to the hole bottom from 17 nm to the hole depth h which is equal to 12 nm.
This work was supported by the Russian Science Foundation Grant No. 15-19-10006 and by Grant of the President of the Russian Federation No. MK-2629.2017.8. The results were obtained using the equipment of the REC and CCU "Nanotechnologies" of Southern Federal University.

1. J.S. Kim, M. Kawabe, and N. Koguchi. "Ordering of high-quality InAs quantum dots on defect-free nanoholes". Appl. Phys. Lett., **88**, pp. 072107, 2006.
2. S.V. Balakirev, M.S. Solodovnik, and O.A. Ageev. "Hybrid Analytical–Monte Carlo Model of In/GaAs(001) Droplet Epitaxy: Theory and Experiment". Phys. Status Solidi B, **255**, pp. 1700360, 2018.

Effect of *in situ* laser radiation on the parameters of the alumina films fabricated by atomic layer deposition

A.V. Miakonkikh[1], I.E. Clemente[1], A.A. Dedkova[2], N.A. Dyuzhev[2], V.Yu. Kireev[2], K.V. Rudenko[1]
1. Institute of Physics and Technology of RAS, 117218, Moscow, Russia, Nakhimovsky av. 34
2. National Research University of Electronic Technology, 124498, Moscow, Zelenograd, Shokina square, 1,

The influence of wafer irradiation with a wavelength of 970 nm light of diode laser on the process of atomic layer deposition (ALD) of aluminum oxide films by precursors trimethylaluminium (TMA) and water vapor is studied. It is supposed that interaction of intensive optical radiation with adsorbed precursors on surface could initiate its local desorption. Selective removal of adsorbed precursors from different materials could be promising for development of area selective atomic layer deposition.
The sample was exposed to laser radiation at the stages of pumping of the reactor after supplying each precursor. As a result of complex researches on the basis of spectral ellipsometry, probe profilometry, x-ray diffractometry and secondary ion mass spectrometry was conducted.
The samples of 20-25 nm thick Al_2O_3 films were deposited in FlexAl ALD tool (Oxford instruments plasma technology, UK). This process is known as truly self limited and hence process dependence on external parameters (wafer temperature, dosage of precursors, pressure) is flat in wide interval [2]. That provides wide “process window”, in which stable and reproducible film properties can be achieved. Table was heated to 300°C. TMA was dosed for 20 ms from the babbler heated to 35°C, and water vapor was dosed for 200 ms, from the vessel cooled to 18°C. The central part of the silicon wafers with a diameter of 3 cm in the process of 200 cycles of ALD in the purge stages was irradiated for 5 seconds by a laser with a wavelength of 970 nm and a power density of 0.29 W/cm^2.
The thickness of alumina (Al_2O_3) films and the uniformity of their distribution over the surface of the wafers were measured by a J.A. Woollam M-2000X spectral ellipsometer with automated moving table in spectral range of 246-988 nm with mapping facilities.
The average density of aluminum oxide films was measured by X-ray reflectometry on the SmartLab tool. The geometry of a parallel beam of X-ray radiation with a wavelength λ ($CuK_{\alpha 1}$) = 0.15406 nm in the scanning mode 2θ with an angular pitch θ = 0.004° was used. The alumina film obtained without *in situ* laser irradiation of the wafer has an average density in the range (3.24-3.23) g/cm^3, while the aluminum oxide film formed in the process with laser radiation had an average density of 2.94-3.05 g/cm^3.
The studies carried out on the SmartSPM scanning probe microscope revealed practically no significant difference in altitude (film thickness) between irradiated and non-irradiated parts of wafer, as well as changes in surface relief (roughness).
SIMS analysis of Al/O ratio depending on the depth was performed, showing negligible differences between treated and untreated parts of wafers.
In addition, local laser irradiation with different power densities during 5 seconds in the purge stages in the process of 200 cycles of ALD of Al_2O_3 films changes (by (0.6-0.74) nm) the total thickness of the films deposited on the wafer, probably due to the heating of the wafers with respect to temperature of table (300°C).

The reported study was carried out under Program of FASO of Russia and was partially supported by RFBR, research project # 18-37-00354.

1. George S.M. "Atomic Layer Deposition: An Overview," Chem. Rev. **110**, 111-131 (2010).
2. Clemente I.E., Miakonkikh A.V. “Application of spectral ellipsometry to in situ diagnostics of atomic layer deposition of dielectrics on silicon and AlGaN” Proceedings of SPIE - The International Society for Optical Engineering **10224**, 1022425 (2016).

Induced bistability into quartz glass by silicon wafer heat treatment in lamp-based reactor

V. Prigara, V. Ovcharov
Yaroslavl Branch of the Institute of Physics and Technology, Institution of Russian Academy of Science, Yaroslavl, Russia, ovcharov.vlad@gmail.com

The net radiation method is applied to obtain formulas for exact expression of thermal radiation heat transfer in a system containing two semitransparent wafers that are radiation-isolated between two opaque grey plates at different temperatures.

Here, the formulas are used for calculation of thermal radiation heat transfer inside the radiation-isolated system modeling a lamp-based reactor and including a heater, a quartz screen, a semiconductor wafer and an absorber of heat. Two semitransparent grey wafers are represented by a quartz screen and a semiconductor wafer, whereas the heater and the absorber possess optical properties corresponding to those of opaque grey bodies. As the semiconductor wafer is treated a standard silicon wafer that reveals bistability under distinct conditions of its thermal treatment in the lamp-based reactor. Optical properties of a quartz screen correspond to the 5 mm thick QI-brand quartz plate [1]. The approach to the calculation of heat transfer in such a system is the development of the ideas proposed in [2] for calculating heat transfer between two grey opaque plates separated by a grey semitransparent screen. To simulate heat transfer in the lamp-based reactor it is suggested that quartz screen is cooled by gas flow and heat from the silicon wafer is extra removed by heat conductivity through a gas-gap between the silicon wafer and the heat absorber that is the elements of the heat system are involved in combined heat transfer. The formulas are used for silicon wafer and quartz glass temperatures with regard to the real optical properties of the heater and absorber and their transfer characteristics are plotted. The results are supplemented by the results of [3] where the system is simulated in conditions of the ideal heater and absorber, all factors being the same. Fig.1 shows the comparison of the transfer characteristics of the silicon wafer (a) and quartz screen (b) for the system containing the heater and the absorber whose optical properties correspond to those of the blackbody (dashed line) and to those of the real materials (solid lines). The induced bistability into quartz glass is also obtained in case for the heater and absorber whose optical properties are real both for ideal heater and absorber. The transfer characteristics of the quartz glass are represented by an S-shaped curve in the same temperature interval of the heater as it occurs in the silicon wafer. As the result, the correcting calculation to be carried out for the real heater confirms the effect of induced bistability into quartz glass that is not prone to non-linear temperature dependence in its optical nature.

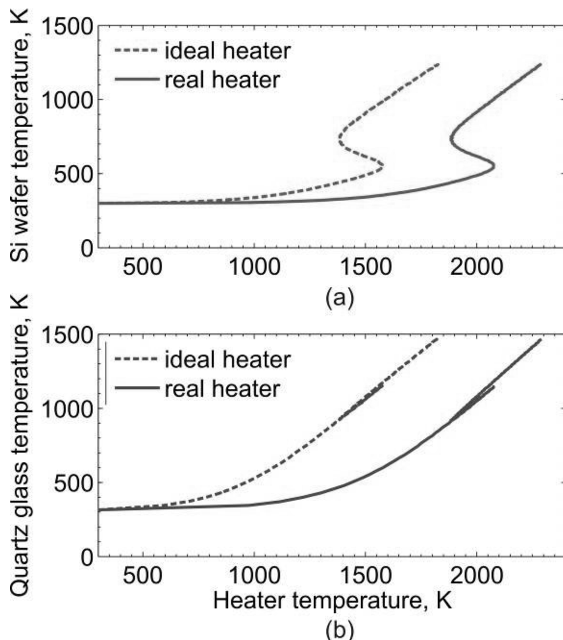

Fig. 1. Transfer characteristics for the silicon wafer (a) and the quartz glass (b) simulated for the heat system that contains the heater and absorber possessing the ideal optical properties (dashed curves) and the real ones (solid curves).

1. V.A. Petrov, S.V.Stepanov, K.S. Muhamedyarov. “Tablitsy standartnyh spravochnych dannyh”. GSSSD 40-82, Gosstandart, Moscow, 1983.
2. J.Zeegers, H.A.L.van Dijk. “A note on the net radiation method applied to a system composed of a semitransparent film between two glazings”. Sol. Energy Mater. and Sol. Cells, **33**, pp. 23-30, 1994.
3. V. Prigara, V. Ovcharov, A. Kurenya, V. Rudakov. “Radiation heat transfer between silicon wafer and lamp-based reactor with inclusion of quartz glass”. Theses of the III International Conference «Modern problems in the physics of surfaces and nanostructures», Yaroslavl, Russia, October, 9-11, 2017. P. 86.

Localization of a thermo-optical travelling wave on an optical inhomogeneity in a silicon wafer under lamp-based heating

V. Ovcharov, V. Prigara, A. Kurenya,V. Rudakov
Yaroslavl Branch of the Institute of Physics and Technology, Institution of Russian Academy of Science, Yaroslavl, Russia, ovcharov.vlad@gmail.com

The thermo-optical travelling wave propagating along the surface of the silicon wafer under its lamp-based heating is a new phenomenon whose model was developed and experimentally confirmed in Ref. [1]. The investigation of this phenomenon that follows makes it possible to study the regularities of the travelling process of the wafer at the change of its stationary temperature states. Parameters of the travelling wave, such as velocity and width of the wave front, depend on both the parameters of the thermal process that a silicon wafer is involved in and on thermal, optical and geometric properties of the silicon wafer. It was shown in Ref. [2] that an isolated inhomogeneity of a finite size may lead to localization (stopping) of the travelling wave propagation at the specific parameters of the homogeneity. Here, a simulation is made of the stopping of a thermo-optical travelling wave in a silicon wafer in the presence of an optic inhomogeneity which essentially changes the balance of heat input and output in the position of travelling wave localization. The optical inhomogeneity is represented by reflecting Ag strip of 1 μm thickness that is sputter-coated on the surface of the silicon wafer. The travelling wave either delays the propagation passing through optical inhomogeneity or stops at the strip boundary. The first approximation width of the optical inhomogeneity may be evaluated supposing that the order of the wave front width is $w_{fr} \sim \sqrt{kd/h_{eff}}$ [1]. Here k is the thermal conductivity of the silicon, d is the silicon wafer thickness; h_{eff} is the effective heat exchange coefficient between the silicon wafer and the water-cooled pedestal. At d =460 μm and h_{eff} =180 W/(m^{2}K) width of the wave front w_{fr} is ~ 2 cm [1]. Fig.1 shows the results of the numerical simulation of the wave propagation along the surface of the silicon wafer having an optical inhomogeneity width 1.5 cm (Fig. (a) and 2.0 cm (Fig. (b)). At Ag strip of 2.0 cm width the travelling wave stops. As a result, the silicon wafer is divided into two regions: high- and low- temperature with temperature difference ~ 640K and gradient across the boundary ~ 430 K/cm. The results may be used in the potential technologies of semiconductor materials.

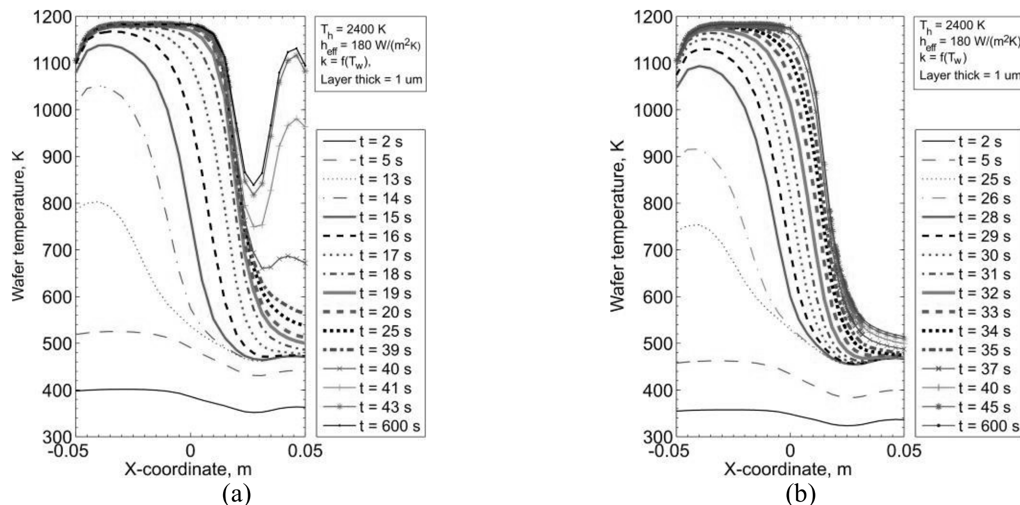

Fig. 1. The time dependence of the temperature profiles of the travelling wave propagating on the surface of 1cm width Ag strip disposed on the silicon wafer surface (travelling wave propagation with slowing down) (a) and of 1.5 cm width (travelling wave stopping) (b).

1. Ovcharov V.V., Kurenya A.L., Rudakov V.I., & Prigara V.P. “Temperature switching waves in a silicon wafer on lamp-based heating”. Proc. of SPIE, **10224,** pp. 1022422-1-1022422-12, 2016.
2. Petrovskii S.V. "Localization of a nonlinear switching wave in an active bistable medium with an isolated inhomogeneity". Technical Physics, **42(**8), pp. 866-871, 1997.

Features of the formation thermite materials based on Al/CuO nanopowders by the electrophoretic deposition technology for reactive bonding

L. Sorokina[1], E. Lebedev[1], D. Gromov[1], Y. Shaman[2], R. Ryazanov[2]

1. Institute of Advanced Materials and Technologies, National Research University of Electronic Technology, Russia, Moscow, Zelenograd

2. Scientific Manufacturing Complex "Technological Centre", Russia, Moscow, Zelenograd

Currently, the development of new technologies and methods for bonding heat-sensitive components is an actual topic of research in the field of 3D assembly. Traditional bonding processes occur with the all components heating. This can damage the heat-sensitive components and reduce the joining quality due to different thermal expansion coefficients. The reactive bonding is a new low-temperature method, which is based on the two surfaces joining due to a high-exothermic reaction. The essence of this method is to use thermite materials as a local heat source, which is placed between two pre-coated with solder surfaces. Intensive heat release occurs after the initiation of a thermite reaction. As a result, the solder melts and a reliable bond is formed. This process finds application not only for soldering and packaging in microelectronics [1], but also for the connection of various surfaces [2, 3], including ceramic, metal and silicon [4, 5]. Traditionally, as local heat sources for joining surfaces multilayer thermite materials are used. However, multilayer films are obtained by low-reproducing magnetron sputtering technology that requires expensive vacuum equipment. From other side, the electrophoretic deposition (EPD) technology is an incredibly promising method of local multicomponent material deposition. This paper presents a room temperature formation thermite materials based on Al/CuO nanopowders by the electrophoretic deposition, which will improve the technology of 3d assembly of integrated circuits.

The EPD process involves the motion of dispersed particles relative to a fluid under the influence of a spatially uniform electric field. In this work the deposition carried out from a suspension consisting of isopropyl alcohol and nanopowders of aluminum and copper oxide (particle size of <100 nm). Stable suspension with total solids loading 1 g L^{-1} in isopropyl alcohol was made using ultrasonic treatment. The thermite coating was formed on a substrate of titanium foil (cathode). Gold foil, which was placed parallel to the cathode at a distance of 1 cm, was used as an anode. The EPD was cycled with a different settling time and applied voltage. The deposition time was from 30 s to 15 min with a voltage of 5 to 160 V. The number of cycles varied from 1 to 10. Morphology and composition of received layers were controlled by scanning electronic microscopy and energy dispersive X-ray analysis. The dependence of the deposit mass on the applied voltage regardless of the amount of cycles was experimentally established. The propagation velocity of the flame front was measured using a high-speed camera. The value of the reaction initiation energy in formed materials was determined with a femtosecond laser. The developed thermite materials were used as local heat sources for different surfaces bonding (Ti, Ni, Cu foil and Si wafers) at room temperature.

This work supported by The Russian Science Foundation (project №16-19-10625)

1. J. Braeuer et al. "A novel technique for MEMS packaging: Reactive bonding with integrated material systems ". J. Sensors and Actuators A: Physical, **188**, pp. 212-219, 2012.
2. W. Zhu et al. "Microstructural and mechanical integrity of Cu/Cu interconnects formed by self-propagating exothermic reaction methods". J. Microelectronic Engineering, **128**, pp. 24–30, 2014.
3. S. Simoes et al. "Microstructure of Reaction Zone Formed During Diffusion Bonding of TiAl with Ni/Al Multilayer". J. Mater. Eng. Perform., **21**, pp. 678–682, 2012.
4. Z. Long et al. "Transient liquid phase bonding of copper and ceramic Al_2O_3 by Al/Ni nano multilayers". J. Ceramics International, **43**, pp. 17000–17004, 2017.
5. F. Baras et al. "Dissolution at Interfaces in Layered Solid-Liquid Thin Films: A Key Step in Joining Process". J. Materials Engineering and Performance, **25**, pp. 3270–3274, 2016.

Fabrication and properties of SOI-based planar silicon nanowire arrays

A. Rogozhin[1, 2], A. Miakonkikh[1, 2], A. Tatarintsev[1], K. Rudenko[1]
1. Institute of Physics and Technology of RAS, Moscow 117218, Russia, rogozhin@ftian.ru
2. Moscow Institute of Physics and Technology (MIPT), Moscow, Russia

There is a strong interest in the fabrication of silicon nanostructures for microelectronic applications. Silicon one-dimensional structures are perspective for application in different nanoelectronic devices, not only for nanoscale field effect transistor and photonics, but also for THz applications [1], biosensors applications allowing progress in increasing sensitivity to adsorbed atoms and molecules [2], quantum devices based on quantum conductivity [3] or Coulomb blockade [4] and even technology for quantum computer formation [5].

We employed two-stage technology of precise anisotropic plasma etching of silicon over e-beam resist and isotropic removal of thermally oxidized defected surface layer of silicon by wet etch to fabricate planar silicon nanowire arrays. Silicon nanowires with diameter of 10-30 nm were obtained {fig. 1). It is simple to get nanowires without oxide or covered with thermal SiO_2. Conductivity of obtained silicon nanowire arrays was measured.

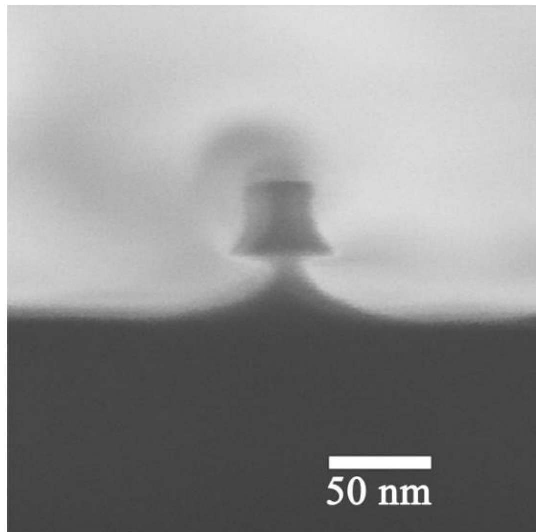

Fig. 1. SEM image of 30 nm – nanowire cross-section.

1. L. Fedichkin, V. Vyurkov, "Quantum ballistic channel as an ultrahigh frequency generator," Appl. Phys. Lett., **64**, 2535-2536 (1994).
2. V.P. Popov, M.A. Ilnitskii, E.D. Zhanaev et al., Semiconductors, **50** (5), 632-638 (2016).
3. H. Namatsu, M. Nagase, K. Kurihara, S. Horiguchi, and T. Makino, Jpn. J. Appl. Phys., Part 1, **35**, 1148 (1996).
4. Y. Takahashi, H. Namatsu, K. Kurihara, K. Iwadate, M. Nagase, and K. Murase, IEEE Trans. Electron Devices, **43**, 1213 (1996).
5. A.A. Orlikovsky, V.V. Vyurkov, and V.F. Lukichev, Book of Abstracts, NATO Advanced Research Workshop Nanoscaled Semiconductor-on-Insulator Structures and Devices, 15-19 October 2006, Sudak, Crimea, Ukraine, pp. 43-44.

Effect of the sublayer material on the growth rate of carbon nanotubes in low-temperature plasma

V.S. Klimin[1,2], A.A. Rezvan[1], O.I. Il'In[1,2], O.A. Ageev[2]
1. Southern Federal University, Institute of Nanotechnologies, Electronics, and Equipment Engineering, Department of Nanotechnologies and Microsystems, Taganrog, Russia, E-mail address: klimimnvs@sfedu.ru
2. Southern Federal University, Research and Education Center "Nanotechnology", Taganrog, Russia, E-mail address: ageev@sfedu.ru

The use of carbon nanomaterials in modern instrument engineering makes it possible to obtain a device with smaller geometric parameters and to reduce the power consumption. Of all modern carbon materials, carbon nanotubes stand apart, which have unique electronic and geometric properties.
However, the processes of obtaining tubes with given geometric and electrical parameters have not been fully studied. In this paper, topical problems of forming nonvolatile memory elements with high speed based on arrays of carbon nanotubes are considered. In the developed instrument, arrays of carbon nanotubes oriented perpendicular to the surface were applied. To form an array of carbon nanotubes with given parameters and a formed lower contact, it is necessary to carefully select the material of the sublayer.
Despite the fact that the catalytic material for the formation of carbon nanotubes is the same, the effect of the catalytic material is obvious. This effect is associated with a different coefficient of thermal expansion and chemical interaction of the catalytic material with the sublayer material. It is also very important that the material of the sublayer interact with the gas atmosphere at which the growth of carbon nanotubes passes. Four different sublayer materials were investigated in this paper.
The formation of carbon nanotubes was carried out by the method of plasma chemical deposition from the vapor phase on the specialized module PECVD of the cluster nanotechnology complex NANOFAB NTK-9 (NT-MDT, Russia). This method allows obtaining carbon nanotubes formed perpendicular to the surface. To select the materials of the sublayer, in our previous works we carried out a theoretical thermodynamic analysis of various structures for the growth of carbon nanotubes.
The data of the conducted thermodynamic analysis made it possible to identify the most promising structures. Perspective was defined as the possibility of growth, so the quality of grown carbon nanotubes. In the experiments for growth, structures such as Ni-Al-Si, Ni-V-Si, Ni-Ti-Si, Ni-Cr-Si were used. Carbon nanotubes were formed in an ammonia atmosphere with a feed rate of N_{Ar} = 150 cc/min, and a carbonaceous gas of acetylene N_{C2H2} = 70 cc/min. The reactor pressure was 4.5 Torr, the growth time was 20 minutes, and the reactor temperature was 750 ° C.
The parameters of the formed catalytic centers and the electrical parameters of the grown carbon nanotubes were monitored using the Ntegra Vita (NT-MDT, Russia).nanotechnology laboratory using a "semi-contact" regime. In addition, the height of the formed arrays of carbon nanotubes was estimated using a scanning electron microscope Nova NanoLab 600 (FEI Company, Netherlands). The obtained dependence has two growth areas. The first section is characterized by intensive growth and lasts about 5 minutes, for the structure of Ni-Cr-Si the growth rate is of the order of 1 μm/min, for the Ni-V-Si structure it is 0.55 μm/min. In the second section, the curve begins to saturate and the growth slows down significantly for the Ni-Cr-Si structure, the growth rate is about 0.2 μm/min, for the Ni-V-Si structure 0.16 μm/min.
In this paper, the regimes of formation of arrays of carbon nanotubes on various structures were studied. It was shown that using different material of the sublayer, different results of geometric parameters and electronic properties of arrays of carbon nanotubes were obtained. The substrate material and the catalytic centers remained the same. In this paper, comparative experiments were conducted to determine the rate of growth of arrays of carbon nanotubes on various sublayer materials.
It was shown that with the growth of an array of carbon nanotubes, two stages are distinguished from the gas phase by plasma enhanced chemical vapour deposition. Using experimental results, we can find optimal regimes for growing carbon nanotube arrays for manufacturing nonvolatile memory elements with high switching speeds.

This research has been supported by the Results obtained using the Research and Education Center and Center for Collective Use "Nanotechnology" South Federal University. This work was supported by the Russian Foundation for Basic Research Project № 18-29-11019 mk.

A Novel Method of Graphene Hydrogenation by MWCVD Plasma

E. Paramonov[1], A. Saveliev[1], M. Rybin[2,3], E. Obraztsova[2], M. Biryukov[4], G. Pavlov[4], A. Molin[5], A. Kusnetsov[5]

1. Laboratory of Carbon Nanomaterials Ltd., Skolkovo, Moscow, Russia, E-mail address: evgeny.s.paramomov@gmail.com

2. General Physics Institute, Moscow, Russia

3. LLC "RUSGRAPHENE", Protvino, Moscow region, Russia

4. JSC NIITM, Zelenograd, Russia

5. LLC "Atommedcenter", Moscow, Russia

Graphene could be next generation nanomaterial for microelectronic industry, variety of sensors and storage systems. Thorough research has been undertaken to analyze, model and produce modified versions of graphene with wide physical and chemical properties. It seems that hydrogenated graphene could be one of the particular interests for the industry. Promising applications in scope of field-effect transistors, hydrogen storages and gas sensors already showed [1]. Further developments in this area need scalable production methods attributed with possibilities of controllable variation of hydrogenation value and limitation of defects introduced by microwave plasma.

We propose a first step towards scalable method of graphene hydrogen adsorption, which gives a material with specified hydrogenated level and corresponding tunable band gap. Graphene is treated in microwave plasma in a CVD reactor. The pressure in the chamber is 2-5 Torr, Microwave 2.45 GHz power is 500-800 W. This method allows dramatically reduce the time of treatment to 10-30 seconds. This is significantly shorter than existing methods that have duration up to 120 minutes. The temperature of the substrate is 200-220 °C and extensive selection of substrates is possible.

The plasma has a diameter of 100 mm, which allows processing samples up to 80 mm in diameter with a uniform distribution of C-H bonds. Samples hydrogenated in range of 2 to 20 percent were obtained. The disadvantage of this method is the possibility of etching graphene in the zones of rupture and gluing. We are exploring this problem now.

Samples of graphene were prepared by LLC "RUSGRAPHENE" together with the Laboratory of Nanomaterials Spectroscopy of General Physics Institute of the Russian Academy of Sciences. Graphene samples were obtained by chemical vapor deposition on the surface of copper foil at a high temperature in a mixture of hydrogen, argon and methane gases. Further, graphene samples from copper foil were transferred onto a quartz substrate for processing in hydrogen plasma, measurements of Raman spectra and optical absorption spectra.

During the Raman spectra studies from graphene samples processed in a hydrogen plasma, an increase in the intensity of the D peak at a shift frequency of 1350 cm^{-1} (excitation energy of 2.33 eV) was observed. The appearance of this peak indicates either disordering (the presence of defects) in graphene, or about the appearance of the sp^3-hybridized state of carbon. However, if the intensity of the 2D peak at a shift frequency of 2680 cm^{-1} does not change, as in our case, then this indicates that the defectiveness of graphene did not increase, but hydrogenation of the material occurred, that is, the chemical bonding of hydrogen atoms to carbon atoms the graphene lattice and carbon transition in graphene from sp^2 to sp^3 hybridization. Moreover, the intensity of the D peak relative to the intensity of the G peak in graphene can be used to refer to the amount of hydrogenated carbon. At 100% hydrogenation, when each hydrogen atom on each side of two-dimensional graphene is bound to each carbon atom in graphene, the intensity of the G peak should not be less than the intensity of the 2D peak in graphene. In the case of complete hydrogenation of graphene, the material acquires other properties and is called graphane. Namely, the graphane is a dielectric with the band gap of 5.4 eV. However, with dosed hydrogenation of graphene, it is possible to control the width of the band gap of the material and make it a semiconductor with the necessary electronic structure.

1. J. Son, S. Lee, S.J. Kim, B.C. Park, H.-K. Lee, S. Kim, J.H. Kim, B.H. Hong, and J. Hong. "Hydrogenated monolayer graphene with reversible and tunable wide band gap and its field-effect transistor", Nature communications, 2016.

PECVD CNT-Si nanocomposite technology for MEMS applications

E. Gusev[1,2], J. Jityaeva[2], N. Rudyk[1], O. Ageev[1,2]
1. Southern Federal University, Institute of Nanotechnology, Electronics and Equipment Engineering, Taganrog, Russia, eyugusev@sfedu.ru
2. Southern Federal University, Research and Educational Centre "Nanotechnologies", Taganrog, Russia, ageev@sfedu.ru

Microelectromechanical systems are actively developing the scientific and industrial direction. The surface micromachining makes it possible to produce MEMS sensors with small overall dimensions, low power consumption and a wide range of sensitivity. Further improvement in output characteristics is associated with weighting of inertial elements, and extension of the side faces of sensitive elements (for capacitive sensors), by increasing the thickness of the structural layer and/or local deposition of additional layers or coatings. It can be achieved by using carbon nanotubes-silicon (CNT-Si) nanocomposite [1].
The technology of CNT-Si composite for MEMS applications and inertial sensors in particular is discussed.
The process flow consists of several stages. First, local deposition of the catalytic centers and next growing of the CNTs is carried out. Then a layer of polycrystalline silicon is deposited on the CNTs arrays. Both CNTs and polysilicon were obtained by the PECVD [2, 3]. The parameters of the catalytic centers and CNTs, in particular, diameter and length of the tubes, intertubular distance, as well as deposition parameters of polysilicon, like grain size, layer thickness, deposition rate, determine the structure and quality of the composite. The study of initial CNTs, silicon thickness and obtained nanocomposite CNT-Si was carried out using scanning electron microscopy and local etching by focused ion beams (FEI, Nova NanoLab 600).

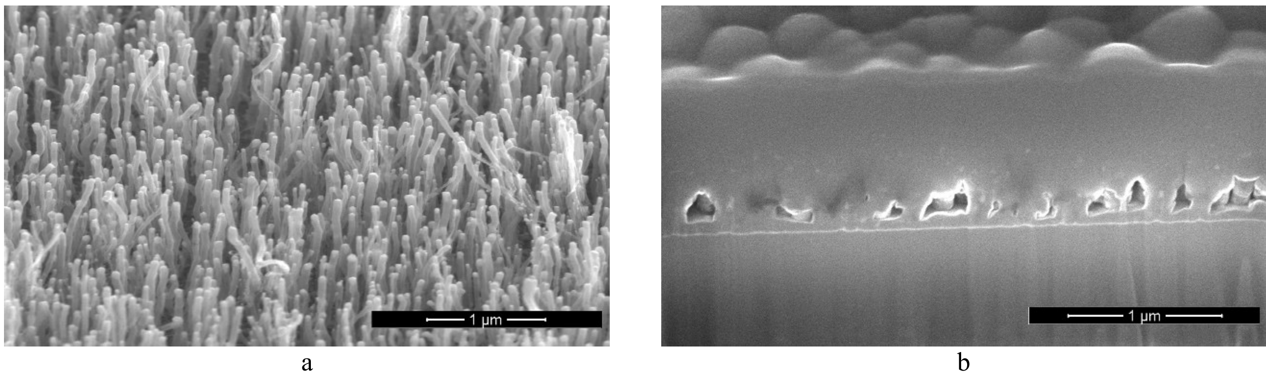

a b

Figure 1. SEM images of (a) CNTs and (b) the nanocomposite.

A series of CNT-Si nanocomposite samples was fabricated (fig. 1). The optimal parameters of the CNTs arrays for the formation of the nanocomposite with the least number of defects were determined. Also, the deposition parameters of the silicon layer were established, ensuring the silicon filling of the intertubular space and obtaining the nanocomposite with an acceptable density of voids. Analysis of the study results showed that the CNT-Si nanocomposite could be used to increase proof masses and to local thickening of critical elements of inertial sensors.
This work was financially supported by Southern Federal University (grant VnGr-07/2017-02). The equipment of the Research and Educational Centre "Nanotechnologies" of Southern Federal University was used for the study.

1. S.M. Ubnoske, E.J. Radauscher, E.R. Meshot, B.R. Stoner, C.B. Parker, J.T. Glass. "Integrating carbon nanotube forests into polysilicon MEMS: Growth kinetics, mechanisms, and adhesion". Carbon*,* **113**, pp. 192-204, 2017.
2. O.I. Il'in, M.V. Il'ina, N.N. Rudyk, A.A. Fedotov, D.I. Levshov, O.A. Ageev. "The influence of activation and growth time on the geometry and structural perfection of multi-walled carbon nanotubes". J. Phys.: Conf. Ser., **1038**, 012062, 2018.
3. E.Yu. Gusev, J.Y. Jityaeva, A.A. Geldash, O.A. Ageev. "Effect of PECVD temperature and RF power on surface structure and refractive index of amorphous and polycrystalline silicon films". J. Phys.: Conf. Ser., **917**, 032029, 2017.

Methods and means of experimental investigation of gas-phase deposition of material layers in MEMS processes

V. Samoylikov, S. Evstafiev
National Research University "MIET", Zelenograd, Russia, madcatse@gmail.com

One of the fundamental processes for the production of micro-nanostructures for various purposes is the gas-phase deposition of layers of different materials realized in CVD and LPCVD technologies. It should be emphasized that the need to obtain layers of a given composition requires careful studies of the physical and chemical laws of processes and the conditions for their commercialization.

To date, there is a large number of works, both experimental and theoretical. However, as shown by the analysis of literary sources, most of these works are performed on the basis of various computer software tools (MATLAB, ANSYS FLUENT, CHEMKIN) [1-3]. What is common in these studies is that the results and conclusions also represent a large set of particular cases, since a particular design of the reactor with specific geometric parameters is being investigated. Such results are difficult to systematize and generalize, which is necessary for advising on the optimization of both design and technological parameters of CVD and LPCVD processes.

In addition, the implementation of such plan requires a significant number of highly qualified specialists (such as mathematicians, physicists, technology specialists, designers and researchers). In addition to the above, the resulting models should be checked for adequacy, which in turn requires significant material and time costs. Therefore, such methods and technical means of research should be used to obtain generalized dependencies that could be used in the design of future reactors with different geometric parameters. Therefore, in our opinion, the creation of analytical models of gas-phase deposition processes is an important component of a comprehensive study of gas-phase processes.

We believe that the results of modeling in finite elements (analysis of particular cases) in conjunction with physical modeling (generalized analysis with engineering calculation techniques) could serve as an effective component of the design of technological equipment.

The methodological basis for the studies of CVD and LPCVD processes was:
- a technique for visualizing the interaction of the ASG flow with the deposition surface (substrates);
- a technique based on the effect of self-doping;
- methods of physical and analog modeling.

Confirmation of the adequacy of the simulation was carried out on a real industrial process with a reliability of ± 10%.

1. N. Haoyin, L. Shijie, C. Caixia. *Modeling and simulation of silicon epitaxial growth in Siemens CVD reactor*. Journal of Crystal Growth, **404**, pp. 89-99, 2014.
2. G. Juergen. *Multiscale Modeling of Chemical Vapor Deposition (CVD). Apparatus: Simulations and Approximations.* Polymers, **5**, pp. 142-160, 2013.
3. I. Zaidi, Y.H. Jang. *Numerical modeling study on the epitaxial growth of silicon from dichlorosilane.* Journal of Crystal Growth, **483**, pp. 1-8, 2018.

Ion-plasma sputtering of (111) textured Pt films with various crystalline structure parameters

R. Selyukov, I. Amirov, M. Izyumov, V. Naumov
Yaroslavl Branch of the Institute of Physics and Technology, Yaroslavl, Russia, E-mail: rvselyukov@mail.ru

Pt films are widely used in MEMS technology [1]. MEMS characteristics are strongly influenced by the surface morphology and the crystalline structure of the Pt films used. The aim of this work was to investigate the effect of ion-plasma treatment on the surface morphology of Pt films having different crystalline structure parameters.

100 nm Pt films were deposited on oxidized Si(100) wafers by magnetron sputtering at room temperature. The type 1 film was deposited with floating potential on the substrate and the type 2 film was deposited with bias -15 V on the substrate. Both films had fiber (111) texture but the type 2 film had the better texture quality and the higher fraction of crystalline phase δ. The FWHM of rocking curves Pt (111) were 12° and 9° for type 1 film and type 2 film respectively. The parameter δ for type 2 film was 15% more than for type 1 film (to calculate δ it was assumed that δ is proportional to the area under rocking curve). After deposition the specimens of both film types were exposed to Ar ion-plasma treatment at room temperature. Treatment regimes were following (ion energy, eV/sputtering time, s/energy fluence Φ_e J·cm^{-2}): 25 eV/300 s/60 J·cm^{-2}, 40 eV/500 s/150 J·cm^{-2}, 65 eV/120 s/60 J·cm^{-2}, 200 eV/10 s/15 J·cm^{-2}. Ar pressure was 0.08 Pa and ion current density was 7.5-7.8 mA/cm^2 in all regimes. The sputtering times were chosen so that the Pt film was thinned to 50 nm at each regime excepting 25 eV. Film thinning doesn't occur in 25 eV regime because this ion energy is less than the Pt sputtering threshold. The surface morphology of specimens was investigated using scanning tunneling microscope GPI-Cryo-SEM at room temperature in high vacuum (10^{-6} mbar). RMS roughness R, correlation length L (L is a parameter characterizing the lateral dimensions of surface objects), and surface area were determined.

It was found that R (and L) are almost equal for as-deposited type 1 and type 2 films (see Fig. 1). Treated film surfaces comprise of grain-like objects with the lateral dimensions of tens nm. In case of 200 eV treatment these objects are covered by smaller clusters. Parameters R and L are smaller for type 2 film than for type 1 film for all regimes excepting 200 eV. After 200 eV treatment R (and L) are almost equal for both film types. It can be concluded that the better crystalline structure of type 2 film restrains the roughening during treatment with lower ion energies (25-65 eV) whereas the influence of structure difference becomes negligible for treatments with higher (200 eV) ion energies. The treatment doesn't change the surface area in the all regimes although R and L change considerably (up to 2.5 and 6 times respectively). This can be explained by significant surface diffusion during treatment.

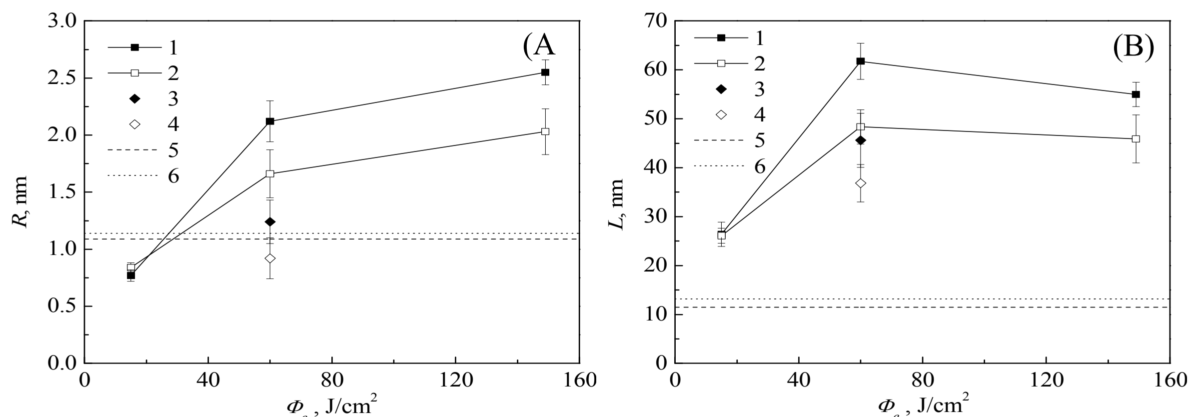

Fig. 1. A - $R(\Phi_e)$. B - $L(\Phi_e)$. 1, 3, 5 - type 1 film, 2, 4, 6 - type 2 film. 1, 2 - sputtering regimes, 3, 4 - 25 eV regime, 5, 6 – as-deposited films.

1. P. Ekkels, X. Rottenberg, R. Puers, H.A.C. Tilmans. "Evaluation of platinum as a structural thin film material for RF-MEMS devices". J. Micromech. Microeng., **19**, 065010, 2009.

Sub-micron inorganic masks for high-quality Josephson structures

S.B. Izyurov[1], V.L. Gurtovoi[1,2], I.N. Khrapach[1,3], V.B. Lubsanov[1], O.V. Astafiev[1,3,4]
1. Moscow Institute of Physics and Technology, 141700 Dolgoprudny, Russia
2. Institute Of Microelectronics Technology and High Purity Materials RAS, 142432 Chernogolovka, Russia
3. Russian Quantum Center, 143025 Skolkovo, Russia
4. Physics Department, Royal Holloway, University of London, Egham, Surrey TW20 0EX, United Kingdom

We describe Ge/Nb bilayer inorganic masks preparation for fabrication of submicron single Josephson junctions and devices on their basis. We fabricated Al/AlO_x/Al Josephson junctions 200x500nm^2 area. High-resistivity silicon substrates were selected as a substrate. The electron-transport characterization in a wide temperature range (20 mK – 1 K) demonstrates high quality of these structures.

Method of shadow evaporation is traditionally used in fabricating structures with Josephson junctions (JJs) as it is described in Dolan work [1]. For this method are widely used masks made with e-beam organic resists like PMMA-MMA. Unfortunately, as it was shown by Pop et al. [2], organic resists contaminate substrates and can outgas organic substance in processes of evaporating metals or forming tunnel insulator by Al oxidation. These organic resists disadvantages can decrease temperature of superconducting transition of evaporated metals and decrease quality of tunnel dielectric. As a result it leads to two-level state formation, decreasing coherence time and increasing noise of detectors with JJs. Also, PMMA-like resists are not suitable for high temperature processes, for example, in epitaxial growth of single crystal Al and Al_2O_3.

These problems can be solved by using inorganic masks Nb-Ge as it was suggested by Welander et al. [3], where germanium is used as a lower supporting layer and niobium as an upper masking layer. But fabricated in [3] structures have leaks through "holes" in single crystalline Al_2O_3 tunnel dielectric and in case of amorphous dielectric AlOx strong suppression of superconducting gap was seen. The main reason of Nb-Ge pair usage is selectivity of germanium etching in an aqueous solution of hydrogen peroxide (H_2O_2) with respect to niobium and resulting Al/AlOx/Al structures. We improved this technology of bilayer Nb-Ge masks to make single submicron JJs and complex structures on their basis like superconducting quantum bits with high coherence time. Fig. 1 shows Nb-Ge mask of SQUID structure on silicon substrate.

For the fabricated SQUID structures current-voltage dependences at different temperatures (Fig. 2) and oscillations of critical current in magnetic field are measured (Fig. 3).
Inorganic mask technology is promising for high quality JJ-nanostructures fabrication.

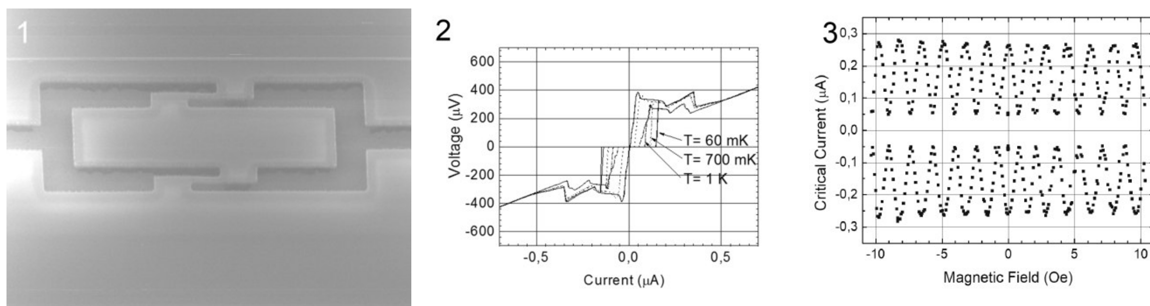

1. Dolan G.J. Offset masks for lift-off photoprocessing. Applied Physics Letters, **31**(5), 337-339 (1977).
2. Pop I.M., Fournier T., Crozes T., Lecocq F., Matei I., Pannetier B., and Guichard W. Fabrication of stable and reproducible submicron tunnel junctions. Journal of Vacuum Science & Technology B, Nanotechnology and Microelectronics: Materials, Processing, Measurement, and Phenomena, **30**(1), 010607 (2012).
3. Welander P.B., Bolkhovsky V., Weir T.J., Gouker M.A., & Oliver W.D. Shadow evaporation of epitaxial Al/Al_2O_3/Al tunnel junctions on sapphire utilizing an inorganic bilayer mask. arXiv preprint arXiv:1203.6007 (2012).

Highly sensitive ultra-low frequency hydrophone

T.V. Krishtop[1], D.A. Zhevnenko[1,2,3], S.V. Kokhanovsky[1], P.V. Dudkin[1,2], A.S. Zlobin[2], A.Y. Belyaev[2,3], V.G. Krishtop[1,4,*]

[1] *LLC «Seysmotronika», Moscow, Russia*

[2] *Moscow Institute of Physics and Technology (State University), Dolgoprudny, Russia.*

[3] *JCS Molecular Electronics Research Institute, Zelenograd, Russia*

[4] *Institute of Microelectronics Technology and High Purity Materials RAS, Chernogolovka, Russia.*

* *krishtop@iptm.ru*

Electrochemical transducers are successfully used in the development and production of high-altitude accelerometers, seismometers, geophones and rotation sensors [1-5]. We designed and developed a microelectronic technology for the production of high-precision planar electrochemical transducers [6-9].

In this paper, we demonstrate a prototype of the highly sensitive ultra-low frequency hydrophone based on an electrochemical planar-type transducer. We designed and produced a new planar electrochemical microchip and invented a mechanical system that is capable to measure alternating pressure at low frequencies. We obtained the sensitivity function of the ULF-hydrophone for converting pressure into an electrical signal. The developed sensing element can become the basis for a family of acoustic pressure receivers, vector acoustic receivers, infrasound pressure gradient detectors in the infrasonic range.

Fig.1. Ultra-low frequency hydrophone

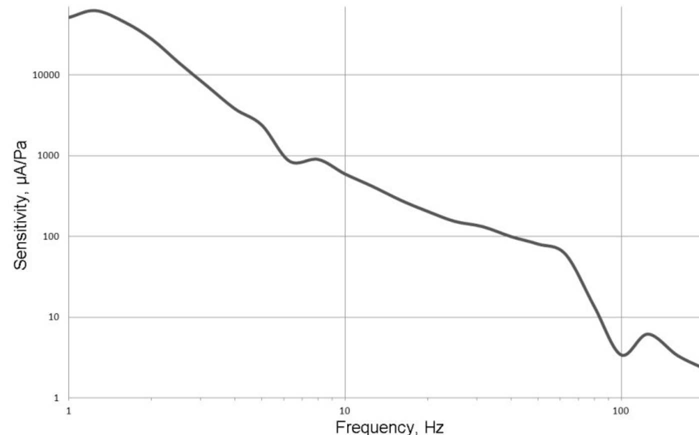

Fig.2. Sensitivity function of the pressure sensor.

1. A.S. Bugaev et al. «Molecular electronic transducers for measuring instruments». Journal of Communications Technology and Electronics (Radiotekhnika i Elektronika), №11, 2018.
2. A.S. Shabalina et al. «Modern measuring instruments based on molecular electronic transducers». Achievements of Modern Radioelectronics, №9, pp. 33-42, 2014.
3. A.S. Shabalina, V.G. Krishtop. «The precision seismometer based on planar electrochemical transducer». Proc. SPIE **10224**, ICMNE-2016, 102241K, 2016.
4. D. Zaitsev, A. Antonov, V. Krishtop. «Angular MET sensor for precise azimuth determination». Proc. SPIE **10224**, ICMNE-2016, 102241H, 2016.
5. D.L. Zaitsev, V.M. Agafonov, E.V. Egorov, A.N. Antonov, V.G. Krishtop. «Precession azimuth sensing with low-noise molecular electronics angular sensors». Journal of Sensors, **2016**, Article ID 6148019, 2016.
6. D.A. Zhevnenko et al. «Mass and charge transfer modeling in planar electrochemical transducers». Electronic Engineering. Series 3. Microelectronics, **164**, №4, pp.31-37, 2016.
7. D.A. Zhevnenko, S.S. Vergeles, T.V. Krishtop, D.V. Tereshonok, E.S. Gornev, V.G. Krishtop. «The simulation model of planar electrochemical transducer». Proc. SPIE **10224**, ICMNE-2016, 102241I, 2016.
8. A.V. Novikov, A.E. Egorchikov, A.N. Dolgov, E.S. Gornev, V.G. Popov, I.V. Egorov, V.G. Krishtop. «The planar silicon-based microelectronic technology for electrochemical transducers». Proc. SPIE **10224**, ICMNE-2016, 102241J, 2016.
9. D.L. Zaitsev et al. «Experimental studies of temperature dependence of transfer function of molecular electronic transducers at high frequencies», IEEE Sensors Journal, **16**, №22, p. 7864, 2016.

Influence of the electromigration on the characteristics of electrochemical microsystems

D.A. Zhevnenko[1,2,3], E.S. Gornev[2,3], V.O. Kuzmenko[2], P.V. Dudkin[1,2], S.N. Zhabin[2], T.V. Krishtop[1], V.G. Krishtop[1,4]

1. Seismotronics LLC, Moscow, Russia

2. Moscow Institute of Physics and Technology (State University), Dolgoprudny, Russia.

3. JCS Molecular Electronics Research Institute, Zelenograd, Russia

4. Institute of Microelectronics Technology and High Purity Materials RAS, Chernogolovka, Russia.

Figure 1. Example of planar ETC.

Planar electrochemical microsystems (Fig.1.) are very effective for design and development of motion parameters sensors. Electrochemical sensors (ECT) have a number of advantages over MEMS and piezoelectric sensors in the infrasonic range [1, 2]. Nowadays, microelectronics fabrication technology of planar electrochemical sensors is actively developing [3-5].

Traditionally, it has been accepted that the electromigration flow in a three-component electrolyte is negligible and almost has no effect on the system characteristics, due to screening by an excess ions of the background component [ex. 1, 2]. However, for now, the dynamic range of electrochemical converters reaches 165 dB [6] or more, and even the effect of electromigration at the level of 0.1-1% is significant for high-precision sensors. Previously, electromigration influence on the characteristics of the system was considered in [7]. Nonlinear characteristics were estimated in [8, 9], but electromigration was not taken into account. In this paper, we took electromigration into account and we simulated the transducing processes in electrochemical transducers with different geometries, estimated the magnitude of the asymmetric electromigration flow (Fig. 2) and calculated the contribution of electromigration to the transfer function and THD.

This work is supported by the Russian Foundation for Basic Research (grant 18-07-01162 A).

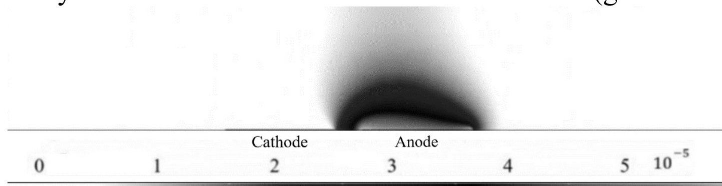

Figure 2. Electromigration additive to full flow of I3- ions.

1. A.S. Shabalina et al. "Modern measuring instruments based on molecular electronic transducers". Achievements of Modern Radioelectronics, **9**, pp. 33-42, 2014.

2. A.S. Bugaev et al, "Molecular electronic transducers for measuring instruments". Journal of Communications Technology and Electronics (Radiotekhnika i Elektronika), **11**, 2018.

3. D.A. Zhevnenko et al. «Mass and charge transfer modeling in planar electrochemical transducers». Electronic Engineering. Series 3. Microelectronics, **164**, №4, pp.31-37, 2016.

4. A.V. Novikov et al. «The planar silicon-based microelectronic technology for electrochemical transducers». Proc. SPIE **10224**, ICMNE-2016, 102241J, 2016.

5. D.A. Zhevnenko, S.S. Vergeles, T.V. Krishtop, D.V. Tereshonok, E.S. Gornev, V.G. Krishtop. «The simulation model of planar electrochemical transducer». Proc. SPIE **10224**, ICMNE-2016, 102241I, 2016.

6. V.M. Agafonov, A.V. Neeshpapa, A.S. Shabalina. "Electrochemical Seismometers of Linear and Angular Motion." Encyclopedia of Earthquake Engineering. Springer, Berlin, Heidelberg, 2015.

7. V. Agafonov, E. Egorov. "Influence of the electrical field on the vibrating signal conversion in electrochemical (MET) motion sensor". International Journal of Electrochemical Science, **3**. pp. 2205-2218, 2016.

8. V.M. Agafonov, A.S. Bugaev, A.A. Oryol. "Nonlinear Effects in Molecular-Electronic Cell of a Planar Type". Nano- and Microsystems Technology, **5**, p.32, 2009.

9. V.M. Agafonov, A.N. Antonov, D.L. Zaitsev. "Intrinsic noise and nonlinearity of diminutive angular molecular-electronics transducers". Sensors & Systems, **1**. pp. 7-12, 2010.

Author Index

Aban'shin N.P. O3-25
Abdullaev D.A. O1-07, O3-19
Ablayev F.M. q2-03, q3-01, P1-38
Ablayev M.F. q3-01, P1-37
Abramov I.I. O1-02
Adonin A.S. O1-17
Afanas'ev V.P. P1-32, P1-33
Afanasiev M.S. P2-08
Afonenko A.A. O2-17
Ageev O.A. O1-04, P1-09, P1-10, P2-20, P2-25, P2-26, P2-27, P2-34, P2-35, P2-41, P2-43
Ahmedov T.I. O2-15
Akchurin G.G. O3-25
Akmaev M.A. P2-16, P2-33
Aleksanyan A.A. P1-13
Aleshkin V.Ya. P2-16
Aleshchenko Yu.A. P2-16
Al-Saman A. O3-09
Amirov I.I. O3-14, O3-15, P2-45
Anchutin S.A. P1-23
Andreev D.V. P1-05, P1-06
Andreev V.G. O3-29, P2-12
Andreev V.V. P1-05
Andrianov S.N. q2-03, P1-37, P1-38
Andrianova N.S. P1-37
Anisimkin V. P1-28
Antonov V.A. L1-04, P2-32
Asadov S.M. P2-21
Astafiev O.V. P2-46
Avdeev S. P2-07
Averkin S.N. O3-11
Averyanov D.V. O1-01
Avetisyan Yu.A. O3-25
Avilov V. P1-09, P1-10
Avosopiants G.V. q2-05, P1-42
Babich A. P2-19
Babukhin D.V. q2-06
Babushkin A. O3-15
Bachurin V. O3-17
Baislamova U. O3-13
Baklanov M.R. O3-13, P2-05, P2-06
Balakirev S.V. P2-34, P2-35
Bandurin D. L2-04
Bantysh B.I. q2-05, q3-06, q3-08, P1-44
Barabanenkov M. O3-27
Baranov G. P2-22
Barinov A.D. P1-32, P1-33
Bazulin D. O3-01
Bdikin I. P2-19
Beginin E.N. P1-16, P1-17
Belikov A.I. O1-08
Belin A.M. P1-22
Beloglazkina E. O2-12
Belov A.Yu. O3-21
Belova N. O1-12
Belyaev A.Y. D-01
Berdnikov A.E. P2-11
Berezin V.A. O1-09
Beterov I.I. qL1-04
Biryukv M. P2-42
Bobrinetskii I. O3-10
Bocharov G.S. P1-32
Bochkin G.A. qL1-03, q1-06, q1-08
Bodisko Y.N. P1-32, P1-33
Bogachev V.V. O1-05
Bogdanov Yu.I. q1-04, q2-05, q2-09, q3-06, q3-08, P1-42, P1-43, P1-44
Bogdanova N.A. q1-04, q3-06, P1-42, P1-43, P1-44
Borzdov A.V. O2-14, P1-12
Borzdov V.M. O2-14, P1-12
Boubanga-Tombet S. L2-01

Author Index

Bozh(j)ev I.V. P1-26, P1-30
Bruk M.A. O2-04, O2-05, P2-23
Burbaev T.M. P2-16
Byrnes T. q1-09
Chaplygin Yu.A. P1-04
Cheinet P. qL1-04
Chekmachev V.G. P1-40
Cherkova S.G. O1-10, P2-14, P2-15
Chernyaev A.P. P1-13
Chernyavskiy A.Yu. q3-04
Chigarev S.G. O2-15
Chinenkov M. P1-24
Chkhalo N.I. O2-01
Chubunov P. P1-03
Chucheva G. P2-01, P2-02, P2-08
Chuev M. O3-20
Chuprina I.N. qL1-02
Churilov A. O3-17
Clemente I. O3-23, P2-20, P2-36
Constantinian K.Y. O3-03
Dagesyan S.A. O2-12, P1-02, P1-28, P1-30
Danelyan E.E. O1-05
Dedkova A.A. P2-36
Demin G.D. O1-20, O2-01, O2-07, O2-08, P1-22
Denicuk S. P1-29
Denisenko Yu.I. P2-03
Devyatov I.A. O3-02
Djuzhev N.A. O1-20, P1-22, P1-24
Dorofeev A.A. P1-26
Drozdetsky M.G. P1-07
Dubinov A.A. L2-01, O2-17
Dudkin P.V. D-01, D-02
Dyuzhev N.A. O2-01, P2-36
Efremov A.M. O3-12
Eletskii A.V. P1-32
Elistratov A.A. q2-06
Entin V.M. qL1-04
Eremenko M.M. P2-34, P2-35
Ermakov R. P1-46
Evsikov I.D. O1-20
Evstafiev S. P1-25, P2-44
Ezhova O.A. O3-07
Fastovets D.V. q1-04, q2-09, q3-06, q3-08, P1-43
Fedichkin L. q3-02, P1-41
Fedorov A. q2-08, q3-09
Fedorov F. O3-10
Fedorov G. L2-04
Fedorov Yu.V P1-01
Fedorova A.V. q1-08
Fedotov S.D. P2-04, P2-24
Fel'dman E.B. qL1-03, q1-06, q1-07, q1-08
Fiegna C. L1-02
Filippov S. q3-05
Fomin L.A. O1-09, O2-06
Galiev R. O2-16
Gasenkova I. P1-29
Gaydamachenko V. O2-12, P1-02
Gayduchenko I. L2-04
Geim A. L2-04
Gerasimenko A. P2-18
Gerasimov K.I. q2-02
Gergel V.A. P1-14
Gismatulin A.A. P2-14
Glinskiy I. O2-16
Glukhenkaya V. P2-18
Glushko A. O3-08
Goldman E. P2-01, P2-02
Golishnikov A.A. P2-31
Goltsman G. L2-04
Goncharov V.E. P1-34
Goncharov Yu. O2-16
Gorbatsevich A.A. O2-11

Author Index

Gorbunov M. P1-07
Gorlachev E.S. O3-14, P1-11
Gornev E.S. O2-02, D-02
Gorshkova N.M. P1-14
Granato E. P1-19
Grishin A.S. O3-03
Gritsenko V.A. O1-06
Gromov D.G. P2-39
Gryazev A.S. P1-32, P1-33
Gulyaev Yu.V. L1-01, P2-02
Gurtovoi V.L. P2-46
Gusev E. P2-07, P2-43
Gushin O.P. O1-13, O2-02, P2-22
Gvozdev V. O1-13
Hansen J.B. O1-15
Henini M. O2-15
Hosotani T. L2-03
Huang B. O1-12
Il'ichev E. O1-03, O3-26
Il'in O.I. P2-41
Ilnitskii M.A. L1-04
Iniguez B. O1-18
Isachenko A. O3-16
Italyantsev A. O3-27
Iurov A. P1-24
Ivanov S.V. P1-08
Izrailev N. O3-16
Izyumov M.O. O3-14, P2-45
Izyurov S.B. P2-46
Jacobsen C.S. O1-15
Jityaev I. O1-04
Jityaeva J. P2-43
Kafanov S. P1-26
Kalachev A.A. qL1-02, P1-37
Kalugin V.V. P1-23
Kalyabin D.V. P1-16, P1-20
Kamaev G.N. O1-06, P2-14
Kaplya P.S. P1-32
Karateev I.A. O1-01
Karaulov V.Yu. P1-31
Karazeev A. q2-08, q3-09
Karuzskii A.L. P1-13
Kashin V. P1-28
Katamadze K.G. q2-05, P1-42
Kateev I.Yu. q2-04, P1-39
Kazachkov A. O3-16
Kazakov I.P. P2-33
Kelm E. O3-18, O3-19
Khabibullin R.A. O2-16, O2-17, P1-14
Khadiev K. q2-07
Khadieva A. q2-07
Kharkov Y. q2-08
Khaustov V. O1-03, O3-26
Khorin I. O3-29
Khoryushin A.V. O1-15
Khrapach I.N. P2-46
Kibalov D. O2-18
Kiktenko E.O. q2-06, q2-08, q3-09
Kim C.-H. O1-19
Kimball J. O1-12
Kireev V.Yu. P2-36
Kiselev D.A. P2-08
Kislinskii Y.V. O3-03
Klekovkin A.V. P2-16, P2-33
Klimin V.S. P2-25, P2-26, P2-41
Knap W. L2-01
Kochurina E.S. P1-23
Kokhanovsky S.V. D-01
Kokin A.A. q1-01
Kolesov V. P1-28
Kolomejtseva N.V. O1-02
Kolotinskiy N. O3-01, P1-15
Komarov I.A. O1-05
Konoplev B. O3-28
Kornev V. O3-01, P1-15
Korobova N. P2-17

Author Index

Korolev A. P1-04
Kostyukov D.A. P2-31
Kotelyanskii I.M. O1-15
Kotova N. P2-06
Kots I.N. P2-25, P2-27
Kovlakov E.V. q3-07
Kozyukhin S. P2-18
Krasnikov G. O1-13, O2-11
Krasukov A. P1-04
Krishtop T.V. D-01, D-02
Krishtop V.G. O2-15, D-01, D-02
Krivospitsky A. O2-10
Kruchinin S. O1-14
Kruchinin V.N. O1-06
Krupenin V.A. P1-26, P1-30
Krupkina T.Yu. P1-04
Krynin A. S1-01
Kshensky O. O1-18
Kublikova D. q3-09
Kucherov M.M. q3-03
Kudrya V.P. O3-24
Kudryavtsev S.E. P1-11
Kulagin A.V. q1-02
Kuleshov A. O1-03, O3-26
Kulik S.P. qL1-01, q2-05, q3-07
Kumar V. O1-10
Kupriayanov A.N. O3-06
Kurbat D. P2-28
Kurenya A. P2-38
Kurochkin V.L. P1-46
Kurochkin Y.V. P1-46
Kuzmenko V. P2-29, P2-30, D-02
Kuznetsov A. P2-42
Kuznetsov P. O1-13
Kuznetsov V.I. O3-04
Kuznetsov Yu.A. P1-44
Kuznetsova E.I. q1-07, P1-36
Kuznetsova I. P1-28
Kwon K.-H. O3-12
Kyaw Z.P. O1-08
Labunov V.A. O1-02, P1-12
Ladunov V.Y. q1-02
Lagodenko N.K. O1-05
Lapshin R.V. P1-22
Lavrukhin D. O2-16
Lazarenko P. P2-18, P2-19
Lazarev I.D. P1-36
Lebedev A.O. P1-08
Lebedev E.A. P2-39
Lebedev K.V. P1-21
Leiman V. L2-02
Leu J. P2-06
Levin D.D. O1-05
Litavrin M. O2-02
Loginov A.P. O3-25
Lomov A. O3-21
Lopatin A.Ya. O2-01
Losev A. P1-46
Lozovik Yu.E. q2-06
Lubsanov V.B. P2-46
Lukichev V.F. O2-10, O2-14, O2-18, O3-11, q1-04, q2-09, q3-06, P1-29, P1-43, P1-44, P2-21, P2-28
Luzanov V.A. O1-15
Lysenko I.E. O3-07
Makarchuk V. O3-08
Makarov M. O3-27
Makhiboroda M.A. O2-01
Makhviladze T.M. P2-13
Malikov I.V. O1-09
Maltsev P.P. L2-02
Manabe S. L2-03
Maslovsky V.M. P1-05, P1-06
Markovets K.E. P2-10
Martynov A.I. P2-24

Author Index

Matuyshkin I.V. O2-02
Maytama M.V. P1-01
Mazaletsky L.A. O3-14
Melesov N. O3-17
Melnikov A. q3-02, P1-28
Menninger N. O1-12
Meshchaninov F. P1-41
Miakonkikh A.V. L1-04, O2-03, O2-10, O2-18, O3-11, O3-13, O3-23, P1-29, P2-20, P2-28, P2-29, P2-30, P2-36, P2-40
Migunov D. O1-03
Mikhailov G.M. O1-09, O2-06
Mikhaylichenko S. O3-08
Mikhaylin I.A. P2-34, P2-35
Miller T. O1-11
Milovanov R. O3-18, O3-19
Minaev V. P2-17
Minkin V.S. P1-14
Minnegaliev M.M. q2-02
Minnullin R. O3-27
Mirofyanchenko A.E. P1-35
Mirofyanchenko E.V. P1-35
Miroshnikova I.N. P1-33
Mitin V. L2-02
Mityagin Yu.A. P1-13
Moiseev S.A. q2-01, q2-02, q2-03, P1-37
Molin A. P2-42
Mordvintsev V.M. P1-11
Morozov O.V. P1-27
Morozova E. O2-12
Mortet V. O1-10
Mozhaev P.B. O1-15
Mozhaeva J.E. O1-15
Mrozovskaya E. P1-03
Mukhanov O. O3-01
Mukhurov N. P1-29
Muratov A.V. P2-16
Murin D. O3-12
Murzin V.N. P1-13
Mustafaeva S.N. P2-21
Myers T. O1-12
Nabiev A. P2-01
Nabiev R. O1-03, O3-26
Naryshkina V. P2-01
Nasibulin A. O3-10
Naumov V.V. O3-22, P2-45
Nekrasov N. O3-10
Nevolin V.K. O3-10, P2-04, P2-24
Nikitov S.A. P1-16, P1-17, P1-20
Nikonov A.V. P1-34
Nikulov A.V. O3-05
Norkin D. q3-09
Novikov A.V. P2-16
Novikov D.V. P1-22
Obraztsova E. P2-42
Omori Y. L2-03
Orlov M.A. O1-05
Orlov O.M. P1-08
Osokin S. P1-20
Otsuji T. L2-01, L2-02, L2-03, O2-16
Ovcharov V. P2-37, P2-38
Ovodov A.I. P1-22
Ovsyannikov G.A. O3-03
Ozhigov Yu.I. q1-02, q1-03
Paliy D. O3-08
Palov A. P2-05
Paporkov V.A. P1-18
Paramonov E. P2-42
Parfenov O.E. O1-01
Parshin E. O3-17
Parshintsev A.A. O2-13
Pashkeev D.A. P1-34

Author Index

Pashkin Yu. P1-26
Pavlov A.A. O2-16
Pavlov A.Yu. P1-01
Pavlov G. P2-42
Pavlov V.Yu. P1-01
Pavlovskiy V.V. O2-17
Perestoronin A.V. P1-13
Perevalov A. P2-09
Perminov N.S. qL1-02
Pestov A.E. O2-01
Pestova A.N. O2-09
Petrosyants K.O. O1-17
Petrukhin G. O1-03, O3-26
Petrzhik A.M. O3-03
Pichkovskiy I.S. P1-45
Pillet P. qL1-04
Pisarenko I.V. O3-28
Pogosov W.V. q2-06
Polohin A.A. P2-18
Polupanov N. P1-09
Polyakova V.V. P2-25, P2-27
Ponomarev D. L2-02, O2-16, O2-17
Popkov A.F. O2-07, O2-08
Popov A.A. P2-11
Popov A.I. P1-32, P1-33
Popov A.V. O2-08
Popov D.A. O1-17
Popov V. P1-17
Popov V.G. O2-15
Popov V.P. L1-04, P2-32
Popov V.V. L2-01
Poyarkov V. O1-18
Presniakov M.Y. P1-33
Presnov D.E. P1-02, P1-26, P1-30
Presnova G.V. P1-30
Prigara V. P2-37, P2-38
Process E.A. O1-12
Prokaznikov A.V. P1-18
Pronin S. O3-29
Putrya M.G. P2-31
Pyrkov A.N. q1-09
Rakhmatov B. O1-19
Rassadin A.E. O2-06
Rau E.I. P1-31, P2-10
Reale F. O1-11
Reggiani S. L1-02
Remes Z. O1-10
Remizov S.V. q2-06
Rezvan A.A. P2-25, P2-26, P2-41
Rezvanov A. O3-13
Ridzel O.Yu. P1-32
Rinnert H. P2-15
Rod I. O3-16
Rogachev M.S. P1-39
Rogozhin A.E. O2-04, O2-05, O2-18, P2-23, P2-40
Romanov V.S. P1-38
Romanova I.A. O1-02
Rubtsova M.Yu. P1-30
Rudakov V.I. P2-38
Rudenko K.V. L1-04, O2-03, O2-10, O2-14, O2-18, O3-11, O3-13, P1-29, P2-20, P2-22, P2-29, P2-30, P2-36, P2-40
Rudenko M. O2-14, O2-18, P2-28
Rudy A. O3-17
Rudyk N. P2-43
Ryabtsev I.I. qL1-04
Ryazanov R.M. P2-39
Rybin M. P2-42
Rychkov G. O1-03, O3-26
Ryndin E.A. O3-09, O3-28
Ryzhii M. L2-01, L2-02, O2-16
Ryzhii V. L2-01, L2-02
Ryzhenkova S. P1-02

Author Index

Sachkov V.A. O1-10
Sadofyev Yu.G. P2-16
Sadovnikov A. P1-17
Safin A. P1-20
Safronov L.N. P2-32
Salashchenko N.N. O2-01
Samoylikov V. P1-25, P2-44
Sangiorgi E. L1-02
Sapegin A. O3-27
Sapkov I.V. P1-02
Sarychev M.E. P2-13
Satou A. L2-01, L2-03
Saveliev A. P2-42
Savelyev M. P2-18
Selberherr S. L1-03
Selyukov R.V. O3-15, O3-22, P2-45
Semenov A.V. O3-02
Semin Yu. O2-10
Semochkin A.I. O1-08
Seredin B. O3-21
Seregin D.S. O1-07, O1-13, O3-13, P2-06
Shadrin A.V. O3-03
Shaman Yu.P. P2-39
Shamiryan D. O3-16
Sharaevskaya A.Yu. P1-16, P1-17
Sharaevskii Yu.P. P1-16
Sharapov A. P2-22
Sharapov N. P1-09
Sharoglazova V. P1-46
Shchavruk N.V. O2-17
Shcherbakova I. O1-02
Sherbin S.N. O1-05
Sherchenkov A. P2-18, P2-19
Shevyakov V.I. P2-09, P2-31
Shishlyannikov A. O2-03, P2-22
Shkarlat R. O1-18
Shorokhov V.V. O2-13, P1-30
Shubin N.M. O2-11
Shupegin M.L. P1-33
Shur M.S. L2-02, O1-18
Sidorov F. O2-04, O2-05
Sigov A. O1-13, P2-06
Simakin S. O2-09, O3-21
Skovoroda N.A. q1-02
Skuratov V. P2-14, P2-15
Slapovskiy D.N. P1-01
Smelova E.M. P2-12
Smirnov A. P1-28
Smirnov V. O2-18, P1-09, P1-10
Sobolev A.S. P1-14
Sokolov I.S. O1-01
Sokolov S. O3-18, O3-19
Soldatov E.S. O2-12, O2-13, P1-28
Solodovnik M.S. P2-26, P2-34, P2-35
Soloviev A.A. P1-38
Sorokina L. P2-39
Spektor I. O2-16
Statsenko V.N. P2-04
Stepanov A. P1-02
Stoffel M. P2-15
Stolyarov A.A. P1-05
Storchak V.G. O1-01
Straupe S.S. q3-07
Struchalin G.I. q3-07
Struchkov N.S. O1-05
Stuchlik J. O1-10
Stuchlikova T.H. O1-10
Suemitsu T. L2-03
Sundaram R.S. O1-11
Sverdlov V. L1-03
Svetlichnyi A. O1-04
Svintsov D. L2-02, L2-04, O2-10, O2-14
Taldenkov A.N. O1-01
Tallarico A. L1-02

Author Index

Tarasov M.A. P1-14
Tatarintsev A.A. O2-03, O3-21, P2-10, P2-22, P2-40
Taylor A. O1-10
Terekhov D. P2-19
Terekhov V. O3-08
Teverovskaya E. O1-03, O3-26
Thomas O. O1-11
Timoshenkov S.P. O1-14, P1-23, P2-17
Tkachenko A.V. O3-07
Tokmachev A.M. O1-01
Tominov R. P1-10, P2-20, P2-26
Tretyakov D.B. qL1-04
Trifonov A.S. P1-26, P1-30
Trushin O.S. O2-09, O3-17, P1-19
Tsarik K.A. P2-04, P2-24
Tsiniaikin I.I. P1-30
Tsukanov A.V. q2-04, P1-39, P1-40
Tsvetkov V.A. P2-33
Tsysar K.M. P2-12
Turin V. O1-18, O1-19
Ulyashova M.M. P1-30
Urmancheev R.V. q2-02
Ushakov D.V. O2-17
Ushakov V.V. P2-16
Uvarov I.V. O3-06, P1-27
Uvarov O.V. P2-33
Vahrushev D.V. P1-38
Vakulov Z.E. P2-20
Valeev A. O1-13
Varzarev Yu.N. P2-20
Vasil'ev S.G. qL1-03
Vasiliev A.V. q2-03, P1-37
Vasiliev S.V. O2-09
Vdovin V.A. O3-29, P2-12
Vdovin V.I. L1-04
Vergnat M. P2-15
Victorova N.B. q1-02
Vishnevskiy A. O3-13, P2-06
Volkov A.N. P1-06
Volkov O.Yu. O2-17
Volodin V.A. O1-06, O1-10, P2-14, P2-15
Vorobyov Y. P2-18
Vorotilov K.A. O1-07, O1-13, O3-13, P2-06
Vyurkov V. O2-10, O2-14, O2-18, P1-12
Wang Y. P2-06
Watanabe T. L2-01
Wei Sh. P2-05
Yachmenev A. O2-16
Yadav D. L2-01
Yakshina E.A. qL1-04
Yakubov A. P2-18, P2-19
Yakunin A.N. O3-25
Ying S.-C. P1-19
Yunin P.A. P2-16
Yurasov D.V. P2-16
Yurischev M.A. q1-05
Yuskaev M.R. P1-34
Yuvchenko S.A. O3-25
Zamburg E. P1-10, P2-20
Zanuccoli M. L1-02
Zavodilenko V. P1-46
Zaytsev K. O2-16
Zaytsev S.V. P1-31
Zebrev G.I. O1-16, O1-18, P1-03, P1-07
Zelensky V.S. P2-12
Zenchuk A.I. q1-06, q1-08
Zhabin S.N. D-02
Zhanaev E.D. P2-32
Zhang J. P2-06
Zharik G. P1-02
Zhevnenko D.A. D-01, D-02

Author Index

Zhikharev E.N.	O2-04, O2-05, P2-23
Zhukov A.A.	q2-06
Ziatdinov M.T.	P1-38
Zimin P.	P1-03
Zimnyakov D.A.	O3-25
Zinchenko L.A.	O3-08
Zlobin A.S.	D-01
Zobov V.E.	q3-03, P1-45
Zotov A.	P2-09
Zubov D.N.	O1-07, O3-18
Zvezdin N.Yu.	P1-18

Научное издание

Труды международной конференции МИКРО- И НАНОЭЛЕКТРОНИКА – 2018

Сборник тезисов

1–5 октября, 2018, г. Звенигород, РФ

Под редакцией:
чл.-корр. РАН *В.Ф. Лукичева*;
д. ф.-м. н. *К.В. Руденко*

Составитель к. ф.-м. н. *В.П. Кудря*

Издание доступно на электронном ресурсе e-library и www.icmne.ftian.ru

Напечатано с готового оригинал-макета

Подписано в печать 20.09.2018 г.
Формат 60x90 1/8. Усл.печ.л. 27,25. Тираж 240 экз. Изд. № 190.

Издательство ООО “МАКС Пресс”
Лицензия ИД N 00510 от 01.12.99 г.

119992, ГСП-2, Москва, Ленинские горы,
МГУ им. М.В. Ломоносова, 2-й учебный корпус, 527 к.
Тел. 8(495)939-3890/91. Тел./Факс 8(495)939-3891.

Отпечатано в типографии ООО «Паблит»
127282, Москва, ул. Полярная, д. 31В, стр. 1
Тел.: (495) 230-20-52
Заказ №